UNIVERSITÉ DES SCIENCES ET TECHNOLOGIES DE LILLE

ÉCOLE DOCTORALE DE BIOLOGIE-SANTÉ

THÈSE DE DOCTORAT

En vue de l'obtention du grade de Docteur en Sciences
de l'Université des Sciences et Technologies de Lille

Présentée par

MARIE DUHAMEL

De la classification moléculaire des gliomes à une nouvelle stratégie thérapeutique de réactivation des macrophages au sein de la tumeur

Soutenue à Lille le 23 septembre 2016

Devant le jury composé de :

Rapporteur	Mr Philippe Bulet	Directeur de recherche (CNRS)
Rapporteur	Mr Pierre Chaurand	Professeur (Université de Montréal)
Examinateur	Mme Anne Régnier-Vigouroux	Chercheur (Johannes Gutenberg Universität Mainz)
Examinateur	Mr Kris Gevaert	Professeur (Ghent University)
Examinateur	Mr Claude-Alain Maurage	Professeur (Lille 2, Droit et Santé)
Examinateur	Mr Michel Salzet	Professeur (Université de Lille 1)
Directrice de Thèse	Mme Isabelle Fournier	Professeur (Université de Lille 1)
Co-encadrant	Mr Maxence Wisztorski	Maître de Conférences (Université de Lille 1)

« Il est bien des choses qui ne paraissent impossibles que tant qu'on ne les a pas tentées. »

André Gide

REMERCIEMENTS

Au terme de ce travail, je tiens à remercier toutes les personnes qui ont contribué à sa réalisation et ont permis par leur soutien et leurs conseils de le mener à bien :

Le Professeur Michel Salzet, directeur du laboratoire PRISM, pour m'avoir accueillie comme doctorante au sein de son laboratoire. Je lui suis reconnaissante pour son soutien, son expérience, ses conseils et sa motivation pour ce projet qui lui tient particulièrement à cœur.

Le Professeur Isabelle Fournier, ma directrice de thèse, qui m'a apporté son expertise et ses conseils dans le domaine de la protéomique.

Le Docteur Maxence Wisztorski, co-encadrant de ma thèse, pour son implication dans le projet, sa disponibilité et ses conseils.

Monsieur Philippe Bulet, directeur de recherche au CNRS, ainsi que Monsieur Pierre Chaurand, Professeur à l'Université de Montréal, qui ont accepté d'être les rapporteurs de ma thèse et pour l'intérêt qu'ils ont porté à mon travail.

Madame Anne Régnier-Vigouroux, Chercheur à l'Université de Mainz, Monsieur Kris Gevaert, Professeur à l'Université de Gand, et Monsieur Claude-Alain Maurage, Professeur à l'Université de Lille 2, qui ont accepté d'examiner mon travail.

L'Université de Lille 1 et le SIRIC ONCOlille pour avoir accepté de financer cette thèse.

L'ensemble des personnes du laboratoire notamment Franck, Annie, Benoit, Jusal, Julien, Céline, Jean-Pascal, Christophe, Françoise, Pierre-Éric, Jacopo, Christelle et Lucie pour leur disponibilité et leur aide.

Les étudiants ou ex-étudiants qui ont permis de créer une atmosphère de travail cordiale et dynamique : Stéphanie, Antonella, Philippe, Tanina, Adriana, Vivian, Khalil, Tony et Dounia.

Enfin, je tiens à remercier mes proches et mes amis Sylvie, Marc, Claire, Jean-Pierre, Ambre, Julien, Elodie et Marion pour leur soutien et leur écoute durant ces trois années.

PUBLICATIONS

Publications acceptées

Duhamel M, Rodet F, Murgoci A.N, Wisztorski M, Day R, Fournier I, Salzet M. Proprotein convertases 1/3 inhibited macrophages: A novel therapeutic based on drone macrophages. *EuPA Open Proteomics.* **11**, 20-22 (2016).

Duhamel M*, Rodet F*, Murgoci A.N, Desjardins R, Gagnon H, Wisztorski M, Fournier I, Day R, Salzet M. The proprotein convertases PC1/3 regulated TLR9 trafficking and the associated signaling pathways. *Scientific Reports*. **6**, 19360 (2016).

Duhamel M, Rodet F, Delhem N, Vanden Abeele F, Kobeissy F, Nataf S, Pays L, Desjardins R, Gagnon H, Wisztorski M, Fournier I, Day R, Salzet M. Molecular Consequences of Proprotein Convertase 1/3 (PC1/3) Inhibition in Macrophages for Application to Cancer Immunotherapy: A Proteomic Study. *Molecular & Cellular Proteomics*. **14**, 2857-77 (2015).

Publications en cours

Duhamel M, Murgoci A.N, Rodet F, Zografidou L, Régnier-Vigouroux A, Vanden Abeele F, Kobeissy F, Nataf S, Pays L, Wisztorski M, Day R, Fournier I, Salzet M. A novel treatment for glioblastoma based on Taxol activation of PC1/3-depleted macrophages: evidence from a proteomic and functional study.

Le Rhun E*, Duhamel M*, Wisztorski M, Zairi F, Escande F, Maurage C.A, Reyns N, Kobeissy F, Salzet M, Fournier I. Glioma Grade III cases study based on non-supervised MALDI Imaging associated to tissue microproteomics linked to patient clinical data.

Proceeding de congrès

Le Rhun E*, Duhamel M* , Wisztorski M, Zairi F, Maurage CA, Fournier I, Reyns N, Salzet M.Metb-07classification of high grade glioma using matrix-assisted laser desorption/ionization mass spectrometry imaging (MALDI MSI): interim results of the gliomic study. Neuro-Oncology 17 (suppl 5), v136-v136

Communications orales

Duhamel M, Rodet F, Delhem N, Vanden Abeele F, Kobeissy F, Nataf L, Pays R, Desjardins R, Gagnon H, Wisztorski M, Fournier I, Day R, Salzet M; Involvement of PC1/3 in macrophages phenotype orientation: study of TLR4 and TLR9 signaling for an application to cancer immunotherapy. 6th workshop du Club Français de NeuroImmunologie, Paris, France, 6 Novembre 2015.

Duhamel M, Rodet F, Delhem N, Vanden Abeele F, Kobeissy F, Day R, Wisztorski M, Fournier I, Salzet M. Deciphering molecular consequences of the PC1/3 inhibition in macrophages for application in immunotherapy. 11ème journées du Club Jeunes de la SFEAP, Marseille, France, 20-22 Mai 2015.

Duhamel M, Rodet F, Wisztorski M, Salzet M, Fournier I. MS analysis of rat alveolar macrophages NR8383 secretomes : Effect of proprotein convertase 1/3 (PC1/3) down-regulation. 10ème journées du Club Jeunes de la SFEAP, Toulouse, France, 14-16 Mai 2014.

Duhamel M, Rodet F, Wisztorski M, Salzet M, Fournier I. MS analysis of rat alveolar macrophages NR8383 secretomes : Effect of proprotein convertase 1/3 (PC1/3) down-regulation. 19ème journées du Club Jeunes de la SFSM, Dieppe, France, 24-28 Mars 2014.

Posters

Duhamel M, Le Rhun E, Wisztorski M, Zairi F, Maurage CA, Fournier I, Reyns N, **Salzet M**. Classification of high grade glioma using matrix-assisted laser desorption/ionization mass spectrometry imaging (MALDI MSI) : interim results of the GLIOMIC study. ITMO 2015.

Duhamel M, **Le Rhun E**, Wisztorski M, Zairi F, Maurage CA, Fournier I, Reyns N, Salzet M. Classification of high grade glioma using matrix-assisted laser desorption/ionization mass spectrometry imaging (MALDI MSI) : interim results of the GLIOMIC study. Society of Neuro-Oncology, Novembre 2015.

Duhamel M, Rodet F, Delhem N, Vanden Abeele F, Kobeissy F, Nataf S, Pays L, Desjardins R, Gagnon H, Wisztorski M, Fournier I, Day R, Salzet M. Deciphering Molecular Consequences of the Proprotein Convertase 1/3 Inhibition in Macrophages for Application in Immunotherapy. EURON, Maastricht, Pays-Bas, 5-6 Octobre 2015.

Duhamel M, Rodet F, Delhem N, Vanden Abeele F, Kobeissy F, Nataf S, Pays L, Desjardins R, Gagnon H, Wisztorski M, Fournier I, Day R, Salzet M. Deciphering Molecular Consequences of the Proprotein Convertase 1/3 Inhibition in Macrophages for Application in Immunotherapy. HUPO 14th Annual World Congress, Vancouver, Canada, 27-30 Septembre 2015.

Duhamel M, Rodet F, Delhem N, Vanden Abeele F, Kobeissy F, Nataf S, Pays L, Desjardins R, Gagnon H, Wisztorski M, Fournier I, Day R, Salzet M. Deciphering Molecular Consequences of the Proprotein Convertase 1/3 Inhibition in Macrophages for Application in Immunotherapy. EUPA 9th Annual Congress, Milan, Italie, 23-28 Juin 2015. 2nd YPI Poster Award.

Duhamel M, Rodet F, Wisztorski M, Salzet M, Fournier I. Mass Spectrometry analysis of rat alveolar macrophages NR8383 secretomes: effect of proprotein convertases 1/3 (PC1/3) down-regulation. HUPO 13th Annual World Congress, Madrid, Espagne, 5-8 Octobre 2014.

Enseignements

2014/2015 : 64h de travaux pratiques en Immunologie, licence 3
2015/2016 : 64h de travaux pratiques en Immunologie, licence 3

Encadrements

Participation à l'encadrement d'étudiants en master et licence :

- Antonella Raffo Romero, 2014, stage de 6 mois
- Blandine Bourigault, 2015, stage de 6 mois
- Daniel Saucier, 2016, stage de 4 mois

TABLE DES MATIÈRES

REMERCIEMENTS iii
PUBLICATIONS iv
TABLE DES MATIÈRES vii
LISTE DES FIGURES ix
LISTE DES TABLEAUX x
LISTE DES ABRÉVIATIONS xi
PROBLÉMATIQUES ET OBJECTIFS 14
BIBLIOGRAPHIE 19
I. Les glioblastomes 19
A. Incidence 19
B. Facteurs de risque et symptômes 20
C. Diagnostic 21
D. Classification histologique de l'OMS de 2007 23
E. Classification moléculaire des glioblastomes 24
F. Traitements 30
II. Utilisation de la spectrométrie de masse pour la caractérisation des tumeurs 33
A. Les différentes techniques utilisées actuellement 33
B. L'imagerie par spectrométrie de masse MALDI-MSI 34
C. Microprotéomique tissulaire et corrélation avec l'imagerie MALDI 39
III. Le microenvironnement tumoral : les macrophages associés aux tumeurs 41
A. Généralités 41
B. Les macrophages associés aux tumeurs (TAM) 42
C. Autres éléments du microenvironnement tumoral 52
IV. Les proprotéines convertases, immunité et cancer 55
A. Généralités 55
B. Fonctions des proprotéines convertases 57
C. Rôle des proprotéines convertases dans l'immunité 60
CHAPITRE 1 63
Classification des gliomes de haut grade basée sur l'imagerie MALDI et la microprotéomique en relation avec les données cliniques des patients 63
Introduction 63
Résultats 64
Conclusion 110
CHAPITRE 2 115
Mise en place d'une approche thérapeutique visant à réactiver les macrophages au sein des tumeurs : effet de l'inhibition de la proprotéine convertase 1/3 115
Introduction 115

Résultats 117
Conclusion 158
CHAPITRE 3 160
Inhibition de la proprotéine convertase 1/3 (PC1/3) dans les macrophages pré-activés au Taxol pour le traitement des glioblastomes 160
Introduction 160
Résultats 161
Conclusion 204
DISCUSSION GÉNÉRALE 213
LISTE DES RÉFÉRENCES 218

LISTE DES FIGURES

Figure 1 : Distribution de tous les types de gliomes du système nerveux central 19
Figure 2 : Coupes histologiques après coloration hématoxyline et éosine de glioblastomes inclus dans l'étude Gliomic. 22
Figure 3 : Stratégie expérimentale de l'imagerie MALDI. 35
Figure 4 : Identification de REG-α comme biomarqueur du cancer de l'ovaire 38
Figure 5 : Hétérogénéité phénotypique des macrophages 45
Figure 6: Rôle des macrophages dans l'angiogenèse 48
Figure 7: Immunosuppression induite par les TAM 50
Figure 8 : La famille des proprotéines convertases 56
Figure 9 : Analyse protéomique de la biopsie de gliome de chien 111
Figure 10 : Protéines identifiées dans la zone tumorale de la biopsie de gliome de chien qui sont communes avec les protéines identifiées chez l'homme 112
Figure 11 : Imagerie peptidique MALDI-MSI de la biopsie de gliome de chien 113
Figure 12 : Etude d'UNC93b1 dans les macrophages NR8383 119
Figure 13 : Schéma décrivant l'impact de l'inactivation de PC1/3 sur l'activation des macrophages 120
Figure 14 : Viabilité des cellules cancéreuses C6 de gliome de rat en présence des sécrétomes des macrophages NT et PC1/3 KD stimulés au CpG-ODN 159
Figure 15 : Effet de l'augmentation de la concentration de taxol sur l'invasion des cellules tumorales C6 en l'absence ou présence de macrophages NT ou PC1/3 KD 205
Figure 16 : TOP 3 TIC des protéines inflammatoires différentiellement sécrétées par les macrophages KD, NT en présence de l'inhibiteur et NT sans l'inhibiteur 207
Figure 17 : Test de différentes concentrations d'inhibiteur des proprotéines convertases sur les sphéroïdes de cellules J3T en co-culture avec les macrophages NR8383 208
Figure 18 : Test de l'inhibiteur (50 µM) sur les sphéroïdes de cellules J3T 209
Figure 19 : Test de l'inhibiteur (50 µM) +/- LPS (200 ng/ml) sur les sphéroïdes de cellules J3T en co-culture avec les macrophages 210
Figure 20 : Test de l'inhibiteur (50 µM) +/- CpG-ODN (1 µM) sur les sphéroïdes de cellules J3T en co-culture avec les macrophages 211
Figure 21 : Test de l'inhibiteur (50 µM) en combinaison avec le Poly(I:C) (25 µg/ml) sur les sphéroïdes mixtes de cellules de glioblastome humain NCH82 et de cellules microgliales humaines 212

LISTE DES TABLEAUX

Tableau 1 : Classification de l'OMS de 2007 des gliomes diffus. 23
Tableau 2 : Fonctions biologiques des principaux biomarqueurs identifiés dans le plasma/sérum et le LCR des patients atteints de GBM. 29
Tableau 3 : Implication de certains substrats des proprotéines convertases dans la tumorigenèse. (Inspiré de Artenstein et Opal, 2011)..... 60

LISTE DES ABREVIATIONS

ACTH,	Adrenocorticotropic Hormone
ANG,	Angiopoietin
ARG1,	Arginase 1
ARN,	Acide Ribonucléique
ATRX,	Alpha Thalassemia/Mental Retardation Syndrome X-linked
CCL,	CC Chemokine Ligand
CCR,	CC Chemokine Receptor
CNDP1,	Carnosine Dipeptidase 1
CpG-ODN,	CpG Oligodeoxynucleotide
CRIP1,	Cysteine Rich Protein 1
CSF-1,	Colony Stimulating Factor 1
CTLA4,	Cytotoxic T-Lymphocyte Associated protein 4
CXCL,	CXC Chemokien Ligand
DHB,	2,5-Dihydroxybenzoic acid
EGF,	Epithelial Growth Factor
EGFR,	Endothelial Growth Factor Receptor
ESI,	Electrospray
FDA,	Food and Drug Administritation
FFPE,	Formalin Fixed Paraffin Embedded
FGF,	Fibroblast Growth Factor
FTL,	Ferritin, Light polypeptide
GBM,	Glioblastome
GM-CSF,	Granulocyte-Macrophage Colony-Stimulating Factor
GNRH,	Gondotropin-Releasing Hormone
GRO,	Growth Related Oncogenes
HCCA,	α-Cyano-4-Hydroxycinnamic Acid
HGF,	Hepatocyte Growth Factor
HIF1α,	Hypoxia-Inducible Factor 1-alpha
HNP-1,	Human Neutrophil Peptide 1
IDH,	Isocitrate Dehydrogenase
IDO,	Indoleamine 2,3-Dioxygénase
IFN,	Interferon
IGF,	Insulin Growth Factor
IGFR,	Insulin Growth Factor Receptor

IL,	Interleukin
IRF,	Interferon Regulatory Factor
IRM,	Imagerie par Résonnance Magnétique
ITO,	Indium Tin Oxide
KO,	Knock-Out
KD,	Knock-Down
LC-MS,	Liquid Chromatography-Mass Spectrometry
LCR,	Liquide Céphalo-Rachidien
LDL,	Low-Density Lipoprotein
LDLR,	Low-Density Lipoprotein Receptor
LPS,	Lipopolysaccharides
MALDI,	Matrix Assisted Laser Desorption Ionization
MCP1,	Monocyte Chimioattractant Protein 1
MDSC,	Myeloid-Derived Suppressor Cells
MGMT,	O^6-methylguanine DNA methyltransferase
MMP,	Matrix Metalloproteinase
MSI,	Mass Spectrometry Imaging
MSP,	Macrophage Stimulating Protein
NADPH,	Nicotinamide Adénine Dinucléotide Phosphate
NCAM,	Neural Cell Adhesion Molecule
NF1,	Neurofibromatose 1
NGS,	Next-Generation Sequencing
NF-κB,	Nuclear Factor-Kappa B
NK,	Natural Killer
NO,	Nitric Oxyde
NOS,	Nitric Oxyde Synthase
NT,	Non-Targeted
OMS,	Organisation Mondiale de la Santé
ORF,	Open Reading Frame
PC,	Proprotein Convertase
PCSK,	Proprotein Convertase Subtilisin Kexin
PD1,	Programmed Death 1
PDGF,	Platelet-Derived Growth Factor
PDGFRA,	Platelet-Derived Growth Factor Receptor, Alpha polypeptide
PDL1,	Programmed Death Ligand 1

$PGE_{2,}$	Prostaglandin E2
PI3K,	Phosphoinositide 3-Kinase
PIP,	Phosphatidylinositol Phosphate
Poly(I:C),	Polyinosinic-polycytidylic Acid
POMC,	Pro-Opiomélanocortine
PTEN,	Phosphatase and Tensin homolog
RB,	Retinoblastome
ROI,	Region Of Interest
ROS,	Reactive Oxygen Species
SDS-PAGE,	Sodium Dodecyl Sulfate-Polyacrylamide Gel Electrophoresis
SKI-1,	Subtilisin Kexin Isozyme 1
SNC,	Système Nerveux Central
SOC,	Store Operated Channel
SRM,	Single Reaction Monitoring
STAT,	Signal Transducer and Activator of Transcription
STIM1,	Stromal Interaction Molecule 1
TAM,	Tumor Associated Macrophage
TCGA,	The Cancer Genome Atlas
TERT,	Telomerase Reverse Transcriptase
TGF,	Tumor Growth Factor
TIL,	Tumor Infiltrating Lymphocyte
TLR,	Toll-Like Receptor
TNF,	Tumor Necrosis Factor
TP53,	Tumor Protein 53
UTR,	Untranslated Region
VAP1,	Vascular Adhesion Protein 1
VCAM,	Vascular Cell Adhesion Molecule
VEGF,	Vascular Endothelial Growth Factor

PROBLEMATIQUES ET OBJECTIFS

Les gliomes ou tumeurs gliales représentent les tumeurs cérébrales les plus fréquentes avec 2500 à 3000 nouveaux cas recensés par an en France (Viegas et al. 2011). Leur incidence est d'environ 5 cas pour 100 000 habitants. Ces tumeurs sont issues du tissu de soutien ou glie. Les glioblastomes sont les tumeurs cérébrales les plus agressives et représentent donc un enjeu thérapeutique majeur. Leur hétérogénéité rend leur classification difficile et par conséquent leur prise en charge n'est pas forcément adaptée. L'étude de cette hétérogénéité est donc primordiale et la prise en compte du microenvironnement tumoral est nécessaire. Les gliomes peuvent être classés en fonction du type de cellules gliales, de la localisation de la tumeur et de l'agressivité des cellules tumorales. Les tumeurs composées d'astrocytes sont appelées astrocytomes et comprennent 4 grades (I-IV) selon la classification de l'Organisation Mondiale de la Santé (Tabatabai et al. 2010). Les astrocytomes de grade I et II correspondent aux tumeurs de bas grade. Les grades III et IV représentent les tumeurs de haut grade. 75% des gliomes diagnostiqués sont de haut grade. Les tumeurs de grade IV sont les tumeurs les plus agressives et correspondent aux glioblastomes. La classification de l'OMS de 2007 utilise les techniques standards d'analyse histopathologique. Elle repose sur le type histologique de la tumeur (présence/absence d'atypies nucléaires, activité mitotique, prolifération microvasculaire, nécrose) pour déterminer le grade tumoral (Louis et al. 2007). Les limites de la classification de l'OMS sont principalement dues à un manque de reproductibilité inter-observateur mais également intra-observateur, pouvant atteindre de 20 à 30% (Varlet et al. 2005). De plus, les tumeurs ayant la même classification histologique présentent de grandes variabilités cliniques et de grandes variabilités de réponses aux traitements. De nouveaux biomarqueurs sont donc nécessaires afin d'adapter la thérapie et d'identifier des facteurs de réponse aux traitements qui pourraient améliorer la durée et la qualité de survie des patients atteints de gliome.

Ces biomarqueurs devraient permettre de mieux stratifier les patients inclus dans des essais cliniques. Des résultats d'études cliniques ont confirmé l'intérêt de la co-délétion des bras chromosomiques 1p et 19q dans la prise en charge des gliomes de grade III, incitant à adapter la prise en charge thérapeutique selon la présence ou non d'une délétion 1p19q. Des délétions 1p19q ont été identifiées dans 50 à 80% des oligodendrogliomes (Smith & Jenkins 2000). Les études récentes les plus marquantes convergent vers des modifications épigénétiques (méthylation de MGMT, phénotype hyperméthylateur des gliomes avec mutation des gènes

IDH1/IDH2, phénotype hypométhylateur des gliomes avec mutation des histones H3). Le statut méthylé ou non du promoteur du gène MGMT a un rôle pronostic très clairement établi (Hegi et al. 2005). Les analyses génomiques ont également permis l'identification de différentes voies dérégulées dans les glioblastomes (voies des récepteurs transmembranaires de facteurs de croissance ou à activité tyrosine kinase dans 90% des cas, voies RB dans 75% des cas, voies TP53 dans 90% des cas). Enfin des mutations IDH1 et 2, mutuellement exclusives, sont observées dans les différents types de gliome selon le type et le grade tumoral, avec une valeur diagnostique et pronostique importante (Yang et al. 2010). Les approches protéomiques, sur de larges cohortes, restent cependant encore rares pour ces pathologies. Les protéines identifiées jusqu'à présent sont généralement peu spécifiques des gliomes, et correspondent principalement à des protéines majoritaires, c'est-à-dire qui participent au fonctionnement de la cellule. Par ailleurs peu d'études ont évalué les corrélations avec la clinique, les données anatomopathologiques, de biologie moléculaire et d'imagerie IRM. Dans ces conditions, il apparaît intéressant de rechercher et valider de nouvelles technologies permettant d'obtenir une classification de ces tumeurs en corrélation avec les données déjà recueillies. Ainsi, la 1ère partie de mon projet de thèse porte sur l'établissement d'une classification moléculaire des gliomes basée sur des signatures moléculaires obtenues grâce à l'imagerie par spectrométrie de masse et la microprotéomique.

Les stratégies thérapeutiques actuelles se basent sur la chimiothérapie et la radiothérapie mais de nombreux phénomènes de résistance sont observés, qui sont dus aux cellules présentes dans le microenvironnement de la tumeur. D'un point de vue moléculaire, une accumulation de cellules microgliales et macrophages est retrouvée au niveau de ces tumeurs suite à la production par les cellules cancéreuses de facteurs chimioattractants comme MCP-1 ou CSF-1 (Carvalho Da Fonseca & Badie 2013). Les cellules cancéreuses produisent également des facteurs inhibiteurs de type IL-10 et TGF-β et, par conséquent, les macrophages perdent leur capacité à produire des cytokines pro-inflammatoires et sont donc incapables de réactiver la réponse immunitaire. Les macrophages pro-inflammatoires M1 et anti-inflammatoires M2 ont des rôles opposés au sein de la tumeur ; tandis que les premiers inhibent la croissance tumorale, les seconds vont la promouvoir en inhibant la réponse anti-tumorale des cellules immunitaires (lymphocytes T, B et cellules NK) (Schmid & Varner 2010). D'autre part, les macrophages sont une source de métalloprotéases matricielles (MMP) pouvant ainsi dégrader la matrice extracellulaire (Galdiero et al. 2013). Ainsi, leur sécrétion dans l'environnement de la tumeur peut aider à augmenter sa propagation en ouvrant la voie à la prolifération et la migration des

cellules tumorales. Des stratégies thérapeutiques ciblant les macrophages sont de plus en plus développées pour diminuer la proportion de macrophages présents au sein de la tumeur ou pour orienter les macrophages d'un phénotype pro-tumoral à un phénotype anti-tumoral (Noy & Pollard 2014). La réactivation des cellules, et notamment les macrophages, pour inhiber la croissance tumorale s'avère être une stratégie prometteuse. La 2nde partie de mon projet de thèse porte donc sur la possibilité de réactiver le système immunitaire au sein de la tumeur.

Les objectifs de ma thèse sont donc les suivants :

Objectif 1

Le but de la première partie de ce projet est de développer une nouvelle classification en intégrant les images IRM des tumeurs, l'analyse génétique et les marqueurs protéiques. Pour ce faire une technique impliquant l'imagerie moléculaire par spectrométrie de masse sera appliquée au niveau des tumeurs. Dans ce projet, les objectifs de ma thèse seront :

1. D'évaluer la concordance et/ou la discordance entre la classification histopronostique OMS 2007 et la classification par spectrométrie de masse des gliomes ;
2. D'évaluer la concordance et/ou la discordance entre la classification OMS 2007 (données anatomopathologiques) couplée à l'analyse moléculaire (1p19q, IDH1, IDH2, MGMT) et à l'interprétation de l'IRM (prise de contraste, nécrose, perfusion…) et la classification par spectrométrie de masse des gliomes ;
3. D'identifier par spectrométrie de masse des marqueurs moléculaires de pronostic des gliomes au sein des prélèvements tumoraux.

Le développement de la méthodologie basée sur la spectrométrie de masse est un point important du 1er objectif de ma thèse. Une classification hiérarchique entre les différents échantillons sera effectuée grâce aux données d'imagerie par spectrométrie de masse. Cette classification permettra de délimiter des régions moléculairement différentes. Les protéines de ces régions seront ensuite identifiées par spectrométrie de masse. Une première étude, afin de mettre en place la méthodologie, sera faite sur des gliomes de grade III. Puis, elle sera étendue sur une cohorte de 50 patients atteints de glioblastome de grade IV.

Objectif 2

La 2nde partie de mon projet de thèse porte sur la possibilité de réactiver le système immunitaire au sein de la tumeur en m'intéressant plus spécifiquement à une enzyme, appelée proprotéine convertase 1/3 (PC1/3). L'expression de PC1/3 est largement associée aux tissus neuroendocriniens. Cependant, des études précédentes au laboratoire ont montré que PC1/3 était aussi exprimé par les cellules immunitaires telles que les macrophages et les lymphocytes et était impliqué dans la régulation de la libération cytokinique dans des souris PC1/3 KO et dans un modèle de macrophage NR8383 PC1/3 KD.

La première partie de ce projet consiste donc à étudier l'effet de l'inhibition de PC1/3 dans les macrophages NR8383 PC1/3 KD afin de comprendre l'impact sur la sécrétion cytokinique et leur état d'activation. Pour cela des études sur les voies de signalisation des récepteurs TLR4 et TLR9 seront effectuées par western blot et analyses protéomiques des sécrétomes et des protéines intracellulaires. Dans ce contexte, j'ai étudié l'impact des facteurs sécrétés par ces macrophages sur la viabilité de cellules cancéreuses.

Ensuite, en vue d'une stratégie thérapeutique visant à réactiver les macrophages, j'ai recherché une stratégie permettant l'activation du TLR4 via un ligand non pathogénique pouvant être utilisé chez le patient. Dans ce contexte, je me suis tournée vers le taxol, qui est un agent anti-cancéreux également connu pour activer le récepteur TLR4. Ainsi il serait donc possible d'utiliser à la fois l'effet anticancéreux du taxol et son effet sur l'activation des macrophages couplé à l'inhibition de PC1/3. Une étude similaire à la précédente sera effectuée, c'est-à-dire des études protéomiques du sécrétome et des protéines intracellulaires. Des expériences de co-culture 3D permettront de déterminer l'effet du taxol et des macrophages PC1/3 KD sur la croissance et l'invasion de sphéroïdes cancéreux.

Ce travail ayant pour finalité de réaliser une étude préclinique chez les chiens car ceux-ci développent des tumeurs spontanées comme l'homme, ils semblent donc être un bon modèle pour réaliser de telles études. Dans ce contexte, des études *in vitro* sur des sphéroïdes 3D ont été initiées sur une lignée de gliome canin (J3T) en présence d'un inhibiteur de proprotéines convertases (PC1/3, PACE4, Furine, PC5/6, PC4) et activation sélective des TLR, en parallèle d'études par imagerie moléculaire et microprotéomique à partir de biopsies de gliomes de chien. Ces études ont permis de préciser la nature moléculaire du gliome chez le chien et ainsi de réaliser des analogies avec celle se développant chez l'homme.

L'ensemble des résultats ouvre une porte vers la possibilité d'une nouvelle stratégie thérapeutique que l'on nomme : la stratégie des drones macrophages ou la stratégie du cheval de Troie qui fera l'objet de la discussion et des perspectives de ce travail.

BIBLIOGRAPHIE

I. Les glioblastomes

A. Incidence

Les glioblastomes (GBM) sont les tumeurs primaires malignes du système nerveux central (SNC) les plus agressives et les plus fréquentes : elles représentent 55% des gliomes diagnostiqués aux Etats-Unis entre 2008 et 2012 (Ostrom et al. 2015) (**Figure 1**). Pour la plupart, les gliomes sont des tumeurs qui infiltrent le parenchyme sain sans délimitation nette. Quatre grades de malignité ont été décrits, depuis le gliome bénin de grade I jusqu'aux gliomes les plus agressifs de grade IV qui sont aussi appelés GBM. A cause de leur fréquence et de leur gravité, les GBM représentent un enjeu thérapeutique majeur.

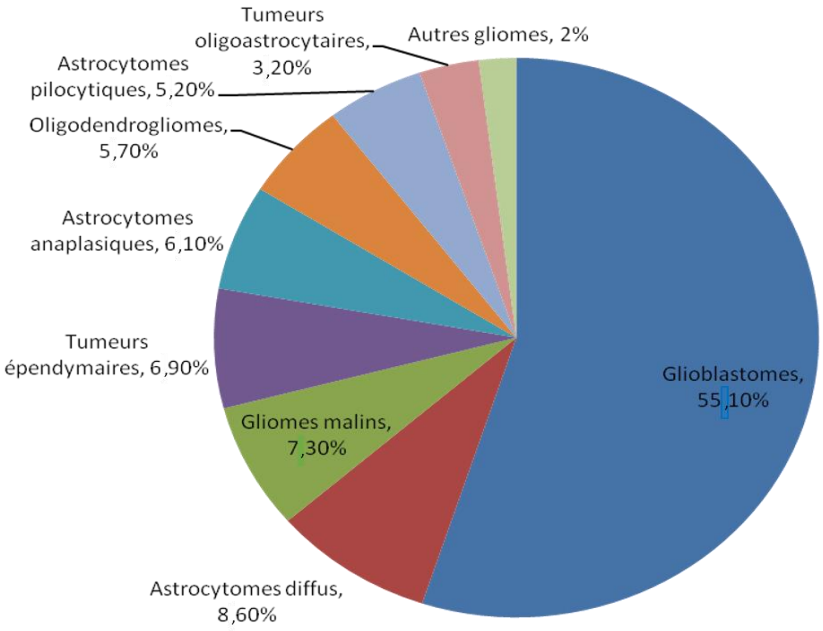

Figure 1 : Distribution de tous les types de gliomes du système nerveux central. Les glioblastomes représentent 55% des gliomes. Adaptée d'Ostrom *et al*, 2015.

L'incidence globale des tumeurs primaires du SNC est d'environ 18 cas pour 100 000 habitants par an dans les pays occidentaux. En France, l'incidence des GBM est de 4 cas pour 100 000 habitants par an (Zouaoui et al. 2012). L'incidence des GBM a augmenté d'environ

1% par an entre les années 1970 et 1990 dans la majorité des pays occidentaux (Deltour et al. 2009; Johannesen et al.; McKinley et al. 2000).

On distingue les GBM primaires des GBM secondaires (Ohgaki & Kleihues 2013). Les premiers sont les plus fréquents et sont dits *de novo* car ils ne se développent pas à partir d'un gliome de grade inférieur contrairement aux GBM secondaires. Ces derniers résultent de la transformation d'un gliome infiltrant de grade II ou III. Ils concernent en majorité les personnes plus jeunes et sont de meilleur pronostic. Les GBM primaires représentent 90% des cas, ils sont plus agressifs et ont des taux de survie plus bas.

L'âge moyen au moment du diagnostic histologique d'un GBM primaire est de 62 ans tandis que l'âge moyen des patients atteints d'un GBM secondaire est de 45 ans (Adamson et al. 2009). En l'absence de traitement, la survie des patients n'excède pas quelques mois. Avec un traitement (chirurgie, chimiothérapie et radiothérapie), la survie des patients est en moyenne de 14.6 mois (Stupp et al. 2005). La récidive survient en moyenne 7 mois après la chirurgie. Ceci peut s'expliquer par la présence de cellules tumorales à distance du foyer primaire (au moins jusqu'à 2 cm autour de la tumeur) (Hochberg & Pruitt 1980). De plus, les cellules initiatrices des gliomes ou cellules souches neurales tumorales sont des cellules dotées d'un potentiel prolifératrice infini et sont résistantes aux agents thérapeutiques (Germano et al. 2010). Une faible quantité de cellules est capable de former une tumeur.

B. Facteurs de risque et symptômes

Les facteurs de prédisposition des GBM sont peu connus. Le seul risque avéré est l'exposition aux radiations ionisantes qui sont suffisamment énergétiques pour exciter les électrons et endommager l'ADN, soit par la radiothérapie soit par la radiochirurgie (Fisher et al. 2007). Le risque de développer un GBM après une radiothérapie est environ de 2.5%. De nombreux autres facteurs ont été suggérés tels que l'exposition aux carcinogènes chimiques (caoutchouc, pétrole, pesticides…). L'exposition aux champs électromagnétiques est encore débattue. Une étude récente retrouvait une association significative entre l'utilisation intensive du téléphone portable et la survenue des gliomes (Hardell et al. 2007). Les traumatismes crâniens ont aussi été suggérés comme étant un facteur de risque possible pour le développement d'un GBM. Une étude a montré que quand les cellules gliales subissent un traumatisme, elles sont hypertrophiées et se multiplient (Magnavita et al. 2003). Des facteurs

intrinsèques sont également retrouvés tels que l'origine ethnique, le sexe, certaines maladies génétiques et des antécédents familiaux de gliome.

Les symptômes développés par les patients atteints de GBM sont variables et dépendent de la taille et de la localisation de la tumeur. Par exemple, un patient avec une tumeur au niveau du lobe temporal pourrait avoir des problèmes de vision et d'ouïe tandis qu'un patient avec une tumeur au niveau du lobe frontal pourrait présenter des troubles de la personnalité. Les symptômes les plus communs des patients atteints de GBM sont des déficits neurologiques, des maux de tête et des crises d'épilepsie (Porter 2012).

C. Diagnostic

Imagerie par Résonnance Magnétique

En cas de suspicion d'un GBM suite à l'apparition de différents symptômes, un scanner sans et avec injection de gadolinium (produit de contraste) et une imagerie par résonnance magnétique (IRM) cérébrale en plusieurs séquences (T1, T1 injectée, T2, FLAIR, diffusion, perfusion et spectroscopie) doivent être réalisés (Adamson et al. 2009). Ces examens vont permettre de localiser la tumeur et évaluer son étendue. Ils permettent également de préciser ses caractéristiques qui sont classiquement, pour un GBM, les suivantes : hyposignal T1, hypersignal T2/FLAIR, prise de contraste périphérique et hétérogène, nécrose centrale…

La biopsie

L'imagerie cérébrale permet de déterminer la présence de la tumeur mais ne permet pas de connaître son degré de malignité. Pour cela, une biopsie est réalisée au moment de la chirurgie afin de réaliser des examens histologiques et moléculaires. Si l'imagerie cérébrale révèle que la tumeur est dans une région qui est inopérable, une biopsie stéréotaxique est réalisée afin de pouvoir faire les analyses biologiques (Porter 2012).

L'observation histologique

Deux traits morphologiques sont essentiels pour établir le diagnostic des GBM : la nécrose (**Figure 2.A et B**) et la présence de proliférations endothélio-capillaires (**Figure 2.C et D**). Les GBM présentent typiquement une grande densité cellulaire (**Figure 2.E et F**) et sont composés d'une variété de types cellulaires présentant une activité mitotique importante.

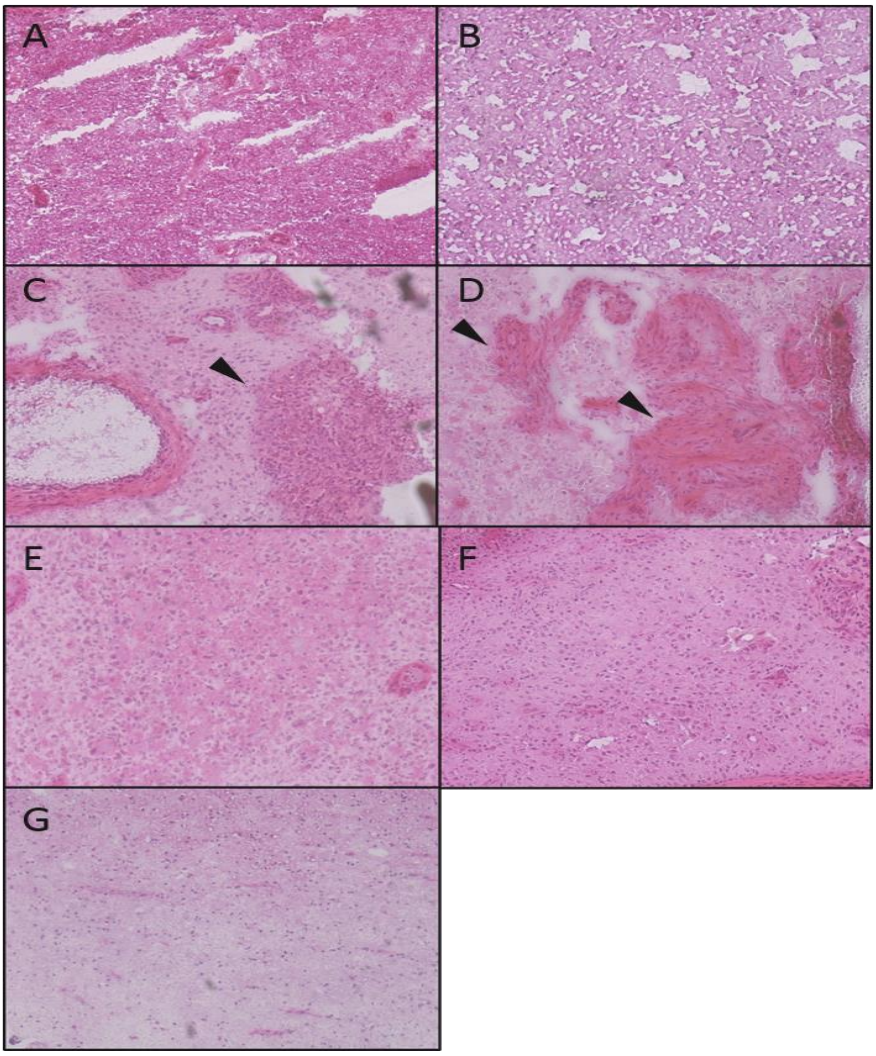

Figure 2 : Coupes histologiques après coloration hématoxyline et éosine de glioblastomes inclus dans l'étude Gliomic. Les images A et B représentent des zones de nécrose. Les images C et D représentent des proliférations endothélio-capillaires (désignées par les flèches). Les images E et F sont des zones très denses en cellules tumorales. L'image G est une zone de parenchyme très peu infiltrée en cellules tumorales.

D. Classification histologique de l'OMS de 2007

La classification de l'Organisation Mondiale de la Santé (OMS) de 2007 des gliomes représente le standard international actuel (Louis et al. 2007). Elle permet de classer les gliomes en fonction des caractéristiques cytologiques et du degré de malignité après une coloration hématoxyline et éosine. Ce système a été employé pour la première fois dans les années 1920 quand Bailey et Cushing ont classé les tumeurs gliales en comparant la similarité des cellules aux cellules gliales connues telles que les astrocytes et les oligodendrocytes. Les caractéristiques cytologiques permettent de définir des catégories de gliomes (**Tableau 1**) :

- Les astrocytomes qui sont composés d'astrocytes,
- Les oligodendrogliomes qui sont composés d'oligodendrocytes,
- Les oligoastrocytomes qui sont des tumeurs mixtes.

Tableau 1 : Classification de l'OMS de 2007 des gliomes diffus.

Type	Grade	Description	Moyenne de survie (années)
Astrocytome	II	Infiltration diffuse, augmentation de la densité cellulaire, pas de mitose	6-8
Oligodendrogliome	II	Apparait dans la matière blanche et le cortex des hémisphères cérébraux, faible activité mitotique, pas de nécrose	12
Oligoastrocytome	II	Tumeur mixte diffuse	3-10
Astrocytomes et oligodendrogliomes anaplasiques	III	Tumeur infiltrante avec une forte activité mitotique, pas de nécrose ni de prolifération vasculaire	3
Glioblastome	IV	Tumeur infiltrante avec nécrose et prolifération micro-vasculaire, taux de mitose important	1 à 2

Il existe ensuite 4 grades pour les gliomes infiltrant. Ces grades sont définis en fonction de critères histologiques et morphologiques dont l'observation d'atypies nucléaires, l'activité mitotique, la prolifération micro-vasculaire et la nécrose.

Les tumeurs de bas grade (I et II) sont bien différenciées, ont une densité cellulaire importante et certaines anomalies cellulaires. Elles possèdent des altérations génétiques particulières qui peuvent corréler avec leur degré de malignité. Les tumeurs de grade élevé (III et IV), dites anaplasiques, présentent une augmentation du nombre de vaisseaux sanguins, des atypies cellulaires, une activité mitotique élevée et une grande densité cellulaire. Les tumeurs de grade IV sont connues sous le nom de GBM. Initialement qualifiés de multiformes, les GBM constituent un groupe très hétérogène de tumeurs.

La classification de l'OMS est un moyen pratique de classer les gliomes et est le seul système accepté à l'échelle internationale. Cependant, ce système est seulement basé sur des critères visuels histologiques et entraîne des problèmes de reproductibilité inter- et intra-observateur. Elle manque de précision en raison de l'existence de plusieurs sous-types moléculaires au sein d'un même sous-type histologique. Avec cette classification, de nombreux cas ne sont pas correctement associés avec l'agressivité de la tumeur, la réponse au traitement et la survie. L'interprétation histologique n'est pas toujours possible à cause de l'hétérogénéité de ces tumeurs. Les tumeurs appartenant au même grade peuvent avoir des évolutions cliniques différentes. Une solution pour améliorer la classification des gliomes diffus est d'utiliser les informations moléculaires.

E. Classification moléculaire des glioblastomes

En plus du diagnostic histologique, un diagnostic moléculaire peut être établi en fonction du contexte génétique de chaque patient (Louis et al. 2016). Les GBM primaires et secondaires peuvent être différenciés par les caractéristiques génétiques des patients. Les biomarqueurs prennent donc une place grandissante dans le diagnostic des GBM.

Les marqueurs génétiques

Les marqueurs génétiques couramment recherchés correspondent à la mutation de gènes, à des modifications chromosomiques ou à la dérégulation épigénétique de certains gènes (Aldape et al. 2015).

❖ TP53 et rétinoblastome

La majorité des tumeurs malignes du cerveau présentent des mutations inactivant la voie TP53 et la voie du rétinoblastome (Adamson et al. 2009). Le facteur de transcription TP53 est sur-régulé en réponse aux stress cellulaires tels que l'exposition aux radiations, aux toxines… Il facilite la réparation de l'ADN en arrêtant le cycle cellulaire pour que les enzymes de réparation puissent fonctionner ou si le dommage est trop important, il induit la mort cellulaire. Les mutations du gène TP53 sont plus souvent retrouvées au niveau des GBM secondaires. Le rétinoblastome, quant-à-lui, contrôle la transition de la phase G1 à la phase S du cycle cellulaire en inhibant l'action du facteur d'élongation E2F1. Dans les GBM, le complexe CDK4/cyclin D1 phosphoryle le rétinoblastome, entraînant la libération du facteur de transcription E2F1 qui active des gènes impliqués dans la transition G1-S. Les mutations de ces deux voies sont donc critiques dans les gliomes.

❖ IDH1/2

Des mutations au niveau du codon 132 du gène IDH1, et moins couramment au niveau du codon 172 du gène IDH2, ont été identifiées dans les gliomes (Parsons et al. 2008). Ces mutations sont fréquentes dans les gliomes de grade II et III (70-90%) et les GBM secondaires (85%) mais sont rarement retrouvées chez les patients ayant un GBM primaire (5%). Les mutations des gènes IDH participent à la transformation des cellules gliales en cellules tumorales. L'enzyme IDH1 mutée entraîne un changement du profil de méthylation des cellules et une altération de la longueur des télomères. La mutation IDH1 diminue la production d'α-cétoglutarate et de NADPH facilitant ainsi la prolifération cellulaire. Les patients présentant ces mutations ont un meilleur pronostic que les patients ne présentant pas la mutation. Cette mutation est associée à une espérance de vie plus longue.

❖ EGFR

Les voies de signalisation des récepteurs à tyrosine kinase (dont EGFR) sont suractivées dans les GBM (Wong et al. 1987). La surexpression d'EGFR est plus souvent retrouvée dans les GBM primaires (40-60%) par rapport aux GBM secondaires (moins de 10%). L'activation d'EGFR provoque la phosphorylation de PIP2 en PIP3 par l'intermédiaire de la kinase PI3K. Ceci permet l'activation de molécules effectrices comme Akt et mTOR déclenchant ainsi la prolifération cellulaire et le blocage de l'apoptose. Ce récepteur est aussi responsable de la résistance à la chimiothérapie. Une relation entre l'âge et l'amplification d'EGFR a été démontrée récemment. Elle serait un facteur de bon pronostic pour les patients de plus de 60 ans et de mauvais pronostic pour les patients plus jeunes.

❖ PTEN

Des mutations du gène PTEN sur le chromosome 10q23 sont fréquentes dans les GBM primaires (Baeza et al. 2003). PTEN contient un centre catalytique qui régule négativement PI3K en déphosphorylant PIP3 et PIP2. Dans le cas de la mutation PTEN, les taux élevés de PIP3 sont utilisés par PI3K pour hyper-phosphoryler le complexe PKB/Akt. Ceci module l'activité de protéines jouant un rôle critique dans la survie cellulaire, l'invasion et la prolifération.

❖ Méthylation de MGMT

Des niveaux élevés de l'enzyme réparatrice de l'ADN MGMT sont caractéristiques des GBM (Aldape et al. 2015). Le gène MGMT code pour une enzyme clé dans les mécanismes de réparation des lésions de l'ADN. La protéine MGMT répare les lésions causées par les agents alkylants dans les cellules tumorales, favorise la survie des cellules tumorales et confère à la tumeur une chimiorésistance. Le gène MGMT a un promoteur qui contient des îlots CpG et la méthylation des îlots CpG empêche la transcription du gène et rend la tumeur chimiosensible. La méthylation du promoteur du gène MGMT a été identifiée dans 36% des cas de gliome. La présence de la mutation améliore l'effet de la chimiothérapie et augmente l'espérance de vie des patients.

❖ ATRX

Des mutations du gène ATRX sont récurrentes chez les patients ayant un GBM secondaire (Aldape et al. 2015). ATRX est une protéine intervenant dans le remodelage de la

chromatine. Elle joue un rôle clé dans le maintien de l'hétérochromatine, particulièrement au niveau des télomères. La mutation du gène ATRX entraîne la production d'une protéine tronquée et est responsable de l'instabilité génomique et une élongation anormale des télomères.

❖ **Perte et gain des chromosomes 7 et 10**

Le gain du chromosome 7 et la perte du chromosome 10 représentent la signature des GBM *de novo* (Aldape et al. 2015). Ces modifications chromosomiques peuvent être également des marqueurs de mauvais pronostic puisque les patients porteurs d'un GBM présentant ces anormalités génomiques ont une survie plus courte.

❖ **Co-délétion 1p/19q**

Avec la classification actuelle, il est difficile de déterminer si les gliomes sont des astrocytomes, des oligodendrogliomes ou des tumeurs mixtes. La délétion des bras chromosomiques 1p et 19q est retrouvée dans 70% des oligodendrogliomes. Les oligodendrogliomes ayant la co-délétion 1p/19q sont sensibles à la chimiothérapie et la radiothérapie. C'est également un marqueur de bon pronostic pour les gliomes de bas grade (Aldape et al. 2015). Des résultats récents d'études cliniques (EORTC 26951, RTOG 9402) ont confirmé l'intérêt de la co-délétion 1p19q dans la prise en charge des gliomes de grade III, incitant à adapter la prise en charge thérapeutique selon la présence ou non d'une délétion 1p19q (Cairncross et al. 2013; van den Bent et al. 2013).

L'ensemble de ces biomarqueurs devrait permettre de mieux stratifier les patients atteints de gliomes inclus dans des essais cliniques. Dans ce contexte, une nouvelle classification des gliomes prenant en compte ces marqueurs moléculaires a émergé en 2016 (Louis et al. 2016b).

Les sous-groupes de GBM primaires

«The Cancer Genome Atlas » (TCGA) a pour la première fois séquencé les GBM en 2008 (Verhaak et al. 2010). Les études ont porté sur l'ADN, les ARNm, les microARN et les profils épigénétiques afin d'identifier de nouveaux sous-types de gliomes ayant des issues cliniques différentes. Ces études ont pu mettre en évidence une hétérogénéité au sein même des GBM primaires. Quatre sous-groupes de GBM primaires ont pu être distingués : classique,

neural, proneural et mésenchymal. Ces sous-classes ont des signatures génétiques différentes et sont caractérisées par des altérations moléculaires et par l'activation de voies de signalisation différentes. Le sous-type classique est caractérisé par une amplification d'EGFR. Le sous-type mésenchymal présente des mutations du gène *NF1* et une surexpression de marqueurs mésenchymateux tels que la chitinase 3 like-1 et le proto oncogène met. Le sous-type proneural est caractérisé par l'altération de PDGFRA, des mutations du gène *IDH1* et de gènes impliqués dans le développement neural tels que *NCAM1*. Enfin, le sous-type neural présente une expression de marqueurs neuronaux tels que la synaptotagmin-1.

Cette hétérogénéité peut aussi s'étendre de façon intratumorale, c'est-à-dire que plusieurs sous-types peuvent être retrouvés chez un même patient. Cela rend l'analyse histologique insuffisante pour le diagnostic des GBM. La caractérisation moléculaire des tumeurs est de plus en plus nécessaire afin d'individualiser la thérapie pour chaque patient en fonction de son profil génétique et protéomique.

Les biomarqueurs protéiques

Les biomarqueurs peuvent être des indicateurs diagnostiques, pronostiques ou thérapeutiques des maladies. Cependant, étant donné l'hétérogénéité tumorale, un marqueur unique n'est pas suffisant pour discriminer des sous-types tumoraux. Les études actuelles développent donc des panels de biomarqueurs qui ne soient pas uniquement génétiques. De plus, les traitements administrés actuellement aux patients atteints d'un GBM primaire ou d'un GBM secondaire sont identiques alors que leurs profils moléculaires sont clairement différents. Des distinctions moléculaires au sein de tumeurs d'un même grade sont donc nécessaires. Les profils protéiques et leurs modifications post-traductionnelles sont tout aussi importants pour définir des sous-types tumoraux.

De nombreuses études protéomiques ont porté sur l'étude des fluides biologiques, obtenus chez des patients atteints de GBM, tels que le plasma/sérum (Jung et al. 2007; Gollapalli et al. 2012; Nijaguna et al. 2015; Gautam et al. 2012) et le liquide céphalo-rachidien (LCR) (Shen et al. 2014; Ohnishi et al. 2009; Schuhmann et al. 2010). L'obtention de ces fluides est non invasive contrairement à l'analyse du tissu tumoral, mais ne permet d'avoir des informations que sur les protéines sécrétées par les cellules cancéreuses ou présentes dans les exosomes. Ces études ont permis de définir plusieurs candidats biomarqueurs tels que des

protéines impliquées dans les réactions inflammatoires et les processus cancéreux (**Tableau 2**). Les protéines FTL, S100A9 et CNDP1 ont montré des modulations d'expression reproductibles dans le sérum de 10 patients atteints de GBM (Gautam et al. 2012). Plusieurs limites ont été associées à l'utilisation du sérum/plasma telles qu'une faible concentration en biomarqueurs comparée aux protéines majoritaires et la présence de la barrière hémato-encéphalique. Pour contrer ces différentes limites, le LCR est de plus en plus étudié. L'avantage est lié au fait que les altérations du contenu protéique du LCR correspondent aux changements se déroulant durant un processus pathologique dans le cerveau. Une étude menée sur le LCR de patients atteints d'astrocytomes de différents grades, a montré que l'expression de la protéine gelsoline diminuait dans les grades élevés (III et IV) (Ohnishi et al. 2009).

Tableau 2 : Fonctions biologiques des principaux biomarqueurs identifiés dans le plasma/sérum et le LCR des patients atteints de GBM.

Fonctions biologiques	Candidats biomarqueurs
Angiogénèse	VEGF
Fonctions immunitaires	CXCL10, IL2, IL2RA, ASGH, APRIL
Composants de la matrice extracellulaire	TIMP1, YKL40, CNDP1, SERPINE1, CTSD, MMP9
Homéostasie calcique	RCVRN, S100A9, S100B, L-CAD
Cytosquelette	FLNA
Migration et invasion	HBA2, NCAM, OPN
Régulateur de croissance	GSN, GFAP, EGFR

L'analyse directe du tissu tumoral représente une approche complémentaire afin de lier la nature de la tumeur et ce qu'elle produit. Plusieurs études protéomiques ont été réalisées sur des biopsies de patients, sur des lignées cellulaires de gliome ou sur des modèles animaux (Vogel et al. 2005; Jiang et al. 2006; Melchior et al. 2009; Niclou et al. 2010). Plusieurs études protéomiques, à partir de biopsies de patients ont également fourni des informations importantes sur la pathophysiologie des GBM. Une étude, réalisée sur 85 tumeurs de différents grades, a permis d'identifier 37 protéines différentiellement exprimées. Parmi elles, de

nombreuses protéines, dont l'expression est augmentée dans les gliomes de haut grade, ont un rôle dans la transduction du signal comme les petites protéines G (Iwadate 2004). Cependant, les techniques utilisées, dites « in-gel », ne permettent d'obtenir des informations que sur les protéines très abondantes.

De plus, la plupart des études menées actuellement ne permettent pas de différencier des sous-régions tumorales au sein du même patient car une analyse globale de la totalité des protéines du tissu est réalisée. C'est dans ce contexte que nous avons donc orienté nos travaux i.e. la prise en compte de l'hétérogénéité tumorale et l'intégration des données cliniques afin d'associer les réseaux physiopathologiques de protéines aux données génétiques (Voir Chapitre II, article 1). Le but étant d'améliorer la classification moléculaire en vue d'un traitement personnalisé.

F. Traitements

Traitement standard

Le traitement standard pour les patients ayant un GBM inclut la résection chirurgicale de la tumeur, la chimiothérapie et la radiothérapie (Adamson et al. 2009). La résection chirurgicale est réalisée dans le but de retirer complètement la tumeur. Dans la plupart des cas une résection complète est impossible due à la localisation de la tumeur et son aspect diffus. Une résection partielle peut être réalisée. Cependant, les taux de survie dans le cas d'une résection partielle sont beaucoup plus bas. Une récidive est souvent observée à partir des cellules tumorales invasives qui n'ont pas été retirées lors de la chirurgie. A défaut d'être curative, la chirurgie permet de réduire les symptômes tels que l'hypertension crânienne améliorant ainsi la qualité de vie des patients.

La radiothérapie commence moins de 6 semaines après la chirurgie. Elle est administrée en combinaison avec la chimiothérapie. La moyenne de survie des patients recevant ce traitement est augmentée de 12,1 à 14,6 mois comparée à la moyenne de survie des patients recevant la radiothérapie seule (Stupp et al. 2005). La moyenne de survie à 2 ans augmente de 10,4% chez les patients recevant la radiothérapie seule à 26,5% chez les patients recevant la combinaison des deux.

La chimiothérapie standard utilisée est le témozolomide. Le témozolomide est un agent alkylant qui inhibe les mécanismes de réparation de l'ADN dans les cellules tumorales. Il provoque une alkylation de la guanine en position O6 et N7 de l'ADN. Cet adduit entraîne un appariement aberrant des bases lors de la réplication de l'ADN, menant à une cassure du brin d'ADN puis une mort cellulaire par apoptose. L'enzyme MGMT permet de réparer les lésions de l'ADN en enlevant le groupement alkyl en position O6 de la guanine. Elle a été associée à la résistance au témozolomide (Hegi et al. 2004).

Traitements futurs

Bien que les GBM soient traités agressivement avec à la fois la chimiothérapie et la radiothérapie, les tumeurs sont souvent résistantes à la thérapie standard et le pronostic des patients est très faible. Les chercheurs développent de nouvelles thérapies dans le but d'améliorer la survie des patients. L'objectif de nombreuses thérapies est de cibler les molécules spécifiques impliquées dans la tumorigenèse (Porter 2012).

Certaines thérapies utilisent des inhibiteurs des molécules VEGF (Miletic et al. 2009), EGFR (Padfield et al. 2015), PDGF (Schäfer et al. 2016) et intégrines (Anderson & Galileo 2016). Ces thérapies ont été développées grâce à une meilleure compréhension des mécanismes moléculaires des GBM et inhibent des molécules spécifiques qui sont dérégulées dans les GBM.

Un autre traitement expérimental développé est l'utilisation des interférons. Ce sont des régulateurs immunitaires qui induisent une activité cytotoxique en altérant l'expression de gènes impliqués dans la prolifération cellulaire et l'apoptose. L'utilisation des interférons permet d'améliorer l'efficacité du témozolomide (Motomura et al. 2011).

Une autre thérapie intéressante est la thérapie génique dans laquelle des virus sont utilisés pour bloquer ou détruire l'expression de gènes spécifiques dans les cellules tumorales. Les thérapies géniques sont souvent administrées pour générer une réponse immunitaire, afin de remplacer un gène perdu ou d'augmenter la sensibilité de la tumeur aux agents thérapeutiques. Des études ont montré que la thérapie génique impliquant l'utilisation du virus de l'herpès (HSV-1 TK) est favorable dans le traitement des gliomes (Klatzmann et al. 1998).

Des essais cliniques d'un vaccin développé spécifiquement pour la mutation d'EGFRvIII ont apporté un espoir pour les patients atteints de GBM (Choi et al. 2009). Ce

vaccin induit des réponses immunitaires humorales spécifiques pour les cellules exprimant EGFRvIII. Les tumeurs ont été analysées et aucune cellule exprimant EGFRvIII n'a été retrouvée.

Immunothérapies

La découverte qu'une réaction immunitaire pouvait être déclenchée dans le système nerveux central a permis d'ouvrir de nouvelles voies pour le développement de traitements des GBM (Chow et al. 2015). Les GBM altèrent le profil immunologique de l'environnement normal du SNC. Les cellules tumorales vont détourner le phénotype des macrophages et cellules microgliales pour inhiber les réponses cytotoxiques des lymphocytes T et ainsi pouvoir se multiplier. Les thérapies développées ciblent des molécules impliquées dans l'activation ou l'inhibition des réponses cytotoxiques des cellules T telles que le couple inhibiteur PD1/PDL1 (Zeng et al. 2013). D'autres stratégies visent à réactiver les macrophages afin qu'ils puissent à nouveau attaquer la tumeur et réactiver les lymphocytes T. C'est cette voie thérapeutique, c'est-à-dire la réactivation des macrophages, que nous avons choisi (Voir Chapitres II et III, Publications 2-5).

II. Utilisation de la spectrométrie de masse pour la caractérisation des tumeurs

Les études récentes les plus marquantes convergent vers des modifications épigénétiques (méthylation de MGMT, phénotype hyperméthylateur des gliomes avec mutation des gènes *IDH1/IDH2*, phénotype hypométhylateur des gliomes avec mutation des histones H3). Une voie alternative à la génétique classique pour la détermination des biomarqueurs moléculaires est la spectrométrie de masse et en particulier, la protéomique tissulaire couplée à l'imagerie moléculaire par spectrométrie de masse.

A. Les différentes techniques utilisées actuellement

La protéomique est une technologique à haut débit générant une grande quantité de données sous la forme de listes de protéines qui sont différentiellement exprimées, reflétant une cause ou une conséquence des processus tumoraux.

La protéomique est de plus en plus utilisée pour comprendre les mécanismes impliqués dans la progression tumorale. Différentes approches ont été menées. Les stratégies les plus employées sont les méthodes shotgun et les méthodes de protéomique ciblées. Les spectromètres de masse à source d'ionisation électrospray (ESI) couplées à des méthodes de séparation comme la chromatographie liquide (LC-MS/MS) est très souvent la méthode de choix. L'approche shotgun repose sur l'identification et la quantification de peptides de digestion provenant d'un mélange complexe de protéines. Les protéines intactes peuvent être séparées par gel SDS-PAGE. Après leur séparation, chaque piste du gel est coupée en plusieurs bandes et ces bandes sont digérées avec une protéase avant l'analyse en LC-MS/MS.

Les techniques de gels 2D permettent de séparer les protéines d'un échantillon complexe en fonction de leur masse moléculaire et de leur point isoélectrique. Cette approche a été souvent utilisée pour analyser les cellules cancéreuses. Elle est habituellement couplée à l'analyse des spots d'intérêt par digestion enzymatique, suivie par l'identification par spectrométrie de masse. Ces techniques basées sur les gels ont l'avantage de fournir une analyse détaillée des modifications post-traductionnelles. Cependant, les protéines peu représentées peuvent être masquées ou non détectées car elles co-migrent souvent avec d'autres protéines

dans le même spot et les protéines de grande masse moléculaire, de grand point isoélectrique ou ayant des propriétés hydrophobes ne sont souvent pas détectées.

D'autres techniques peuvent également être utilisées telles que les puces à protéines qui permettent de mesurer l'expression de centaines de protéines et de détecter des biomarqueurs protéiques qui sont liés au développement et/ou la progression de la tumeur. Les approches de protéomiques ciblées SRM (single reaction monitoring) ont été développées pour détecter des protéines connues dans des tissus cancéreux (Addona et al. 2009).

Toutes ces techniques permettent d'identifier un grand nombre de protéines mais ne permettent pas de corréler les protéines identifiées à leur localisation dans le tissu. Pour contrer ce problème, le couplage de méthodes de protéomique et d'imagerie MALDI a permis d'identifier des candidats biomarqueurs pour différents types de cancer. Cette stratégie produit des données plus proches de la réalité clinique car elle prend en compte l'environnement de la tumeur. Elle permet de déterminer l'expression de protéines au niveau de régions de tissu intactes sans étape de lyse qui est généralement effectuée lors des approches de protéomique classique.

B. L'imagerie par spectrométrie de masse MALDI-MSI

Principe

Le but de l'imagerie MALDI-MSI est de créer des images moléculaires représentant la distribution d'un certain nombre de biomolécules contenues dans un échantillon. Cela permet ainsi de déterminer la complexité moléculaire de tissus biologiques par la distribution spatiale de molécules à la fois dans des tissus sains et pathologiques (Franck et al. 2009; Angel & Caprioli 2013).

La spectrométrie de masse (MS) permet l'analyse de molécules basée sur leur rapport masse sur charge (m/z). Un spectromètre de masse est constitué d'une source d'ionisation, d'un analyseur de masse et d'un détecteur. L'analyse de tissu directe est possible grâce aux sources MALDI. L'analyse MALDI des coupes de tissus permet d'acquérir des profils d'expression tout en maintenant l'intégrité cellulaire et moléculaire. L'imagerie MALDI fournit une grande spécificité moléculaire par le fait que les molécules sont ablatées, ionisées et détectées

directement à partir du tissu. Plusieurs centaines de molécules du tissu peuvent être imagées en même temps.

Stratégie expérimentale

Les résultats obtenus de l'imagerie MSI sont dépendants d'un certain nombre de paramètres tels que la collection des échantillons et leur préparation, l'instrumentation et l'analyse des données (**Figure 3**). L'expérience commence avec le choix des molécules à analyser. Ces dernières peuvent être des métabolites issus d'un médicament, des lipides, des peptides ou des protéines.

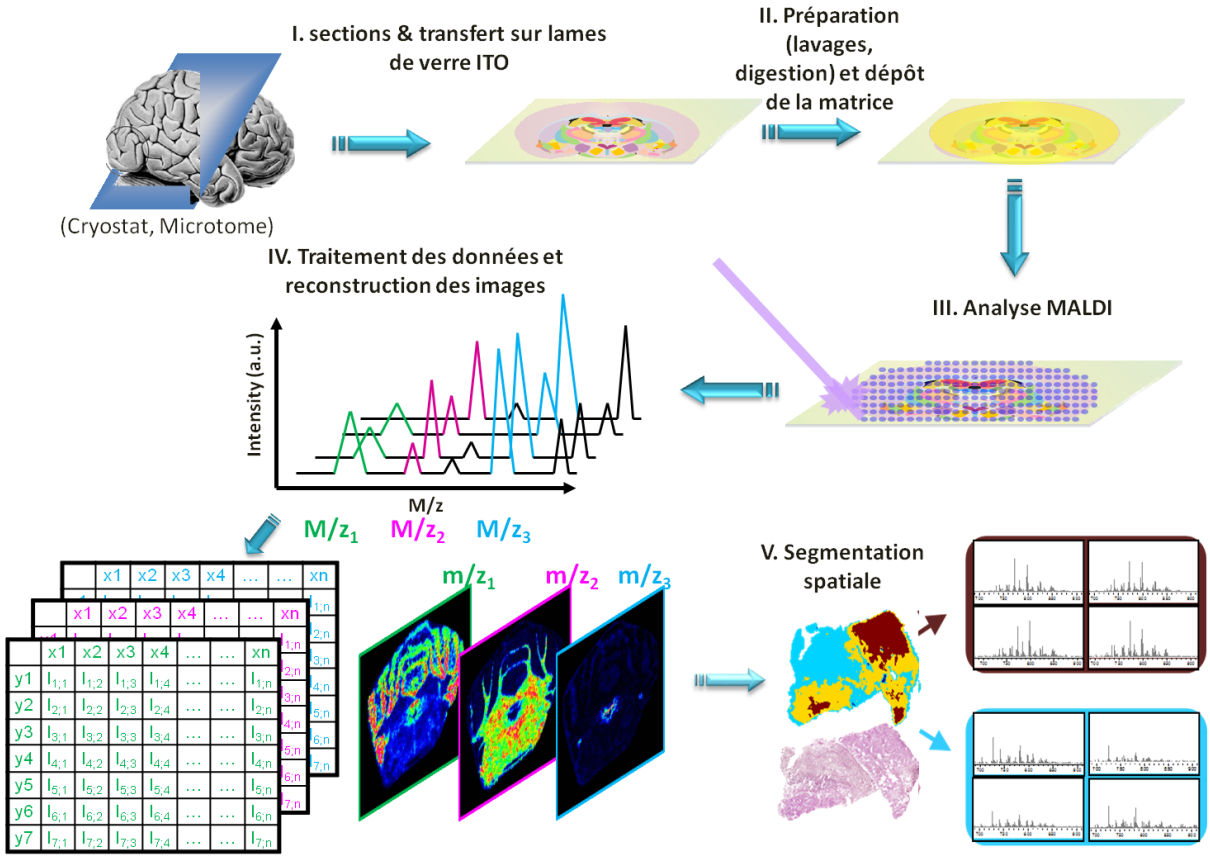

Figure 3 : Stratégie expérimentale de l'imagerie MALDI. Après avoir réalisé des coupes de tissu et les avoir transférées sur des lames conductrices, la matrice est déposée. Les spectres de masse sont enregistrés pour chaque point du tissu. Les spectres de masse enregistrés avec leurs coordonnées sur le tissu sont traités et les images moléculaires peuvent être générées et représentent la localisation des molécules sur le tissu. (Adaptée de Franck et *al*, Molecular and Cellular Proteomics, 2009).

Les échantillons doivent être conservés dans de bonnes conditions afin d'éviter de modifier la morphologie des tissus. Les tissus frais et congelés permettent l'analyse de toutes les molécules par imagerie MSI contrairement aux tissus fixés et enrobés dans la paraffine (FFPE) qui ne permettent l'analyse que des peptides obtenus après digestion trypsique. Les tissus frais et congelés sont coupés avec un cryostat à une épaisseur pouvant aller de 7 à 12 µm. Sur certains instruments (MALDI-TOF) les tissus doivent être déposés sur des lames histologiques particulières conductrices (lames Oxyde Idium Etain (ITO) pour éviter l'accumulation de charges lors de l'analyse, une tension de 20kV étant appliquée sur le porte échantillon.

La source de production d'ions de type MALDI requière l'utilisation d'un composé organique, nommé matrice (Karas & Krüger 2003). Les matrices sont des molécules organiques acides de faible poids moléculaire qui absorbent l'énergie du laser et qui, ajoutées en large excès, permettent d'assurer la désorption/ionisation des analytes. La matrice doit être co-cristallisée avec les composés à analyser. Lors d'une analyse MALDI conventionnelle cette étape est réalisée en mélangeant la solution matrice avec l'échantillon à analyser. Pour le mode imagerie, la solution de matrice est déposée sur la surface du tissu. Pour éviter une délocalisation des composés à étudier au sein de la section de tissu et afin de pouvoir réaliser des images avec une plus grande résolution spatiale, le dépôt de la matrice est le plus souvent réalisé par des techniques de nébulisation. Afin de garantir une grande reproductibilité des dépôts, ces micro-nébulisations sont réalisées à l'aide de robots permettant de contrôler certains paramètres tels que le débit, la taille des gouttes et l'épaisseur du dépôt. Le choix de la matrice dépendra de la nature des molécules à analyser. Pour les peptides, des signaux intenses sont obtenus avec l'α-cyano-4-hydroxy-cinnamic acid (HCCA). Pour les lipides, la matrice 2,5-dihydroxybenzoic acid (DHB), la 9-aminoacridine ou encore les acides cinnamiques sont privilégiés.

Après la préparation des échantillons, les images sont acquises en mode point par point suite au déplacement du porte échantillon sous le faisceau laser. Un spectre de masse représentant les peptides/protéines ou lipides présents à chaque point est enregistré. La résolution spatiale des images est déterminée par la distance entre deux points d'analyse. Une plus grande résolution spatiale permet une observation plus fine des sous-structures anatomiques précises. En général, la résolution spatiale pour une coupe entière de tissu se situe entre 50 et 100 µm.

L'acquisition est suivie par un processus de traitement de données. Ce traitement est essentiel pour assurer ensuite une analyse des données et une interprétation des résultats d'imagerie. Les spectres MS bruts individuels sont d'abord lissés et le bruit de fond est soustrait. Une étape de réalignement des spectres est également réalisée afin de corriger les variations de m/z des pics liées à la position du porte échantillon dans l'instrument ainsi que les variations de rugosité de la surface étudiée. Par la suite, une étape de normalisation est effectuée pour corriger les variations d'intensité du courant ionique total d'un point à un autre. Ce processus n'affecte pas les intensités relatives qui, bien que les intensités absolues globales puissent varier, restent similaires. La normalisation permet donc de diminuer les variations inter-spectres au cours de la même acquisition. Les données traitées sont, par la suite, utilisées pour reconstruire des cartes de densité ionique 2D de la distribution des composés au sein des tissus. Pour un signal particulier, correspondant à un composé spécifique, la variation des intensités mesurées pour chaque spectre enregistré avec ses coordonnées d'acquisition, est reportée sur une échelle de couleur. Différentes représentations peuvent être utilisées, comme la visualisation de chaque composé individuellement, ou de 2-3 composés, sur une même image. Sur les données retraitées, il est également possible d'utiliser des outils bioinformatiques, afin de faciliter l'interprétation des données, ou d'extraire une information à partir d'un profil moléculaire complexe global (Jones et al. 2012). Ainsi l'utilisation d'algorithme d'analyse statistiques permet d'extraire les m/z des signaux spécifiques à des régions particulières (appelées Région d'intérêt ou ROI) ou encore de déterminer des ressemblances dans les profils spectraux pour délimiter des régions de tissus correspondant à des phénotypes moléculaires semblables ou différents. Cette analyse dite de Hierachical Clustering ou segmentation, offre l'accès à une information non visualisable sur les images brutes comme nous le verrons dans la suite de ce manuscrit.

Applications de l'imagerie MALDI en oncologie

Grâce à l'imagerie MALDI, plusieurs biomarqueurs ont été identifiés dans différents cancers. Pour les grades III et IV du cancer de l'ovaire, un biomarqueur ayant un ratio m/z de 9744 et correspondant à un fragment de la sous-unité régulatrice du protéasome 11S (REG-α) a été mis en évidence (**Figure 4**) (Lemaire et al. 2007). Ce marqueur permet de discriminer la transition des cellules d'un état bénin à un état malin, permettant ainsi un diagnostic précoce.

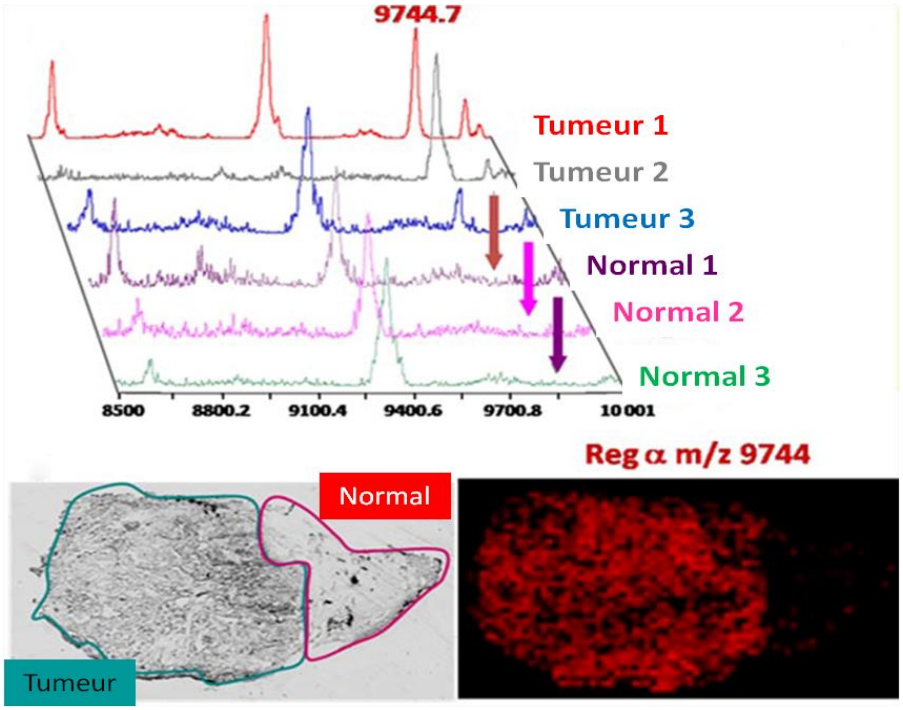

Figure 4 : Identification de REG-α comme biomarqueur du cancer de l'ovaire. Profils MALDI de trois échantillons de cancer de l'ovaire versus trois échantillons sains et image moléculaire du fragment de REG-α (m/z 9744) a une résolution de 50 µm d'une section de tissu de cancer de l'ovaire. (Adaptée de Franck et *al*. Molecular and Cellular Proteomics, 2009).

L'imagerie MALDI permet également de déterminer les marges de la tumeur. Les tissus adjacents à la tumeur qui paraissent histologiquement sains peuvent montrer des signatures moléculaires caractéristiques du tissu tumoral. Une étude sur la détermination des marges d'une tumeur du rein a été faite par Oppenheimer et al. 2010. Les auteurs ont démontré que des cellules sans caractéristiques phénotypiques de cellules tumorales présentent des signatures moléculaires typiques de la tumeur. Les spectres de masse ont été comparés entre 4 régions différentes : la tumeur, la marge tumorale, la marge saine et le tissu sain. Des profils caractéristiques de la tumeur ont été retrouvés dans la marge saine du tissu. Des protéines impliquées dans le système mitochondrial de transport des électrons sont sous-exprimées dans la tumeur et également dans la marge saine annotée histologiquement.

Enfin, l'imagerie MALDI peut être utilisée pour identifier des signatures moléculaires qui corrèlent avec la progression de la tumeur et par conséquent avec la survie des patients. Dans ce cas, les données obtenues de l'imagerie MALDI ont une valeur pronostique. Par exemple, une étude de Balluff et al. 2011 a mis en évidence des profils protéiques permettant de prédire la survie des patients atteints de cancers gastro-intestinaux. Des protéines

biomarqueurs ont été identifiées telles que HNP-1, CRIP1 et S100-A6. Une forte expression de ces protéines est associée à des taux de survie plus courts.

L'imagerie MALDI permet de déterminer la localisation de molécules au sein du tissu et ainsi des signatures moléculaires en fonction des régions. L'identification de ces molécules, et par exemple des protéines, est possible par spectrométrie de masse en réalisant des microextractions dans ces régions d'intérêt.

C. Microprotéomique tissulaire et corrélation avec l'imagerie MALDI

L'imagerie MALDI permet de mettre en évidence des marqueurs de phénotype cellulaire particuliers associés à un mécanisme physiopathologique mais ne donne pas accès directement à l'identification de ces marqueurs. L'identification peut être réalisée *in-situ* sur les tissus par des expériences de MS2 au moment de l'acquisition des images, c'est-à-dire que les ions sont fragmentés pour permettre leur identification. Ces stratégies restent assez difficiles pour l'identification des protéines, qui peuvent être obtenues sur la fragmentation des peptides issus de la digestion enzymatique in-situ (digestion trypsique le plus couramment). Cependant, le nombre de protéines identifiées par ces stratégies est limité à quelques dizaines de protéines parmi les plus abondantes localement sur le tissu ; et ce, bien que plusieurs centaines de peptides (en moyenne 500) de digestion soient observables dans les spectres. En effet, la grande majorité des peptides ont une intensité de signal trop faible et conduisent à des spectres MS/MS présentant un nombre insuffisant de fragments pour permettre une identification fiable de la protéine dont ils sont issus par interrogation des banques de données. Bien que la fragmentation des composés de plus faible poids moléculaire (Mw<1000 u.), tels que les lipides et les métabolites, soit plus facile compte-tenu de la taille de ces composés et des méthodes d'activation et de fragmentations utilisées ; le nombre de composés identifiés directement à partir des tissus reste limité, cela étant lié au trop grand nombre d'espèces présentes en mélange localement qui contribuent à l'existence de phénomènes de suppression d'ions. Ainsi, afin de pouvoir remonter à des identifications à grande échelle des composés (et en particulier des protéines) dans des ROI mises en évidence dans les expériences d'imagerie et permettre une meilleure compréhension des processus physiopathologiques et du microenvironnement tumoral, de nouvelles stratégies ont été développées ces dernières années au laboratoire. Ces stratégies, appelées micro-protéomique, permettent de réaliser l'identification à grande échelle des protéines à partir d'un micro-environnement à une échelle d'environ 500 µm. Le principe

est de réaliser des microdigestions sur des régions sélectionnées du tissu. Après la microdigestion, la région d'intérêt est soumise à une extraction des peptides par microjonction liquide (Quanico et al. 2013; Wisztorski et al. 2016). Grâce à des solvants appropriés, les peptides de digestion ou les protéines entières sont extraits du tissu pour ensuite être analysés par LC-MS/MS en vue de leur identification.

Cette technique a déjà été utilisée avec succès sur des tumeurs de l'ovaire par (Wisztorski et al. 2013). Les auteurs ont démontré que plusieurs protéines identifiées dans la région tumorale étaient impliquées dans la voie p53 et des protéines connues pour être surexprimées dans ce type de cancer ont été retrouvées, prouvant la fiabilité de cette technique. L'enjeu à l'heure actuelle est donc la mise en corrélation des données cliniques aux données d'imagerie MALDI et de protéomique afin d'améliorer le diagnostic, le pronostic et *in fine*, d'adapter le traitement. L'intégration globale des données nécessite le développent de nouveaux algorithmes permettant d'uniformiser les données de OMICS. Cependant pour préciser le diagnostic, il sera nécessaire d'y intégrer les données sur le microenvironnement tumoral. En effet, l'hétérogénéité tumorale est un élément clé dans la résistance et la rechute aux traitements.

III. Le microenvironnement tumoral : les macrophages associés aux tumeurs

A. Généralités

La communication entre les cellules et leur microenvironnement est essentielle à la fois pour l'homéostasie des tissus sains et pour la croissance tumorale. Les tumeurs se développent dans un microenvironnement dynamique. Celui-ci étant composé de différents types cellulaires tels que les cellules stromales, les cellules endothéliales et les cellules immunitaires. Ces cellules interagissent entre elles et avec les cellules tumorales. Ce microenvironnement complexe régule la croissance de la tumeur et la formation de métastases. Le microenvironnement tumoral ne cesse de changer au cours de la progression de la maladie, ce qui permet d'affirmer qu'il possède un rôle clé dans les processus tumoraux (Quail & Joyce 2013).

Le lien entre l'inflammation chronique et la tumorigenèse a été proposé pour la première fois par Rudolf Virchow en 1863 après qu'il ait observé des leucocytes infiltrant les tumeurs (Balkwill & Mantovani 2001). Par la suite, de nombreuses études ont démontré que l'inflammation influençait fortement l'initiation et l'invasion tumorale. En effet, les tissus présentant une inflammation chronique ont également un fort risque de développer une tumeur (Sangiovanni et al. 2004). Nous pouvons citer, par exemple, le cancer du foie qui est une des causes les plus importantes de décès des patients atteints de cirrhose. L'inflammation chronique, due à la cirrhose, permet à la tumeur de se développer suite à la production de TNF-α et de ROS (Reactive Oxygen Species). L'exposition au TNF-α active la voie NF-κB et induit alors l'expression de gènes qui inhibent l'apoptose et permettent la survie cellulaire. De plus, l'inflammation facilite la progression de la tumeur en supprimant l'immunité adaptative et les fonctions des cellules T. Au contraire, les réponses immunitaires altérées peuvent également être corrélées avec une forte incidence de développer un cancer. Chez les personnes immunodéprimées (par exemple en cas de greffe d'organe ou de SIDA), la probabilité de développer une tumeur est plus élevée que chez des personnes saines (Gallagher et al. 2001; Stewart et al. 1995).

Il apparait donc clair que la tumorigenèse est modulée par des réponses immunitaires aberrantes et une homéostasie altérée. En cas de cancer, les interactions intercellulaires qui sont

présentes dans les tissus normaux sont rompues. La tumeur a la capacité de contourner ces évènements cellulaires et, à terme, le microenvironnement s'accommode à la tumeur.

B. Les macrophages associés aux tumeurs (TAM)

Généralités

Les macrophages sont retrouvés dans tous les tissus où ils jouent divers rôles anatomiques et fonctionnels. Ils ont des rôles dans le développement, la réparation et l'homéostasie des tissus et les réponses immunitaires. Ce sont des cellules qui répondent aux changements physiologiques. Durant ces adaptations, les macrophages peuvent aussi être recrutés à partir des réservoirs monocytiques du sang, de la rate et de la moelle osseuse (Cortez-Retamozo et al. 2012). Dans les tissus normaux, une blessure ou une infection par un pathogène entraîne l'expression locale d'une grande variété de facteurs de croissance tels que les facteurs CSF-1, GM-CSF, MSP, TGF-β1 et les chémokines CCL2, CCL7, CCL8, CCL3 ou CCL4 (Nathan 2002). Ces facteurs permettent de recruter des monocytes circulants et de les différencier en macrophages. Les macrophages vont alors déclencher les réponses immunitaires, tuer les pathogènes, stimuler l'angiogenèse et réparer les tissus lésés. Cependant, très souvent ces fonctions réparatrices et homéostatiques sont reversées et, dans ce cas, les macrophages sont associés à des états pathologiques comme c'est le cas pour la fibrose, l'obésité et le cancer.

Dans les tumeurs, on retrouve une grande population de macrophages. Dans ce cas, ils sont appelés macrophages associés aux tumeurs (TAM). Ils peuvent représenter jusqu'à 50% de la masse tumorale. Dans le cas des gliomes, 30 à 50% des cellules présentes dans le microenvironnement sont des cellules microgliales ou des macrophages (Morantz et al. 1979). Généralement, une forte accumulation de macrophages est associée à un faible pronostic dans la plupart des cancers humains (Zhang et al. 2012). Les TAM sont des régulateurs importants de la tumorigenèse, ils participent à l'initiation de la tumeur, la progression tumorale et la formation de métastases. Des études sur les cancers du sein et sur les gliomes ont démontré que les TAM facilitent l'invasion cellulaire par un circuit paracrine impliquant les facteurs CSF-1 (colony stimulating factor 1) et EGF (epidermal growth factor) (Wyckoff et al. 2004). Les TAM sont également une source de protéases, telles que les cathepsines, qui permettent la

progression de la tumeur et la résistance thérapeutique dans de nombreux types de cancer (Gocheva et al. 2010).

Les macrophages sont des effecteurs de la réponse immunitaire. Ils devraient normalement reconnaitre les cellules cancéreuses comme étrangères car elles expriment des antigènes uniques. Cependant, le microenvironnement tumoral est immunosuppresseur empêchant les macrophages d'exercer leur fonction.

Origine et recrutement des TAM

Les TAM sont soit des monocytes sanguins eux-mêmes originaires de la moelle osseuse soit des macrophages résidents. Les macrophages résidents sont dérivés de progéniteurs érythro-myéloïdes qui se développent dans le sac vitellin embryonnaire (Ostuni et al. 2015). Dans l'environnement tumoral, les macrophages résidents locaux sont retrouvés avec les monocytes sanguins et sont recrutés en grand nombre par l'environnement inflammatoire. La proportion de monocytes circulants et de macrophages résidents dépend du type de cancer. Par exemple, pour les gliomes, des interactions complexes ont lieu entre les cellules microgliales résidentes et les monocytes circulants traversant la barrière hémato-encéphalique. Les macrophages résidents et les monocytes circulants peuvent être différenciés par l'expression à leur surface de marqueurs (CX3CR1, CD45, CCR2) (Hambardzumyan et al. 2015).

Après avoir atteint la tumeur, les monocytes subissent une maturation spécifique qui peut être observée par une modification de leurs marqueurs de surface, notamment les molécules Ly6C et MHCII (Ostuni et al. 2015). Les monocytes se différencient en macrophages en réponse à un vaste spectre de chémokines et facteurs de croissance produits par les cellules stromales et les cellules cancéreuses. Dans des conditions pathologiques « normales », le recrutement des macrophages passe par l'expression locale d'un grand nombre de facteurs de croissance tels que les facteurs CSF-1, GM-CSF, TGF-β1, MSP et de chémokines comme la CCL2, CCL7, CCL8, CCL3, CCL4 et MIF. Ces facteurs permettent de recruter les monocytes circulants et de les stimuler pour qu'ils se différencient en macrophages. Ces macrophages vont alors déclencher la réponse immunitaire et éliminer les pathogènes.

Dans l'environnement tumoral, les TAM sont recrutés par des facteurs sécrétés par les cellules stromales et les cellules néoplasiques. La chémokine CCL2 et la cytokine CSF-1 sont deux des facteurs les plus importants pour le recrutement des macrophages au niveau des

tumeurs (Pollard 2004). D'autres facteurs tels que la fibronectine, le fibrinogène, le VEGF et PDGF sont aussi impliqués dans le recrutement des monocytes. Par contre, quand la tumeur progresse, des changements apparaissent dans le microenvironnement. Les macrophages vont alors subir des modifications phénotypiques.

Plasticité phénotypique des macrophages

Les macrophages sont des cellules qui se différencient à partir des monocytes qui sont eux-mêmes des phagocytes sanguins. Ce sont des cellules ayant une grande plasticité phénotypique. Le phénotype de ces cellules dépend de leur localisation anatomique et du contexte physiologique et/ou pathologique. Ils peuvent s'accommoder aux conditions physiologiques. Quand ils sont exposés aux signaux de leur environnement, les macrophages peuvent se reprogrammer et adopter soit un phénotype pro-inflammatoire soit un phénotype anti-inflammatoire.

Les macrophages peuvent présenter deux états de polarisation en analogie avec la classification des lymphocytes Th1 et Th2 (Ostuni et al. 2015). Les macrophages dits « M1 » produisent des cytokines pro-inflammatoires, participent à la présentation des antigènes et ont un rôle anti-tumoral. Ils peuvent être activés soit par l'interféron-γ soit par les lipopolysaccharides bactériens (LPS). Ils peuvent sécréter des cytokines telles que le TNF-α, l'IL12, l'IL23 et l'IL6 en grande quantité, ces dernières vont stimuler les lymphocytes Th1 afin qu'ils détruisent les pathogènes. Certains marqueurs sont spécifiques du phénotype M1 tels que NOS2. Au contraire, les macrophages dits « M2 » produisent des cytokines anti-inflammatoires et ont des fonctions pro-tumorales. Ils sont impliqués dans une réponse lymphocytaire Th2. Ils peuvent être activés par différentes cytokines inhibitrices telles que l'IL4 et l'IL10. Les marqueurs M2 sont, par exemple, ARG1 et CD206 (**Figure 5**). Cette classification phénotypique des macrophages est cependant simplifiée et ne représente pas la complexité d'activation des macrophages. Neuf états d'activation différents ont été décrits (Xue et al. 2014). De plus, les marqueurs décrits pour les phénotypes M1 et M2 ne permettent pas de les discriminer. Par exemple, ARG1 qui est induit par l'IL4 est aussi induit par d'autres stimuli tels que le LPS ou l'IFN-γ (El Kasmi et al. 2008).

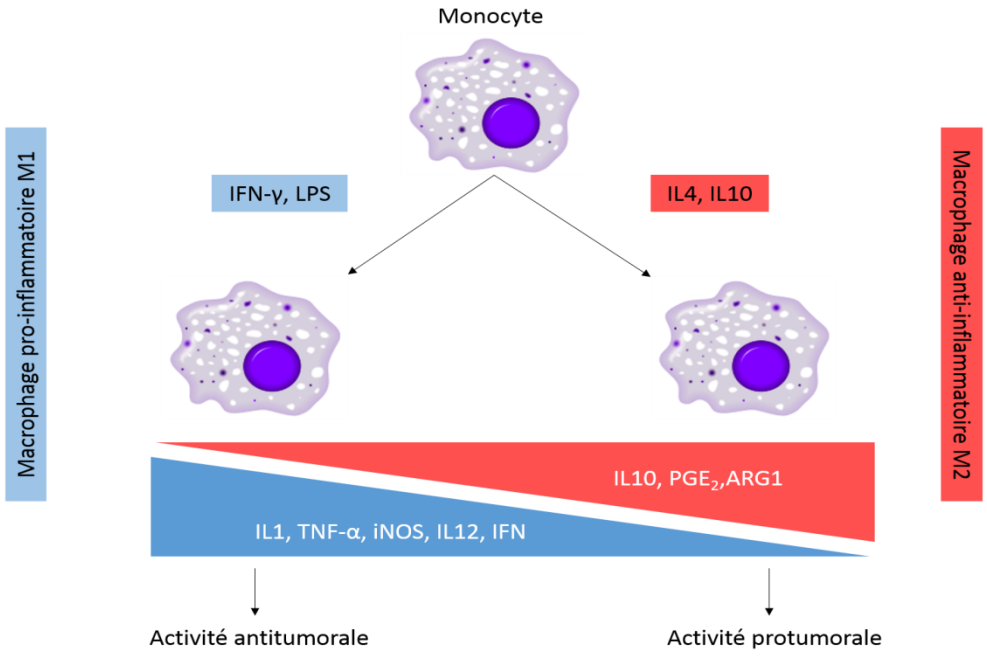

Figure 5 : Hétérogénéité phénotypique des macrophages. Les monocytes sanguins et macrophages résidants peuvent se différencier en réponse à leur environnement. Les TAM présentent des caractéristiques de macrophages M2 et contribuent à la progression tumorale.

Les TAM ressemblent aux macrophages M2, ils sécrètent en grande quantité de l'IL10 et ont des fonctions anti-inflammatoires. Au sein du microenvironnement tumoral, différentes cytokines sont exprimées et bloquent les fonctions immunitaires des macrophages. Ils vont alors passer d'un état anti-tumoral M1 à un état pro-tumoral M2 (Ostuni et al. 2015). Un composant de ce mélange cytokinique est le facteur CSF-1 qui bloque la maturation des cellules dendritiques. Par conséquent, ils sont incapables de présenter les antigènes. Durant les différentes étapes du développement de la tumeur, les macrophages subissent des modifications dynamiques de leur phénotype. La plupart des fonctions pro-tumorales des TAM sont induites par des molécules typiques du phénotype M2 telles qu'ARG1, VEGFA et HIF1α tandis que les molécules pro-inflammatoires M1 telles que l'IL12 ont des actions anti-tumorales. Cette vision est simplifiée car les TAM vont également exprimer des molécules pro-inflammatoires telles que NOS2 qui peuvent favoriser la croissance tumorale (Hofseth et al. 2003).

Actuellement, le basculement des macrophages d'un phénotype anti-tumoral vers un phénotype pro-tumoral n'est pas complètement compris. Une étude a démontré que l'hypoxie présente au niveau des tumeurs pouvait expliquer cette transition (Murdoch et al. 2005).

La tumeur contrôle le phénotype des TAM

Les facteurs présents dans le microenvironnement vont orienter le phénotype des TAM et peuvent être classés en trois catégories : les signaux dérivés des réponses immunitaires, la mort des cellules tumorales et le métabolisme des cellules tumorales.

❖ Les signaux dérivés des réponses immunitaires

Certains facteurs contrôlant le phénotype des TAM coïncident avec l'activation des macrophages M2 tels que l'IL10, l'IL4, l'IL13 et le TGF-β. Ces signaux sont, pour la plupart, libérés au niveau de la tumeur par les cellules immunitaires infiltrantes et influencent les fonctions des macrophages (Ostuni et al. 2015).

Dans un modèle de carcinome de la peau, les immunoglobulines dérivées des lymphocytes B permettent de promouvoir l'activation des cellules myéloïdes. Les macrophages acquièrent un phénotype pro-tumoral. Cibler les lymphocytes B peut être une stratégie thérapeutique pour le traitement des carcinomes de la peau. Dans une étude récente, la déplétion des lymphocytes B a démontré une réduction de la progression tumorale dans un modèle murin, corrélant à la fois avec une réduction de la production d'immunoglobulines et avec une diminution du nombre de cellules immunitaires infiltrantes (Affara et al. 2014).

Les cytokines pro-inflammatoires peuvent aussi conférer un phénotype pro-tumoral aux TAM. Par exemple, l'IFN-γ peut déclencher l'expression d'enzymes immunosuppressives telles que NOS2 et IDO par les TAM, les cellules dendritiques, et les cellules myéloïdes (Pallotta et al. 2011).

Les cellules stromales et tumorales sont également une source majeure de signaux immunitaires contrôlant les fonctions des TAM. De nombreuses lignées cellulaires cancéreuses humaines peuvent sécréter de l'IL10, du TGF-β et des PGE_2 *in vitro* et *in vivo.* Ces facteurs entraînent la différenciation des macrophages en TAM (Ostuni et al. 2015).

❖ Les signaux dérivés de la mort des cellules tumorales

La mort des cellules tumorales, soit spontanée soit induite par la thérapie, est associée à la libération de signaux de danger dans l'environnement extracellulaire. Les cellules immunitaires infiltrantes dont les TAM sont sensibles à ces signaux. Ils stimulent l'activation des macrophages via l'inflammasome ou la voie de signalisation du récepteur TLR4. Il a été montré que la libération d'ADN par les cellules tumorales mourantes pouvait stimuler les

réponses immunitaires contre les cellules cancéreuses via l'activation d'IRF3 et la production d'IFN-β (Ostuni et al. 2015).

❖ **Les signaux dérivés du métabolisme des cellules tumorales**

Le microenvironnement tumoral est hypoxique et est caractérisé par une forte concentration de lactate. Les forts taux d'acide lactique dans les tumeurs sont dus au métabolisme des cellules très prolifératives qui convertissent le glucose en lactate. Cette production énergétique supporte la croissance cellulaire par la production d'intermédiaires métaboliques qui agissent comme précurseurs pour les voies de biosynthèse (Vander Heiden et al. 2009). Des altérations métaboliques similaires sont observées dans les macrophages exposés au LPS et reflètent des adaptations cellulaires pour apporter l'énergie nécessaire. Les signaux métaboliques des cellules cancéreuses conditionnent le phénotype des TAM. L'acide lactique induit l'expression, par les macrophages, de gènes pro-tumoraux tels que *Vegf1* et *Arg1* (Colegio et al. 2014).

Fonctions des TAM

Les macrophages sont donc des cellules multifonctionnelles dont le phénotype est modulé par l'environnement local. La tumeur éduque les macrophages pour qu'ils favorisent sa progression vers un stade plus agressif. Les fonctions des macrophages peuvent résulter en l'initiation et le développement de la tumeur.

❖ **Rôle des TAM dans l'angiogenèse**

Il est largement reconnu que les tumeurs ont besoin d'être très irriguées pour se développer. En effet, les vaisseaux sanguins permettent d'apporter les nutriments et l'oxygène nécessaire pour la croissance de la tumeur. Ce processus d'angiogenèse implique de nombreux facteurs tels que le bFGF, le VEGF, les angiopoïétines (ANG1 et ANG2), l'IL1, l'IL8, le TNF-α et les métalloprotéases matricielles (MMP9 et MMP2). Ces molécules permettent la prolifération et la migration des cellules endothéliales, le remodelage de la matrice extracellulaire et la formation de vaisseaux sanguins. Les TAM produisent en grande quantité le VEGF qui est un composant clé des processus d'angiogenèse (Kitamura et al. 2015). Des études ont montré qu'une forte accumulation de TAM est caractéristique des régions où le taux d'angiogenèse est très fort. Il a été également suggéré que l'hypoxie ou les molécules libérées

en réponse à l'hypoxie attirent les macrophages. L'hypoxie déclenche une surexpression d'HIF-1α par les macrophages qui induit l'expression de molécules pro-angiogéniques tels que le VEGF (Semenza 2013).

Les TAM produisent d'autres facteurs pro-angiogéniques comme le TNF-α et l'IL1β. Ils induisent l'expression de MMP9 permettant la libération de VEGF actif. Les TAM libèrent également de l'oxyde nitrique (NO) synthétisé par l'enzyme iNOS. Une augmentation des taux de NO résulte en une vasodilatation (Rahat & Hemmerlein 2013).

Les TAM sont donc recrutés au niveau des zones de la tumeur où une vascularisation est nécessaire. Ces cellules produisent des facteurs angiogéniques qui permettent la formation de nouveaux vaisseaux sanguins (**Figure 6**). Ceci va alors permettre à la tumeur de se développer et de pénétrer dans la circulation sanguine. Un mélange complexe de facteurs, allant de l'hypoxie aux cytokines, contrôle l'expression de ces régulateurs.

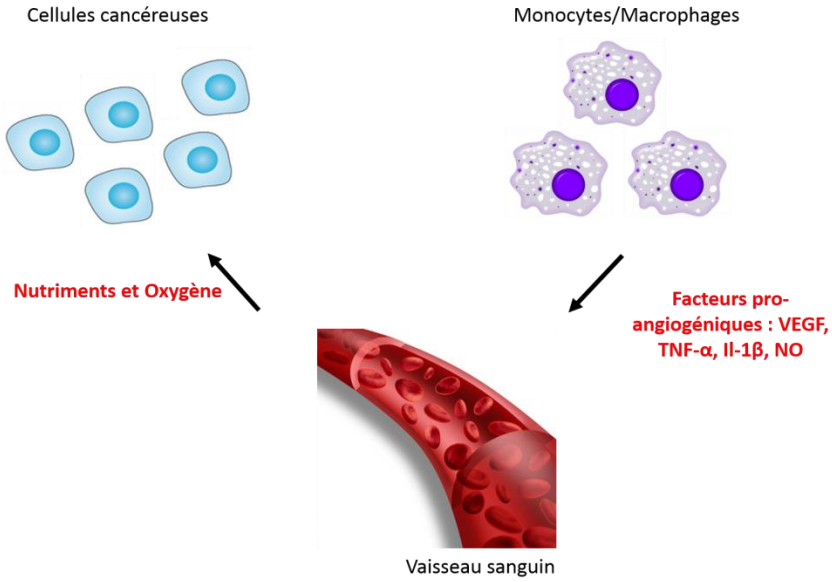

Figure 6 : Rôle des macrophages dans l'angiogenèse. Les vaisseaux sanguins apportent les nutriments et l'oxygène nécessaires aux cellules cancéreuses pour proliférer. La formation de ces nouveaux vaisseaux sanguins est induite par des facteurs libérés par les TAM.

❖ Rôle des TAM dans la formation de métastases

Pour établir un foyer métastatique, les cellules tumorales ont besoin de migrer à travers le stroma et de pénétrer dans les vaisseaux sanguins. Les TAM contribuent à ces phases précoces de la formation des métastases en augmentant la densité des vaisseaux sanguins. Ils

aident également les cellules cancéreuses à envahir les tissus environnants. En effet, ils produisent des protéases qui dégradent la membrane basale permettant aux cellules tumorales de pénétrer dans le stroma (Pollard 2004). Ils expriment également une grande variété de facteurs de croissance qui peuvent stimuler la croissance et la motilité des cellules cancéreuses. Parmi ceux-ci, on retrouve le FGF, l'HGF, les ligands d'EGFR, le PDGF et le TGF-β. L'EGF sécrété par les TAM active les récepteurs EGFR, situés sur la surface des cellules cancéreuses, qui les rend alors plus mobiles (Pollard 2004). Les facteurs de croissance peuvent aussi empêcher les cellules tumorales d'entrer en apoptose et promouvoir leur prolifération. Les TAM permettent également la formation de métastases par la sécrétion de CCL18 et d'ostéonectine qui modulent les propriétés d'adhésion des cellules cancéreuses à la matrice extracellulaire (Sangaletti et al. 2008; Chen et al. 2011).

Les cellules tumorales circulantes ont besoin de survivre dans les vaisseaux sanguins pour pouvoir former les métastases. Les TAM protègent ces cellules cancéreuses d'une attaque immunitaire et des stress environnementaux. En effet, les caillots sanguins formés après la pénétration des cellules cancéreuses dans les vaisseaux sanguins, activent les cellules endothéliales qui expriment les molécules VCAM1 et VAP1. Ces protéines permettent de recruter les macrophages (Ferjančič et al. 2013). Ces macrophages se lient alors aux cellules cancéreuses et leur transmettent des signaux de survie.

❖ Suppression des réponses immunitaires

Une activité majeure des TAM est la suppression des réponses immunitaires anticancéreuses (**Figure 7**). Ceci repose sur le fait que les TAM sont incapables de sécréter des molécules immunostimulatrices telles que l'IL12. L'IL12 est une cytokine pro-inflammatoire qui déclenche les actions tumoricides des cellules natural killer (NK) et les activités cytotoxiques des lymphocytes Th1. Par contre, les TAM produisent des cytokines inhibitrices telles que l'IL10, le TGF-β et les prostaglandines E2 afin de recruter les lymphocytes T régulateurs (Karavitis et al. 2012; Ostuni et al. 2015). L'IL10 sécrétée par les TAM régule négativement la production d'IL12 et stimule la différenciation des cellules Th2 qui libèrent de grande quantité d'IL4 et d'IL13. Ces cytokines renforcent le phénotype pro-tumoral des TAM. L'IL10 réduit également l'efficacité des thérapies basées sur l'immunité anti-tumorale.

La suppression des fonctions des cellules T par les TAM passe par l'activité d'une enzyme appelée arginase 1 (ARG1). ARG1 contrôle le catabolisme de la L-arginine. Son activité est déclenchée par une variété de signaux tumoraux tels que l'IL4, l'IL10 et l'hypoxie.

Cette enzyme inhibe les fonctions des cellules T en limitant la quantité disponible de L-arginine. L'arginine est aussi le substrat de la nitric oxide synthase (NOS2) qui l'utilise pour produire un médiateur crucial pour la cytotoxicité des cellules myéloïdes. NOS2 est induit par les macrophages durant l'inflammation. Dans les tumeurs, cette enzyme peut supprimer les fonctions des cellules T (Ostuni et al. 2015). Les TAM peuvent aussi entraîner l'apoptose des cellules T en exprimant à leur surface les molécules inhibitrices de la famille B7 telles que les facteurs PD-L1 et CTLA4 (Fife & Bluestone 2008). Ces signaux inhibiteurs empêchent les cellules T cytotoxiques d'éliminer les cellules cancéreuses.

Les fonctions pro-tumorales des TAM reposent aussi sur les effets prolifératifs de certaines cytokines pro-inflammatoires comme l'IL6, le TNF-α et l'IL11 qui déclenchent la prolifération des cellules cancéreuses du foie, du poumon et de l'estomac via les voies de signalisation NF-κB et STAT3 (Grivennikov et al. 2010). Ces facteurs peuvent aussi agir sur les cellules souches cancéreuses pour déclencher la tumorigenèse.

L'immunosuppression est un problème majeur des thérapies anti-cancéreuses. La régulation de la différenciation et de l'activation des cellules myéloïdes est considérée comme une nouvelle approche thérapeutique.

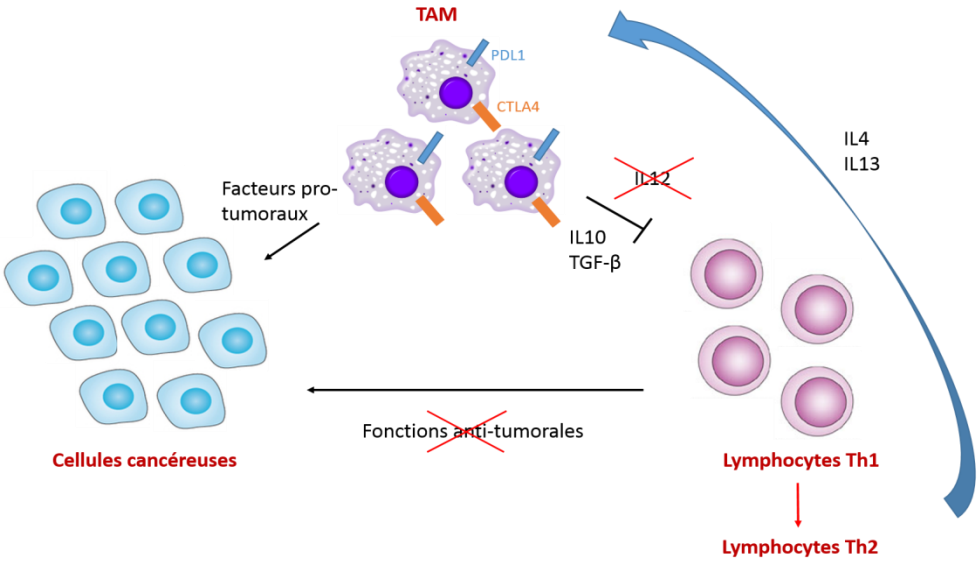

Figure 7: Immunosuppression induite par les TAM. Les TAM sécrètent des facteurs immunosuppresseurs qui vont orienter les lymphocytes vers un phénotype Th2. Les lymphocytes n'exercent donc plus leurs fonctions anti-tumorales. Les cellules Th2 vont renforcer le phénotype anti-inflammatoire des TAM en sécrétant de l'IL4 et de l'IL13. Les lymphocytes peuvent aussi entrer en apoptose par les interactions PD1/PDL1 et CTLA4. Tous ces phénomènes permettent aux cellules cancéreuses de se multiplier.

Opportunités thérapeutiques

Les TAM peuvent influencer l'efficacité des thérapies anti-cancéreuses. Plusieurs drogues ont des effets directs sur les TAM. Par exemple, la Trabectédine est un agent thérapeutique qui entraîne des dommages au niveau de l'ADN des TAM. Son administration réduit la croissance tumorale et corrèle avec une diminution de la densité des TAM (Germano et al. 2013). Le Docétaxel diminue également le nombre de macrophages au niveau de la tumeur (Kodumudi et al. 2010).

L'interaction entre les TAM et les traitements anti-cancéreux ne se limite pas à la chimiothérapie. De faibles doses d'irradiations γ, au niveau d'un modèle murin de cancer du pancréas, reprogramment les TAM vers un phénotype anti-tumoral caractérisé par une augmentation de leur capacité à stimuler les cellules T (Klug et al. 2013).

La manipulation des TAM peut être exploitée pour traiter le cancer, soit seule ou en combinaison avec la chimiothérapie. Actuellement, l'approche la plus avancée repose sur l'appauvrissement de la tumeur en TAM via l'inhibition de la signalisation CSF-1/CSF-1R. Des essais cliniques combinent l'utilisation d'inhibiteurs du récepteur CSF-1 et la chimiothérapie pour le traitement des cancers métastatiques. Bloquer le récepteur CSF-1 permet d'augmenter l'efficacité du traitement au Paclitaxel dans des modèles murins de cancer du sein. Un anticorps monoclonal (RG7155) dirigé contre le récepteur CSF-1 humain inhibe la signalisation du récepteur en bloquant sa dimérisation induite par la liaison de ses ligands CSF-1 ou IL34 (Ries et al. 2014). Une première phase d'essai clinique testant l'administration de l'anticorps RG7155 à des patients atteints de tumeurs diffuses à cellules géantes (Dt-GCT) a montré des résultats encourageants chez un patient où la tumeur s'est désagrégée (West et al. 2006). Cet effet est corrélé à la diminution du nombre de TAM de la biopsie tumorale et une augmentation de l'infiltration de cellules T CD8+. L'inhibition de CSF-1R a également été provoquée par un peptide perméable à la barrière hémato-encéphalique dans un modèle de glioblastome (Pyonteck et al. 2013). L'inhibition de CSF-1R réduit significativement la progression de la tumeur.

Ces différentes stratégies représentent une avancée majeure vers l'identification de thérapies anti-cancéreuses ciblant les fonctions pro-tumorales des TAM. Cependant, les macrophages autres que les TAM sont également touchés par ces traitements. Les anticorps anti-CSF-1R ne ciblent pas spécifiquement les TAM. De plus, l'inhibition de CSF-1R peut aussi

entraîner une surexpression des récepteurs PD-1 et CTLA-4 qui inhibent les cellules T (Ostuni et al. 2015).

Une autre approche pour cibler spécifiquement les TAM repose sur l'inhibition du recrutement des monocytes par la tumeur. Ceci peut être mené en interférant sur la signalisation CCL2-CCR2. Des anticorps permettant de bloquer CCL2 inhibent le recrutement des TAM dans des tumeurs primaires et métastatiques du sein (Bonapace et al. 2014; Qian et al. 2011). Cependant, l'interruption du traitement entraîne une augmentation rapide de l'infiltration des monocytes et accélère la formation de métastases. Cet effet négatif montre que cibler le recrutement des TAM peut ne pas être suffisant pour un traitement durable.

Une stratégie plus attrayante pour la thérapie anti-cancéreuse repose sur la reprogrammation des TAM afin d'améliorer leurs propriétés anti-tumorales. Par exemple, l'inhibition de la signalisation IL10 dans un modèle murin de cancer du sein a permis d'augmenter l'efficacité de la chimiothérapie (Ruffell et al. 2014). L'IL10 bloque la capacité des macrophages à produire de l'IL12, et inhibe ainsi les réponses anti-tumorales des lymphocytes T CD8+.

C. Autres éléments du microenvironnement tumoral

Les cellules myéloïdes MDSC

L'immunosuppression observée chez les patients ayant une tumeur passe en partie par les activités des cellules myéloïdes MDSC (myeloid-derived suppressor cells) (Almand et al. 2001). Les MDSC sont des cellules myéloïdes immatures et immunosuppressives qui maintiennent l'homéostasie des tissus en réponse à des infections ou des stress traumatiques. Les MDSC infiltrent les tumeurs où elles augmentent la vascularisation et altèrent les mécanismes d'immunosurveillance comme la présentation des antigènes par les cellules dendritiques, l'activation des cellules T, la polarisation des macrophages M1 et l'inhibition de la cytotoxicité des cellules NK (Talmadge & Gabrilovich 2013).

Les lymphocytes T régulateurs

Les lymphocytes T régulateurs représentent un autre type cellulaire retrouvé dans le microenvironnement tumoral. Dans des conditions physiologiques, les cellules T régulatrices modulent l'activation des lymphocytes T et B. Dans certains types de tumeurs, comme les tumeurs du sein et du foie, une augmentation des lymphocytes T régulateurs corrèlent avec une diminution de la survie des patients (Bates et al. 2006; Fu et al. 2007) tandis que dans d'autres types de cancers, comme les cancers colorectaux, ils sont associés à une meilleure survie (Frey et al. 2010). Les lymphocytes T régulateurs suppriment la présentation des antigènes par les cellules dendritiques et inhibent les fonctions cytotoxiques des cellules Th1 (von Boehmer & Daniel 2013).

Les fibroblastes

Les fibroblastes sont prédominants dans les tissus connectifs. Ils déposent la matrice extracellulaire et les composants de la membrane basale, régulent la différenciation des cellules épithéliales et modulent les réponses immunitaires (Kalluri & Zeisberg 2006). Les fibroblastes associés aux tumeurs sont différents des fibroblastes normaux. Une fois qu'ils s'accumulent dans le microenvironnement tumoral, ils sont activés par des facteurs de croissance et des cytokines. Les facteurs TGF-β, MCP1, PDGF, FGF et les protéases sécrétées ont été impliqués dans l'activation des fibroblastes (Marsh et al. 2013). Suite à leur activation, les fibroblastes sécrètent des facteurs de croissance qui permettent à la tumeur de se développer. Par exemple, le VEGF participe à la perméabilité vasculaire et l'angiogenèse (Fukumura et al. 1998). Ils produisent également des facteurs pro-inflammatoires qui activent la voie de signalisation NF-κB pour promouvoir la tumorigenèse (Erez et al. 2010).

La matrice extracellulaire

La matrice extracellulaire a la capacité de limiter l'initiation tumorale à des stades précoces et induit la progression tumorale à des stades tardifs. Par conséquent, la composition de la matrice extracellulaire du microenvironnement tumoral permet de prédire le pronostic clinique. Pour le cancer du sein, 4 sous classes peuvent être définies en fonction de la composition de la matrice extracellulaire (Bergamaschi et al. 2008). Les tumeurs exprimant

fortement les inhibiteurs de protéases dans leur matrice extracellulaire, sont associées à un bon pronostic tandis que les tumeurs exprimant fortement les intégrines et les métalloprotéases matricielles sont associées à un mauvais pronostic.

Le système vasculaire

L'angiogenèse est une caractéristique des cancers en réponse à un besoin en oxygène et en nutriments provenant de la circulation sanguine. La vascularisation tumorale nécessite la coopération de nombreuses cellules du microenvironnement dont les cellules vasculaires endothéliales, les péricytes et les cellules précurseurs dérivées de la moelle osseuse (Quail & Joyce 2013). En plus des cellules formant les vaisseaux sanguins, d'autres cellules incluant les macrophages, les cellules souches mésenchymateuses et les fibroblastes libèrent des facteurs pro-angiogéniques dans le microenvironnement.

IV. Les proprotéines convertases, immunité et cancer

A. Généralités

Les modifications post-traductionnelles augmentent la diversité des protéines présentes dans un organisme. Dans la plupart des cas, elles influencent la fonction des protéines et sont introduites dans les protéines cibles via des enzymes spécifiques. Plus de 200 modifications post-traductionnelles sont connues, incluant les glycosylations, les phosphorylations, l'ajout de motifs lipidiques, les acétylations, les méthylations, les ubiquitinylations, les oxydations … Les modifications post-traductionnelles réversibles permettent l'adaptation des cellules aux conditions physiologiques et/ou aux stress.

Une modification post-traductionnelle irréversible est, par exemple, la protéolyse des protéines au niveau de sites spécifiques. La protéolyse est effectuée par des protéases qui clivent des liaisons peptidiques particulières pour libérer de multiples produits. L'analyse des génomes humain et murin a révélé la présence d'environ 600 protéases différentes, appartenant à 5 classes d'enzymes protéolytiques : aspartic, métallo, cysteine, sérine et thréonine protéases (Puente et al. 2003).

Parmi elles, on retrouve les sérines protéases caractérisées par la présence d'un site actif qui est utilisé pour hydrolyser les liaisons peptidiques de leur substrat. Ces protéases appartiennent à la classe enzymatique la plus abondante et la plus diversifiée. Les sérines protéases peuvent être classées en deux familles : les homologues à la chymotrypsine et les homologues à la subtilisine. Les subtilases sont sous-divisées en deux groupes dont l'un d'eux comprend les proprotéines convertases (**Figure 8**) (Siezen & Leunissen 1997).

Les sept premiers membres de la famille des proprotéines convertases (proprotéine convertase 1/3 (PC1/3), PC2, furine, PC4, PC5, PACE4 (paired basic amino acid cleaving enzyme 4) et PC7) clivent les protéines précurseurs au niveau de résidus basiques dans les granules de sécrétion immatures, dans les endosomes, dans l'appareil de Golgi, à la surface cellulaire ou dans la matrice extracellulaire. Elles sont responsables de l'activation, et parfois de l'inactivation, de nombreuses protéines telles que les hormones, les facteurs de croissance et leur récepteur, les molécules d'adhésion et les enzymes. Elles sont souvent importantes pour la progression de maladies diverses comme le cancer, l'inflammation et les infections pathogènes (Seidah & Prat 2012).

Le huitième membre de cette famille est l'enzyme SKI-1 (subtilisin kexin isozyme 1) qui active des facteurs de transcription et des protéines spécifiques qui transitent par l'appareil de Golgi. C'est une enzyme majeure contrôlant la synthèse du cholestérol et des acides gras et qui régule des fonctions biologiques importantes telles que la réponse des cellules aux stress, la minéralisation des os, la survie des neurones et la direction des protéines vers les lysosomes (Seidah et al. 1999).

Le dernier membre est la proprotéine convertase PCSK9 (proprotein convertase subtilisin kexin 9) qui agit d'une façon non enzymatique pour améliorer la dégradation endosomale et lysosomale de récepteurs de surface. Le plus important est le récepteur LDLR (low-density lipoprotein receptor) (Park et al. 2004). Ce récepteur a un rôle majeur dans la sur-régulation des niveaux de cholestérol-LDL circulants. Une augmentation de son activité est associée à une hypercholestérolémie.

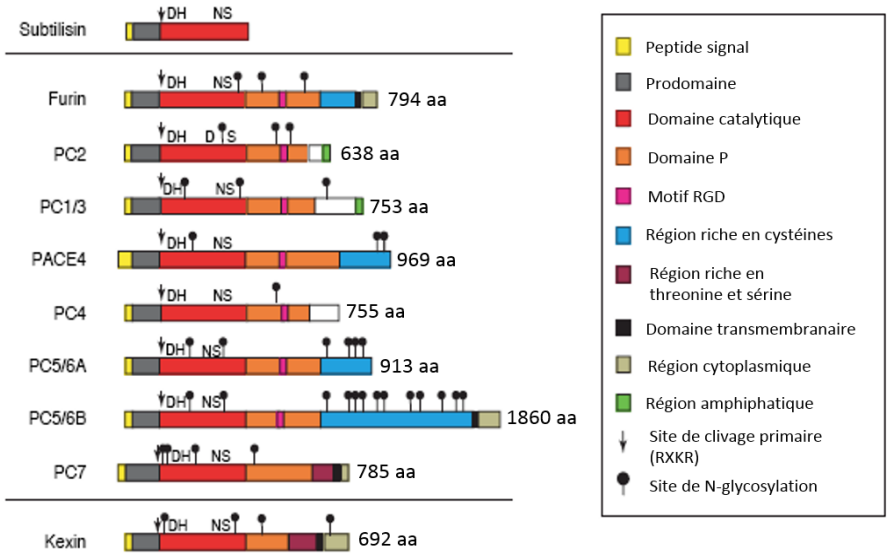

Figure 8 : La famille des proprotéines convertases. Les proprotéines convertases présentent une structure N-terminale hautement similaire ainsi qu'une région C-terminale plus variable. (Adaptée de Seidah *et al*, 2012)

Des modèles de souris knock-out ont permis de déterminer les substrats de chacune de ces enzymes. Par exemple, les souris PC1/3 et PC2 knock-out (KO) sont viables mais les souris qui n'expriment ni PC1/3 ni PC2 meurent durant l'embryogenèse, suggérant une redondance de ces enzymes (Seidah & Prat 2012). L'inhibition du gène *Pcsk1* entraîne des retards de

croissance qui sont dus à une déficience de l'hormone GHRH (growth hormone-releasing hormone) (Zhu, Orci, et al. 2002). Le précurseur de cette hormone est clivé à son extrémité C-terminale par PC1/3. Les précurseurs et les formes intermédiaires de cette hormone s'accumulent dans les souris PC1/3 KO, ainsi que la POMC, la pro-insuline et le pro-glucagon (Zhu, Zhou, et al. 2002). Cependant, les souris PC1/3 KO peuvent toujours cliver partiellement la POMC pour produire l'ACTH (adrenocorticotropic hormone) probablement grâce à l'action d'une autre proprotéine convertase. Une déficience complète pour l'enzyme PC1/3 résulte en une obésité massive, une déficience de l'homéostasie du glucose et une infertilité d'origine hypothalamique qui sont dues en partie aux faibles taux d'ACTH et d'insuline.

Des inhibiteurs et régulateurs de ces proprotéines convertases peuvent par conséquent avoir de nombreuses applications dans le traitement de maladies telles que le cancer et la formation de métastases, les infections virales, les maladies inflammatoires et l'hypercholestérolémie.

B. Fonctions des proprotéines convertases

Activation

Comme la plupart des précurseurs protéiques qui subissent de nombreuses modifications post-traductionnelles avant d'être actifs, les proprotéines convertases sont elles-mêmes l'objet de modifications avant de devenir complètement fonctionnelles. Les premiers événements se font dans le réticulum endoplasmique où les précurseurs perdent leur peptide signal et sont glycosylés à de nombreux sites. Les précurseurs résultants (pro-proprotéines convertases) acquièrent leur conformation dans le réticulum endoplasmique, permettant le clivage autocatalytique de leur pro-segment. Le pro-segment clivé reste lié à la protéase mature, la retenant dans un état inactif. La seule proprotéine convertase qui ne suit pas ce cheminement est la PC2 qui est transportée avec la protéine 7B2 dans les granules de sécrétion acides, où elle est autoclivée (Seidah & Prat 2012).

Localisation cellulaire et expression tissulaire

L'expression tissulaire et la localisation cellulaire de chaque proprotéine convertase est différente. PC1/3 et PC2 sont largement localisées dans les granules de sécrétion des cellules neurales et neuroendocrines et sont impliquées dans la maturation de la plupart des prohormones (Day et al. 1992). On les retrouve également dans les cellules immunitaires (macrophages, lymphocytes) (Lansac, Dong, Claire M. Dubois, et al. 2006). La furine est ubiquitaire et est transportée du réseau trans-golgien à la surface cellulaire (Thomas 2002). PC4 est exclusivement exprimée dans les cellules germinales des testicules et des ovaires et au niveau du placenta (Gyamera-Acheampong & Mbikay 2009). PC5 est exprimée dans les neurones du système nerveux central, dans les cellules du tube digestif, dans les tissus ovariens et dans les cellules germinales testiculaires (Lusson et al. 1993). PACE4 est retrouvée abondamment dans le cervelet, la moelle épinière, l'hypophyse, le tractus gastro-intestinal, le cœur, le foie, les reins, les ovaires ainsi que la prostate (Dong et al. 1995). PC5 et PACE4 se lient à des inhibiteurs des métalloprotéases à la surface cellulaire ou dans la matrice extracellulaire via leur domaine C-terminal. PC7 est également ubiquitaire mais est exprimée plus fortement dans le système nerveux central, dans les tissus reproductifs, dans les cellules intestinales… Une partie des enzymes PC7 est dirigée vers la surface cellulaire par la voie de sécrétion non conventionnelle (Rousselet et al. 2011). SKI-1 peut être localisée dans l'appareil de Golgi, dans les endosomes et les lysosomes (Pullikotil et al. 2007). PCSK9, qui est exprimée dans le foie, l'intestin et les reins, est une enzyme soluble qui est sécrétée sous forme inactive (Zaid et al. 2008). Après la liaison à sa cible, le complexe est dirigé vers les endosomes et lysosomes pour être dégradé (Maxwell et al. 2005).

Mode d'action des proprotéines convertases

Les proprotéines convertases sont impliquées dans le clivage protéolytique de nombreuses protéines. Parmi ces protéines, on retrouve des hormones, récepteurs, molécules d'adhésion, enzymes et protéines d'origine virale ou bactérienne. Les sept premières convertases (PC1/3, PC2, furine, PC4, PC5, PACE4 et PC7) clivent les précurseurs protéiques au niveau d'un motif consensuel (R/K)X_n-R/K↑. La flèche indique le site de clivage et X_n correspond à 0, 2, 4 ou 6 acides aminés sauf une cystéine. L'enzyme SKI-1 clive au niveau de résidus non basiques de l'extrémité C-terminale du motif RX(L/V/I)X↑. PCSK9 se clive elle-

même au niveau de son résidu VFAQ et une fois clivée, cette protéine n'a plus le rôle de protéase mais agit en se liant à des récepteurs de surface spécifiques (Seidah & Prat 2012).

Rôle en conditions pathologiques : le cancer

Les proprotéines convertases jouent un rôle important dans les mécanismes de néoplasie en facilitant la prolifération, la migration des cellules cancéreuses et la formation de métastases. Différents cancers humains et lignées de cellules tumorales montrent une forte expression des proprotéines convertases qui corrèle avec leur croissance et leur invasion (Khatib et al. 2002). Les rôles des proprotéines convertases sont variables en fonction du type de tumeur.

Il a été démontré que la surexpression de PACE4 était suffisante pour induire la différenciation de kératinocytes murins en cellules malignes. Ceci est dû à l'augmentation de la conversion des pro-MMP en leur forme active par l'enzyme PACE4 (Bassi et al. 2005). La surexpression de PACE4 a également été observée dans le cancer de la prostate (D'Anjou et al. 2011). La furine a été associée à la transformation maligne des cellules cancéreuses pour les cancers tête et cou, les cancers des ovaires et les cancers du sein (Cheng et al. 1997; Bassi et al. 2001; Page et al. 2007). D'autres études ont reporté un rôle de PC1/3 et PC2 dans les cancers neuroendocriniens incluant les phéochromocytomes, les adénomes hypophysaires et les carcinoïdes (Jin et al. 1999; Konoshita et al. 1994). Elles sont également surexprimées dans les tumeurs du poumon. L'enzyme PC7 est associée au cancer du sein et de l'ovaire.

Les proprotéines convertases peuvent avoir des rôles importants dans la progression tumorale dus à la grande variété de leurs substrats qui incluent des MMP, des molécules d'adhésion, des facteurs de croissance et leurs récepteurs (Khatib et al. 2002). Le **Tableau 3** décrit des exemples de substrats des proprotéines convertases qui ont des rôles dans la progression tumorale.

Tableau 3 : Implication de certains substrats des proprotéines convertases dans la tumorigenèse. (Inspiré de Artenstein et Opal, 2011)

Facteurs de croissance et récepteurs	IGF-1R	Acquisition d'un phénotype malin
	IGF1 PDGF TGF-β	Prolifération et angiogenèse
	VEGF	Angiogenèse
Molécules d'adhésion	Cadhérines	Métastase
	α-intégrines	Angiogenèse et métastase
Protéases	MT1-MMP ADAM ADAM-TS Stromelysin-3 MMP2	Dégradation de la matrice extracellulaire et de la membrane basale

Les facteurs de croissance et leurs récepteurs ont un rôle important dans la progression tumorale. Les facteurs de croissance et récepteurs clivés par les proprotéines convertases incluent les IGF, IGFR, PDGF, TGF-β1 et VEGF (Artenstein & Opal 2011). Ils peuvent intervenir au niveau de la prolifération, la formation de vaisseaux sanguins et la différenciation des cellules en cellules cancéreuses. Des pro-métalloprotéases sont également clivées par les proprotéines convertases (Artenstein & Opal 2011). Ces molécules dégradent la matrice extracellulaire pour faciliter la mobilité des cellules cancéreuses et donc la formation de foyers métastatiques. Enfin, les molécules d'adhésion sont aussi des substrats des proprotéines convertases. Parmi elles, on retrouve les intégrines et cadhérines (Müller et al. 2004). Les intégrines permettent la liaison des cellules à la matrice extracellulaire et favorisent la formation des métastases. Les cadhérines, quant à elles, sont impliquées dans l'adhésion des cellules entre-elles et diminuent la mobilité des cellules. Une perte de fonction des cadhérines est associée à une agressivité plus importante des tumeurs.

C. Rôle des proprotéines convertases dans l'immunité

Les proprotéines convertases sont aussi des régulateurs importants des réponses immunitaires. L'inhibition de leur activité empêche l'activation protéolytique des toxines bactériennes et l'entrée des virus. La furine est connue pour réguler le clivage et donc l'activité du récepteur TLR7 (Hipp et al. 2013). De plus, l'inhibition de l'expression de *Pcsk1* chez des

souris est associée à des réponses inflammatoires exacerbées (Refaie et al. 2012). Des analyses biochimiques ont aussi démontré que les proprotéines convertases contrôlent la maturation de plusieurs protéines importantes pour les réponses immunitaires telles que les intégrines, les métalloprotéases matricielles et les cytokines.

Furine

La furine est exprimée de façon ubiquitaire mais dans les cellules T son expression est fortement régulée suite à leur activation. De plus, la furine est une cible directe du facteur de transcription STAT4 (Pesu et al. 2006). Des études ont montré que la furine clivait plusieurs protéines impliquées dans la biologie des lymphocytes T dont Notch1 et TGF-β (Thomas 2002). Chez des souris qui ont des lymphocytes T déficients pour la furine, des taux élevés de cytokines pro-inflammatoires (IL6, IFN-γ et IL13) ont été retrouvés dans leur sérum tandis que les taux de cytokines anti-inflammatoires (IL10) étaient plus faibles (Pesu et al. 2008). Les réponses immunitaires exacerbées, dans ces souris, peuvent être dues à une diminution de la disponibilité de la cytokine TGF-β1 dans les cellules T. Une autre étude a montré que le récepteur TLR7 était clivé par la furine pour être activé. Les stimuli pro-inflammatoires augmentent l'expression de la furine dans les cellules immunitaires, suggérant un mécanisme de rétroaction positif pour le clivage du récepteur TLR7 (Hipp et al. 2013).

PCSK9

Une diminution de l'activité de PCSK9 augmente la quantité des récepteurs aux LDL à la surface des cellules du foie et augmente donc la clairance du LDL. La clairance des lipides provenant des pathogènes peut être régulée par PCSK9, comme par exemple pour le LPS. Une étude a montré que des souris PCSK9 knock-out produisaient moins de cytokines pro-inflammatoires en réponse au LPS. Dans les cellules humaines du foie, PCSK9 inhibe l'assimilation du LPS qui est une étape nécessaire pour son élimination. L'inhibition de PCSK9 améliore la survie des patients ayant subi un choc septique (Walley et al. 2014).

PC1/3

La plupart des études fonctionnelles menées jusqu'à maintenant ont porté sur les fonctions neuroendocrines de PC1/3. Après une étude histologique ayant permis de mettre en évidence la présence de celle-ci au sein d'organes immunitaires effecteurs (Salzet et al. 2000; Salzet 2002; Lansac, Dong, Claire M Dubois, et al. 2006), une étude, sur des souris PC1/3 KO, s'est intéressée aux fonctions immunitaires de l'enzyme (Refaie et al. 2012). L'expression de PC1/3 est régulée par les motifs moléculaires associés aux pathogènes et plus spécialement par le LPS qui active la voie de signalisation TLR4 (Lansac, Dong, Claire M. Dubois, et al. 2006). Ces souris PC1/3 KO présentent une désorganisation et une augmentation du volume de leur rate (Refaie et al. 2012), indiquant un manque de communication entre les cellules immunitaires telles que les macrophages, les cellules B et les cellules T. De plus, une injection de LPS a montré une augmentation de la sécrétion des cytokines pro-inflammatoires dans le plasma démontrant que PC1/3 joue un rôle dans l'immunité innée. L'expression de PC1/3 co-localise avec le marqueur CD14, qui est un marqueur spécifique des macrophages (Lansac, Dong, Claire M. Dubois, et al. 2006). Des études sur des modèles de macrophages ont ensuite été menées pour aller plus en détail dans le rôle de PC1/3 dans l'immunité (Refaie et al. 2012; Gagnon et al. 2013). Ces études ont démontré que l'inhibition de PC1/3 dans ces macrophages déclenchait une sécrétion plus importante de cytokines pro-inflammatoires.

Parce que de nombreuses maladies sont liées à la réponse des macrophages et leur capacité à activer les cellules T telles que les maladies auto-immunes, les allergies chroniques ou encore le cancer (comme décrit dans la section III.B), l'étude du rôle de PC1/3 dans l'immunité pourrait permettre de mieux comprendre ces maladies et de développer des stratégies thérapeutiques.

CHAPITRE 1

Classification des gliomes de haut grade basée sur l'imagerie MALDI et la microprotéomique en relation avec les données cliniques des patients

Introduction

Les gliomes de haut grade représentent un challenge que ce soit pour leur classification histologique ou leur prise en charge thérapeutique. La classification de l'OMS de 2007 est basée sur des observations morphologiques de la tumeur et, par conséquent, des problèmes de reproductibilité intra- et inter-observateurs sont fréquents (Louis et al. 2007). Récemment, une mise à jour de cette classification a été faite. Cette dernière prend en compte les données moléculaires pour chaque patient qui sont majoritairement : les mutations IDH1/IDH2, le gain du bras chromosomique 7q et la perte du bras chromosomique 10q, les mutations au niveau du promoteur de TERT, les mutations d'ATRX, la co-délétion des bras chromosomiques 1p/19q, les mutations de TP53 et les mutations de PTEN (Louis et al. 2016b). Cependant, les approches génomiques sont limitées car certains gènes (normaux, surexprimés ou mutés) peuvent ne pas être exprimés. En effet, des contradictions sont observées entre les profils transcriptomiques et protéomiques dans les gliomes (Persson et al. 2009). L'intégration des données histologiques, génomiques et protéomiques permettrait de définir une meilleure classification et une meilleure caractérisation des gliomes.

La plupart des études protéomiques menées jusqu'à maintenant portent sur l'analyse des fluides biologiques tels que le plasma ou le liquide céphalo-rachidien (Gautam et al. 2012; Ohnishi et al. 2009). Elles ont permis d'obtenir des informations sur les protéines sécrétées par la tumeur et ont identifié des facteurs de croissance (VEGF), des protéines du système immunitaire (cytokines, chémokines), des protéines impliquées dans l'angiogenèse et la migration … Les études, à partir de biopsies de patients, utilisent en général des techniques « in-gel » et ne permettent pas d'obtenir des informations sur les protéines très minoritaires. De plus, l'analyse est faite sur la globalité du tissu sans prendre en compte l'hétérogénéité tumorale.

Dans notre étude, nous nous sommes intéressés à la protéomique des gliomes de grade III via l'utilisation de l'imagerie MALDI associée à la segmentation non supervisée et couplée à des études microprotéomiques. La question sous-tendue à cette étude est la possibilité de corréler les données d'imagerie MALDI et de microprotéomique et de les comparer aux données

cliniques des patients pour améliorer la classification et le diagnostic voir même, in fine, le pronostic.

Résultats

Une première analyse sur cinq échantillons de gliome de grade III a été réalisée puis validée sur cinq autres échantillons analysés en aveugle. Nous avons tout d'abord défini par imagerie MALDI des profils moléculaires, au sein de la tumeur et également entre les différents patients. Des analyses non supervisées suivies d'une classification hiérarchique ont ensuite été effectuées afin de délimiter des régions de profils moléculaires différents. Nous avons voulu comparer, dans un premier temps, les annotations histologiques faites par l'anatomo-pathologiste avec nos données d'imagerie. Des contradictions ont été observées pour certains tissus. Certaines tumeurs homogènes, d'un point de vue histologique, présentent en fait des régions hétérogènes d'un point de vue moléculaire. La classification hiérarchique globale, en prenant en compte les cinq tissus, a permis d'identifier trois groupes différents alors qu'ils sont tous classés en grade III par la classification de l'OMS de 2007. Nous avons ensuite identifié les protéines dans ces régions grâce à une stratégie de microprotéomique couplée à une analyse shotgun. Les trois groupes, déterminés par imagerie MALDI, ont aussi été retrouvés lors des analyses statistiques des données de microprotéomique. Des protéines surexprimées dans chacun de ces trois groupes ont été identifiées. Le premier groupe est caractérisé par un profil néoplasique et de nombreuses protéines sont impliquées dans le métabolisme des ARNm. Les protéines surexprimées dans le second groupe sont des protéines liées à la pathologie du gliome et sont caractéristiques d'une infiltration en cellules immunitaires telles que les macrophages et cellules microgliales. Le troisième groupe est associé à un profil de régénération neuronale. Nous avons ensuite voulu valider notre classification par imagerie MALDI en prenant cinq nouveaux échantillons. Ces cinq échantillons se sont bien reclassés dans les trois groupes identifiés. La classification hiérarchique des dix échantillons a permis de montrer que deux des trois groupes étaient en fait très similaires. Pour simplifier notre classification, nous avons donc gardé deux groupes. Des protéines spécifiques à chacun de ces deux groupes ont été retrouvées. Le premier groupe présente des protéines spécifiques en lien avec l'épissage des ARN, l'expression et la régulation des ARNm mais aussi dans le recyclage des ARN non codants. Le groupe 2, quant-a-lui, intègre des protéines déjà connues pour être impliqués dans les gliomes mais aussi des protéines liées aux cellules souches. Une récente étude de séquençage par NGS sur 121 gliomes de tout grade a récemment montré l'existence de 2 groupes moléculaires pour

les gliomes de grade III (Zacher et al. 2016). Dans notre étude, les patients du groupe 1 présentent en majorité une mutation de TP53, une perte d'ATRX et les chromosomes 1p/19q ne sont pas co-délétés. Des anomalies sur les chromosomes 7 et 10 sont observées chez 3 patients sur 4. Les patients du groupe 2 ne présentent pas de mutation de TP53 (3 patients sur 4) et n'ont pas d'anomalies sur les chromosomes 7 et 10 (3 patients sur 4). Un point également important dans cette étude est en lien avec la présence de protéines issues d'ORF alternatifs au sein des échantillons. Outre le fait de la présence de ces protéines non connues car issues des 5' et 3'UTR des ARN ou des autres cadres de lecture, celles-ci montrent une répartition en fonction des 2 groupes. Le rôle de ces protéines est encore inconnu mais leur présence pourrait être un élément supplémentaire pour améliorer le diagnostic et voir même le pronostic après une étude systématique sur une cohorte plus importante.

Cette étude avait pour objectif de valider notre technologie pour l'établissement d'une classification des gliomes par protéomique intégrant les données cliniques. Une étude sur un nombre plus important de patients est en cours.

BBA - research article

Evaluation of Non-Supervised MALDI Mass Spectrometry Imaging Combined to MicroProteomics for Glioma Grade III Classification

Emilie Le Rhun[1,2*], Marie Duhamel[1*], Maxence Wisztorski[1], Jean-Pascal Gimeno[3], Fahed Zairi[1,4], Fabienne Escande[5], Nicolas Reyns[4], Firas Kobeissy[6], Claude Alain Maurage[5], Michel Salzet[1], Isabelle Fournier[1]**

(1) Univ. Lille, INSERM U1192, Laboratoire Protéomique, Réponse Inflammatoire et Spectrométrie de Masse (PRISM) F-59000 Lille, France; email address: marie.duhamel@etudiant.univ-lille1.fr, emilie.lerhun@chru-lille.fr, maxence.wisztorski@univ-lille1.fr, fahed.zairi@chru-lille.fr, michel.salzet@univ-lille1.fr, isabelle.fournier@univ-lille1.fr

(2) CHU Lille, Department of Neurosurgery, Neuro-oncology, F-59000 Lille, France; Breast unit, Department of Medical Oncology, Oscar Lambret Center, Lille, France; email address: emilie.lerhun@chru-lille.fr

(3) ONCOLille, Maison Régionale de la Recherche Clinique, F-59000 Lille, France; email address: jean-pascal.gimeno@univ-lille1.fr

(4) CHU Lille, Department of Neurosurgery, F-59000 Lille, France; email address: fahed.zairi@chru-lille.fr, nicolas.reyns@chru-lille.fr

(5) CHU Lille, Pôle Pathologie Biologique, Service Anatomie Pathologique, F-59000 Lille, France; email address: fabienne.escande@chru-lille.fr, claude-alain.maurage@chru-lille.fr

(6) Department of Biochemistry and Molecular Genetics, Faculty of Medicine, American University of Beirut. Department of Psychiatry, Center of Neuroproteomics and Biomarkers Research, University of Florida, Gainesville, FL, USA; email address: firasko@gmail.com

***Co-contributing author**

****Corresponding author**
Pr Isabelle Fournier, U-1192 Inserm, Laboratoire de Protéomique, Réponse Inflammatoire, Spectrométrie de Masse (PRISM), Université de Lille 1, Cité Scientifique, 59655 Villeneuve d'Ascq Cedex, France. Email: **isabelle.fournier@univ-lille1.fr**

ABSTRACT

An integrated diagnosis using molecular features is recommended in the updated World Health Organization (WHO) classification. Our aim was to explore non-targeted molecular classification using MALDI Mass Spectrometry Imaging (MALDI MSI) associated to Microproteomics in order to classify anaplastic glioma by integration of clinical data. We used fresh-frozen tissue sections to perform MALDI MSI of proteins based on their digestion peptides after *in-situ* trypsin digestion of the tissue sections and matrix deposition by micro-spraying. The generated 70 µm spatial resolution image datasets were further processed by individual or global segmentation in order to classify the tissues according to their molecular proteins signature. The clustering gives 3 main distinct groups. Within the tissues the ROIs defined by this groups were used for MicroProteomics by micro-extraction of the tryptic peptides after on-tissue enzymatic digestion. More than 2500 proteins including 22 alternative proteins (AltProt) are identified by the ShotGun Microproteomics. Statistical analysis on the basis on the label free quantification of the proteins shows a similar classification to the MALDI MSI segmentation into 3 groups. Systemic biology performed on each group reveals sub-networks related to neoplasia for group 1, glioma with inflammation for group 2 and neurogenesis for group 3. This demonstrates the interest of these new non-targeted large molecular data based on, bridged MALDI MSI to microproteomics, for tumors classification. This analysis provides new insights into Grade III glioma organization. This specific information could allow a more accurate classification of the biopsies according to the prognosis and the identification of potential new targeted therapeutic options.

KEYWORDS

Anaplastic glioma, WHO classification, Matrix-Assisted Laser Desorption/Ionization Mass Spectrometry Imaging, microproteomics

HIGHLIGHTS

- Unsupervised clustering of MALDI MS Imaging data classifies Grade III gliomas into 3 groups
- Shotgun Tissue microproteomics confirm MALDI MS Imaging clustering.
- MALDI MS Imaging add new information to the histological and molecular features of the 2016 WHO classification and represents a promising new tool that could help in developing precision medicine for glioma

ABBREVIATIONS

A: Astrocytoma; ACN: Acetonitrile; ATRX: Apha-thalassemia/mental retardation syndrome X-linked; CDKN2A: Cyclin-Dependent Kinase Inhibitor 2A; CGH-array: Comparative genomic hybridization; DNA: Deoxyribonucleic acid; EGFR: Epidermal Growth Factor Receptor; F: Female; FDR: False Discovery Rate; FFPE: Formalin-Fixed Paraffin-Embedded; gCIMP: CpG Island Methylator Phenotype; HCD: Higher Energy Collision Dissociation; HES: Hematoxylin Eosin Safran; IDH: Isocitrate Dehydrogenase; LC: Liquid Chromatography; H3F3A: H3 Histone, Family 3A; LESA : Liquid Extraction Surface Analysis ; LFQ: Label Free Quantification; M: Male; MALDI: Matrix-Assisted Laser Desorption/Ionization; MALDI MSI: MALDI Mass Spectrometry Imaging; TOF: Time-of-Flight; MeOH: Methanol; MGMT: O-6-Methylguanine-DNA Methyltransferase; MRI: Magnetic Resonance Imaging; MSI: Mass Spectrometry Imaging; O: Oligodendroglioma; OA: Oligo-astrocytoma; PSM: Peptide Spectrum Matches; PTEN: Phosphatase and Tensin Homolog; ROI: Region of Interest; RNA: Ribonucleic acid; SNEA: Subnetwork Enrichment Analysis; TERT: Telomerase Reverse Transcriptase; TFA: Trifluoroacetic acid; TP53: Tumor Protein P53; WHO: World Health Organization

1. INTRODUCTION

Histological classification and clinical management of gliomas remains challenging. The World Health Organization (WHO) classification is the standard classification for gliomas and is used to guide the clinical management according to the subtypes of tumors. Shortcomings in the prior 2007 WHO classification based on morphological features have been reported [1]. A highly variable clinical outcome was observed between same subtypes of gliomas, and a high intra and interobserver discrepancy between pathologists has been noted [2].

A new update of the WHO classification has recently been published [3]. The goal of these classifications is to provide strong information on the prognosis of patients in a pre-determined subtype of tumors and to guide clinical decisions. The integration of immunohistochemical markers and molecular markers to the standard pathological analysis add objectivity and permits a better prognostic classification by improving the definition of prognostically distinct subtypes of gliomas [1, 4]. In the WHO 2016 classification, grades II or III glioma with a glioblastoma-like profile, including *IDH1/2* wild-type status, frequent gains on 7q and losses on 10q and frequently telomerase reverse transcriptase (TERT) promoter mutations, mostly associated with a glioblastoma, an anaplastic astrocytoma or oligoastrocytoma pathological patterns have usually the worse outcome [1]. Thus, the determination of the presence of a +7q/-10q in patients with *IDH1/2* wild-type WHO grade II and III gliomas is relevant [1]. Tumors with an *IDH1/2* mutation, a 1p/19q codeletion and an oligodendroglial histological subtype have the best prognosis [1, 5, 6]. Most of these tumors show a proneural glioblastoma-like expression profile, associated with a better outcome [1, 7, 8]. Yet *IDH1/2* mutation / CpG island methylator phenotype (gCIMP), 1p/19q co-deletion represent the main molecular features required for a better classification of gliomas [1, 2, 7, 8]. Other biological markers of interest are often added, such as *TERT* promoter mutations, gain on chromosome arm 7q (+7q), loss on chromosome arm 10q (−10q), tumor protein p53 (*TP53*), alpha-thalassemia/mental retardation syndrome X-linked (*ATRX*) gene mutations predominantly found in astrocytomas, phosphatase and tensin homolog (PTEN), and Notch pathway genes mutations or (H3 Histone, Family 3A) H3F3A and BRAF mutations [1, 9-20]. However, their implications and their relevance in refining prognostic information for grade II and grade III gliomas remain to be confirmed [1].

Immunohistochemistry and molecular based classification of glioma have improved the determination of the prognosis and integrated diagnosis should now be required as part of tumor assessment in the clinical practice and help to guide the therapeutic decisions [17, 18, 21, 22]. Although genomic approaches are limited, as some normal, upregulated or mutated genes may not be transcribed [23] and discrepancies have been identified between m-ribonucleic acid (mRNA) and proteomics expression profiles in gliomas [24, 25]. The addition of proteomics findings could as well lead to the discovery of new prognostic information and to a better characterization of tumors subtypes, and may also improve clinical decision making. Over the past years, technological advances have been realized in the proteomics analysis. The proteomics approach gives access to large proteins identification and relative quantification, determination of post-translational modifications and could also help to identify personalized clinical strategies by determining specific molecular pathways and cellular functions [24, 26-30].

In the present study, we aim to investigate Glioma grade III molecular features and classification by non-targeted molecular approach using MALDI MS Imaging (MALDI MSI) and Spatially-Resolved Microproteomics. This is achieved by performing MALDI MSI of trypsin digested protein [31] in order to retrieve proteins distribution within tissues of patients with anaplastic glioma and further non-supervised classification of the molecular data [32]. From such classification, regions of interest (ROIs) are selected for the Spatially-Resolved Shotgun Proteomics [33, 34]. Comparison between proteomics data and histological ones is investigated in order to search concordance or discordance.

2. MATERIALS AND METHODS

2.1. Patient samples and consent

Samples were prospectively collected from histologically confirmed anaplastic glioma recruited between September 2014 and July 2015 at Lille University Hospital, France according the protocol setup for the gliomic study (NCT 02473484). The study adhered to the principles of the Declaration of Helsinki and the Guidelines for Good Clinical Practice. All patients gave written informed consent before enrollment. Patients enrolled in this cohort had all a newly diagnosed anaplastic glioma according to the WHO classification of the central nervous system [3] after

pathological examination by the same pathologist (CAM) in routine practice conditions. Other criteria of inclusion included an age of 18 or more year old, the absence of other prior cancer or of cancer treatment, the absence of genetic disease potentially leading to cancer. Tumors samples were processed within 2 hours after sample extraction in the surgery room to limit the risk of proteins degradation.

2.2. Glioma tissue samples for immunohistochemistry and molecular analyses

2.2.1. Immunohistochemistry analyses

IDH1-R132H mutations, ATRX, protein 53 (P53) and epidermal growth factor receptor (EGFR) statuses were determined by immunohistochemistry on formalin-fixed paraffin-embedded (FFPE) tumor tissue samples. 4 µm sections were labeled in an Ultra automate (Ventana-Roche Tissue Diagnostics, Tucson AZ), after antigen retrieval procedures (ATRX, IDH1 and P53: citrate pH 6.0 ; EGFR: proteinase 2), according to suppliers protocols. A punch of positive control tumor was stained on the same slide for IDH1 labeling (tumor tissue from an IDH1 R132H mutated, non-codeleted, astrocytoma). ATRX was determined as positive when cases with more than 10% positive tumor cells were scored positive (ATRX expression). P53 was considered expressed when 10% or more nuclei were deeply stained, EGFR expression was semi-quantified according to Hirsch score, allowed by comparison to the multiscale control. A multiscale positive control was stained in the same series for EGFR labeling. IDH1 R132H was explored using Diavona clone H09, mouse monoclonal at 1/40 dilution, ATRX using Sigma, ref HPA001906 Rabbit polyclonal, at dilution 1/200 dilution, P53 using Dako, clone DO-7, mouse monoclonal, at 1/100 dilution, and EGFR using Invitrogen, clone 31G7, mouse monoclonal, at 1/20 dilution.

2.2.2. Deoxyribonucleic acid (DNA) extraction and quantification

Molecular analyses were performed on FFPE tissues. The following tests were performed: Comparative genomic hybridization (CGH)-array, O-6-methylguanine-DNA methyltransferase (MGMT) promoter methylation and IDH1/IDH2 mutations. All tissues used for DNA extraction were histologically evaluated to determine the tumor cell content. Only tissue samples with a minimum of tumor cell content of 70% or more were analyzed. DNA extraction from FFPE was performed using the kit QIAamp DNA FFPE Tissue (Qiagen). CGH Profiles were determined using a

SurePrint G3 Human CGH Microarray Kit, 8x60K (Aligent) and the CytoGenomics v2.7 software. The limit of resolution was 1 Mb. Presence of 1p/19q codeletion, gain of chromosome 7, loss of chromosome 10, amplification of the EGFR gene and homozygous deletion of the Cyclin-Dependent Kinase Inhibitor 2A (CDKN2A) gene has been systematically evaluated. Mutations affecting codon 132 of *IHD1* (ref seq NM_005896.2), codon 172 of IDH2 (ref seq NM_ 002168.2) were validated by PCR-sequence Sanger when immunohistochemistry was negative. The MGMT promoter methylation status (CpGs 74-78) was determined after bisulfite treatment by pyrosequencing on a PyroMark Q96 with kit MGMT PyroMark (Qiagen). The presence of a methylation was score positive when a minimum of 8% of methylation was observed.

2.3. MALDI Mass Spectrometry Imaging (MALDI MSI)

2.3.1. Tissue preparation and image acquisition

Twelve micrometers sections were cut using a cryostat (Leica Microsystems, Nanterre, France) to perform tryptic peptides MALDI MSI analysis. These tissue sections were deposited on ITO-coated glass slides (BrukerDaltonics, Bremem, Germany) and dried for 15 min in a desiccator. Several washes were performed to remove as much as possible abundant lipids: (1) 1 minute in 70% ethanol, (2) 1 minute in 100% ethanol, (3) 1 minute in acetone and (4) 30 seconds in chloroform. These two last steps were repeated twice. The tissue was dried between each washing step in a desiccator. Trypsin (60 µg/ml, dissolved in NH_4HCO_3 50 mM) was then micro-sprayed on the tissue surface using an electrospray nebulizer attached to a 500 µL syringe at a flow rate of 180 nL/min. The nebulizer was moved uniformly throughout the tissue surface for 15 min. Incubation was performed using ImagePrep (Bruker Daltonics, Bremen, Germany) by microspraying water heated at 37 °C for 2 hours. The digestion procedure includes 60 cycles, each cycle corresponding to 2s spraying, 180s incubation and 60s drying using the nitrogen flow of the instrument. During all the procedure the Imaprep tank was filled with water at 95°C to maintain a constant humidity atmosphere for digestion improvement. This water as well as the 37°C water used for spraying was replaced every 30 min during the 2H of total digestion procedure. Once digestion was over, matrix deposition was performed using ImagePrep. The used matrix was the solid ionic matrix HCCA/ANI [35]. HCCA/ANI is prepared just before use by acido/basic reaction between the

conventional HCCA matrix and the organic base aniline in a ratio 1:1 equivalent. Briefly, 36 µL of aniline were added to 5 ml of a solution of 10 mg/mL HCCA dissolved in ACN/0.1% TFA aqueous (7:3, v/v). The formation of the organic salt is obtained after a few minutes sonication of the solution. This solution was then loaded into the Imageprep. Uniform deposition of the matrix on the tissue was ensured careful control of the deposition parameters by monitoring scattered light in real-time during all the process through the optical sensor equipping the instrument. A method specially developed for the HCCA/ANI matrix was used. This methods includes 4 steps of spraying cycles with optimized parameters. Briefly, step 1 comprises 5 cycles at 0.1V with 1s spraying, 10s incubation and 180s drying. Step 2 includes 8 cycles at 0.2V including 1.25s spraying, 30s incubation and 120s drying. In step 4, 37 cycles at 0.3V were performed with 1.55 s spraying, 20s incubation and drying monitor according to sensor control (25%). Finally, 3 cycles were realized on step 4 with 2s spray, 20s incubation and 2/3 drying according to sensor control (25%) and 1/3 allow to complete drying. After, HCCA/ANI deposition, the slides were directly transferred to the MS instrument. Images were performed on an Ultraflex II MALDI-TOF/TOF instrument (Bruker Daltonics, Bremen, Germany) upgraded with a smartbeam II solid state laser operating up to 200Hz repetition rate. Mass spectra were acquired in the positive delayed extraction reflectron mode on using 800-4000 m/z range. Recorded spectra were averaged from 400 laser shots per pixel. Images were performed using 70 µm spatial resolution raster.

2.3.2. MALDI MSI data processing and analysis

SCiLS Lab (SCiLS Lab 2015b, SCiLS GmbH) software was used for unsupervised spatial segmentation of anaplastic glioma. MALDI MSI raw data were first imported into SCiLS Lab [36]. Data analysis starts with a preprocessing step of baseline removal using an iterative convolution with sigma 20. A peak picking was realized with a step of alignment and a normalization according to the Total Ion Count applied to every 16^{th} spectrum selecting 100 peaks per spectrum. Afterwards, edge-preserving image denoising was carried out using weak filtering. The resulting denoised data were spatially segmented using the bisecting k means algorithm. Different spatial segmentations were performed. First each tissue (individual segmentation) were segmented separately. Then all the tissues (global segmentation) were segmented together. Briefly, the segmentation algorithm groups

spectra according to similarity of data after features extraction. Results of segmentations were represented on a dendogram, with each branch representing a group of spectra for which a color was attributed to be localized on the resulting molecular image. This gives a segmentation map where regions of distinct molecular composition were color-coded according to the dendogram. For this step five samples were submitted to an individual or a global segmentation. A detailed description of this pipeline can be found in reference [37]. For each region, images of specific mass-to-charge (m/z) ratio of ions were reconstructed. The global spatial segmentation allowed us to determine regions of interest (ROIs). These identified ROIs can then be subjected to on-tissue microdigestion followed by microextraction for proteins identifications.

A classification model was then generated. The first five patients were used as a training group and five new patients were included as a test group. For the training, three groups were created according to the ROIs defined by the spatial segmentation (blue group, brown group and green/orange group). In each group, a total of three regions were selected to establish the classification model. The validation of the model was done using two different regions in each group. Then the generated model was blind tested with the test group.

2.4. Tissue ShotGun Microproteomics

2.4.1. On-tissue LysC-Tryptic microdigestion on tissue

Spatially-resolved microproteomics were realized on the ROIs according to the previously published protocol [34]. Briefly, 20-µm sections were cut using a cryostat (Leica Microsystems, Nanterre, France) and subjected to proteins microdigestion. These tissue sections were deposited on poly-lysine glass slides and dried for 15 minutes in a desiccator. Several washes were performed to remove lipids: (1) 1 minute in 70% ethanol, (2) 1 minute in 100% ethanol, (3) 1 minute in acetone and (4) 30 seconds in chloroform. These two last steps were repeated twice. The tissue was dried between each step of washing in a desiccator. Then, the LysC-trypsin solution (40 µg/ml, diluted in Tris-HCl 50 mM, pH 8.0) was deposited using the piezoelectric microspotter Chemikal Inkjet Printer (CHIP-1000, Shimadzu, CO, Kyoto, Japan). The digestion was performed on a total area of 1 mm^2 made out of a 4 x 4 pitch of micro-spots. Each spot is 200 µm in diameter and correspond to a droplet volume of 100 pL/cycle. Enzyme was spot for 30 min in a row and changed. This was repeated 4

folds in 2H. After enzyme deposition 0.1%TFA was spotted for 25 cycles with 100 pL on each spot /cycle.

2.4.2. Microextraction by Liquid Microjunction

After the microdigestion, the peptides within selected regions of tissue sections (ROIs) were extracted using the TriVersa Nanomate platform (Advion Biosciences Inc., Ithaca, NY, USA) with Liquid Extraction Surface Analysis (LESA) option. Briefly, a volume of solvent was aspirated and deposited onto the digested region and then aspirated again to be dispensed into a low binding tube. Three steps per extraction were done: (1) 0.1% TFA, (2) ACN/0.1% TFA (8:2, v/v), (3) MeOH: 0.1% TFA (7:3, v/v). Two extractions per point were performed to increase quantity of material collected.

2.4.3. NanoLC-MS & MS/MS analysis

After liquid microjunction extraction, collected samples were dried under vacuum, reconstituted with 20 µl of 0.1% TFA solution and subjected desalting using C-18 Ziptip (Millipore, Saint-Quentin-en-Yvelines, France) eluted by 60% ACN and dried under vacuum. Dried samples were reconstituted in 0.1% FA aqueous / ACN (98:2, v/v). The samples were separated by online reversed-phase chromatography using a Thermo Scientific Proxeon Easy nLC 1000 system equipped with a Proxeon trap column (100 µm ID x 2 cm, Thermo Scientific) and a C18 packed-tip column (75 µm ID x 50 cm, Thermo Scientific). Separation was achieved using an increased amount of acetonitrile (5-35% over 100 minutes) at a flow rate of 300 nL/min. Data were acquired on a Thermo Scientific Q-Exactive mass spectrometer set to acquire top 10 MSMS in data-dependent mode. The survey scans were done at a resolving power of 70,000 FWHM (m/z 400), in positive mode and using an AGC target of 3e+6. Default charge state was set at 2, unassigned and +1 charge states were rejected and dynamic exclusion was enabled for 25s. The scan range was set to 300-1600 m/z. For ddMS², the scan range was between 200-2000m/z, 1 microscan was acquired at 17,500 FWHM with an isolation window of 4.0 m/z and a HCD Normalized Collision Energy (NCE) of 30 was used.

2.4.4. Data analysis

All MS data were processed with MaxQuant [38, 39] (Version 1.5.3.30) using the Andromeda [40] search engine. The proteins were identified by searching MS and MS/MS data against the Decoy version of the complete proteome for Homo sapiens in the UniProt database [41] (Release February 2016, 70615 entries) combined with 262 commonly detected contaminants. A second search was also done combining the Human database with an AltORF database previously published [42]. Trypsin specificity was used for digestion mode, with N-terminal acetylation and methionine oxidation selected as variable. We allowed up to two missed cleavages. An initial mass accuracy of 6 ppm was selected for MS spectra, and the MS/MS tolerance was set to 20 ppm for the HCD data. FDR at the peptide spectrum matches (PSM) and protein level was set to 1%. Relative, label-free quantification of the proteins was conducted into Max-Quant using the MaxLFQ algorithm [43] with default parameters. The data sets and Perseus result files used for analysis were deposited at the ProteomeXchange Consortium [44] (http://proteomecentral.proteomexchange.org) via the PRIDE partner repository [44] with the data set identifier PXD004437 (for reviewer access only, Username: reviewer85761@ebi.ac.uk; Password: VgKBKrC2). Analysis of the identified proteins was performed using Perseus software (http://www.perseus-framework.org/) (version 1.5.0.31). The file containing the information from the identification were used and hits from the reverse database, proteins with only modified peptides and potential contaminants were removed. The LFQ intensity was logarithmized (log2(x)). Categorical annotation of the rows was used to define the different group depending on the following: (1) the group (Group 1, Group 2, Group 3) and (2) the patient (case 1, case 2, case 3, case 4 and case 5). Statistical Multiple-sample tests were performed using ANOVA with a FDR of 5%. To evaluate the enrichment of the categorical annotations (Gene Ontology terms and KEGG pathway), Fisher's exact test was performed taking into account the results of the ANOVA for each group. Normalization was achieved using a Z-score with matrix access by rows. Only proteins that were significant by ANOVA were used. Hierarchical clustering was first performed using the Euclidean parameter for the distance calculation, and the average option for linkage in the rows and columns of the trees with a maximum of 300 clusters. Functional annotation and characterization of the identified proteins were performed using PANTHER software (version 9.0, http://www.pantherdb.org) and STRING (version 9.1, http://stringdb.org) [[45] **(Supplementary Table 1 & 2)**

2.4.5. Subnetwork Enrichment Pathway Analyses and statistical Testing

The Elsevier's Pathway Studio version 10.0 (Ariadne Genomics/Elsevier) was used to deduce relationships among differentially expressed proteomics protein candidates using the Ariadne ResNet database [46, 47]. "Subnetwork Enrichment Analysis" (SNEA) algorithm was selected to extract statistically significant altered biological and functional pathways pertaining to each identified set of protein hits among the different groups. SNEA utilizes Fisher's statistical test set to determine if there are nonrandom associations between two categorical variables organized by specific relationship. Integrated Venn diagram analysis was performed using "the InteractiVenn": a web-based tool for the analysis of comlex data sets [48]. See **Supp. Tables 3, 4 and 5** as supplemenatry data for the listed differential pathways

3. RESULTS

3.1 Clinical, pathological and molecular description

Five patients were first analyzed. The median age was 36 years (minimum 27, maximum 45), 3 patients were male. No necrotic aspect was observed on brain MRI, but contrast enhancement was present in all tumors. Tumors included 2 oligoastrocytomas, 2 astrocytomas and 1 oligodendroglioma. IDH1 mutations were observed in 4 samples, 1p/19q codeletion in 2 samples, ATRX was positive in 2 samples, P53 was noted in 2 tumors, EGFR in 3 tumors with a median Hirsch score of 200 (range, minimum 120, maximum 350), and a methylated MGMT promoter was found in 5 samples, with a median percentage of methylation of 32% (range, minimum 14.6%, maximum 64.8%). 7 gain and 10 losses were observed in 1 sample. Initial treatment included surgery (complete resections in 1 case, subtotal resection in 3 cases and partial resection in 1 case), followed by radiation therapy in two cases, by radiation therapy then 6 cycles of temozolomide in one case and by radiation therapy and concomitant/maintenance temozolomide in two cases). Median follow-up time was 14.5 months (range, minimum 9 months, and maximum 19.5 months). Two patients among the 5 analyzed presented with a progression (patients 1 and 3). Only one patient died of disease progression 14.4 months after initial diagnosis after two more lines of treatment for recurrent disease (patient 3). This patient had an IDH1 negative and non 1p/19q codeleted tumor. The clinical characteristics and the results of pathological and molecular analysis are presented in **Table 1**.

Five other patients were then analyzed as a validation cohort. The median age was 40 years (minimum 30, maximum 60), 4 patients were male. As for cases, no necrotic aspect was observed on brain MRI, but contrast enhancement was present in all tumors. Tumors included 2 oligodendrogliomas, 2 astrocytomas and 1 oligoastrocytoma. IDH1 mutations were observed in all the 5 samples, 1p/19q codeletion in only 1 sample, ATRX was expressed in 1 sample, P53 was noted in 3 tumors, EGFR in 5 tumors with a median Hirsch score of 200 (range, minimum 110, maximum 300), and a methylated MGMT promoter was found in 4 samples, with a median percentage of methylation of 23% (range, minimum 13.8%, maximum 47.8%). No 7 gain and 10 loss was observed. Initial treatment included surgery (complete resections in 4 cases and subtotal in 1 case), followed by radiation therapy in two cases, by radiation therapy then 6 cycles of temozolomide in one case and by radiation therapy and concomitant/maintenance temozolomide in four cases). Median follow-up time was 12.5 months (range, minimum 8 months, and maximum 35 months). No progression was observed during the follow-up and all patients are still alive. The clinical characteristics and the results of pathological and molecular analysis are also reported in **Table 1** (validation cohort).

3.2. Histological and molecular studies of the 5 tissue samples in the training cohort

After Hematoxylin Eosin Safran (HES) staining, the tissue was annotated by the pathologist (**Figure 1A**). Necrosis, parenchyma infiltrated by tumor cells, tumor tissues have been delimited by the pathologist (CAM) in each sample before subjected to MALDI MSI analyses. Cases 1 and 3 presented large tumor areas and small necrosis parts whereas in Case 2, necrosis constituted the main part of the tissue sample. Cases 4 and 5 were homogeneous tumor tissues (**Figure 1A**).

The MALDI MS images were generated from trypsin digested tissue sections, thus monitoring proteins through their tryptic peptides. From the raw MALDI MSI data obtained from each tissue sample, individual clustering was then realized (**Figure 1B)** by subjecting resulting spectra of each tissue sample to spatial segmentation. This allows to find out the regions of specific molecular profiles within the tissues. The segmentation map clearly shows discrepancies between classical pathological annotations based on morphological criteria and molecular histology realized by MALDI MSI for certain tissues. In case number 1, three regions of interest (ROIs) are

well delimited on the segmentation map in accordance with the pathological annotations (**Figure 1B).** For case number 2, molecular clustering and pathological annotations revealed mainly the presence of 3 different ROIs as previously defined by the pathologist. However, a fourth ROI is observed with MSI imaging in the necrotic part, sharing molecular characteristics of the region identified as parenchyma region by the pathologist (**Figure 1B).** In case number 3, four ROIs are delimited thanks to MSI imaging while the pathologist only identified two distinct regions. For cases number 4 & 5, the pathologist defined tissue samples as homogeneous tumors, but the MSI data identified heterogeneous samples with 3 different ROIs observed on the segmentation map in both cases (**Figure 1B**).

Individual analyses confirmed the presence of specific ions delimiting these regions (**Figure 1C**). In case number 1, ion at m/z 1952.01 is specific of the tumor region as designed by the pathologist whereas the ion at m/z 1428.17 is specific of the necrosis part. On the other side, ions at m/z 2430.95 and 2608.94 are present in both regions (**Figure 1C)**. For case number 2, m/z 1148.94 ion is specific of the infiltrated parenchyma; when m/z 2043.54 is specific of the tumor region and m/z 1686.27 and 1920.71 are related to the necrosis region (**Figure 1C).** For case number 3, m/z 1149.95 and 1510.72 are specific of the tumor region (**Figure 1C).** In cases number 4 and 5, considered as homogeneous tumors, two regions are identified. These two regions present specific molecular profiles characterized by ions at m/z 1217.92 and 1307.04 for case number 4 and ions at m/z 1499.25 and 1605.44 for case number 5 (**Figure 1C).**

Based on these data, we decided to perform a spatial segmentation of the entire set of samples together in order to compare them to each other's and determine if common features can be found between the different cases (**Figure 1D**). Global segmentation shows that different cases share common molecular features. Indeed, cases number 1 & 4 presented the same molecular similarities and are grouped together (blue root). Green and orange regions are found on the same root and are molecularly very similar, so we decided to group them together. Case number 5 and parts of cases number 2 and 3 belong to the green/orange region. Brown region is on a distinct root and comprise parts of cases number 2 and 3 (**Figure 1D**).

3.3. Tissue microproteomics, protein identification and classification

From these global segmentation results, we could thus identify three molecularly different groups among the grade III tissue samples **(Figure 1D)**. In order to identify the proteins related to each group and in each region of the tissues defined from the MALDI MSI data, we performed microproteomics. For each sample, microextractions were achieved after in-situ on-tissue digestion. For cases number 1, 2, 3 and 5, three different microextractions were performed per tissue (see Figure 1D, 1.1, 1.2 and 1.3, 5.1, 5.2, and 5.3, 22.1, 22.2 and 22.3, 20.1, 20.2 and 20.3 respectively). For case number 4, two microextraction were realized and referenced as 6.1 and 6.2. After extractions, each of the 14 extraction spots were submitted to Shotgun analyses. Proteins with an abundance that was significantly different among the samples were determined according to the MaxQuant and Perseus software. Heat maps were generated from the proteins found to be significant according to ANOVA test using a significance threshold of $P<0.05$ (**Figure 2A**). More than 2500 proteins were identified combining all analyses (**Suppl. Table 1**). Hierarchical clustering revealed two main branches, separating cases number 1 and 4 (corresponding to the blue region) from the other ones **(Figure 2A**). Cases number 2, 3 and 5 were molecularly closer as they belonged to the same branch of the heat map. This branch is then divided into samples 5.2, 5.3 and 22.3 (corresponding to the brown region) for one part and samples 20.1, 20.2, 20.3, 5.1, 22.1 and 22.2 (corresponding to the green/orange region) for the other part (**Figure 2A**) which can be associated to green/orange regions. This classification based on the proteins up or down regulation expressions profiles,is well in line with the classification obtained by clustering of the MALDI MSI data (**Figure 1D**). Indeed, MALDI MSI classified cases number 1 and 4 together and cases number 2, 3 and 5 together. These three last samples are molecularly heterogeneous because different regions are found within each tissue separating points 5.2, 5.3 and 22.3 and 5.1, 20.1, 20.2, 20.3, 22.1 and 22.2 (**Figure 1D**). We decided to classify samples 5.1, 20.1, 20.2, 20.3, 22.1 and 22.2 together because they belong to the same branch of the tree. They are molecularly closed based on the spatial segmentation.

Thus, to simplify the denomination of each group, we named them Group 1, Group 2 and Group 3. Extraction spots 1.1, 1.2, 1.3, 6.1 and 6.2 belong to Group 1. Group 2 corresponds to extraction points 5.2, 5.3 and 22.3. Group 3 is constituted by extraction spots 20.1, 20.2, 20.3, 5.1, 22.1 and 22.2 (**Figure 2A**). Considering the overexpressed proteins, 386 proteins are overexpressed in Group 1, 198 in Group 2

and 315 in Group 3. The overexpressed proteins specific to each of these 3 clusters are listed in **Suppl. Table 2.** Comparison of the biological process and molecular functions of the three groups showed that Group 1 was in majority involved in metabolic process, binding and catalytic activity **(Figure 2B**) and included specific proteins such as chaperones and nucleic acid binding proteins (**Figure 2C)**. String network analysis reveals two major clusters *i.e.* RNA splicing and proteins localized in endoplasmic reticulum; and RNA catabolic process (**Figure 2D**). Several proteins are of particular interest due to their involvement in glioma and tumor cell growth promotion e.g. BAG family molecular chaperone regulator 3 (BAG3), Hematopoietic lineage cell-specific protein (HS1), Leukotriene A-4 hydrolase (LTA4H), Programmed cell death 6-interacting protein (PDC6IP), Pre-B-cell leukemia transcription factor-interacting protein 1 (PBXIP1). Group 2 is found to be specifically involved in reproduction biological functions but also in developmental, cellular and metabolic processes (**Figure 2B**). For protein class, proteins in group 2 are more involved in cytoskeleton and hydrolase (**Figure 2C**). No specific cluster can be observed with String analysis for this group (**Supp. Figure1**). Interestingly, some of the proteins identified have ever been described in Glioma such as Lethal (2) giant larvae protein homolog 1 (LLGL1), MTSS1-like protein (MTSS1L), Shootin-1 (KIAA1598), LanC-like protein 1 (LANC1). By contrast, Isocitrate dehydrogenase [NADP] cytoplasmic (IDH1, IDH2), Breast carcinoma-amplified sequence 1 (BCAS1), Optineurin (OPTN), WD repeat-containing protein 44 (WDR44) are overexpressed in group 2 and are proteins known to play a key role in aggressive glioma (**Supp. Data 2**). For group 3, binding, receptor activity, metabolic activity are the most important modulated functions (**Figure 2B**). String analysis confirms the presence of two clusters one being related to metabolic process and the other one to endocytosis (**Supp. Figure 2**). IDH3, IDH3A, IDH3G, Neural cell adhesion molecule L1-like protein (CHL1) Disks large homolog (DLG1, DLG2, Neuronal growth regulator 1 (NGR1), Rho-associated protein kinase 2 (ROCK2) Neural cell adhesion molecule L1 (L1CAM), Tumor protein D52 (TDP52) are overexpressed in group 3 and known to be involved in glioma.

Systemic biology analysis was then performed on the overexpressed proteins of each group (**Figure 3**)**.** Differential distribution of unique & common/intersected biological and functional pathways among the three different groups (Groups 1, 2 and 3) are depicted in **Figure 3 (3A, 3B, 3C).** Unique statistical significant pathways were identified including 61 pathways (group 3); 43 pathways (group 2); 58 pathways

(Group 1) (Please refer to **Suppl. Tables 6, 7, and 8** for the identity of each of the unique pathways.). Combined differential pathways were analyzed across the three groups. 17 pathways were shared between groups 2 & 3, 20 pathways were shared between groups 2 & 1, and 2 pathways were shared between groups 1 & 3. 20 pathways were shared among the groups 1, 2 & 3. Please refer **to Suppl. Table 9 & 10** for the pathways identity, implicated proteins and the specific P value of each of the unique pathways. Integrated Venn diagram analysis was performed using "the InteractiVenn": a web-based tool for the analysis of comlex data sets [48]. See **Supp. Tables 3, 4 and 5** as supplemenatry data for the listed differential pathways. Overexpressed proteins in group 1 (**Figure 3A**) are involved in neoplasia, innate immune response, autophaghy, response to oxydative stress, mRNA metabolism, protein folding, spliceosome, regulation of translation which is line with neoplasia and necrosis. For group 2 (**Figure 3B**), the subnetwork is mainly glioma, inflammation, microglia activation, neoplasma and metastasis, cell migration, motility, microtubule cytoskeleton assembly which is line with aggressive glioma. For group 3 (**Figure 3C)**, the pattern is more related to nerve cell differenciation, neurite outgrowth, axon guidance, filopodia formation, secretory pathway which is line with neuronal stem cells profile.

We therefore characterized each group thanks to its protein expression profiles. Group 1 is mainly associated to neoplasia showing many proteins involved in tumor cell growth. Group 1 corresponds to aggressive tumor. Group 2 regroupsmany proteins involved in inflammation and metastasis. Group 3 has a neuronal stem cell profile with proteins specific to nerve cell differenciation and neurite outgrowth.

3.4 Validation test and association to clinical data

In order to validate the classification obtained with the first set of 5 samples (training group), a blind set of 5 samples (case 6 to case 10) were tested. Peptides images were performed with MALDI MSI followed by segmentation. 5 regions in each of the groups defined by the classification obtained on the training groups were used to build classification model (**Figure 4A, Top**). This model was applied to the 5 next samples conserved for blind tests (**Figure 4A, Bottom**). As a result, cases number 6 (a part), 8 and 10 (a part) are classified within group 1 as confirmed by the distribution of ions at m/z 1599.218 and 2281.756 which are found in cases 1, 4, 8 and partially in 6 and in 10 (**Figure 4B**). Case number 9 is very similar to the large

area brown area of case number 2 and therefore belongs to group 2. Ions at m/z 1155.958 and 1433.345 confirm the similarity of cases number 2 and 9 **(Figure 4B**). Group 3 regroups cases number 5, 7 with a part of cases number 2, 3, 6 and 9. Ions at m/z 1149.785 and 1540.143 were specific of this group **(Figure 4B**). From these data, we can conclude that group 1 regroups cases number 1, 4, 8, part of 6 and part of 10. Groups 2 and 3 were difficult to separate completely due to the fact that some parts of the tissues belong to one group and other to another group. However, we previously observed on the heat map and on the global segmentation that these two groups were molecularly very close (**Figure 1D and 2A**). Thus, taking into account this point, the two groups can be merged as a single group that will be named as "group 2" which is divided into two sub-groups. Thus, Cases 2, 3, 5, 7, part of 6 and part of 9 belonged to group 2.

Then, a complete unsupervised segmentation using the 10 samples was realized (**Figure 4C)**. From this segmentation only two main groups can be deduced. The first regroups cases number 1, 4, 8 and 10 (deep and light blue). The second one regroups cases number 2, 3, 5 and 7 (red, orange and brown). Cases number 6 and 9 are more difficult to classify, the tissues presenting molecular signatures characteristic of both groups.

Taken into account these two groups, we searched which proteins were only expressed in each of these groups in order to find potential biomarkers (**Table 2**). Sixteen protein have been detected in group 1 *i.e.* HLA-DRA, Destrin (DSTN), CD74, Glucosidase alpha acid (GAA), P450 oxydoreductase (POR), Ribosomal Protein L12 (RPL12), Scaffold attachment factor B2 (SAFB2), Poly(A) binding protein nuclear 1 (PABPN1),CDC5 cell division cycle 5-like (CDC5L), Golgy reassembly stacking protein 2 (GORASP2), Golgi integral membrane protein 4 (GOLIM4), Ribophorin II (RPN2), Nidogen 1 (NID1), chromobox homolog 5 (CBX5), Aspartate beta-hydrolase (ASPH) (**Table 2**). Group 2 contains Myelin basic protein (MBP), CYBRD1, Small VCP:p97 intracting protein (SVIP), Ermin (ERMN), Anillin (ANLN), Oligodendrocytic myelin paranormal and inner loop protein (OPALIN), Glycolipid transfer protein (GLTP), Hyaluronan and proteoglycan link protein 2 (HAPLN2), MAP6 domain containg 1 (MAP6D1), CD9, Glycerol-3 phosphatase dehydrogenase-1 (GPD1), ectonucleotide gyrophosphatase/phosphodiesterase 6 (ENPP6), Mysoin (MYO1D), Dynein cytoplasmic 1 intermediate chain 1 (DYNC1I1) (**Table 2**).

Even though the patient cohort remains limited and is not large enough to properly reflect the new WHO classification markers (only 1 case IDH1 negative), a first comparison between the MALDI MSI/proteomics data shows that a correlation cannot be directly drawn. Indeed, Group 1 regroups cases 1, 4, 8, and 10. Out of these 4 cases, it can be retrieved from the clinical data that 4 have ATRX loss, 3 are EGRF positive, 4 are P53 positive, 3 are IDH1 positive and 4 have no 1p/19q codeletion. All are MGMT 5 methylated. 3 on the 5 have on chromosomes 7 and 10 abnormalities i.e. 2 are 7p gain and 10p gain, one 7 loss and 1 no abnormalities. For Group 2, including cases 2, 3,5 and 7, 3 have ATRX expressed, 3 P53 negative, 2 have 1p:19q codeletion and 2 no. All are MGMT methylated and IDH1 positive. For chromosome 7 and 10, 3 have no abnormalities. Cases 6 and 9 present a mixed up of the two other groups. Case 6 is negative in immunocytochemistry but the molecular analysis confirm the presence of IDH1 mutation. It is ATRX loss, P53 negative, no codeletion 1p/19q and is EGRF positive. It has no MGMT methylation and have chromosome 7 loss. Case 9 is IDH1 positive. It present 1p/19q codeletion. It expressed ATRX, MGMT methylation and no chromosoem7 and 10 abnormalities. It must be noticed that the molecular data are only reported for defined targets when our approach is performed on large scale data. Moreover, the proteomics data are collected in different parts of the tissue for tissues showing a heterogeneous profile when the biological data are only confirmed as present or absent for a tissue. It is also important to notice that no correlation are found between the MSI/Proteomics classification and the histological one.

4. DISCUSSION

Previous proteomics studies have been reported on Glioma. These include a large panel of different studies based of different methodologies and including profiles determined from glioma cell lines [49-51], animal models [49-52], patients fluids [50, 51, 53] and patients samples [50, 51, 53-59] . To date, mainly two methodologies were used for such glioma proteomics studies namely gel-based protein profiling ([56, 57, 59] and quantitative proteomics [55, 60-63]. However, none of these previous studies used MALDI MSI methodology coupled to label-free tissue microproteomics [33, 34, 64]. The MALDI MSI methodology authorizes molecular imaging of different classes of biomolecules obtained from tissue samples without requiring antibodies, tagged or labeled probes [31]. Here we were interested by evaluating the classification resulting from the non-supervised analysis using MALDI MSI data of proteins and compare this to the pathologist annotation and the patients

molecular data. Microproteomics was combined to the non-supervised clustering to evaluate the observation of specific su-signaling pathways and retrieve corresponding biomarkers. A set of five grade III glioma samples were thus analyzed by MALDI MSI looking to the digestion peptides of proteins followed by individual and global non-supervised hierarchical clustering. In our study, molecular discrepancies were identified between annotations of the neuropathologist and the molecular histology done by MALDI MSI, with more regions of interest identified by the MALDI MSI analysis. Indeed, based on the WHO classification, some samples are categorized as homogeneous tumors whereas MALDI MSI data clearly state that the tumor is molecularly heterogeneous. This point confirms the fact that MALDI MSI can be a tool for helping pathologists to confirm their diagnoses. The global clustering of the five samples revealed three groups of different molecular profiles. Proteins up- and down-regulated or specific to these groups were further identified by Shotgun tissue Microproteomics. Proteins identified in group 1 are in majority involved in metabolic process, binding and catalytic activity. This was confirmed by systemic biology analysis. All pathways are involved in neoplasia, innate immune response, autophagy, response to oxidative stress, mRNA metabolism, protein folding, spliceosome, and regulation of translation. Part of the proteins identified within this group were also found in the study of Polisetty *et al.* where differentially expressed proteins in anaplastic astrocytoma were mainly associated to mRNA processing [54]. Group 2 is specifically involved in reproduction biological functions but also in developmental, cellular and metabolic processes. The pathways analysis confirms that this group is mainly involved in glioma pathology, inflammation, microglia activation, neoplasm and metastasis, cell migration, motility and microtubule cytoskeleton assembly. Microglia/macrophages infiltration has previously been reported in glioma and these cells are responsible for the chemoresistance, metastasis and tumor progression [65-67]. Group 3 is more related to with nerve cell differentiation, neurite outgrowth, axon guidance, filopodia formation and secretory pathway.

Then, validation of the classification was realized by using 5 blind samples with MALDI MSI. They were classified into two main groups i.e. group 1 and a merge of group 2 and group 3. This classification was validated by the segmentation performed on the 10 samples. Despite only a few samples were evaluated in this study, some common molecular features were shared between samples among the

proteomics subgroups. Group 1 is constituted by specific proteins involved in major histocompatibility complex, mRNA formation, DNA and histone H3 binding, cell trafficking in Golgi apparatus, metabolism, cell cycle and cell attachment. CD74 and HLA-DR are linked to macrophages or microglia tumour infiltration [68]. Expression of CD74 in high grade glioma is associated with resistance to temozolomide treatment [69]. GORASP2, GOLIM4, CD74, and HLA-DR have recently been identified in glioblastoma membrane proteomic study [63]. RNP2, as well as CBX5, are considered as markers of glioma and seem to be therapeutic targets [70, 71]. Considering SAFB2, PABPN1, CDC5L, these proteins are involved in RNA splicing and recently in non-coding RNA turn-over [72-74]. Group 2 contains proteins known to be implicated in glioma like Ermin, HAPLN2, MAP6D1, ENPP6, DYNC1I1, MBP [75] Moreover. Anillin, OPALIN and GPD1 are markers of glioma stem cells [76]. In conclusion, we demonstrated that the use of MALDI MSI combined to microproteomics may allow the generation of tumors classification associated to the identification of specific signaling pathways and set of potential markers. In this first study on 10 grade III glioma patients we show that the classification allow for two main groups to be distinguished. First data demonstrate that a direct comparison to the molecular and clinical data is not straightforward. MALDI MSI/proteomics data do not seem to show correlation with the histological type which is in line with the recently rebuilt of the classification based on the molecular data. Correlation with molecular data is not immediate and would necessitate a larger patient cohort to be investigated. This will also require the development of bioinformatics tools that can cope with the integration of clinical, histological, targeted molecular data to our large scale non-targeted proteomics data.

Nevertheless, this study is prospective and this approach needs to be realized on a larger cohort of patients where we will be able to correlate proteomics data to genomic data. However some interesting points can still be drawn. In fact group 1 integrates several proteins link to RNA Splicing, mRNA expression and regulation of specific transcripts but also on long noncoding RNAs (lncRNAs) turnover. This can be associated to the presence of several alternative proteins issued from alternative ORF [42]. We detect using our in silico AltORF databank, 22 alternative proteins in the whole of the proteomics data without correspondence with known human proteins and specific AltProt of each Group was also detected (**Table 3**). Such alternative

proteins can be useful for diagnosis and prognosis and need to be investigated in this way.

By identifying protein expression, proteomics analysis may add new information to improve the classification of gliomas and to identify novel potential therapeutic targets. This kind of analysis can provide new candidate biomarkers and can improve the knowledge of glioma biology. Our results need further validation on a larger prospective cohort of gliomas with various IDH and 1p19q codeletion statuses.

ACKNOWLEDGEMENTS

This research was supported by grants from the Ministère de L'Education Nationale, de L'Enseignement Supérieur et de la Recherche, ANR (IF), the Université de Lille (MD), Métropole Européenne de Lille (MD), SIRIC ONCOLille (IF, MD), Grant INCa-DGOS-Inserm 6041aa, and INSERM. We would like to thank Sylvie Janas and the Tumorothèque Régionale of Nord Pas de Calais. We also would like to thank Prof. Xavier Roucou (Université deSherbrooke, Canada) for supplying the library of alternative proteins.

CONTRIBUTIONS

ELR: conception and design, data acquisition, data analysis, manuscript writing, final approval

MD: conception and design, data acquisition, data analysis, manuscript writing, final approval

MW: conception and design, data acquisition, data analysis, manuscript writing, final approval

FZ: data acquisition, manuscript writing, final approval

FE: conception and design, data acquisition, manuscript writing, final approval

CAM: conception and design, data acquisition, data analysis, manuscript writing, final approval

NR: conception and design, data acquisition, data analysis, manuscript writing, final approval

FK: data analysis, manuscript writing, final approval

MS: conception and design, data acquisition, data analysis, manuscript writing, final approval

IF: conception and design, data acquisition, data analysis, manuscript writing, final approval

COMPETING FINANCIAL INTERESTS

The authors declare no Competing Financial Interests

REFERENCES

[1] M. Weller, R.G. Weber, E. Willscher, V. Riehmer, B. Hentschel, M. Kreuz, J. Felsberg, U. Beyer, H. Loffler-Wirth, K. Kaulich, J.P. Steinbach, C. Hartmann, D. Gramatzki, J. Schramm, M. Westphal, G. Schackert, M. Simon, T. Martens, J. Bostrom, C. Hagel, M. Sabel, D. Krex, J.C. Tonn, W. Wick, S. Noell, U. Schlegel, B. Radlwimmer, T. Pietsch, M. Loeffler, A. von Deimling, H. Binder, G. Reifenberger, Molecular classification of diffuse cerebral WHO grade II/III gliomas using genome- and transcriptome-wide profiling improves stratification of prognostically distinct patient groups, Acta Neuropathol, 129 (2015) 679-693.

[2] M.J. van den Bent, Interobserver variation of the histopathological diagnosis in clinical trials on glioma: a clinician's perspective, Acta neuropathologica, 120 (2010) 297-304.

[3] D.N. Louis, H. Ohgaki, O.D. Wiestler, W.K. Cavenee, P.C. Burger, A. Jouvet, B.W. Scheithauer, P. Kleihues, The 2007 WHO classification of tumours of the central nervous system, Acta neuropathologica, 114 (2007) 97-109.

[4] W. Wick, M. Weller, [Anaplastic glioma. Neuropathology, molecular diagnostics and current study concepts], Nervenarzt, 81 (2010) 928-930, 932-925.

[5] N. Hata, S.O. Suzuki, H. Murata, R. Hatae, Y. Akagi, Y. Sangatsuda, T. Amano, K. Yoshimoto, T. Tahira, M. Mizoguchi, Genetic analysis of a case of glioblastoma with oligodendroglial component arising during the progression of diffuse astrocytoma, Pathol Oncol Res, 21 (2015) 839-843.

[6] K. Fukuoka, T. Yanagisawa, Y. Watanabe, T. Suzuki, M. Shirahata, J. Adachi, K. Mishima, T. Fujimaki, M. Matsutani, S. Wada, A. Sasaki, R. Nishikawa, Brainstem oligodendroglial tumors in children: two case reports and review of literatures, Childs Nerv Syst, 31 (2015) 449-455.

[7] L.A. Cooper, D.A. Gutman, Q. Long, B.A. Johnson, S.R. Cholleti, T. Kurc, J.H. Saltz, D.J. Brat, C.S. Moreno, The proneural molecular signature is enriched in oligodendrogliomas and predicts improved survival among diffuse gliomas, PloS one, 5 (2010) e12548.

[8] A. Idbaih, A. Omuro, F. Ducray, K. Hoang-Xuan, Molecular genetic markers as predictors of response to chemotherapy in gliomas, Current opinion in oncology, 19 (2007) 606-611.

[9] P.J. Killela, C.J. Pirozzi, Z.J. Reitman, S. Jones, B.A. Rasheed, E. Lipp, H. Friedman, A.H. Friedman, Y. He, R.E. McLendon, The genetic landscape of anaplastic astrocytoma, Oncotarget, 5 (2014) 1452-1457.

[10] P.J. Killela, C.J. Pirozzi, P. Healy, Z.J. Reitman, E. Lipp, B.A. Rasheed, R. Yang, B.H. Diplas, Z. Wang, P.K. Greer, Mutations in IDH1, IDH2, and in the TERT promoter define clinically distinct subgroups of adult malignant gliomas, Oncotarget, 5 (2014) 1515-1525.

[11] Y. Jiao, P.J. Killela, Z.J. Reitman, B.A. Rasheed, C.M. Heaphy, R.F. de Wilde, F.J. Rodriguez, S. Rosemberg, S.M. Obashinjo, S.K.N. Marie, Frequent ATRX, CIC, FUBP1 and IDH1 mutations refine the classification of malignant gliomas, Oncotarget, 3 (2012) 709-722.

[12] B. Wiestler, D. Capper, T. Holland-Letz, A. Korshunov, A. von Deimling, S.M. Pfister, M. Platten, M. Weller, W. Wick, ATRX loss refines the classification of anaplastic gliomas and identifies a subgroup of IDH mutant astrocytic tumors with better prognosis, Acta neuropathologica, 126 (2013) 443-451.

[13] G. Cairncross, M. Wang, E. Shaw, R. Jenkins, D. Brachman, J. Buckner, K. Fink, L. Souhami, N. Laperriere, W. Curran, Phase III trial of chemoradiotherapy for anaplastic oligodendroglioma: long-term results of RTOG 9402, Journal of Clinical Oncology, 31 (2013) 337-343.

[14] G. Cairncross, B. Berkey, E. Shaw, R. Jenkins, B. Scheithauer, D. Brachman, J. Buckner, K. Fink, L. Souhami, N. Laperierre, Phase III trial of chemotherapy plus radiotherapy compared with radiotherapy alone for pure and mixed anaplastic oligodendroglioma: Intergroup Radiation Therapy Oncology Group Trial 9402, Journal of Clinical Oncology, 24 (2006) 2707-2714.

[15] M. Weiler, W. Wick, Molecular predictors of outcome in low-grade glioma, Current opinion in neurology, 25 (2012) 767-773.

[16] X.-Y. Liu, N. Gerges, A. Korshunov, N. Sabha, D.-A. Khuong-Quang, A.M. Fontebasso, A. Fleming, D. Hadjadj, J. Schwartzentruber, J. Majewski, Frequent ATRX mutations and loss of expression in adult diffuse astrocytic tumors carrying IDH1/IDH2 and TP53 mutations, Acta neuropathologica, 124 (2012) 615-625.

[17] D.E. Reuss, F. Sahm, D. Schrimpf, B. Wiestler, D. Capper, C. Koelsche, L. Schweizer, A. Korshunov, D.T. Jones, V. Hovestadt, ATRX and IDH1-R132H immunohistochemistry with subsequent copy number analysis and IDH sequencing as a basis for an “integrated” diagnostic approach for adult

astrocytoma, oligodendroglioma and glioblastoma, Acta neuropathologica, 129 (2015) 133-146.

[18] J.E. Eckel-Passow, D.H. Lachance, A.M. Molinaro, K.M. Walsh, P.A. Decker, H. Sicotte, M. Pekmezci, T. Rice, M.L. Kosel, I.V. Smirnov, Glioma groups based on 1p/19q, IDH, and TERT promoter mutations in tumors, New England Journal of Medicine, 372 (2015) 2499-2508.

[19] D. Rohle, J. Popovici-Muller, N. Palaskas, S. Turcan, C. Grommes, C. Campos, J. Tsoi, O. Clark, B. Oldrini, E. Komisopoulou, An inhibitor of mutant IDH1 delays growth and promotes differentiation of glioma cells, Science, 340 (2013) 626-630.

[20] M. Weller, R. Stupp, G. Reifenberger, A.A. Brandes, M.J. van den Bent, W. Wick, M.E. Hegi, MGMT promoter methylation in malignant gliomas: ready for personalized medicine?, Nat Rev Neurol, 6 (2010) 39-51.

[21] D.N. Louis, A. Perry, P. Burger, D.W. Ellison, G. Reifenberger, A. Deimling, K. Aldape, D. Brat, V.P. Collins, C. Eberhart, International Society of Neuropathology-Haarlem consensus guidelines for nervous system tumor classification and grading, Brain pathology, 24 (2014) 429-435.

[22] M. Weller, S.M. Pfister, W. Wick, M.E. Hegi, G. Reifenberger, R. Stupp, Molecular neuro-oncology in clinical practice: a new horizon, Lancet Oncol, 14 (2013) e370-379.

[23] K. Krapfenbauer, E. Engidawork, N. Cairns, M. Fountoulakis, G. Lubec, Aberrant expression of peroxiredoxin subtypes in neurodegenerative disorders, Brain research, 967 (2003) 152-160.

[24] R.F. Deighton, T. Le Bihan, S.F. Martin, A.M. Gerth, M. McCulloch, J.M. Edgar, L.E. Kerr, I.R. Whittle, J. McCulloch, Interactions among mitochondrial proteins altered in glioblastoma, Journal of neuro-oncology, 118 (2014) 247-256.

[25] O. Persson, U. Brynnel, F. Levander, B. Widegren, L.G. Salford, M. Krogh, Proteomic expression analysis and comparison of protein and mRNA expression profiles in human malignant gliomas, PROTEOMICS-Clinical Applications, 3 (2009) 83-94.

[26] A.A. Khalil, Biomarker discovery: a proteomic approach for brain cancer profiling, Cancer science, 98 (2007) 201-213.

[27] J.-M. Lemée, E. Com, A. Clavreul, T. Avril, V. Quillien, M. De Tayrac, C. Pineau, P. Menei, Proteomic analysis of glioblastomas: what is the best brain control sample?, Journal of proteomics, 85 (2013) 165-173.

[28] J. Kalinina, J. Peng, J.C. Ritchie, E.G. Van Meir, Proteomics of gliomas: initial biomarker discovery and evolution of technology, Neuro-oncology, 13 (2011) 926-942.

[29] S.P. Niclou, F. Fack, U. Rajcevic, Glioma proteomics: status and perspectives, Journal of proteomics, 73 (2010) 1823-1838.

[30] S. Khaghani-Razi-Abad, M. Hashemi, M. Pooladi, M. Entezari, E. Kazemi, Proteomics analysis of human oligodendroglioma proteome, Gene, 569 (2015) 77-82.

[31] J. Franck, K. Arafah, M. Elayed, D. Bonnel, D. Vergara, A. Jacquet, D. Vinatier, M. Wisztorski, R. Day, I. Fournier, M. Salzet, MALDI imaging mass spectrometry: state of the art technology in clinical proteomics, Mol Cell Proteomics, 8 (2009) 2023-2033.

[32] D. Bonnel, R. Longuespee, J. Franck, M. Roudbaraki, P. Gosset, R. Day, M. Salzet, I. Fournier, Multivariate analyses for biomarkers hunting and validation through on-tissue bottom-up or in-source decay in MALDI-MSI: application to prostate cancer, Anal Bioanal Chem, 401 (2011) 149-165.

[33] M. Wisztorski, B. Fatou, J. Franck, A. Desmons, I. Farre, E. Leblanc, I. Fournier, M. Salzet, Microproteomics by liquid extraction surface analysis: application to FFPE tissue to study the fimbria region of tubo-ovarian cancer, Proteomics Clin Appl, 7 (2013) 234-240.

[34] J. Quanico, J. Franck, C. Dauly, K. Strupat, J. Dupuy, R. Day, M. Salzet, I. Fournier, M. Wisztorski, Development of liquid microjunction extraction strategy for improving protein identification from tissue sections, J Proteomics, 79 (2013) 200-218.

[35] R. Lemaire, D. Wisztorski, M. Hendra, Exploring direct analysis using ionic matrices, Proceedings of 53rd ASMS conference on Mass Spectrometry, San Antonio, Texas, June 5, 9 (2005).

[36] H. Thiele, S. Heldmann, D. Trede, J. Strehlow, S. Wirtz, W. Dreher, J. Berger, J. Oetjen, J.H. Kobarg, B. Fischer, P. Maass, 2D and 3D MALDI-imaging: conceptual strategies for visualization and data mining, Biochim Biophys Acta, 1844 (2014) 117-137.

[37] T. Alexandrov, M. Becker, S.O. Deininger, G. Ernst, L. Wehder, M. Grasmair, F. von Eggeling, H. Thiele, P. Maass, Spatial segmentation of imaging mass

spectrometry data with edge-preserving image denoising and clustering, J Proteome Res, 9 (2010) 6535-6546.

[38] S. Tyanova, T. Temu, A. Carlson, P. Sinitcyn, M. Mann, J. Cox, Visualization of LC-MS/MS proteomics data in MaxQuant, Proteomics, 15 (2015) 1453-1456.

[39] J. Cox, M. Mann, MaxQuant enables high peptide identification rates, individualized p.p.b.-range mass accuracies and proteome-wide protein quantification, Nat Biotechnol, 26 (2008) 1367-1372.

[40] J. Cox, N. Neuhauser, A. Michalski, R.A. Scheltema, J.V. Olsen, M. Mann, Andromeda: a peptide search engine integrated into the MaxQuant environment, J Proteome Res, 10 (2011) 1794-1805.

[41] C. UniProt, UniProt: a hub for protein information, Nucleic Acids Res, 43 (2015) D204-212.

[42] B. Vanderperre, J.F. Lucier, C. Bissonnette, J. Motard, G. Tremblay, S. Vanderperre, M. Wisztorski, M. Salzet, F.M. Boisvert, X. Roucou, Direct detection of alternative open reading frames translation products in human significantly expands the proteome, PLoS One, 8 (2013) e70698.

[43] J. Cox, M.Y. Hein, C.A. Luber, I. Paron, N. Nagaraj, M. Mann, Accurate proteome-wide label-free quantification by delayed normalization and maximal peptide ratio extraction, termed MaxLFQ, Mol Cell Proteomics, 13 (2014) 2513-2526.

[44] J.A. Vizcaino, E.W. Deutsch, R. Wang, A. Csordas, F. Reisinger, D. Rios, J.A. Dianes, Z. Sun, T. Farrah, N. Bandeira, P.A. Binz, I. Xenarios, M. Eisenacher, G. Mayer, L. Gatto, A. Campos, R.J. Chalkley, H.J. Kraus, J.P. Albar, S. Martinez-Bartolome, R. Apweiler, G.S. Omenn, L. Martens, A.R. Jones, H. Hermjakob, ProteomeXchange provides globally coordinated proteomics data submission and dissemination, Nat Biotechnol, 32 (2014) 223-226.

[45] D. Szklarczyk, A. Franceschini, M. Kuhn, M. Simonovic, A. Roth, P. Minguez, T. Doerks, M. Stark, J. Muller, P. Bork, L.J. Jensen, C. von Mering, The STRING database in 2011: functional interaction networks of proteins, globally integrated and scored, Nucleic Acids Res, 39 (2011) D561-568.

[46] A. Bonnet, S. Lagarrigue, L. Liaubet, C. Robert-Granie, M. Sancristobal, G. Tosser-Klopp, Pathway results from the chicken data set using GOTM, Pathway Studio and Ingenuity softwares, BMC proceedings, 3 Suppl 4 (2009) S11.

[47] A. Yuryev, E. Kotelnikova, N. Daraselia, Ariadne's ChemEffect and Pathway Studio knowledge base, Expert opinion on drug discovery, 4 (2009) 1307-1318.

[48] H. Heberle, G.V. Meirelles, F.R. da Silva, G.P. Telles, R. Minghim, InteractiVenn: a web-based tool for the analysis of sets through Venn diagrams, BMC Bioinformatics, 16 (2015) 169.

[49] T. Bock, H. Moest, U. Omasits, S. Dolski, E. Lundberg, A. Frei, A. Hofmann, D. Bausch-Fluck, A. Jacobs, N. Krayenbuehl, M. Uhlen, R. Aebersold, K. Frei, B. Wollscheid, Proteomic analysis reveals drug accessible cell surface N-glycoproteins of primary and established glioblastoma cell lines, J Proteome Res, 11 (2012) 4885-4893.

[50] J. Kalinina, J. Peng, J.C. Ritchie, E.G. Van Meir, Proteomics of gliomas: initial biomarker discovery and evolution of technology, Neuro Oncol, 13 (2011) 926-942.

[51] S.P. Niclou, F. Fack, U. Rajcevic, Glioma proteomics: status and perspectives, J Proteomics, 73 (2010) 1823-1838.

[52] R. Ait-Belkacem, C. Berenguer, C. Villard, L. Ouafik, D. Figarella-Branger, O. Chinot, D. Lafitte, MALDI imaging and in-source decay for top-down characterization of glioblastoma, Proteomics, 14 (2014) 1290-1301.

[53] P. Gautam, S.C. Nair, M.K. Gupta, R. Sharma, R.V. Polisetty, M.S. Uppin, C. Sundaram, A.K. Puligopu, P. Ankathi, A.K. Purohit, G.R. Chandak, H.C. Harsha, R. Sirdeshmukh, Proteins with altered levels in plasma from glioblastoma patients as revealed by iTRAQ-based quantitative proteomic analysis, PLoS One, 7 (2012) e46153.

[54] R.V. Polisetty, P. Gautam, M.K. Gupta, R. Sharma, M.S. Uppin, S. Challa, P. Ankathi, A.K. Purohit, D. Renu, H.C. Harsha, A. Pandey, R. Sirdeshmukh, Heterogeneous nuclear ribonucleoproteins and their interactors are a major class of deregulated proteins in anaplastic astrocytoma: a grade III malignant glioma, J Proteome Res, 12 (2013) 3128-3138.

[55] M.B. Nijaguna, C. Schroder, V. Patil, S.D. Shwetha, A.S. Hegde, B.A. Chandramouli, A. Arivazhagan, V. Santosh, J.D. Hoheisel, K. Somasundaram, Definition of a serum marker panel for glioblastoma discrimination and identification of Interleukin 1beta in the microglial secretome as a novel mediator of endothelial cell survival induced by C-reactive protein, J Proteomics, 128 (2015) 251-261.

[56] T. Guo, X. Wang, M. Li, H. Yang, L. Li, F. Peng, X. Zhan, Identification of Glioblastoma Phosphotyrosine-Containing Proteins with Two-Dimensional Western Blotting and Tandem Mass Spectrometry, Biomed Res Int, 2015 (2015) 134050.

[57] P. Simeone, M. Trerotola, A. Urbanella, R. Lattanzio, D. Ciavardelli, F. Di Giuseppe, E. Eleuterio, M. Sulpizio, V. Eusebi, A. Pession, M. Piantelli, S. Alberti, A unique four-hub protein cluster associates to glioblastoma progression, PLoS One, 9 (2014) e103030.

[58] M.S. Heroux, M.A. Chesnik, B.D. Halligan, M. Al-Gizawiy, J.M. Connelly, W.M. Mueller, S.D. Rand, E.J. Cochran, P.S. LaViolette, M.G. Malkin, K.M. Schmainda, S.P. Mirza, Comprehensive characterization of glioblastoma tumor tissues for biomarker identification using mass spectrometry-based label-free quantitative proteomics, Physiol Genomics, 46 (2014) 467-481.

[59] R.F. Deighton, T. Le Bihan, S.F. Martin, M.E. Barrios-Llerena, A.M. Gerth, L.E. Kerr, J. McCulloch, I.R. Whittle, The proteomic response in glioblastoma in young patients, J Neurooncol, 119 (2014) 79-89.

[60] I.D. Popescu, E. Codrici, L. Albulescu, S. Mihai, A.M. Enciu, R. Albulescu, C.P. Tanase, Potential serum biomarkers for glioblastoma diagnostic assessed by proteomic approaches, Proteome Sci, 12 (2014) 47.

[61] V.N. Patel, G. Gokulrangan, S.A. Chowdhury, Y. Chen, A.E. Sloan, M. Koyuturk, J. Barnholtz-Sloan, M.R. Chance, Network signatures of survival in glioblastoma multiforme, PLoS computational biology, 9 (2013) e1003237.

[62] K. Motomura, A. Natsume, R. Watanabe, I. Ito, Y. Kato, H. Momota, R. Nishikawa, K. Mishima, Y. Nakasu, T. Abe, H. Namba, Y. Nakazato, H. Tashiro, I. Takeuchi, T. Mori, T. Wakabayashi, Immunohistochemical analysis-based proteomic subclassification of newly diagnosed glioblastomas, Cancer Sci, 103 (2012) 1871-1879.

[63] R.V. Polisetty, P. Gautam, R. Sharma, H.C. Harsha, S.C. Nair, M.K. Gupta, M.S. Uppin, S. Challa, A.K. Puligopu, P. Ankathi, A.K. Purohit, G.R. Chandak, A. Pandey, R. Sirdeshmukh, LC-MS/MS analysis of differentially expressed glioblastoma membrane proteome reveals altered calcium signaling and other protein groups of regulatory functions, Mol Cell Proteomics, 11 (2012) M111 013565.

[64] M. Wisztorski, A. Desmons, J. Quanico, B. Fatou, J.P. Gimeno, J. Franck, M. Salzet, I. Fournier, Spatially-resolved protein surface microsampling from tissue sections using liquid extraction surface analysis, Proteomics, (2016).

[65] B. Badie, J.M. Schartner, J. Paul, B.A. Bartley, J. Vorpahl, J.K. Preston, Dexamethasone-induced abolition of the inflammatory response in an experimental glioma model: a flow cytometry study, J Neurosurg, 93 (2000) 634-639.

[66] D. Hambardzumyan, D.H. Gutmann, H. Kettenmann, The role of microglia and macrophages in glioma maintenance and progression, Nat Neurosci, 19 (2016) 20-27.

[67] K.M. Lewis, C. Petritsch, Asymmetric Cell Division: Implications for Glioma Development and Treatment, Translational neuroscience, 4 (2013) 484-503.

[68] W. Roggendorf, S. Strupp, W. Paulus, Distribution and characterization of microglia/macrophages in human brain tumors, Acta neuropathologica, 92 (1996) 288-293.

[69] G.J. Kitange, B.L. Carlson, M.A. Schroeder, P.A. Decker, B.W. Morlan, W. Wu, K.V. Ballman, C. Giannini, J.N. Sarkaria, Expression of CD74 in high grade gliomas: a potential role in temozolomide resistance, Journal of neuro-oncology, 100 (2010) 177-186.

[70] Y.-H. Yu, G.-Y. Chiou, P.-I. Huang, W.-L. Lo, C.-Y. Wang, K.-H. Lu, C.-C. Yu, G. Alterovitz, W.-C. Huang, J.-F. Lo, Network biology of tumor stem-like cells identified a regulatory role of CBX5 in lung cancer, Scientific reports, 2 (2012).

[71] D.L. Masica, R. Karchin, Correlation of somatic mutation and expression identifies genes important in human glioblastoma progression and survival, Cancer research, 71 (2011) 4550-4561.

[72] L. Collins, D. Penny, Complex spliceosomal organization ancestral to extant eukaryotes, Molecular biology and evolution, 22 (2005) 1053-1066.

[73] M. Kretz, Z. Siprashvili, C. Chu, D.E. Webster, A. Zehnder, K. Qu, C.S. Lee, R.J. Flockhart, A.F. Groff, J. Chow, Control of somatic tissue differentiation by the long non-coding RNA TINCR, Nature, 493 (2013) 231-235.

[74] Y.B. Beaulieu, C.L. Kleinman, A.-M. Landry-Voyer, J. Majewski, F. Bachand, Polyadenylation-dependent control of long noncoding RNA expression by the poly (A)-binding protein nuclear 1, PLoS Genet, 8 (2012) e1003078.

[75] S. Delic, N. Lottmann, K. Jetschke, G. Reifenberger, M.J. Riemenschneider, Identification and functional validation of CDH11, PCSK6 and SH3GL3 as novel glioma invasion-associated candidate genes, Neuropathology and applied neurobiology, 38 (2012) 201-212.

[76] C.J. Sandberg, E.O. Vik-Mo, J. Behnan, E. Helseth, I.A. Langmoen, Transcriptional profiling of adult neural stem-like cells from the human brain, PloS one, 9 (2014) e114739.

TABLES AND FIGURES LEGENDS

TABLES

Table 1: Clinical characteristics, pathological and molecular data of the patients

Table 2: Proteins specifically identified by Shotgun Microproteomics in group 1 and group 2. Proteins are groups according to the microextraction spot in which they are found.

Table 3: Human alternative proteins identified by ShotGun Microproteomics that don't show any correspondence to reference human proteins found in the conventional databases.

FIGURES

Figure 1: Histological and MALDI MSI data of the 5 grade III glioma cases. (A) Scanned pictures after hematoxylin-eosin staining and anathomo-pathologist annotations. **(B)** Individual segmentation maps for each case. The segmentation map shows 3 clusters for cases number 1, 2, 4 and 5 and 4 clusters for case number 3. Colors represent molecularly different regions as shown in the corresponding dendogram. Note that for 2 different tissues, similar colors are not equivalent to similar molecular groups **(C)** MALDI MSI images of characteristics m/z observed for the different cases. **(D)** Global segmentation maps of all tissues together. Colors represent molecularly different regions as shown in the corresponding dendogram. The segmentation map gives 4 main clusters. Cases number 1 and 4 are molecularly similar and are represented in blue (Group 1). Cases number 2, 3 and 5 are grouped together based on their molecular profiles and are represented in orange, green and brown. These last cases can be divided into two groups with brown region (Group 2) in one group and green/orange regions in another group (Group 3). Microextraction spots (1.1, 1.2, 1.3 for case 1, 5.1, 5.2, 5.3 for case 2, 6.1, 6.2 for case 4, 20.1, 20.2, 20.3 for case 3, 22.1, 22.2 and 22.3 for case 5) are localized on the segmentation maps in the different ROIs of each tissue and are indicated by a white cross.

Figure 2: Shotgun Microproteomics analysis. ShotGun proteomics was performed after on-tissue trypsin digestion followed by microextraction at the spots determined

from MALDI MSI data. **(A)** Heat map of proteins with different regulation profiles as determined after label free quantification in the three groups highlighting the presence of 3 clusters. **(B)** Diagrams giving the molecular functions and biological processes associated to the overregulated proteins after analyzing protein clusters with Panther software. **(C)** Protein classes of the overregulated proteins after analyzing protein clusters with Panther software. **(D)** String analysis of proteins overregulated in group 1.

Figure 3: Molecular pathways associated to overregulated proteins. Overregulated proteins in **(A)** Group 1, **(B)** Group 2 and **(C)** Group 3.

Figure 4: Validation of the classification on 5 additional patients. (A) A classification model was generated. The training group presents three classes. In the first class, 3 regions of the blue group were used and 2 regions were used for the validation. In the second class, 3 regions of the green/orange group were used and 2 regions were used for the validation. In the third class, 3 regions of the brown group were used and 2 regions were used for the validation. This model was used to classify the five new samples. Sample 7 is classify in the green region. Sample 8 is classify in the blue region and samples 6, 9 and 10 are heterogeneous. (B) Specific m/z images were extracted for each group. (C) MALDI imaging segmentation map of all the 10 tissues. The segmentation map shows 2 main clusters: blue vs orange/brown. Colors represent molecularly different regions.

SUPPLEMENTARY DATA

Supplementary Figure 1: String analysis of overregulated proteins in group 2.

Supplementary Figure 2: String analysis of overregulated proteins in group 3.

Supplementary Table 1: List of proteins identified in all the analyses.

Supplementary Table 2: List of overregulated proteins in group 1, group 2 and group 3.

Supplementary Table 3: Validation of the interaction Map for group 1

Supplementary Table 4: Validation of the interaction Map for group 2

Supplementary Table 5: Validation of the interaction Map for group 3

Supplementary Table 6: Enriched significant pathways were identified in group 1.

Supplementary Table 7: Enriched significant pathways were identified in group 2.

Supplementary Table 8: Enriched significant pathways were identified in group 3.

Supplementary Table 9: Unique Enriched pathways in the 3 groups

Supplementary table 10: Common pathways through the three groups

Cases	sex	age at diagnosis	topography	necrosis on MRI	contrast enhancement on MRI	first progression	death	histological type	WHO grade	IDH1	1p/19q codeletion	ATRX	P53	EGFR (Hirsch score)	MGMTp status (%)	chromosomes 7 and 10
1	M	69	fronto-temporo-parietal, left	no	yes	yes	no	OA	3	positive	no codeletion	loss	positive	positive (220)	methylated (64.8%)	7p gain, 10p gain
2	M	27	parietal, right	no	yes	no	no	OA	3	positive	codeletion	expressed	negative	negative (200)	methylated (14.6%)	no abnormalities
3	F	45	frontal, right	no	yes	no	no	O	3	positive	codeletion	expressed	negative	positive (170)	methylated (32%)	7 gain, 10 loss
4	F	24	temporo insular, right	no	yes	yes	yes	A	3	negative	no codeletion	loss	positive	negative (120)	methylated (16%)	no abnormalities
5	M	45	frontal, left	no	yes	no	no	A	3	positive	no codeletion	loss	negative	positive (350)	methylated (58%)	no abnormalities
Validation Cohort																
6	M	30	frontal, right	no	yes	no	no	O	3	mutant*	no codeletion	loss	negative	positive (200)	non methylated (2.4%)	7 gain
7	M	40	frontal, left	no	yes	no	no	OA	3	positive	no codeletion	loss	positive	positive (200)	methylated (14%)	no abnormalities
8	M	35	temporal, right	no	yes	no	no	A	3	positive	no codeletion	loss	positive	positive (110)	methylated (16.2%)	7 loss
9	F	54	frontal, right	no	yes	no	no	O	3	positive	codeletion	expressed	negative	positive (300)	methylated (47.8%)	no abnormalities
10	M	60	pariertal, right	no	yes	no	no	A	3	positive	no codeletion	loss	positive	positive (130)	methylated (13.8%)	7p gain, 10p gain

Table 1

Abbreviations

M: male, F: female, MRI: Magnetic Resonance Imaging, OA: oligo-astrocytoma, A: astrocytoma, O: oligodendroglioma, WHO: world health organization, IDH1: Isocitrate Dehydrogenase, ATRX: alpha-thalassemia/mental retardation syndrome X-linked, P53, MGMTp: MGMT promoter

Identified proteins	Protein names	Gene names
Group 1		
Common to 1.1/1.2/1.3/6.1/6.2		
Q30118	HLA class II histocompatibility antigen, DR alpha chain	**HLA-DRA**
F6RFD5	Destrin	**DSTN**
P04233-2	HLA class II histocompatibility antigen gamma chain	**CD74**
P10253	Lysosomal alpha-glucosidase;76 kDa lysosomal alpha-glucosidase;70 kDa lysosomal alpha-glucosidase	**GAA**
Common to 1.1/1.2/6.1/6.2		
H0Y4R2	NADPH--cytochrome P450 reductase	**POR**
P30050	60S ribosomal protein L12	**RPL12**
Q14151	Scaffold attachment factor B2	**SAFB2**
Q86U42-2	Polyadenylate-binding protein 2	**PABPN1**
Q99459	Cell division cycle 5-like protein	**CDC5L**
Q9H8Y8-2	Golgi reassembly-stacking protein 2	**GORASP2**
Common to 1.1/1.3/6.1/6.2		
F8W785	Golgi integral membrane protein 4	**GOLIM4**
P04844-2	Dolichyl-diphosphooligosaccharide--protein glycosyltransferase subunit 2	**RPN2**
P14543-2	Nidogen-1	**NID1**
P45973	Chromobox protein homolog 5	**CBX5**
Q12797-10	Aspartyl/asparaginyl beta-hydroxylase	**ASPH**
F8W785	Golgi integral membrane protein 4	**GOLIM4**
Group 2		
Common to 20.1/20.2/20.3/22.1/22.2/22.3/5.1/5.2/5.3		
P02686-4	Myelin basic protein	**MBP**
Q53TN4-3	Cytochrome b reductase 1	**CYBRD1**
Q8NHG7	Small VCP/p97-interacting protein	**SVIP**
Q8TAM6	Ermin	**ERMN**
Q9NQW6	Actin-binding protein anillin	**ANLN**
Common to 20.1/20.3/22.1/22.2/22.3/5.1/5.2/5.3		
A0A0A0MTN4	Opalin	**OPALIN**
F5H0U5	Glycolipid transfer protein	**GLTP**
Q9GZV7	Hyaluronan and proteoglycan link protein 2	**HAPLN2**
Q9H9H5	MAP6 domain-containing protein 1	**MAP6D1**
Common to 20.1/20.2/20.3/22.1/22.2/22.3/5.1/5.2		
A6NNI4	Tetraspanin;CD9 antigen	**CD9**
P21695-2	Glycerol-3-phosphate dehydrogenase [NAD(+)], cytoplasmic	**GPD1**
Q6UWR7	Ectonucleotide pyrophosphatase/phosphodiesterase family member 6	**ENPP6**
Common to 20.1/20.2/20.3/22.1/22.2/5.1/5.2/5.3		
K7EIG7	Unconventional myosin-Id	**MYO1D**
Common to 20.2/20.3/22.1/22.2/22.3/5.1/5.2/5.3		
O14576-4	Cytoplasmic dynein 1 intermediate chain 1	**DYNC1I1**

Table 2

GENE REFERENCES	WHOLE ID PROTEOMICS	GROUP 1	GROUP 2
ALTHES2	IP_058211.1		
ALTSFPQ	IP_062363.1	IP_062363.1	
ALTEDARADD	IP_079312.1	IP_079312.1	
ALTRYR2	IP_079402.1		IP_079402.1
ALTLMAN2L	IP_088021.1		IP_088021.1
ALTPLA2R1	IP_091451.1	IP_091451.1	
ALTTTN	IP_092840.1	IP_092840.1	
ALTSTC2	IP_134213.1		
ALTSNHG18	IP_135449.1		IP_135449.1
ALTFOXF2	IP_136674.1		
ALTPRDM13	IP_143952.1		
ALTHCG18	IP_148329.1		IP_148329.1
ALTRP3-323P13.2	IP_149055.1		IP_149055.1
ALTPON2	IP_154527.1		IP_154527.1
ALTLINC00094	IP_180218.1		IP_180218.1
ALTANXA8	IP_183058.1	IP_183058.1	
ALTZCCHC24	IP_185288.1	IP_185288.1	
ALTAC068858.1	IP_204724.1	IP_204724.1	
ALTTRAF7	IP_240015.1		IP_240015.1
ALTHIF3A	IP_276654.1	IP_276654.1	
ALTIGSF5	IP_289664.1	IP_289664.1	
ALTCSF2RB	IP_294011.1	IP_294011.1	

Table 3

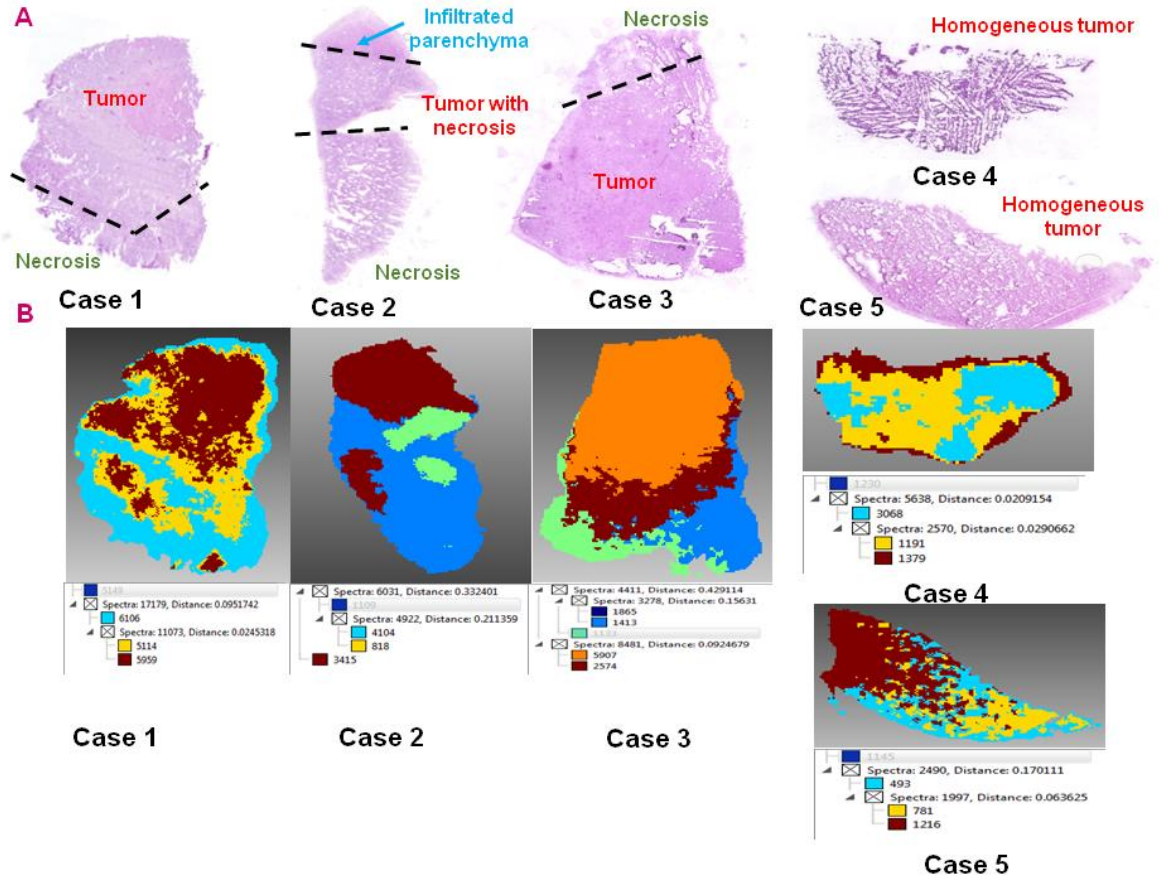

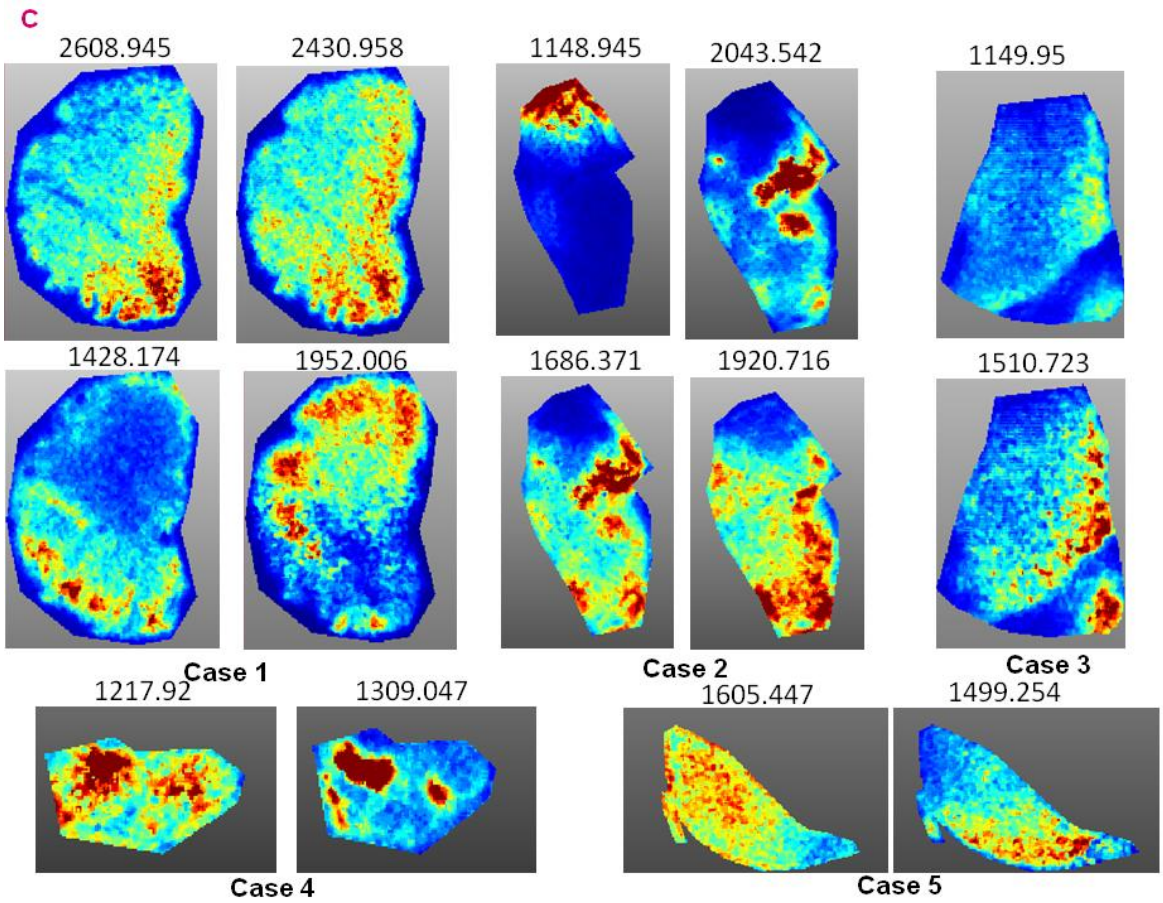

D

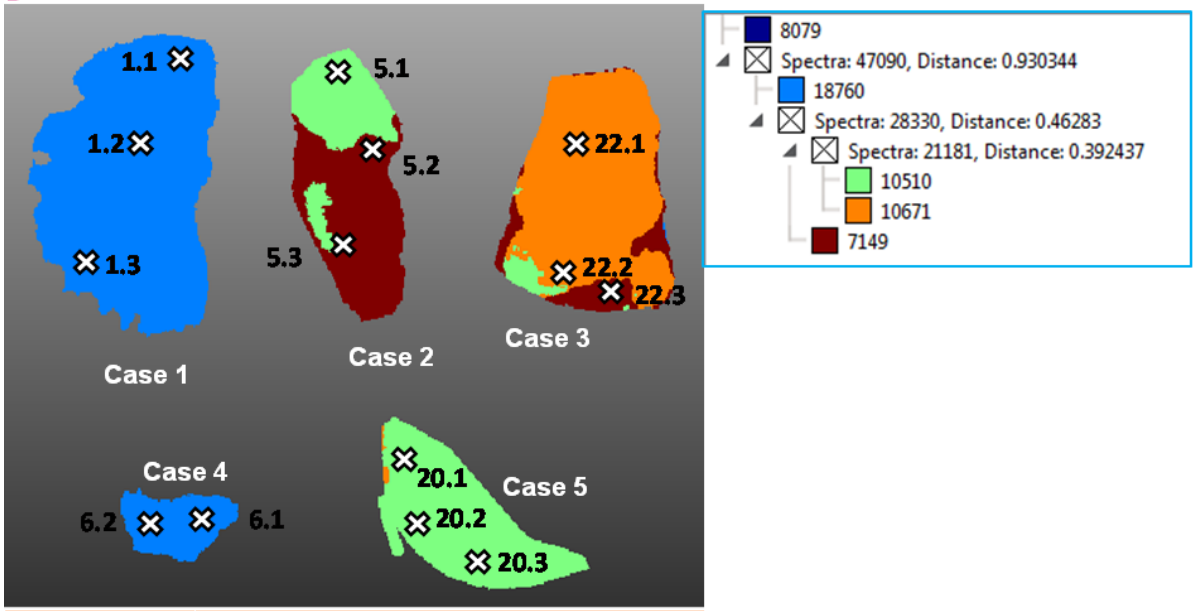

Segments	Microextraction points
Blue	1.1/1.2/1.3/6.1/6.2
Brown	5.2/5.3/22.3
Green + Orange	20.1/20.2/20.3/5.1/22.1/22.2

Figure 1

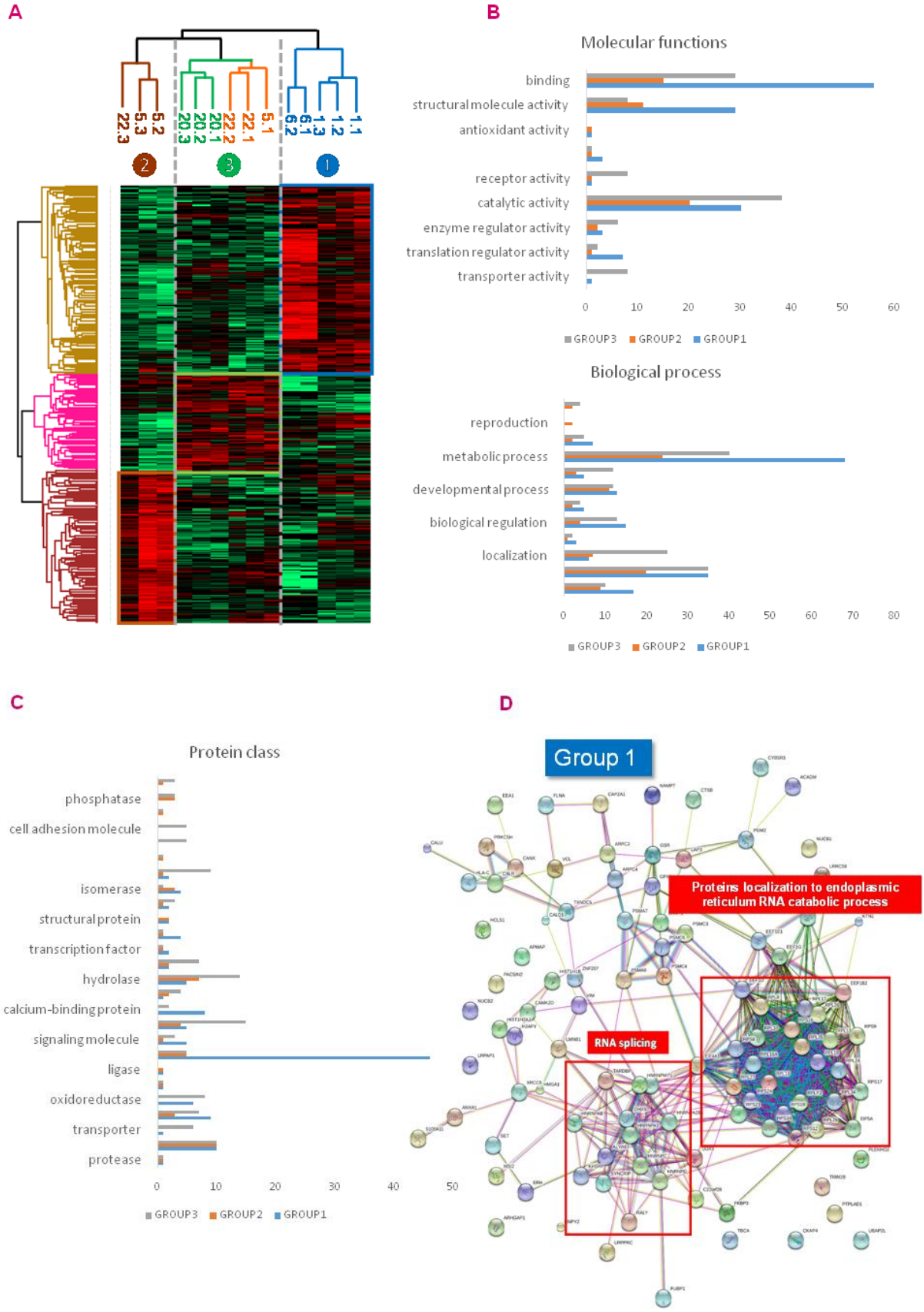

Figure 2

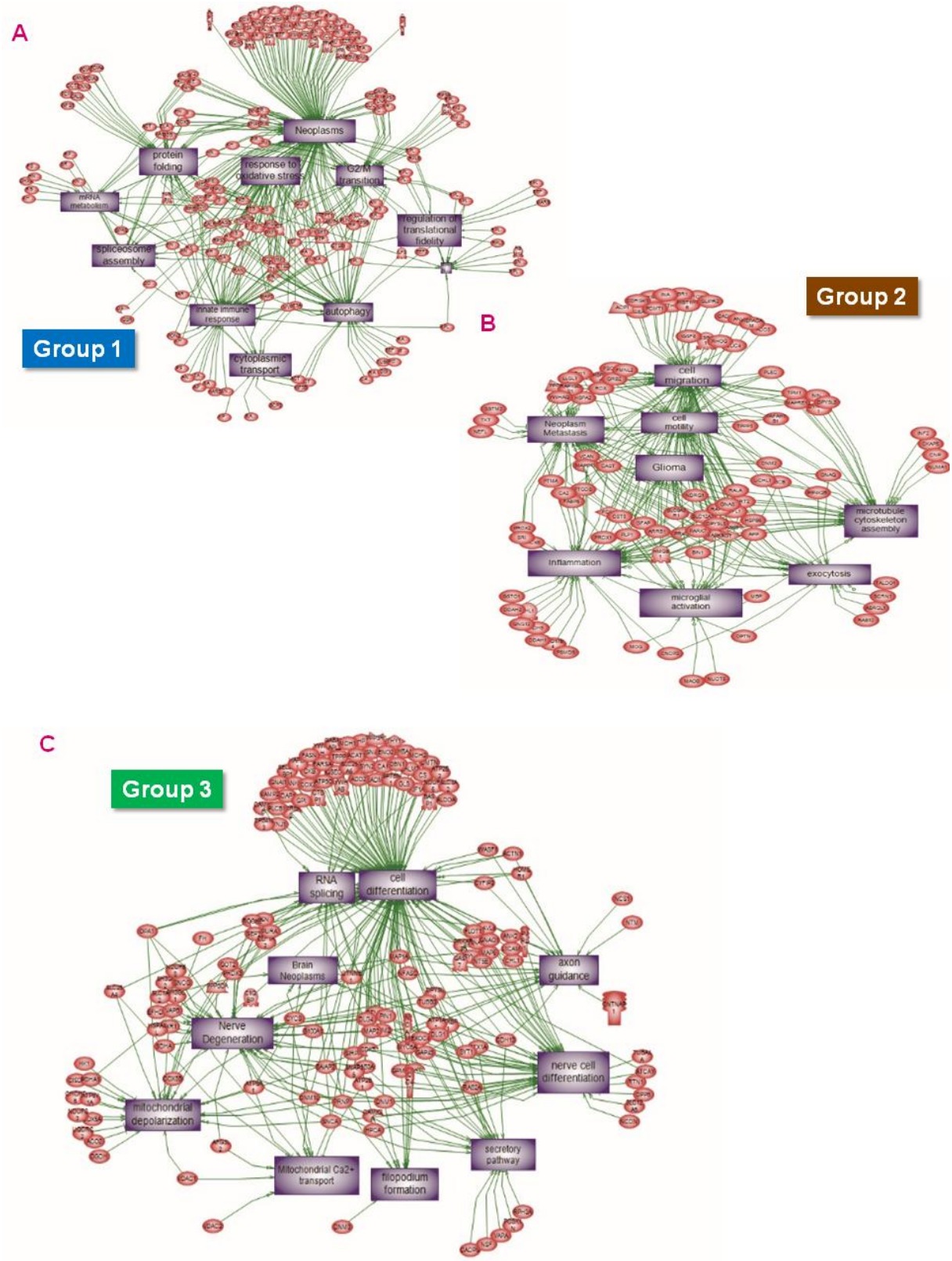

Figure 3

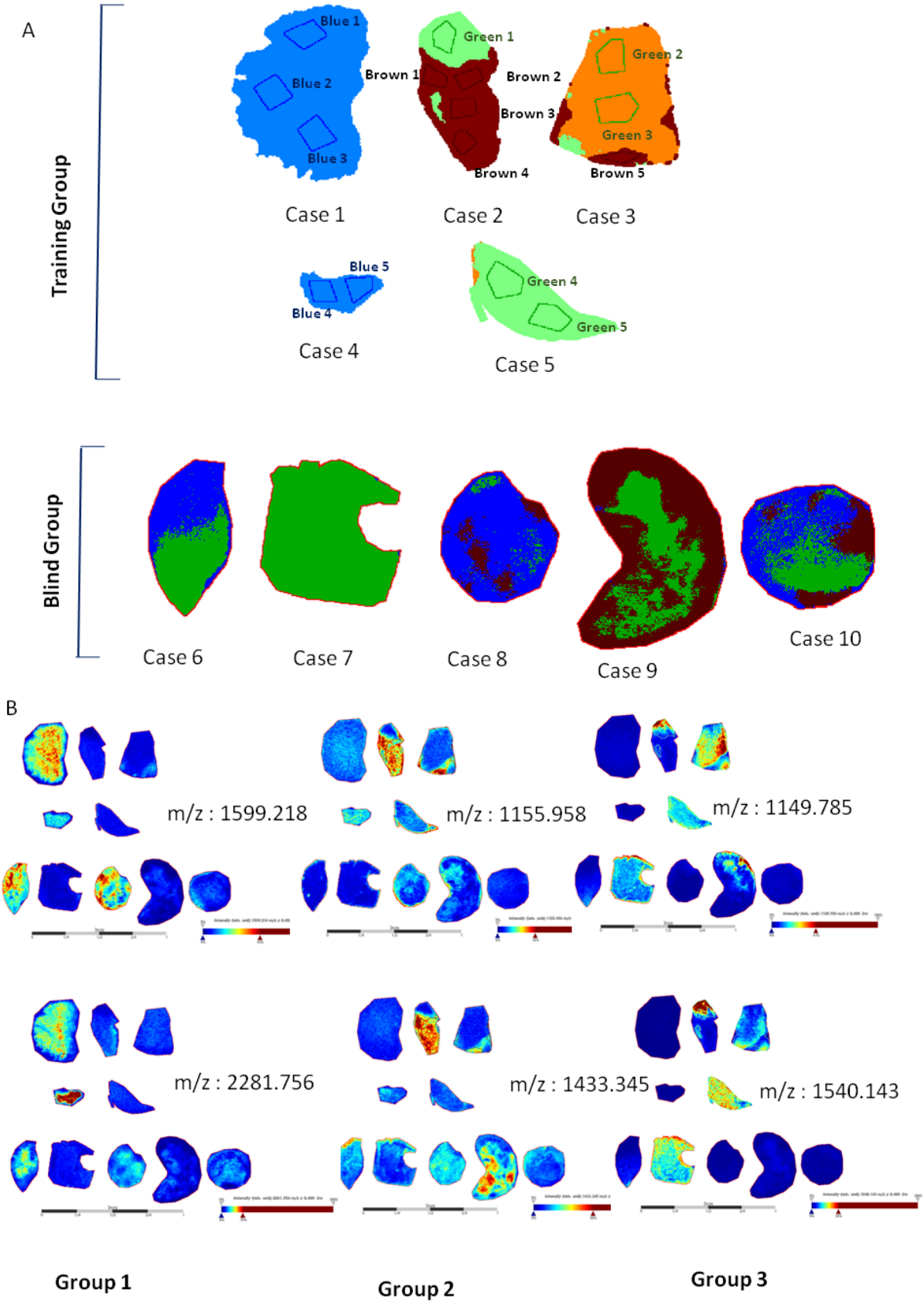

C

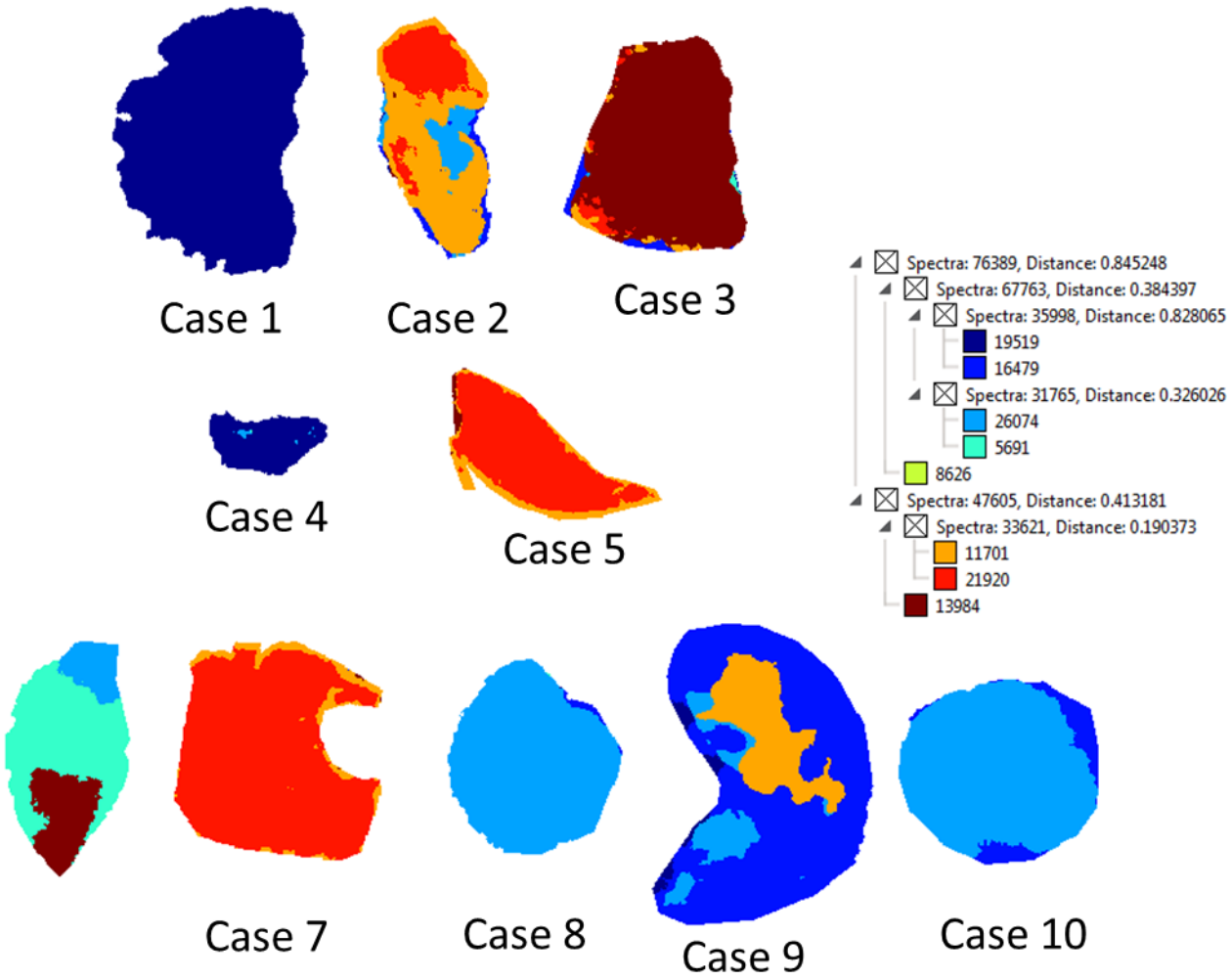

Figure 4

Conclusion

Nous avons démontré avec cette étude que l'imagerie MALDI couplée à la microprotéomique permettait d'établir de nouvelles classifications des gliomes, que l'on peut mettre en lien avec les données cliniques des patients. Cette première étude a été faite sur une petite cohorte, il faudra bien sûr, par la suite, augmenter la cohorte de patients pour augmenter la robustesse de l'étude. Néanmoins, cette étude nous a permis de mettre en évidence certains points importants. Un des points essentiels est l'hétérogénéité moléculaire de ces tumeurs, cette diversité n'étant pas forcément retrouvée d'un point de vue histologique. L'hétérogénéité tumorale est une problématique difficile à appréhender et l'inefficacité d'une thérapie basée uniquement sur une chimiothérapie, de type témozolomide, le montre malheureusement souvent avec de nombreuses résistances. Il est nécessaire de combiner les agents pharmacologiques. Un essai préclinique est en cours depuis 2015, intégrant le crocétinate de sodium combiné avec le témozolomide et la radiothérapie (NCT01465347). Pour réaliser de telles études, des nouveaux modèles sont donc nécessaires. Les modèles chiens semblent les plus appropriés, eu égard au fait qu'ils développent des tumeurs spontanées comme chez l'homme. Dans ce contexte, nous avons récemment engagé une étude protéomique préliminaire chez le chien en collaboration avec la clinique vétérinaire Oncovet. Une biopsie de glioblastome de chien a été étudiée d'une part par microprotéomique et d'autre part par imagerie MALDI MS. Ces études ont conduit à identifier un total de 836 protéines avec un minimum de 2 peptides par protéine (0.1% de faux positif). Parmi les protéines identifiées, 350 sont spécifiques de la zone bénigne et 156 de la zone tumorale. Il est intéressant de noter que l'identification des protéines par l'algorithme de SEQUEST réalisée avec soit la base FASTA humaine ou FASTA canine n'a montré que 19 protéines différentes au niveau de la zone cancéreuse, confirmant ainsi la proche parenté entre les deux modèles d'étude. Les protéines spécifiques de la zone tumorale sont impliquées dans différents évènements cellulaires jouant un rôle dans la progression de la tumeur. L'analyse avec le logiciel Cytoscape a montré que les protéines surexprimées dans la zone tumorale sont impliquées dans la régulation des ARN alors que les protéines sous-exprimées jouent un rôle dans le métabolisme enzymatique (**Figure 9A**).

26 protéines déjà identifiées dans des études précédentes comme étant de potentiels biomarqueurs des gliomes chez l'homme ont été retrouvées dans nos analyses (CRYAB, APOA1, cathepsine D, FABP7, UCH-L1, …) (**Figure 9B**).

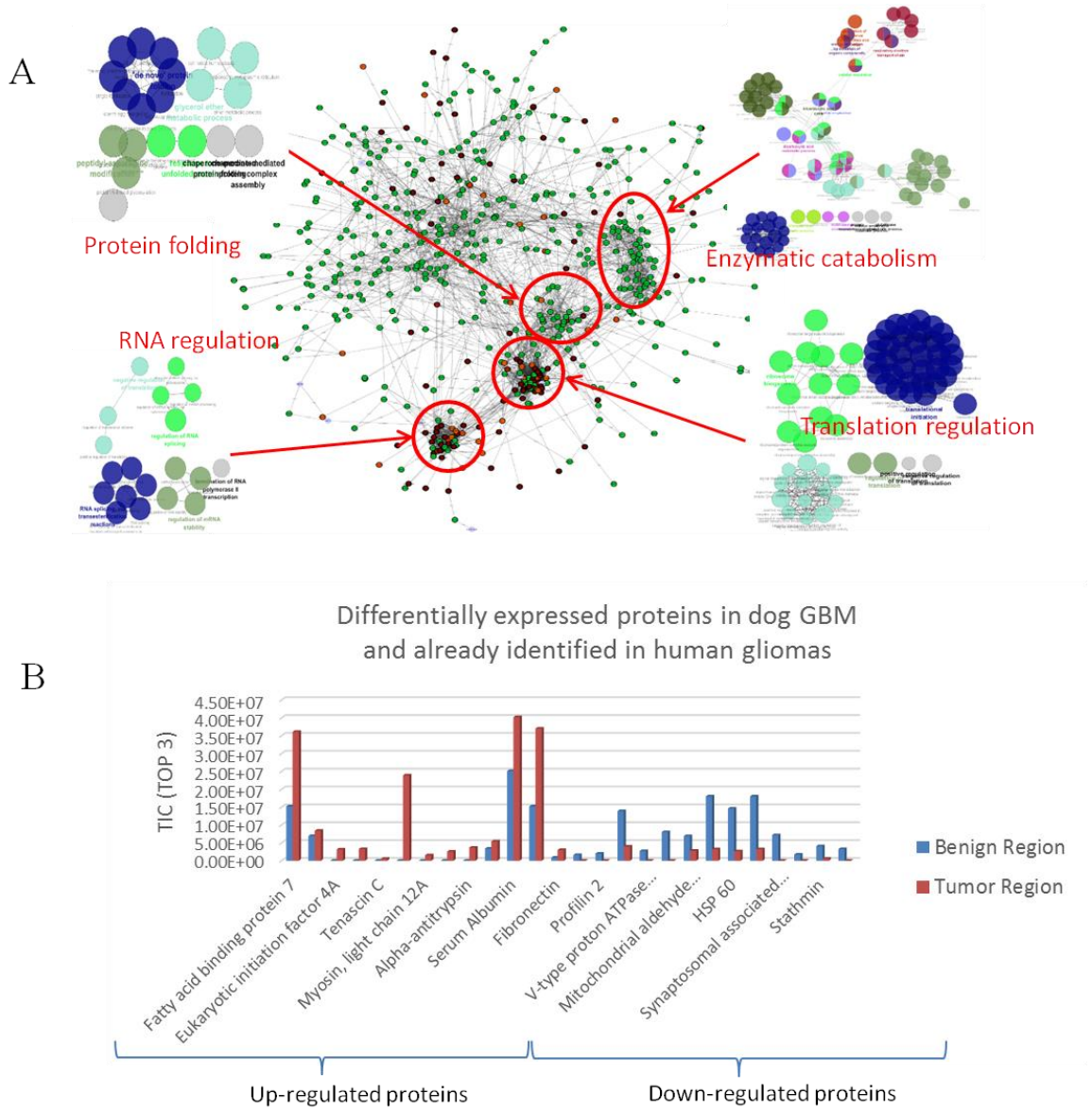

Figure 9 : Analyse protéomique de la biopsie de gliome de chien. A. Réseaux protéiques et fonctions biologiques des protéines identifiées en utilisant le logiciel Cytoscape (les protéines en vert sont sous-exprimées dans la région cancéreuse alors que les protéines en rouge sont sur-exprimées). B. Quantification relative des protéines différentiellement exprimées dans la biopsie de gliome de chien et déjà connues pour avoir une implication dans les gliomes humains.

Dans le contexte de notre étude sur les gliomes de grade III chez l'homme, nous pouvons retrouver 45 protéines identifiées dans la zone cancéreuse chez le chien qui sont communes avec les protéines identifiées chez l'homme. 37 protéines se classent dans le groupe 1, 6 protéines se classent dans le groupe 2 et 2 protéines se classent dans le groupe 3. La zone cancéreuse de la biopsie de gliome de chien ressemble donc largement, d'un point de vue

moléculaire, aux échantillons du groupe 1. En effet, de nombreuses protéines sont impliquées dans la régulation des ARN (**Figure 10**).

GROUP 1		GROUP 2	GROUP 3
ILF2	H2B	CA2	DPP6
MSN	RPLP2	DDAH2	PRKAR2A
CHCHD3	RPS21	PAICS	
DDX5	DBI	RNH1	
RPL10L	PPIB	DARS	
PTBP1	RPS23	UBA2	
HP1BP3	TPM4		
CNN3	RPL35a		
PSPC1	RPS20		
PPT1	RPL35		
VCL	MYL12a		
CTSD	RPL27		
ZYX	RPL18A		
APOA4	RPL34		
RTCB	GNB2L1		
SF3B2	SERBP1		
PA2G4	ATXN2L		
SAFB	DHX9		
	TNC		

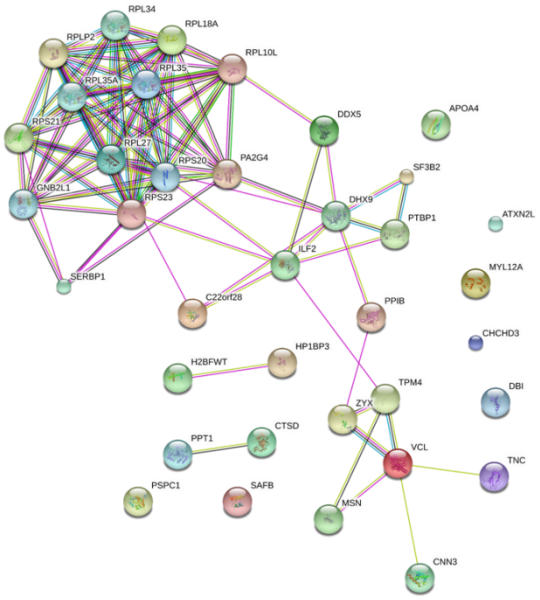

Figure 10 : Protéines identifiées dans la zone tumorale de la biopsie de gliome de chien qui sont communes avec les protéines identifiées chez l'homme. La majorité des protéines identifiées font partie du groupe 1 et sont impliquées dans la régulation des ARN.

Les données d'imagerie MALDI-TOF ont permis de mettre en évidence trois régions sur la coupe avec, pour chacune des régions, des protéines spécifiques (**Figure 3A**). Ensuite, les peptides identifiés dans les expériences de microprotéomique ont été recherchés afin de reconstruire les images MALDI-Orbitrap correspondant à ces composés. Cela est possible grâce à la résolution du MALDI-Orbitrap. Nous nous sommes plus particulièrement intéressés à la localisation du marqueur IDH1 qui est retrouvé principalement dans la zone cancéreuse (**Figure 11**).

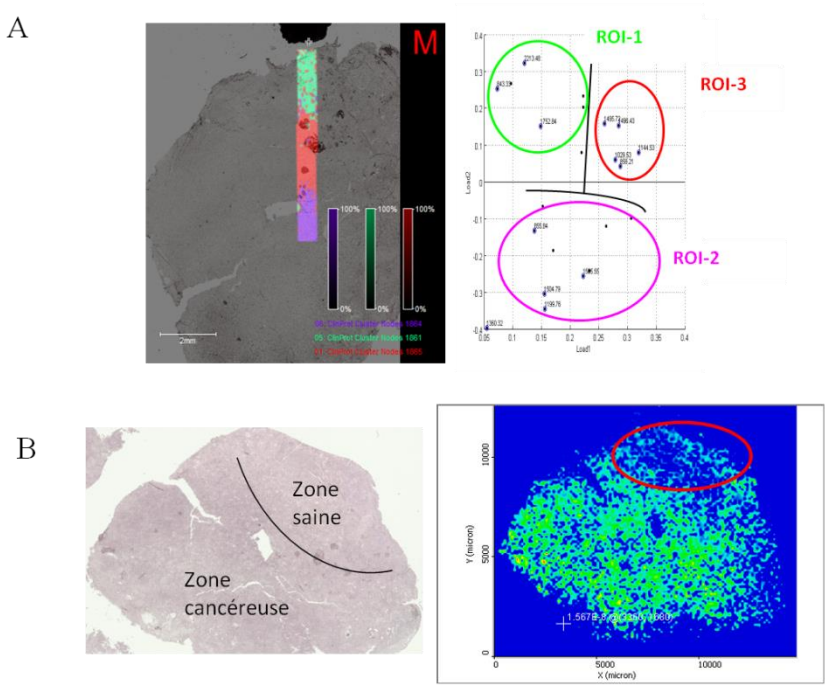

Figure 11 : Imagerie peptidique MALDI-MSI de la biopsie de gliome de chien. A. Imagerie MALDI-TOF MS de la biopsie. L'analyse biostatistique par hierarchical clustering sur une partie de la section permet de démontrer que trois sous-régions (ROI1, ROI2, ROI3) présentent un profil moléculaire distinct. B. Imagerie MALDI-Orbitrap MS de la biopsie. L'image représente la distribution du fragment de digestion trypsique à m/z 1341.69 de la protéine IDH1. La partie entourée correspond à la zone saine. IDH1 est exprimé principalement dans la zone cancéreuse.

Ces résultats préliminaires sont encourageants. En effet, les profils protéiques retrouvés chez le chien présentent de fortes similarités avec ceux retrouvés chez l'homme. Les protéines surexprimées dans la zone cancéreuse chez le chien sont impliquées, notamment, dans la régulation des ARN, comme nous l'avons observé dans notre étude sur les gliomes de grade III chez l'homme. De plus, de nombreuses protéines biomarqueurs, identifiées dans d'autres études chez l'homme, sont également retrouvées chez le chien, telles que la protéine IDH1. Afin de confirmer ces résultats, ces études seront prolongées sur une cohorte plus importante d'échantillons et comparées aux résultats de l'étude chez l'homme.

Ces résultats permettent de mettre en exergue la proche parenté entre les patients chiens et les patients humains et donc ainsi la pertinence des études sur le chien. Ces études confirment la notion d'hétérogénéité tumorale tant chez le chien que chez l'homme. Elles montrent la nécessité de considérer cette hétérogénéité dans le cadre du traitement. En effet, des protéines impliquées dans la réponse immunitaire ont été identifiées. La présence de nombreux types cellulaires différents au sein des gliomes contribuent à cette hétérogénéité. Parmi eux, on

retrouve les cellules microgliales et macrophages. Cette infiltration en cellules immunitaires permet à la tumeur de se développer rapidement et peut expliquer la résistance à certains traitements. Le développement de nouveaux traitements doit donc prendre en compte la présence de ces cellules dans le microenvironnement tumoral. Ce dernier point fait l'objet de mon deuxième chapitre de thèse où nous avons étudié la réactivation des macrophages vers un phénotype cytotoxique, en vue d'une stratégie thérapeutique, suite à l'inhibition d'une enzyme appelée proprotéine convertase 1/3 (PC1/3). Notre objectif final étant l'utilisation d'un inhibiteur de ces proprotéines convertases pour le traitement des gliomes avec une réactivation des macrophages au sein de la tumeur via les TLRs.

Dans ce contexte, je me suis axée sur les macrophages car ces cellules sont la porte d'entrée de la réponse immunitaire et de son orientation. Ce travail fait donc l'objet de mon second volet des résultats de ma thèse.

Il a pour but de répondre à deux questions:

1. Peut-on modifier le phénotype d'un macrophage pour le réactiver sans qu'il revienne vers un phénotype tolérant ?
2. Peut-on orienter et contrôler la nature des facteurs secrétés par ces macrophages ?

CHAPITRE 2

Mise en place d'une approche thérapeutique visant à réactiver les macrophages au sein des tumeurs : effet de l'inhibition de la proprotéine convertase 1/3

Introduction

Les macrophages sont impliqués dans de nombreuses maladies. Ils sont recrutés durant l'inflammation pour exercer leurs fonctions phagocytaire et inflammatoire. La population macrophagique n'est pas homogène. En effet, ces cellules peuvent présenter différents phénotypes dont l'orientation est influencée par leur environnement. L'activation des macrophages est souvent représentée de manière simplifiée de deux façons : le phénotype pro-inflammatoire M1 anti-tumoral et le phénotype anti-inflammatoire M2 pro-tumoral. En fait, ce schéma est très simplifié car les macrophages peuvent présenter jusqu'à neuf états d'activation différents (Xue et al. 2014).

Durant la tumorigenèse, les macrophages sont recrutés par les cellules cancéreuses et sont alors appelés macrophages associés à la tumeur ou TAM. La tumeur crée un environnement immunosuppresseur qui oriente les TAM vers un phénotype de type anti-inflammatoire M2 (Hambardzumyan et al. 2015). Un des challenges des thérapies basées sur les macrophages est de contrer ce microenvironnement immunosuppresseur. De plus en plus de thérapies sont développées pour réorienter les macrophages vers un phénotype pro-inflammatoire afin de réactiver la réponse immunitaire dans les cancers (Vicari et al. 2002; Kakinoki et al. 2010; Tsuchiyama et al. 2008). Les macrophages peuvent être activés par différents stimuli déclenchant des cascades de signalisation jusqu'à la synthèse de protéines spécifiques. Comme exemple de stimuli, nous pouvons citer les ligands des récepteurs « Toll-Like » (TLR) tels que le LPS, le CpG-ODN, le Poly-IC … Une thérapie, ciblée sur l'activation des macrophages via les TLR, représente donc une bonne opportunité. Trois agonistes des TLR sont approuvés par la FDA pour une utilisation en oncothérapie (Iribarren et al. 2016). Le premier est le picibanil qui est un agoniste du TLR4 et est approuvé au Japon pour le traitement de différents carcinomes. Il est administré en combinaison de la chimiothérapie. Le monophosphoryl lipid A est utilisé comme adjuvant d'un vaccin contre le papillomavirus humain. L'imiquimod cible le récepteur TLR7 pour activer la réponse immunitaire anti-cancéreuse et est utilisé pour le traitement des cancers de la peau. Cependant, des études

récentes démontrent que l'activité de l'imiquimod ne passe pas par le TLR7 (Walter et al. 2013). Le développement de thérapies ciblées sur de nouveaux agonistes des TLR est donc nécessaire. Actuellement, 6 études cliniques complètes ont été réalisées utilisant des agonistes des récepteurs TLR. Plusieurs essais ont été menés avec un agoniste du TLR9 IMO-2055, en combinaison avec d'autres inhibiteurs ou anticorps thérapeutiques. Ces études ont montré des effets significatifs sur des patients atteints de cancer du poumon et de cancer colorectal (Smith et al. 2014; Chan et al. 2015). Un agoniste du TLR4 (G100) a également été testé sur des patients atteints de cancer de la peau (Bhatia et al. 2015).

Dans ce deuxième chapitre de ma thèse, nous avons cherché à réactiver les macrophages en travaillant sur une enzyme appelée proprotéine convertase 1/3. Cette enzyme est largement associée au système neuroendocrinien mais récemment son expression a aussi été découverte dans les cellules immunitaires telles que les lymphocytes et les macrophages (Salzet et al. 2000; Day & Salzet n.d.; Lansac, Dong, Claire M Dubois, et al. 2006; Refaie et al. 2012). Nous avons donc voulu comprendre son rôle au niveau des macrophages. Nous nous sommes appuyés sur des travaux précédents du laboratoire qui montraient que des souris PC1/3 knock-out (KO) présentaient un fort taux de cytokines pro-inflammatoires dans leur plasma (Refaie et al. 2012). L'isolement des macrophages péritonéaux de ces souris PC1/3 KO a également prouvé que leur sécrétion cytokinique était augmentée. Une autre étude a confirmé le rôle de PC1/3 dans la libération cytokinique dans les macrophages de rat NR8383 (Gagnon et al. 2013).

Sur la base des données précédentes, nous avons voulu déterminer l'impact de l'inhibition de cette enzyme sur le trafic et la signalisation intracellulaire de récepteurs de l'immunité innée i.e. les TLR et plus spécifiquement TLR4 (récepteur membranaire) et TLR9 (récepteur endosomal).

Notre premier objectif était de comprendre l'impact de l'inhibition de PC1/3 sur la sécrétion des facteurs immunitaires (cytokines, signaux de dangers etc..) dépendamment du récepteur TLR concerné. L'idée sous-jacente était de connaître la voie de signalisation (MyD88 dépendante ou indépendante) impliquant PC1/3 et ensuite de rechercher à quel niveau de la voie cette enzyme contrôlait la signalisation intracellulaire des TLR.

Le second objectif était de savoir si l'inhibition de PC1/3 modifiait le phénotype des macrophages et si ces derniers secrétaient des facteurs permettant la réactivation de la réponse immunitaire au sein de la tumeur. Pour ce faire, nous avons entrepris une étude par protéomique sur les sécrétomes et les contenus protéiques intracellulaires des macrophages. L'impact des

facteurs sécrétés par les macrophages PC1/3 knock-down (KD) a également été évalué sur la viabilité de lignées de cellules cancéreuses et le recrutement de cellules immunitaires.

Résultats

Nous avons analysé par protéomique les sécrétomes des macrophages PC1/3 KD stimulés avec du LPS de 1h à 72h. Plus de 1400 protéines ont été identifiées et 18 protéines sont spécifiques de l'inhibition de PC1/3. Certaines d'entre-elles sont impliquées dans l'activation des lymphocytes Th1 et la réponse inflammatoire. Nous avons aussi identifiés des cytokines et chémokines sécrétées de façon plus précoce par les macrophages PC1/3 KD par rapport aux macrophages contrôles NT (non-targeted). Les analyses par « cytokines array » ont confirmé la sécrétion cytokinique plus abondante des macrophages PC1/3 KD sous LPS et CpG-ODN. Un point à noter ici est que la sécrétion des macrophages suite à une stimulation du récepteur TLR4 (LPS) ou du récepteur TLR9 (CpG-ODN) n'est pas la même. En effet, sous LPS, les facteurs sécrétés sont majoritairement de type : CXCL9, CCL20, CXCL1 et IL-1β tandis que les facteurs sécrétés sous CpG-ODN sont majoritairement la CXCL2 et l'IL-1α. Des tests fonctionnels ont été réalisés tels que des tests de chémoattraction et de viabilité de cellules cancéreuses. Les sécrétomes des cellules PC1/3 KD stimulés au LPS attirent de façon importante les lymphocytes T CD4+. De plus, ils présentent une activité anti-tumorale sur des cellules de cancer du sein (SKBR3) et de l'ovaire (SKOV3). Ces macrophages sécrètent donc des facteurs tuant les cellules cancéreuses lorsque la voie TLR4 est activée. Une étude a montré que l'activation du récepteur TLR4 via le LPS pour le traitement des glioblastomes montrait des effets significatifs (Chicoine et al. 2007). Une autre étude a démontré que la stimulation des cellules microgliales avec le LPS et l'IFN-γ déclenchait la sécrétion de facteurs anti-tumoraux (Mora et al. 2009).

Afin de comprendre pourquoi ces macrophages PC1/3 KD sécrètent de façon massive des cytokines et chémokines, nous avons ensuite étudié les modulations des protéines intracellulaires. Une des découvertes les plus frappantes est la réorganisation du cytosquelette lorsque PC1/3 est absente. Un marquage à la phalloïdine a confirmé le fait que les cellules PC1/3 KD présentaient un grand nombre de filopodes, qui sont un gage de l'activation macrophagique, leur permettant ainsi d'être plus mobiles (Patel et al. 2012). Un grand nombre de protéines surexprimées dans les macrophages PC1/3 KD est connu pour être spécifique des exosomes et corps multi-vésiculaires, pouvant en partie expliquer la sécrétion observée. La

réorganisation du cytosquelette a des effets importants sur le trafic et les voies de signalisation intracellulaires (Németh et al. 2004). Des études par immunofluorescence ont montré une modulation du trafic du récepteur TLR9 quand PC1/3 est inhibée, avec une accumulation au niveau des corps multi-vésiculaires.

L'ensemble de ces éléments nous a conduit à analyser les voies de signalisation en aval des récepteurs TLR4 et TLR9. Le premier point observé est l'augmentation de la libération calcique par les cellules PC1/3 KD. La signalisation calcique est impliquée dans la libération cytokinique et la translocation des facteurs de transcription (Heo et al. 2015). Le facteur de transcription NF-κB est plus activé dans les macrophages PC1/3 KD sous LPS et CpG-ODN. Au contraire l'activation du facteur de transcription STAT3, qui est connu pour inhiber la voie NF-κB, diminue lorsque PC1/3 n'est pas présente. L'inhibition de STAT3 est très intéressante d'un point de vue thérapeutique car des inhibiteurs de STAT3 sont développés pour traiter différents cancers (tête et cou, sein, poumon, colorectal, prostate…) (Siveen et al. 2014).

Notre étude a permis de démontrer, grâce à la protéomique, que les macrophages PC1/3 KD présentent des caractéristiques de macrophages pro-inflammatoires activés. Les voies de signalisation des récepteurs TLR4 et TLR9 sont renforcées menant à la sécrétion de cytokines et chémokines. La stimulation du récepteur TLR4 mène, en plus, à la sécrétion de facteurs anti-tumoraux

En ce qui concerne les voies de signalisation, nous avons pu mettre en évidence que les voies TLR4 et TLR9 Myd88-dépendante sont activées, conduisant à la sécrétion des facteurs immunitaires. Dans le cadre de TLR4, nous avons mis en évidence que l'inhibition de PC1/3 et la stimulation du TLR4 par du LPS conduit à la fois à une augmentation de NF-κB mais aussi du calcium interne. Les expériences d'imagerie calcique montrent que les cellules PC1/3 KD présentent une forte concentration de calcium à l'état basal et après stimulation au LPS. Nous avons également démontré que les canaux SOCs (Store Operated Channels) étaient en partie impliqués dans ce phénomène. La thapsigargine va entraîner un stress du réticulum endoplasmique et activer ainsi les canaux SOCs membranaires pour permettre l'entrée de calcium dans la cellule. Cependant, ces canaux ne sont pas les seuls impliqués dans cette entrée massive de calcium car lorsque l'on ajoute 2 mM de Ca^{2+} extracellulaire, la concentration calcique augmente. On peut suggérer l'implication d'ORAI1 et STIM1. Ce travail est en cours d'analyse. Néanmoins, les modifications du cytosquelette observées sont à mettre en lien avec

la signalisation calcique et permet ainsi d'expliquer la forte libération cytokinique par les macrophages PC1/3 KD.

Pour le TLR9, l'inhibition de PC1/3 conduit à une translocation du récepteur actif plus rapidement vers les endosomes, ce qui suggère que PC1/3 jouerait un rôle de régulateur dans cet adressage. En effet, des travaux préliminaires révèlent une expression plus importante de la protéine UNC93b1, la chaperonne du récepteur TLR9, en l'absence de PC1/3 (**Figure 12**). Les données d'immunofluorescence des cellules NT montrent un délai au niveau de la co-localisation entre UNC93b1 et TLR9 sous CpG-ODN. Il faut plus de 3h pour obtenir cette co-localisation (**Figure 12**). Les mêmes analyses sur les cellules PC1/3 KD sont en cours afin de savoir si la co-localisation d'UNC93b1 et de TLR9 se fait plus rapidement. UNC93b interagit avec le récepteur TLR9 (Brinkmann et al. 2007) pour permettre son trafic vers les endosomes (Lee et al. 2013).

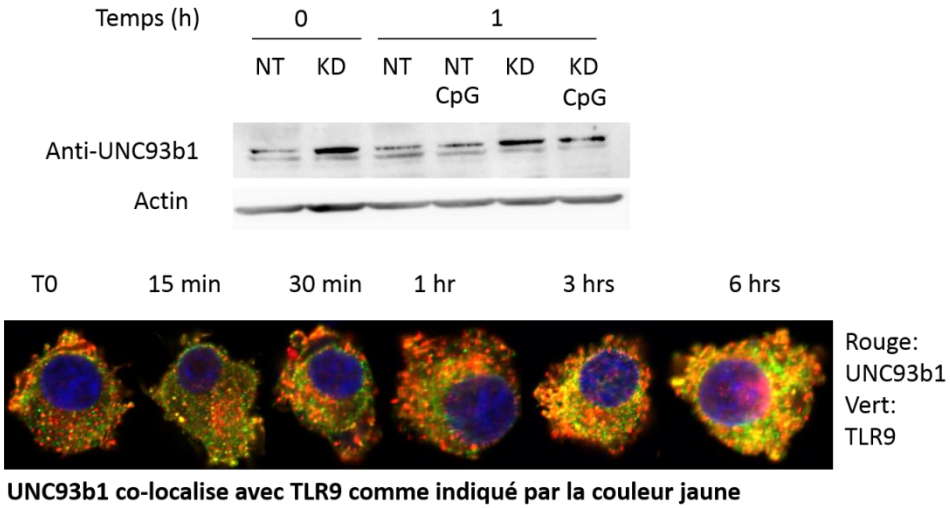

Figure 12 : Etude d'UNC93b1 dans les macrophages NR8383. L'analyse par western blot montre qu'UNC93b1 est plus exprimé dans les cellules KD que dans les cellules NT. Des études par immunofluorescence démontrent qu'UNC93b1 et TLR9 co-localisent dans les macrophages à partir de 3h de stimulation au CpG-ODN. Ces résultats ont été réalisés par Rinaldo van Meel et à l'initiative du Dr Franck Rodet.

Ces résultats confirment donc que la nature des facteurs libérés par les macrophages PC1/3 KD est différente en fonction des TLR activés bien que ceux-ci activent la voie MyD88-dépendante.

L'ensemble de ces résultats montre que la proprotéine convertase PC1/3 est un élément important dans le trafic et la signalisation intracellulaire de ces récepteurs MyD88-dépendant

(**Figure 13**). D'autres ligands des récepteurs TLR sont également à l'étude tels que le taxol comme nous le verrons dans le chapitre 3.

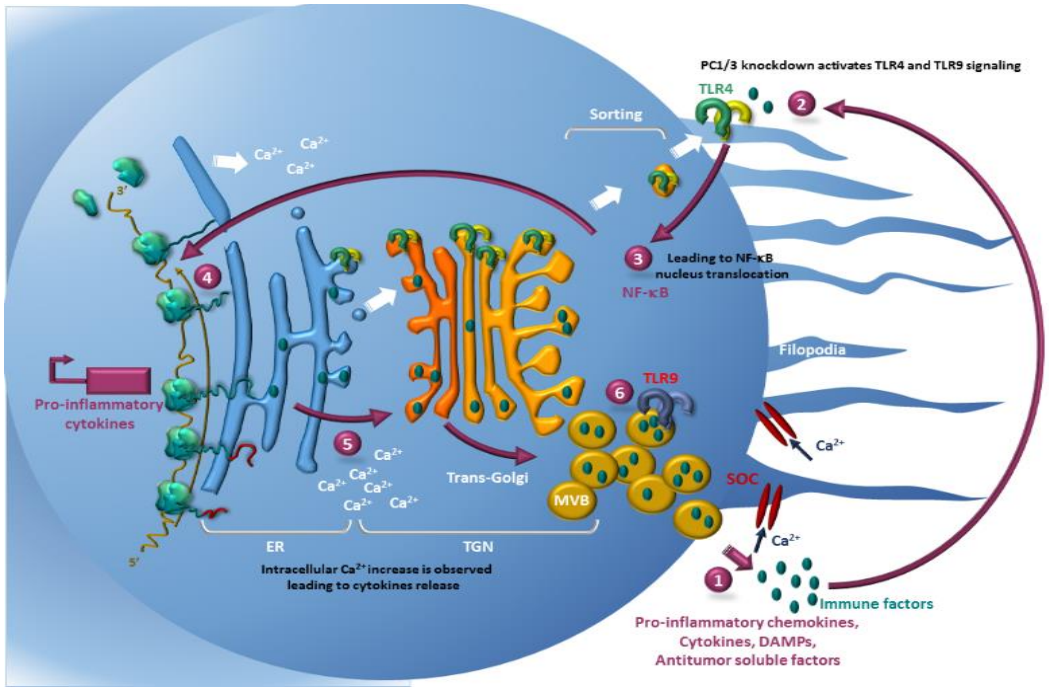

Figure 13 : Schéma décrivant l'impact de l'inactivation de PC1/3 sur l'activation des macrophages. L'inhibition de PC1/3 favorise la formation de corps multi-vésiculaires pour la libération de chémokines et cytokines (1). Les molécules sécrétées peuvent activer les récepteurs TLR4 et TLR9 (2) et induire la voie de signalisation MyD88-dépendante (3) avec la translocation du facteur NF-κB dans le noyau (4) et l'augmentation du calcium interne (5). Ces phénomènes, ainsi que le remodelage du cytosquelette, permettent la libération de cytokines et chémokines (6).

Research

Molecular Consequences of Proprotein Convertase 1/3 (PC1/3) Inhibition in Macrophages for Application to Cancer Immunotherapy: A Proteomic Study*[S]

Marie Duhamel‡, Franck Rodet‡, Nadira Delhem§, Fabien Vanden Abeele¶, Firas Kobeissy‖, Serge Nataf, Laurent Pays**, Roxanne Desjardins‡‡, Hugo Gagnon§§, Maxence Wisztorski‡, Isabelle Fournier‡, Robert Day‡‡, and Michel Salzet‡¶¶**

Macrophages provide the first line of host immune defense. Their activation triggers the secretion of pro-inflammatory cytokines and chemokines recruiting other immune cells. In cancer, macrophages present an M2 anti-inflammatory phenotype promoting tumor growth. In this way, strategies need to be develop to reactivate macrophages. Previously thought to be expressed only in cells with a neural/neuroendocrine phenotype, the proprotein convertase 1/3 has been shown to also be expressed in macrophages and regulated as a function of the Toll-like receptor immune response. Here, we investigated the intracellular impact of the down-regulation of the proprotein convertase 1/3 in NR8383 macrophages and confirmed the results on macrophages from PC1/3 deficient mice. A complete proteomic study of secretomes and intracellular proteins was undertaken and revealed that inhibition of proprotein convertase 1/3 orient macrophages toward an M1 activated phenotype. This phenotype is characterized by filopodial extensions, Toll-like receptor 4 MyD88-dependent signaling, calcium entry augmentation and the secretion of pro-inflammatory factors. In response to endotoxin/lipopolysaccharide, these intracellular modifications increased, and the secreted factors attracted naïve T helper lymphocytes to promote the cytotoxic response. Importantly, the application of these factors onto breast and ovarian cancer cells resulted in a decrease viability or resistance. Under inhibitory conditions using interleukin 10, PC1/3-knockdown macrophages continued to secrete inflammatory factors. These data indicate that targeted inhibition of proprotein convertase 1/3 could represent a novel type of immune therapy to reactivate intra-tumoral macrophages. ***Molecular & Cellular Proteomics 14: 10.1074/mcp.M115.052480, 2857–2877, 2015.***

From the ‡Inserm U-1192, Laboratoire de Protéomique, Réponse Inflammatoire, Spectrométrie de Masse (PRISM), Université Lille 1, Cité Scientifique, 59655 Villeneuve D'Ascq, France; §Institut de Biologie de Lille, UMR 8161 CNRS, Institut Pasteur de Lille, Université Lille 1, Lille, France; ¶Inserm U-1003, Equipe labellisée par la Ligue Nationale contre le cancer, Laboratory of Excellence, Ion Channels Science and Therapeutics, Université Lille 1, Cité Scientifique, 59655 Villeneuve d'Ascq, France; ‖Department of Biochemistry and Molecular Genetics, Faculty of Medicine, American University of Beirut; **Inserm U-1060, CarMeN Laboratory, Banque de Tissus et de Cellules des Hospices Civils de Lyon, Université Lyon-1; ‡‡Institut de Pharmacologie, Département de Chirurgie/Service d'Urologie, Faculté de Médecine et des Sciences de la Santé, Université de Sherbrooke, Sherbrooke, J1H 5N4 Québec, Canada; §§PhenoSwitch Bioscience Inc. 3001 12e Ave Nord, Sherbrooke, Qc, Canada, J1H 5N4

Received June 3, 2015, and in revised form, August 25, 2015
Published, MCP Papers in Press, September 1, 2015, DOI 10.1074/mcp.M115.052480
Author's contributions: MS, MD, RD wrote the paper. MD, FR, MW, FVA, ND, FK, HG, RoD performed the experiments. MS, IF, RD received financial support for the project and corrected the manuscript. All authors reviewed the manuscript.

Innate immunity is the first line of immune defense and is common to all metazoans (1, 2). In this immune system, macrophages play a crucial role in the maintenance of tissue homeostasis. These cells are involved in almost every disease through their immunological and wound-healing functions (1, 2). During a pathogenic infection, trauma or neurodegeneration, macrophages are recruited and activated contributing to the phagocytosis of pathogens and the secretion of cytokines and chemokines activating other immune cells. Macrophages can develop into classically pro-inflammatory (M1) or alternatively (M2) activated macrophages. M1 macrophages are characterized by the secretion of pro-inflammatory cytokines whereas M2 macrophages secrete anti-inflammatory cytokines (3). Stimulation of macrophages with LPS activates TLR4 signaling leading to the nucleus translocation of NF-κB or IRF3 which activate genes encoding proteins involved in innate immune response (4). Many of these proteins are secreted (cytokines, chemokines…) to attract and activate other immune cells like T lymphocytes. In tumors, macrophages are oriented toward the M2 phenotype and promote cancer growth by suppressing immune cells function (5). Current

research in the therapeutic field focus on ways to reactivate macrophages.

Surprisingly, we have shown that during immune responses, macrophages secrete typical neuroendocrine molecules (6–8), such as neuropeptides (9) or the proprotein convertases (PC)[1] PC2 and PC1/3 and that PC1/3 is an important regulator of innate immune responses (10–12). Proprotein convertases cleave precursor proteins which can lead to the activation, inactivation or functional changes. PC2 and PC1/3 operate within the regulated secretory pathway. Their expression is not restricted to neuroendocrine tissues, they are also expressed in macrophages and lymphocytes (12). In a previous study from our group, PC1/3 knockout (KO) in mice challenged with LPS caused innate immune defects and uncontrolled cytokine secretion (10). Th1 pathway is enhanced in PC1/3 KO mice. Following LPS treatment, PC1/3 colocalized with TLR4 in the endosomal compartment (11). We concluded that PC1/3 contributes to the regulation of TLR4 signaling and the resulting cytokine secretion.

The NR8383 rat pulmonary macrophage cell line was previously shown as a good model to study the role of PC1/3 in the macrophage innate immune response (13). In the present study, we developed a PC1/3-knockdown (K_D) NR8383 cell line using lentiviral-delivered shRNAs. Our aim is to understand the cellular impact of PC1/3 inhibition in macrophages and the consequences on their activation. Proteomic analysis of secreted proteins allowed us to identify pro-inflammatory cytokines and alarmins already at 24h of LPS stimulation in PC1/3-K_D secretomes which was confirmed by cytokines array. Proteomic studies of PC1/3-K_D NR8383 cellular extracts revealed an important perturbation in the intracellular trafficking machinery through the disorganization of cytoskeletal protein expression. These results were confirmed on macrophages from PC1/3 KO mice. Cytokines secretion and cytoskeleton reorganization can be linked to intracellular calcium increase in PC1/3-K_D cells. Moreover, we showed that MyD88-dependant TLR4 signaling was sustained when PC1/3 is down-regulated. We describe here that inhibition of PC1/3 induced classically activated phenotype (M1) in macrophages. The chemotactic and anti-tumor properties of the PC1/3-K_D macrophage secretome promoted the cytotoxic immune response and inhibited cancer cell viability. The down-regulation of PC1/3 could be used in cancer immunotherapy to reactivate macrophages.

[1] The abbreviations used are: PC, proprotein convertase; KO, knock-out; LPS, lipopolysaccharide; TLR, Toll-like receptor; KD, knock-down; SOC, Store-operated channel; NT, nontarget; PFA, paraformaldehyde; OVA, ovalbumine; FBS, fetal bovine serum; FASP, filter aided sample preparation; HCD, higher energy collision dissociation; FDR, false discovery rate; NK, natural killer; RLU, relative light unit; CCL, chemokine (C-C motif) ligand; CXCL, chemokine (C-X-C motif) ligand; MIF, macrophage migration inhibitory factor; WASP, Wiskott–Aldrich syndrome protein; TGN, trans-golgi network; ECV, endosome carrier vesicle; MVB, multivesicular body; TG, thapsigargin; ER, endoplasmic reticulum; SOCE, store-operated calcium entry; NA, nonactivated; A, activated; shRNA, small hairpin RNA; NaF, sodium fluoride; NP40, Nonidep P-40; LFQ, label free quantification; HBSS, Hank's balanced salt solution; PBMC, peripheral blood mononuclear cell.

EXPERIMENTAL PROCEDURES

Cell Culture—The rat alveolar macrophage cell line NR8383 (CRL-2192) was obtained from ATCC (Manassas, VA). NR8383 PC1/3-K_D and NR8383 nontarget (NT) shRNA cell lines were cultured in Ham's F12K medium supplemented with 15% fetal bovine serum and 12 μg/ml puromycin at 37 °C in a humidified atmosphere (5% CO_2). NR8383 PC1/3 K_D was performed using lentivirus transduction as described previously (11).

Confocal Microscopy—The NR8383 cells were grown in culture flasks and treated or not with LPS (InvivoGen, Toulouse, France) at a concentration of 200 ng/ml before being subjected to immunofluorescence studies. For actin immunostaining, the cells were fixed with 4% paraformaldehyde (PFA) for 10 min, washed with PBS, permeabilized with 0.2% Triton X-100 for 10 min at room temperature, blocked with 1% BSA, 1% OVA and 1% normal donkey serum for 1 h and stained with phalloidin labeled with rhodamine (1/100, Santa Cruz Biotechnology, Heidelberg, Germany) at 4 °C for 30 min. After washing with PBS, the nuclei were stained with Hoechst 33342 (1/10000), and the cells were visualized by confocal microscopy. Fluorescence analysis was conducted using a Zeiss LSM 510 confocal microscope (488 nm excitation for Alexa 488 and 543 nm for Alexa 546) connected to a Zeiss Axiovert 200 M with a 63X1.4 numerical aperture oil immersion objective. Both channels were excited, collected separately and then merged to examine the colocalization. The image acquisition characteristics (pinhole aperture, laser intensity, scan speed) were the same throughout the experiments to ensure comparability of the results.

Identification of Cytokines and Chemokines Using Rat Cytokine Antibody Arrays—NR8383-K_D and -NT cells were plated on sterile six-well plates until confluence was attained. The cells were starved overnight with Ham's F12K medium supplemented with 2% FBS and stimulated for 24 h with 20 ng/ml IL-10 (Peprotech) in serum-free medium or left untreated. The medium was then replaced, and the cells were stimulated for 24 h with 200 ng/ml LPS or left untreated. The cell supernatants were collected, centrifuged at 500 × g, passed through a 0.22-μm filter to remove cells and immediately frozen in liquid nitrogen.

The Rat Cytokine Array Panel A from R&D system was used to probe the cytokines in the secretome of stimulated and nonstimulated NR8383 cells by following the procedures recommended by the manufacturer. The membranes were quantified by densitometry using ImageJ software. Statistical analyses were performed using the paired *t* test. Error bars represent the S.E.

Total and Nuclear Protein Extracts—NR8383-K_D and -NT cells were plated on sterile six-well plates until confluent. For LPS stimulation, the cells were starved overnight with Ham's F12K medium supplemented with 2% FBS. The cells were stimulated with 200 ng/ml LPS in serum-free medium or left untreated. At 1 h, 3 h, 6 h (for Western blot analysis), and 24 h (for FASP), the cells were collected, washed once with ice-cold PBS and then lysed with RIPA buffer for total protein extraction (150 mM NaCl, 50 mM Tris, 5 mM EGTA, 2 mM EDTA, 100 mM NaF, 10 mM sodium pyrophosphate, 1% Nonidet P-40, 1 mM PMSF, 1X protease inhibitors). Cell debris was removed by centrifugation (20000 × *g*, 10 min, 4 °C); the supernatants were collected. For the nuclear extracts, NE-PER Nuclear and Cytoplasmic Extraction Reagents were used (Thermo Scientific) according to the manufacturer's instructions. The supernatants were collected, and the protein concentrations were measured using the Bio-Rad Protein Assay.

Western Blot Analysis—The total cell extracts (40 μg) or nuclear extracts (5 μg) were then analyzed by Western blot assays. Primary antibodies were rabbit anti-IRF3, mouse anti-phospho-IκBα, mouse anti-IκBα (1:1000, from Cell Signaling Technology, Leiden, The Netherlands) and rabbit anti-lamin A (1:1000, from Abcam). Horseradish peroxidase-coupled goat antimouse and goat anti-rabbit secondaries (Jackson ImmunoResearch) were used at 1:30000 and 1:20000 respectively. ImageJ software was used to quantify the bands.

Filter-aided Sample Preparation (FASP)—The total protein extract (0.1 mg) was used for FASP analysis as described previously (14). We performed FASP using Microcon devices YM-10 (Millipore) before adding trypsin (Promega) for protein digestion (40 μg/ml in 0.05 M NH_4HCO_3). The samples were incubated overnight at 37 °C. The digests were collected by centrifugation, and the filter device was rinsed with 50 μl of NaCl 0.5 M. Next, 5%TFA was added to the digests, and the peptides were desalted with a Millipore ZipTip device before LC-MS/MS analysis.

Secretome Preparation and Protein Digestion—NR8383-K_D and -NT cells were plated in sterile 24-well plates until confluent. For LPS stimulation, the cells were starved overnight with Ham's F12K medium supplemented with 2% FBS. The cells were stimulated with 200 ng/ml LPS in serum-free medium or left untreated. At 1, 16, 24, 48, and 72 h, the cell supernatants were collected, centrifuged at 500 × *g*, passed through a 0.22-μm filter to remove the cells and immediately frozen in liquid nitrogen. The experiments were performed in biological triplicates.

Four hundred microliters of the secretome was collected for each condition. The volume was reduced to 100 μl in a SpeedVac. Secretome digestion was performed as previously described (15). In brief, the cell supernatants were denatured with 2 M urea in 10 mM HEPES, pH 8.0 by sonication on ice. The proteins were reduced with 10 mM DTT for 40 min followed by alkylation with 55 mM iodoacetamide for 40 min in the dark. The iodoacetamide was quenched with 100 mM thiourea. The proteins were digested with 1 μg LysC/Trypsin mixture (Promega) overnight at 37 °C. The digestion was stopped with 0.5% TFA. The peptides were desalted with a Millipore ZipTip device in a final volume of 20 μl of 80% ACN elution solution. The solution was then dried using the SpeedVac. Dried samples were solubilized in water/0.1% formic acid before LC MS/MS analysis.

LC MS/MS Analysis—The samples were separated by online reversed-phase chromatography using a Thermo Scientific Proxeon Easy-nLC system equipped with a Proxeon trap column (100 μm ID × 2 cm, Thermo Scientific) and a C18 packed-tip column (75 μm ID × 10 cm, Thermo Scientific). The peptides were separated using an increasing amount of acetonitrile (5–35% over 100 min) at a flow rate of 300 nl/min. The LC eluent was electrosprayed directly from the analytical column, and a voltage of 1.7 kV was applied via the liquid junction of the nanospray source. The chromatography system was coupled to a Thermo Scientific Q Exactive mass spectrometer that was programmed to acquire in a data-dependent Top 10 method. The survey scans were acquired at a resolution of 70 000 at *m/z* 400.

Data Analyses—All MS data were processed with MaxQuant (25) using the Andromeda (26) search engine. The proteins were identified by searching MS and MS/MS data against the Decoy version of the complete proteome for Rattus norvegicus in the UniProt database (UniProt Consortium. Reorganizing the protein space at the Universal Protein Resource (UniProt. Nucleic Acids Res. 2012, 40 (Database issue), D71–5.) (Release June 2014, 33675 entries) combined with 262 commonly detected contaminants. Trypsin specificity was used for digestion mode, with N-terminal acetylation and methionine oxidation selected as variable, and carbamidomethylation of cysteines set as a fixed modification. We allowed up to two missed cleavages. For the MS spectra, an initial mass accuracy of 6 ppm was selected, and the MS/MS tolerance was set to 20 ppm for the HCD data. For identification, the FDR at the peptide spectrum matches (PSM) and protein level was set to 0.01. Relative, label-free quantification of the proteins was conducted using the MaxLFQ algorithm (27) integrated into MaxQuant with default parameters. The data sets and Perseus result files used for analysis were deposited at the ProteomeXchange Consortium (*28*) (http://proteomecentral.proteomexchange.org) via the PRIDE partner repository (29) with the data set identifier PXD001984 for cellular extracts (For reviewer access only Username: reviewer62003@ebi.ac.uk; Password: zokVruKN) and PXD001986 for the secretome analyses (For reviewer access only Username: reviewer19925@ebi.ac.uk; Password: PUUJeVfO). Analysis of the identified proteins was performed using Perseus software (http://www.perseus-framework.org/) (version 1.5.0.31). The file containing the information from the identification and hits from the reverse database were used, and proteins with modified peptides and potential contaminants were removed. The LFQ intensity was logarithmized (log2(x)). Categorical annotation of the rows was used to define the different group depending on the following: (1) the cell line (NT or K_D); (2) the treatment (Ctrl/LPS); and 3) the kinetics of the secretomes (1 h, 16 h, 24 h, 48 h, or 72 h). Multiple-sample tests were performed using ANOVA with a FDR of 5% and preservation of the group randomization. To evaluate the enrichment of the categorical annotations (Gene Ontology terms and KEGG pathway), Fisher's exact test was performed taking in account the results of the ANOVA for each group. Normalization was achieved using a Z-score with matrix access by rows. Only proteins that were significant by ANOVA were used for the statistical analysis. Hierarchical clustering was first performed using the Euclidean parameter for the distance calculation, and the average option for linkage in the rows and columns of the trees was used with a maximum of 300 clusters. To quantify fold changes in proteins across the samples, we used MaxLFQ. To visualize these fold changes in the context of individual protein abundances in the proteome, we projected them onto the summed peptide intensities normalized by the number of theoretically observable peptides. Specifically, to compare the relative protein abundances between and within samples, the protein length normalized to the log 2 protein intensities (termed the "iBAQ" value in MaxQuant) was included in the MaxLFQ differences. Functional annotation and characterization of the identified proteins were performed using PANTHER software (version 9.0, http://www.pantherdb.org) and STRING (version 9.1, http://string-db.org). The GeneMANIA Cytoscape plugin (30) was used to generate co-expression networks from cell extracts proteomics data. A "basal" network composed of 95,886 recognized interactions was generated from the data obtained by the analysis of K_D or NT cells under basal conditions. A supervised clustering was then performed to identify the top 100 molecules that coregulated with Anxa6 in this "basal network." The list of 100 genes which encoded molecules were identified was then assessed for gene set enrichment using EnrichR (31) and the GO classification. Following the same approach, two "LPS-stimulated" networks were then generated from the data obtained by the analysis of: (1) unstimulated or LPS-stimulated K_D cells (89,017 recognized interactions) and (2) unstimulated or LPS-stimulated NT cells (96 563 recognized interactions). A supervised clustering was then performed to identify the top 100 molecules that coregulated with NFKB1 in each of these "LPS-stimulated" networks. Both lists of 100 genes that encoded molecules were identified and then assessed for gene set enrichment using EnrichR and the GO classification. Finally, subnetworks of genes presenting significant enrichments for specific GO terms were selected and visualized on Cytoscape. For presentation purposes, nodes were assigned equal weights and subnetworks were slightly distorted to avoid nodes superimposition.

Systems Biology Analysis—The altered pathways relevant to overexpressed proteins in K_D PC1/3 cells were analyzed using Pathway Studio software v.10 (Ariadne Genomics, Rockville, MD). This soft-

ware helps to interpret biological meaning based on gene (protein) expression, to build and analyze pathways, and to identify relationships among genes, proteins, cell processes, and diseases. This software contains a built-in resource named ResNet, which is a database of molecular interactions based on natural language processing of scientific abstracts in PubMed. Using ResNet, a researcher can analyze the gene product/protein list and build a pathway using well-known interactions that are discussed in the existing literature. The program searches the current pathway database and ResNet for interactions with the selected entities and then adds them to the pathway. After the new pathway was constructed, we were able to obtain more detailed information regarding the putative pathways that were altered in response to LPS treatment.

Data Analysis of Mouse Peritoneal Macrophages—An analysis of previously publish data was done to obtain information concerning modifications of proteins induced in peritoneal macrophages from wild type (WT) or PC1/3 KO (KO) mice challenged by LPS (8 h) or not (10). Briefly, peritoneal macrophage from wild type (WT) and PC1/3 knocked out (KO) mice were collected as described previously (10). Cytosolic and membrane fractions were then prepared according to (16) and processed for Gel-LC-MSMS as described in 10. The resulting tryptic peptides were purified and identified by reversed-phase chromatography coupled to an LTQ-Orbitrap Velos (Thermo Scientific). For identification, raw files were filtered for high quality spectra and converted to mgf files using scaffold software (4.4.5) (17) and analyzed using ProteinPilot software 4.5 (18). For each samples all gel band of a particular condition were combined for protein identification. FDR was calculated using PSPEP files (Sciex) and protein alignment was done with the protein alignment template 2.0 (Sciex) using a local protein FDR of 95% (19) over a combined list of all identified proteins. Only proteins with a score of over 6, which represents the proteins identified with two or more unique peptides and at least a fold change of 4 (converted log2 value) were kept for analysis. The relative protein expression was calculated based on the protein score, which was shown to be an adequate relative indicator of the relative differential expression (20). Ratio between WT and KO was calculated using the sum of corresponding fractions. Gene ontology analysis was performed using Blast2go (21).The network analysis was performed as follows: The gene names of identified proteins were used as input to retrieve a network from STRING (22), and this network was then loaded into Cytoscape 3.2 (23, 24). with relative expression data using Id mapper. The Reactome FI pluggin was used to select a subnetwork of gene ontology terms and NCI database-associated specific proteins

Calcium Imaging—Cells were plated onto glass coverslips and loaded with 4 μM Fura-2 AM at room temperature for 45 min in growth medium. Recordings were performed in HBSS containing the following: 140 mM NaCl, 5 mM KCl, 2 mM $MgCl_2$, 0.3 mM Na_2HPO_3, 0.4 mM KH_2PO_4, 4 mM $NaHCO_3$, 5 mM glucose, and 10 mM HEPES adjusted to pH 7.4 with NaOH. The cells were then washed three times in HBSS. The fluorescence intensity of Fura-2 in each cell was monitored and recorded at 340 and 380 nm. To represent the variation in the intracellular free calcium concentration, the fluorescence intensity ratio represented by F340/F380 was used as an indicator of the changes in cytosolic Ca^{2+} concentrations.

Isolation of Human Immune Cell Subsets for the Migration Assay—Human blood samples were collected from healthy adult donors with informed consent obtained in accordance with Institutional Review Board approval from the Institut de Biologie de Lille. Mononuclear cells (PBMCs) were isolated from peripheral blood samples by density gradient centrifugation using Ficoll. Human NK, CD8+ and $CD4^+CD25^-$ conventional T cells were purified from PBMCs by magnetic separation using NK and T cell isolation kits as described by the manufacturer (Miltenyi Biotech, Bergisch Gladbach, Germany). The purity of the isolated NK, $CD8^+$, and $CD4^+$ T cells was >95%. NK cells were activated using recombinant IL-2 (200 UI/ml, BD Pharmingen, San Jose, CA) and IL-15 (200 UI/ml, BD Pharmingen). $CD8^+$ and $CD4^+$ T cells were activated with plate-bound anti-CD3 (1.5 μg/ml, Clinisciences, Nanterre, France) antibody and incubated at 37 °C for 2 h prior to culturing. Soluble mouse anti-human CD28 antibody (100 ng/ml, Clinisciences) was added to the cells at the time of culture.

Migration Assay—The different NK and T cell populations were harvested and suspended at a concentration of 10^6 cells/ml in RPMI 1640. The chemotaxis protocol was performed as previously described (32) using a 48-well microchemotaxis Boyden chamber with 5-μm pore polycarbonate filters. The cells were incubated for 2 h 30 min at 37 °C in 5% CO_2 with NR8383 secretomes (NT and PC1/3-K_D nonstimulated or stimulated with 200 ng/ml LPS for 24 h). Each condition was performed in triplicate. Cells that migrated through the filter were counted in the inferior well. The results are expressed as the number of activated cells that were attracted by each secretome compared with the nonactivated ones.

Cell Viability Measured by the CellTiter-Glo Assay—SKBR3 and SKOV3 cells were seeded into 96-well white plates (6500 and 3000 cells per well, respectively) with NR8383 secretomes obtained after 24 h of LPS stimulation or no stimulation. The assay was conducted for 24, 48, 72, or 96 h. For the 96 h+ medium, conditioned secretomes were removed at 72 h and replaced with fresh ones. CellTiter-Glo reagent (Promega) was added to the wells and incubated at room temperature for 10 min protected from light. The luminescence was recorded using a Berthold luminometer Centro LB960. The results are expressed as relative light units (RLUs).

RESULTS

PC1/3-knockdown NR8383 Cells Express an Inflammatory Profile—A stable PC1/3-K_D cell line has been developed by lentiviral delivery of shRNAs (11). To better understand the interaction and regulation of TLR4 by PC1/3, we used these PC1/3-K_D NR8383 cells in the present study. A proteomics analysis was performed to identify secreted proteins subsequent to PC1/3 silencing in NR8383 cells, before and after LPS challenge. Shotgun proteomics of secreted proteins (from 1 h to 72 h after stimulation) was performed for nontarget (NT) control cells and K_D cells (Fig. 1). More than 1400 proteins were identified in all analyses of the NR8383 secretomes (supplemental Data S1).

Comparison of the identified proteins between resting K_D or NT cells and cells challenged with LPS allowed the identification of 28 specific proteins that were directly related to PC1/3 (Fig. 1*A*). These proteins were only secreted by K_D cells, both resting and those stimulated with LPS. The proteins are involved in different functions, *e.g.* responses to stimuli, RNA processing, endocytosis, regulation of transcription, catabolism, protein binding, regulation of axogenesis and immune responses (Table I).

This study was then further coupled to a kinetic study at 1 h, 16 h, 24 h, 48 h, and 72 h after LPS challenge. Proteins with an abundance that was significantly different among the conditions were determined according to the MaxQuant and Perseus software. As a criterion of significance, we applied an ANOVA significance threshold of $p < 0.05$, and heat maps were created. A total of 125 proteins in the cell culture super-

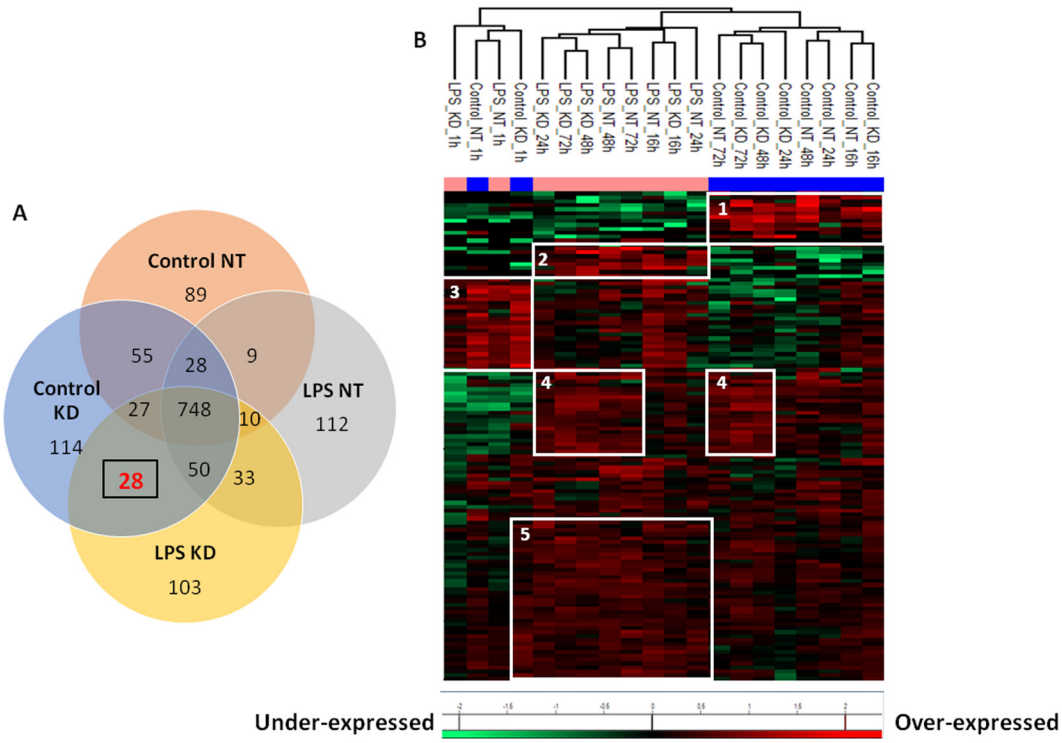

FIG. 1. **Secretome analysis strategy.** *A*, NR8383 cells were stimulated with LPS or were nonstimulated (control), and the supernatants were collected (from 1 h to 72 h). After the proteomic approach, the samples were analyzed by LC-MS/MS. The numbers of identified secreted proteins found in common or specific for K_D and NT macrophages (nonstimulated or stimulated with LPS) are represented in a Venn diagram. Twenty-eight proteins were specific to the PC1/3 K_D. *B*, Heat map of proteins with different secretion profiles in NR8383 macrophages stimulated with LPS *versus* nonstimulated (control). Distinct clusters are highlighted.

natants of the macrophages stimulated with LPS *versus* non-stimulated macrophages were considered reliable based on the statistical analysis (Fig. 1*B*, supplemental Data S2).

Two major branches of the heat map separate the 1-h series from the other time points. In the second branch, two branches distribute the control *versus* the stimulated cells. Each experiment was performed 3 times, and each sample corresponded to the statistical data obtained per condition. Five specific clusters of over-expressed proteins were retrieved. Cluster 1 is specific to the control (16 h–72 h). Clusters 2 and 5 are specific to LPS stimulation (16 h–72 h). Cluster 3 represents proteins found after 1 h in both control and LPS-stimulated cells. Cluster 4 is specific to later time points (48 h and 72 h). For each cluster, proteins with specific functions were characterized. For example, in cluster 2, proteins implicated in macrophage activation and the immune response were specific to LPS stimulation. In cluster 1, the majority of the proteins were implicated in protein synthesis associated with early stimulation. The complete list of proteins in these clusters is provided in Table II.

Among the proteins identified in clusters 4 and 5 (Table II) were the alarmins (*e.g.* GRP78, HSP84, HSP86, HSP73, calreticulin, capthepsin B, nucleolin, and granulins)(33). Alarmins are produced by immune cells through the endoplasmic reticulum (ER)-Golgi secretion pathway and are involved in triggering the adaptive immune response. Analyses of the other clusters revealed the release of chemokines (CXCL10 and CCL3), cytokines (MIF), interferon-inducible protein (IFI30) and growth factor (GDF15). Both chemokines and alarmins have known functions in immune responses. These proteins recruit and activate receptor-expressing cells of the innate immune system, including dendritic cells and CD4+ cells, and they also directly or indirectly promote adaptive immune responses (34).

To analyze the chemokine/cytokine pattern between NT and K_D PC1/3 NR8383 cells in detail, time course analyses of chemokine and cytokine protein expression were performed without quantification (Fig. 2*A*).

Both nonstimulated and challenged K_D cells secreted CCL3, CCL6, CCL9, CXCL10, CXCL2, MIF, and IL-1RA. Challenged K_D cells also secreted CCL7, CCL2, and CXCL3. Comparisons with NT cells revealed that most chemokines were released by both cell types. However, differences in the timing and nature of the secreted chemokines were evident. CXCL3 was only secreted by K_D cells, whereas the inhibitory chemokine TGF-β was secreted by NT cells. MIF protein was not secreted by NT cells in response to LPS stimulation. To validate these results and to quantify the chemokine and cytokine levels released by NR8383 cells, cytokine arrays were performed after 24 h of stimulation (Fig. 2B). As shown, NR8383

TABLE I
List of 28 secreted proteins specific to PC1/3 knockdown from Figure 2A

Protein Name	Biological Function
Protein Arap1	Response to stimuli, signal transduction
Choline-phosphate cytidylyltransferase A	
STE20-like serine/threonine-protein kinase	
Mitogen-activated protein kinase 14	
Inositol polyphosphate-1-phosphatase	
Paired immunoglobulin-like type 2 receptor alpha	T cell activation, regulation of inflammatory responses
Galectin-1	
Protein Vnn1	
Insulin-like growth factor-binding protein 2	
Heterogeneous nuclear ribonucleoprotein M	RNA processing
DEAH box polypeptide 9	
Protein Ddx6	
rRNA 2′-O-methyltransferase fibrillarin	
Mitochondrial import inner membrane translocase	Protein folding and localization, endocytosis
Protein Txndc5	
Peptidyl-prolyl cis-trans isomerase	
Vacuolar protein sorting-associated protein 26A	
Protein RGD1309995	
UDP-glucose:glycoprotein glucosyltransferase 1	
H2-K region expressed gene 2	
ATPase Asna1	
Canopy 2 homolog	Regulation of transcription
Protein Cbx1	
Protein Raly	
Phospholipase A2	Catabolic processes
Xaa-Pro dipeptidase	
Protein Ubap21	Protein binding
Reticulon-4	Regulation of axonogenesis

cells secreted several chemokines, including CCL5, CCL3, CXCL9, CCL20, CXCL10, CXCL1, and CXCL2. We established that without LPS challenge, NR8383 K_D cells produced significantly more CCL5, CXCL1, CXCL2, CXCL10, IL-6, and TNF-α than NT cells (Fig. 2*B*). Moreover, following LPS challenge, K_D cells additionally produced CXCL9 and CCL20 and concomitantly released the previous cytokines and chemokines CXCL1, CXCL2, CXCL10, IL-1α, and IL-1β. These chemokine and cytokine profiles are characteristic of secretion through the unconventional secretory pathway, which involves synthesis in the cytoplasm and release without passing through the ER and Golgi complex (35).

PC1/3-K_D NR8383 Cells and Modulation of the Intracellular Trafficking Machinery—Members of the IL-1 cytokine family, particularly IL-1α and IL-1β are key inflammatory cytokines that are released through the unconventional secretory pathway. Unconventional vesicular or organellar pathways have been discussed. To determine whether the secretory pathway is affected by PC1/3 K_D, proteomic studies of the cellular contents were undertaken in NT and K_D cells under either resting conditions or at 24 h post-LPS stimulation (Fig. 3, supplemental Data S3). For the ANOVA test, the samples were classified between NT and K_D. Two clear clusters were highlighted. Cluster number 1 represents over-expressed proteins in K_D cells, whereas cluster number 2 groups over-expressed proteins in NT cells (Fig. 3*A*, Table III and supplemental Data S4). The proteins in each cluster were then analyzed using PANTHER software (http://www.pantherdb.org) to determine the biological functions based on the protein classes. Using this analysis, we demonstrated that over-expressed proteins in K_D cells were implicated in cell adhesion, extracellular matrix or cytoskeleton, whereas in NT cells, over-expressed proteins were involved in nucleic acid binding or oxidoreduction functions (Fig. 3*B*). For a more detailed analysis, we performed a systems biology analysis for network identification of the over-expressed proteins in PC1/3-K_D cells (Fig. 3*C*). Differential pathways were generated using the "direct interaction" algorithm to map the relationships of the identified proteins (supplemental Data S5). We found that among the 85 altered proteins, 32 proteins had direct regulatory relationships, including binding, post-translational modifications and transcriptional regulation. Different biological processes are represented by the over-expressed proteins in PC1/3 K_D cells (Fig. 3*C*). For instance, these proteins are involved in actin organization, inflammatory responses, cytoskeletal assembly, T cell activation and calcium channels. Several of the identified proteins were clustered under certain functional classes, such as cellular remodeling (Cluster 1, supplemental Data S5), immune activation and calcium export (Cluster 2, supplemental Data S5), which is consistent with the

TABLE II
List of proteins identified in specific clusters after Perseus analyses from Figure 2B and Supplementary data 2

Cluster 1	Cluster 2	Cluster 3	Cluster 4	Cluster 5
Alcam	Sqstm1	LOC685186	Rplp2	Hspa8
Mif	Marcks	Eef2	P4hb	Atic
Lpl	Sdc4	Txn	Hspa5	Aldoa
Ifi30	Cxcl10	Pgk1	Ncl	Pygl
Smpdl3a	Ccl3	Tcp1	Calr	Rpl5
Gpnmb	Hn1	Ywhab	Vim	Cltc
Ganab	Ndrg1	Rhoa	Fabp5	Pkm
Fkbp2	Gdf15	Eef1a1	Arhgdia	Hsp90ab1
Axl		Gm15013	Tpm3	Cfl1
Lyz2		Ran	Hnrnpa3	Vcp
Ctsd		Gnb2l1	Prdx5	Tpi1
Npc2		Actg1	Prg4	Tkt
		Ywhaq	Calu	Gdi2
		Clic1	Akr1b8	Ywhag
		Tuba1b	Grn	Rps11
		Cdc42	Ahnak	Tmsb4x
		Rpl7	Ctsb	Atp6v1b2
		Cct8	Tpm4	Ywhah
		Tubb4b	Eef1b2	Hsp90aa1
		Ugp2		Pgd
		Eif4a1		Cap1
		Rpl4		Vat1
				Eif5a
				Actr3
				Cct2
				Prdx1
				Myl6
				Eef1d
				Cndp2
				Cct4
				Pdcd6ip
				Flna
				Atp6v1a
				Cct7
				Msn
				Kpnb1
				Iqgap1
				Tln1
				Cct6a

results obtained using PANTHER software analysis (Fig. 3*B*). Further demonstrating the impact of PC1/3 K_D on the cytoskeleton organization, we found that molecules co-up-regulated with Anxa6 in K_D cells were highly significantly related with the GO terms "actin binding" or "extracellular vesicular exosome" (Fig. 4*A*).

Next, we focused on proteins that are important for the cytoskeleton (Table III). Among these cytoskeletal proteins, STRING analysis revealed that most of them are known to be involved in the ARP2/3 complex and the WAVE complex (WASF2, ACTR3, ARPC1B) (supplemental Data S6). Wiskott-Aldrich syndrome protein (WASP) is known to lead to upstream signals resulting in activation of the ARP2/3 complex, which causes a burst of actin polymerization and the formation of a lamellipodium structure. ARP2/3-complex-mediated actin polymerization is crucial for the reorganization of the actin cytoskeleton at the cell cortex during processes such as cell movement and vesicular trafficking (36). Moreover, macrophage activation promotes changes in macrophage cell elasticity that depend on actin polymerization. Cytoskeletal rearrangements are observed between activated and nonactivated macrophages: activated macrophages are elongated, whereas nonactivated cells are more circular (37).

To validate our hypothesis regarding cytoskeletal rearrangements, we incubated NR8383 macrophages with phalloidin to stain the actin filaments. We clearly demonstrated that resting PC1/3-K_D cells were more elongated and expressed a high level of directional actin-filled structures compared with NT cells (Fig. 4*B*a and b). In this context, PC1/3-K_D cells were polarized, with long actin filopodia that emanated from one side of the cell and actin-associated membrane

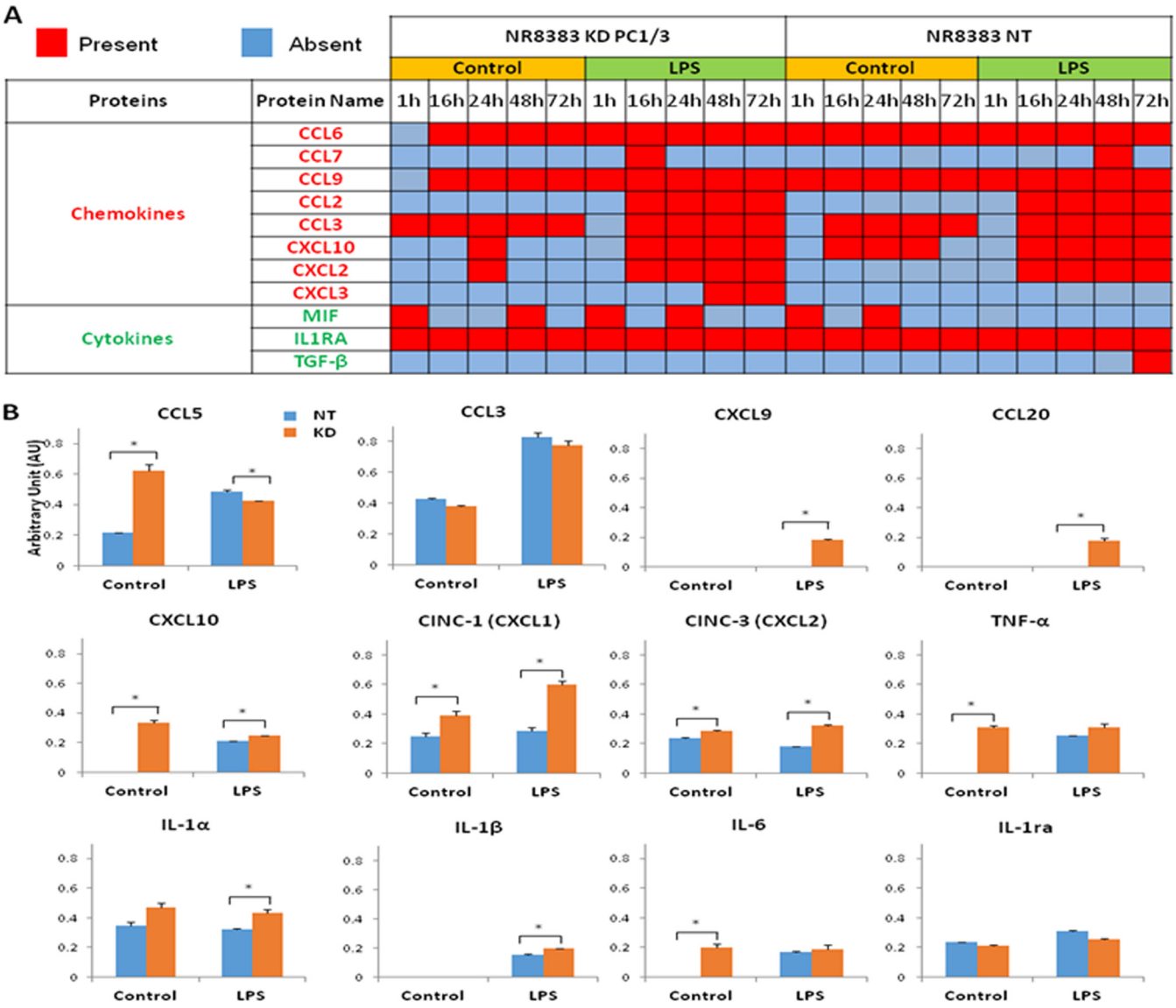

FIG. 2. **Chemokines and cytokines secreted by NT and K_D cells over the time that were challenged or not with LPS.** *A*, Mass spectrometry analyses allowed for the identification of chemokines and cytokines over time. For identification, FDR was set at 0.01. Blue indicates proteins that were absent, whereas red shows proteins that were present in the secretome. *B*, Rat cytokine array assay. Cells were untreated (control) or treated with LPS for 24 h. The NT cell secretomes are shown in blue, and the K_D cell secretomes are in orange. The bar diagrams represent the ratio of the spot mean pixel densities/reference point pixel densities. Significant differences were analyzed using Student's *t* test. $^*p < 0.05$.

ruffling on the other side (Fig. 4*B*b). Thus, PC1/3-K_D cells expressed an activated phenotype, and, in response to LPS challenge, the number of filopodia increased corresponding to a higher level of activation in these cells (Fig. 4*B*c and d). Filopodia in LPS-stimulated NT cells increased as compared with control cells demonstrating an activation state under LPS. These results are consistent with the data obtained using proteomics for cytoskeletal reorganization (Figs. 3 and 4*A*).

It has been shown that the cytoskeleton regulates cell polarity, migration and cytokine secretion via vesicular trafficking. Based on the proteomic data, proteins specific to Golgi vesicle transport were clearly under-expressed in K_D cells (Table IV).

Among them, we found the following proteins in the same cluster: STX7, USO1, NSF, and COPG1. These proteins are required for transport from the endoplasmic reticulum to the Golgi stack (38) and catalyze the fusion of transport vesicles within the Golgi cisternae. By contrast, endosome-specific proteins (early, late, recycling) APPL1, VAC14, EHD4, VPS4B, ANXA6, and RAP2B and GGA2 proteins involved in protein trafficking between the trans-Golgi network (TGN) and endosomes were over-expressed in K_D cells (Table IV). These

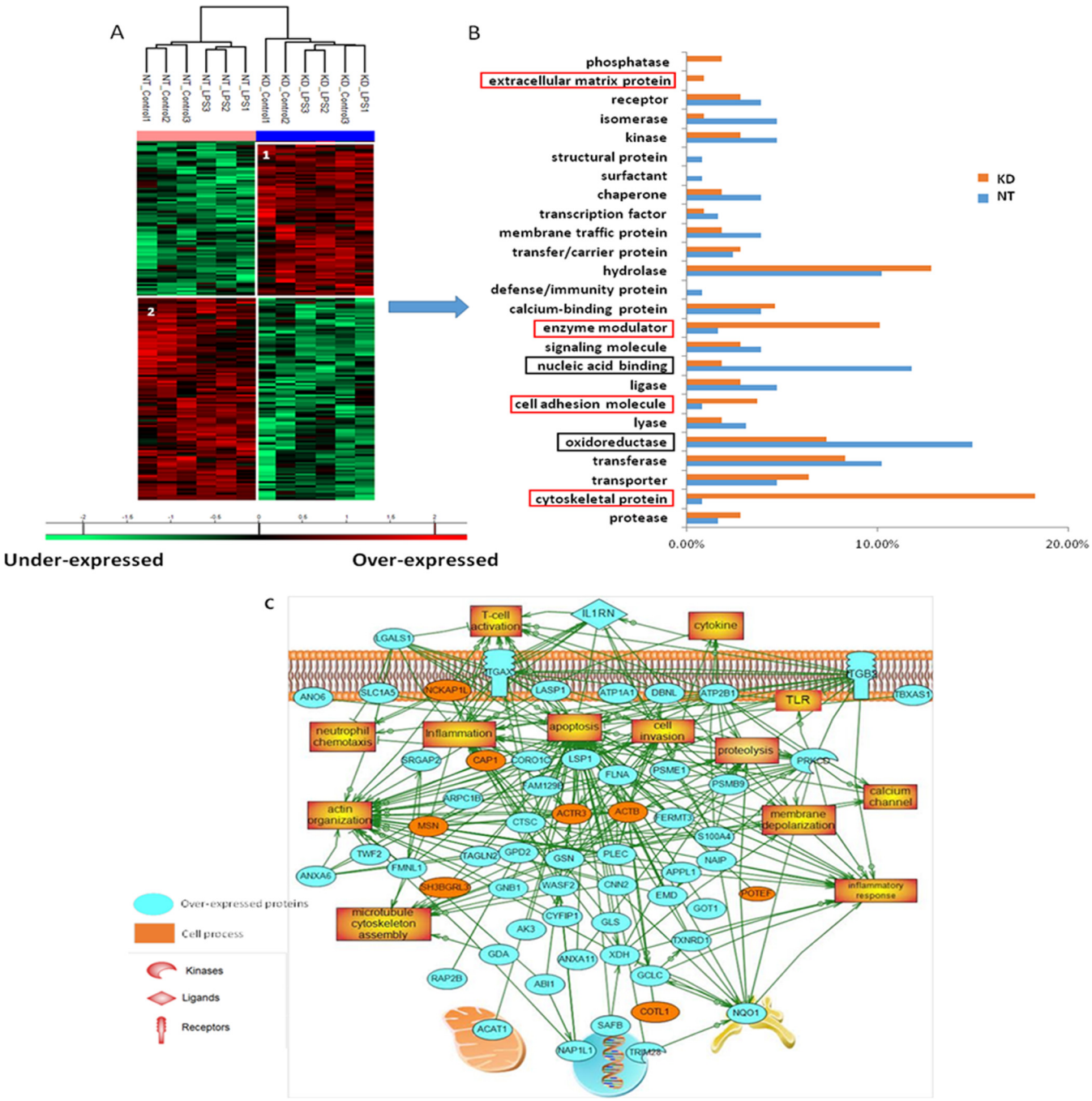

FIG. 3. **Whole-cell extract analysis strategy.** *A*, NR8383 cells were stimulated with LPS (200 ng/ml) or not (control) and lysed before FASP and LC-MS/MS analysis. MaxQuant and Perseus software were used for the statistical analysis, and a heat map was generated to show proteins that were significantly different between NT and PC1/3-K_D NR8383 macrophages in the cell extracts. Two clusters are highlighted. *B*, The proteins in each cluster were analyzed using Panther software. The biological functions associated with these proteins are shown. The functions framed in red correspond to those of proteins that were over-expressed in K_D cells, whereas the functions framed in black correspond to those of proteins that were over-expressed in NT cells. *C*, Global pathway analysis of the over-expressed proteins identified in PC1/3-K_D cells. Over-expressed proteins in PC1/3-K_D cells were involved in global altered molecular pathways. The different colors reflect the degree of expression. Proteins in blue are over-expressed in PC1/3-K_D cells, whereas those in orange show no expression differences between NT and K_D cells.

proteins are required for the regulation of cell proliferation in response to extracellular signals from an early endosomal compartment and also play a role in the biogenesis of endosome carrier vesicle (ECV)/multivesicular body (MVB) transport intermediates from early endosomes (38). Moreover, these proteins are involved in the late steps of the endosomal

TABLE III
List of proteins identified in specific clusters after Perseus analyses from Fig. 3A and supplementary Data S4

Cluster 1			Cluster 2		
LOC684352	Lgals1	Slc1a5	Fcgr2b	Hspa5	Ephx2
Cotl1	Got1	Bpnt1	Colgalt1	Eno2	Aldh3b1
Acad9	Gls		Rpl22l2	Manf	Ogdh
Fermt3	Gclc		Acad11	Acaca	Aarsd1
Fam129b	Il1rn		Uap1l1	Pdia3	Pdk1
Flna	Plec		Sh3bgrl	Ncl	Nucb1
Nckap1l	Gpd2		Ganab	Etfa	Camk1
Atp2b1	Acadvl		Hist1h1b	Anxa3	Cd14
Fmnl1	Anxa6		Ktn1	Pgk1	Aldh7a1
Nmral1	Tbxas1		Cul4b	Ppib	Atg7
Naip5	Pdhb		Ube2m	Pgam1	Npl
Gsdmd	Gnb1		Plod1	Scarb2	Nasp
Cnn2	Rap2b		Eif4g1	Aldh1l1	Snd1
Itgax	Ctsc		Siglec1	Psmb6	G3bp2
Srgap2	Ctbs		Usp5	Pfkl	Atp6v1d
Ahcyl1	Nit2		Naglu	Pebp1	Gpi
Vsig8	Vps4b		Atp6v1a	Uso1	Nampt
Cyfip1	Lsp1		Apobr	Idh1	Ero1l
Anxa6	Actr3		Fam120a	Tpi1	Pcyox1
Cct8	Wdr1		Rab32	P4ha1	Cth
Ipo7	Tagln2		Hyou1	Prkaa1	Fam129a
Wasf2	Anxa11		Fdps	Timm10	Slc9a3r1
Msn	Ech1		Hexb	Vamp3	Bche
Xdh	Adk		Slc25a13	Dnaja1	Uggt1
Slc25a12	Gsn		Dst	Phb	Fkbp4
Ano6	Tuba3a		Gale	Fabp4	Dnajc3
Itgb2	Psmb9		Calu	Eif2s3	Ak4
Coro1c	Ak3		Atp13a1	Ssrp1	Tpmt
Hnrnpd	Psme1		Acly	Eif3a	
Nap1 l1	Emd		Psmd5	Vat1	
Strn	Hdhd2		Aldh3a2	Ddhd1	
Gga2	Cct4		Vav1	Txndc12	
Safb	Vac14		M6pr	Pgm1	
Arpc1b	Ehd4		Gaa	Copg1	
Txnrd1	Lasp1		Stx7	Creld2	
Nqo1	Dbnl		Por	Fam162a	
Atp1a1	Sfxn3		Ldha	Creld1	
Prkcd	Gda		Gapdh	Ufm1	
Aldh4a1	Abi1		Aldoa	Lpcat3	

MVB pathway. MVBs contain intraluminal vesicles that are generated by the invagination and scission from the limiting membrane of the endosomes and are mostly delivered to lysosomes, enabling the degradation of membrane proteins. This phenomenon indicates that PC1/3 K_D remodels the endosomal compartment, which is consistent with our data obtained using macrophages isolated from PC1/3-KO mice. Ontogenic enrichment of proteins issued from our previous publish proteomic analyses of peritoneal macrophages (10) from wild type (WT) or PC1/3 KO (KO) mice challenged by LPS (8 h) or not, confirms the over-expression of cytoskeleton proteins as well as GTPase activity (5 Go terms) (Fig. 5*A*). STRING analysis of proteins with GTPase activity has been performed and the network subsequently analyzed using the visualization tool Cytoscape followed by the Integrated Reactome FI analysis tool which selects subnets with specific ontogenetic functions. The biological interaction network GTPase proteins included 202 proteins. Among the groups of proteins with specific ontogenic functions two groups are overexpressed in KO samples *i.e.* receptor activity and vesicles trafficking. We focused our attention on the last one (Fig. 5*B*). The network consists mainly of small G proteins and Rab proteins responsible for their regulation. The center of the network, the protein Agfg1 (Arf-GAP domain and FG repeats-containing protein (1), has an important role in endocytosis (39) At the periphery of this protein, several Rab show a similar expression profile which is over-expressed in unstimulated KO sub-sample and expressed when stimulated with LPS. These Rab (Rab8, Rab11, Rab14 and Rab27) all have a common function that is exocytosis and secretion (40). This disruption of molecular pathways secretion and the increase of membrane targeted molecules involved in vesicle-associated functions in PC1/3 KO mice (Fig. 5*C*) correlate with dysregulated cytokine secretion as well as intracellular disruption as we found in NR8383 PC1/3 K_D cells. Moreover, these results in both NR8383 PC1/3 K_D cells and PC1/3 KO macrophages are also consistent with the data obtained from the kinetic study of secretion showing a lot of proteins involved in exosomes.

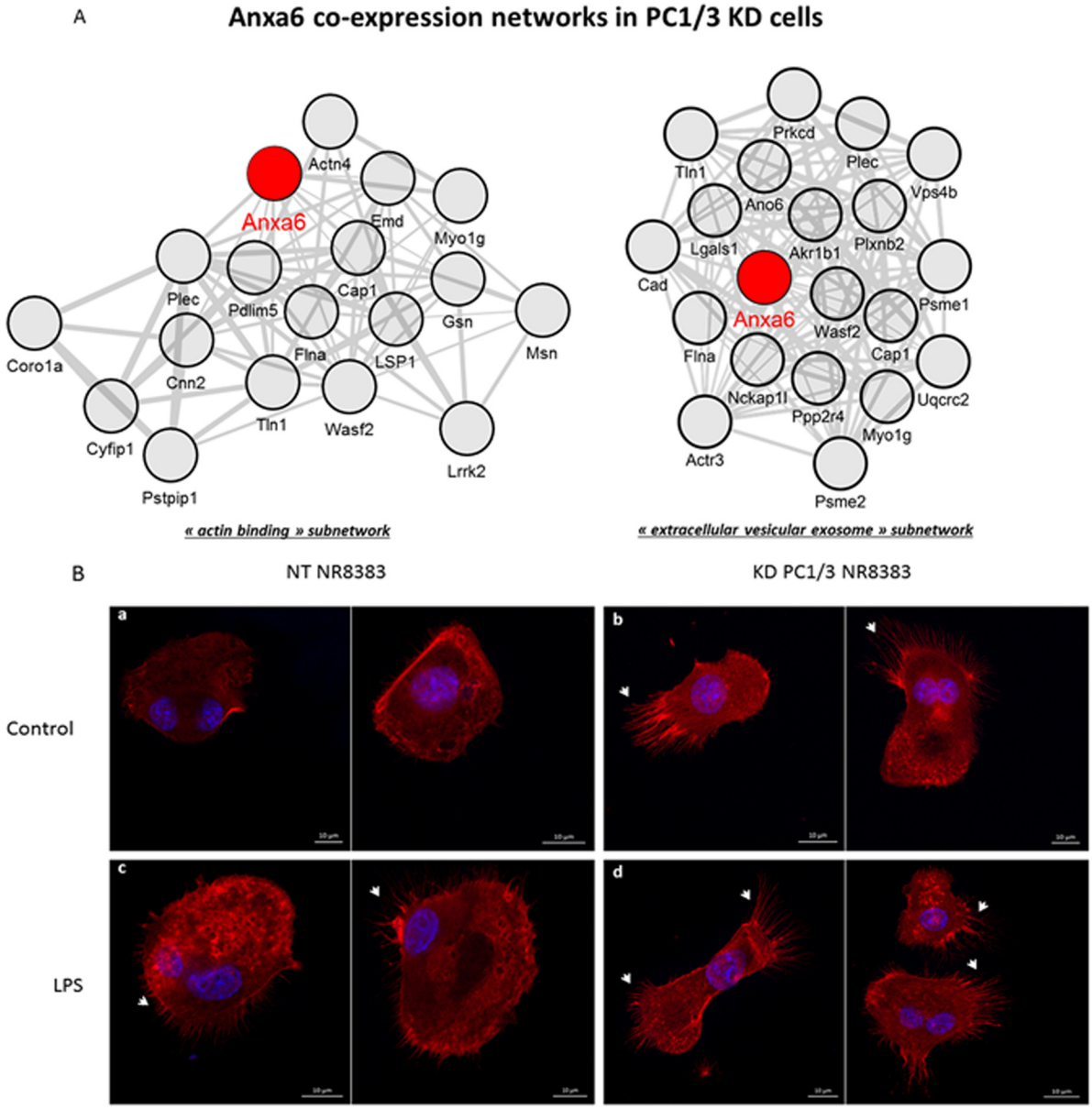

FIG. 4. **PC1/3-K_D cells exhibit cytoskeletal reorganization.** A, Analysis of co-expression network identifies cytoskeletal reorganization in K_D cells. The 100 genes which encoded molecules were the most tightly coregulated with Anxa6 in unstimulated K_D cells were identified and assessed for gene set enrichment. Shown are subnetworks of genes annotated by the GO terms "actin binding" (adjusted *p* value for enrichment significance = 6.1e-8) (left panel) or "extracellular vesicular exosome" (adjusted *p* value for enrichment significance = 3.1e-10) (right panel). Only 18 out of 50 genes forming the subnetwork "extracellular vesicular exosome" are shown. *B,* Confocal imaging of NR8383 cells stained with rhodamine-phalloidin (1/100^e). The nuclei were counterstained with Hoechst 33342 (blue). The cells were stimulated with LPS (**c** and **d**) or left untreated (**a** and **b**) for 24 h. Scale bar, 10 μm.

The large amount of inflammatory cytokines produced by the activated PC1/3-K_D cells is consistent with MVB discharge. Interestingly, the cytoskeleton, MVB discharge (38, 41) and Ca^{2+} signaling are linked. Indeed, increasing intracellular Ca^{2+} levels stimulate exosome secretion (41). Moreover, the disruption of actin filaments inhibits Ca^{2+} signaling (42). It has been shown that T cells deficient in WAVE2 and WASP present impaired Ca^{2+} mobilization (43). Gelsolin is another protein that promotes the assembly of actin filaments and has Ca^{2+} binding sites. A low concentration of Ca^{2+} inhibits actin binding, whereas a high Ca^{2+} concentration exposes actin binding sites (44). We have shown that in PC1/3-K_D cells, gelsolin and certain proteins implicated in the WAVE2 and WASP complexes are over-expressed (Table III). Moreover, cytokine secretion is dependent on an increase in intracellular Ca^{2+} (45). The inhibition of store-operated channels (SOCs) leads to a decrease in TNF-α and IL-6 secretion (46). To determine whether calcium homeostasis was impacted in

TABLE IV
List of proteins implicated in the canonical and non-canonical pathway of cytokine secretion

Cellular compartment	Protein name	NT		KO	
		control	LPS	control	LPS
Early endosome	Filamin A	27.3099	26.6311	28.113	27.8758
	DCC-interacting protein 13 alpha	18.3755	18.6619	19.6669	19.7339
	Protein Vac 14	22.4716	21.1599	22.9718	22.4599
	EH-domain containing protein 4	23.5251	22.8681	25.4616	25.3642
	Vacuolar protein sorting associated	22.3025	21.3796	23.1595	22.149
Late endosome	Annexin A6	26.8954	26.0519	27.7486	27.0312
Recycling endosome	Ras-related protein Rap-2b	22.2046	21.6395	23.7746	22.9046
	Vesicle-associated membrane protein 3	26.1284	25.8384	25.4235	24.6955
Golgi vesicle transport	General vesicular transport factor p115	25.111	24.2455	24.2114	23.9002
	Vesicle-fusing ATPase	24.2388	23.3532	23.4758	22.3273
	Syntaxin-7	25.0211	24.8745	23.6678	23.9568
	Coatomer subunit gamma 1	23.9452	23.0883	23.0444	22.6604
Clathrin mediated endocytosis	Sialoadhesin	23.0034	23.3274	19.2157	21.5666
	Twinfilin-2	23.0461	23.0252	23.5662	23.9651
TGN to endosomes	ADP ribosylation factor-binding protein	21.8125	19.7305	23.7937	22.5062

NR8383 cells, we performed calcium imaging experiments (Fig. 6).

For that purpose, we used the calcium probe fura-2AM to evaluate the cytosolic calcium concentration ((Ca^{2+})) in sterile conditions or in response to LPS exposure. We clearly demonstrated that LPS ($n = 3$) rapidly induced a pronounced elevation of (Ca^{2+})c in NR8383-K_D cells compared with NT cells (Fig. 6*A*, 6*B*). Fig. 6*A* shows the Ca^{2+} signals from individual cells, which are quantified in Fig. 6*B*. We next investigated whether other features important for calcium homeostasis were affected in NR8383-K_D cells. Fig. 6*C* shows the quantitative results obtained from original traces of similar Ca^{2+} imaging experiments. Resting (Ca^{2+})c levels were significantly increased in NR8383-K_D cells. To more thoroughly investigate how the (Ca^{2+})c in NR8383-K_D cells was affected, we examined two key processes that determine the basal (Ca^{2+})c in cells. First, we measured store-operated calcium entry (SOCE) mediated by SOCs. SOCs are located in the plasma membrane and are activated by depletion of the internal Ca^{2+} store in response to stimulation of the surface receptor-coupled signaling pathway (47). Ca^{2+} entry mediated by SOCE directly influences (Ca^{2+})c. New intracellular Ca^{2+} imaging experiments were conducted using the SERCA pump inhibitor thapsigargin (TG) as a store-depleting agent (48). As expected, the addition of 2 mM extracellular calcium to NR8383 cells that had been pre-incubated for 10 min with TG (1 μM) in Ca^{2+}-free medium to achieve complete ER Ca^{2+} store depletion resulted in marked and sustained elevation of the (Ca^{2+})c because of the activation of SOCE (Fig. 6*D*). The peak (Ca^{2+})c elevation in relation to SOCE increased by ~70% in K_D NR8383 cells (Fig. 6*E*). Moreover, an increasing (Ca^{2+}) in the bathing solution from 0 mM to 2 mM produced more significant elevations of the basal (Ca^{2+})c in K_D NR8383 compared with NT cells (Figs. 6*F*, 6*G*). Notably, we observed higher resting (Ca^{2+})c levels in NR8383-K_D cells compared with NT cells at normal 2 mM external Ca^{2+} concentrations prior to the application of TG (Fig. 6*F*). This finding suggests that the PC1/3 K_D also promoted enhanced basal Ca^{2+} influx and not only SOCE. The application of TG in the presence of 2 mM extracellular calcium clearly showed that SOCE was not sustained in control cells compared with NR8383-K_D cells. Taken together, these results demonstrate that the basal (Ca^{2+})c increased in K_D NR8383-K_D cells in relation to SOCE and the increase in the constitutive Ca^{2+} influx, which is consistent with the results obtained for the cytoskeletal rearrangements and cytokine release in these cells.

PC1/3-K_D NR8383 Cells and the TLR4 Intracellular Signaling Pathway—As shown previously, in response to LPS treatment, PC1/3 and TLR4 colocalize in the endosomal compartment (11). In PC1/3-K_D cells, this compartment is disorganized (10, 11) (Table IV), and uncontrolled cytokine secretion is observed following LPS stimulation (10). Altogether, these results indicate that PC1/3 or its products may contribute to the regulation of TLR4 signaling. Proteomic data for the cellular extracts allowed us to focus on proteins implicated in immune system responses, particularly TLR signaling (Table V, supplemental Data S3).

LPS stimulation of TLR4 results in the activation of MyD88-dependent signaling and subsequently NF-κB signaling activation. TLR4 can also mediate the activation of MyD88-independent signaling after its internalization leading to the activation of interferon response factor (IRF) 3 (4). It appears that proteins involved in TLR4 signaling were modulated in NR8383-K_D cells. Most importantly, the relative abundance of IRF3 decreased, whereas that of NF-κB1 (also known as p105) increased (Table V). This finding demonstrated that NF-κB was solicited rather than IRF3 and, thus, suggested that the TLR4 MyD88-dependent pathway was activated in K_D cells. Detailed analyses of the results reinforced this hypothesis (supplemental Data S3). Indeed, we observed an over-expression of interleukin-1 receptor accessory protein

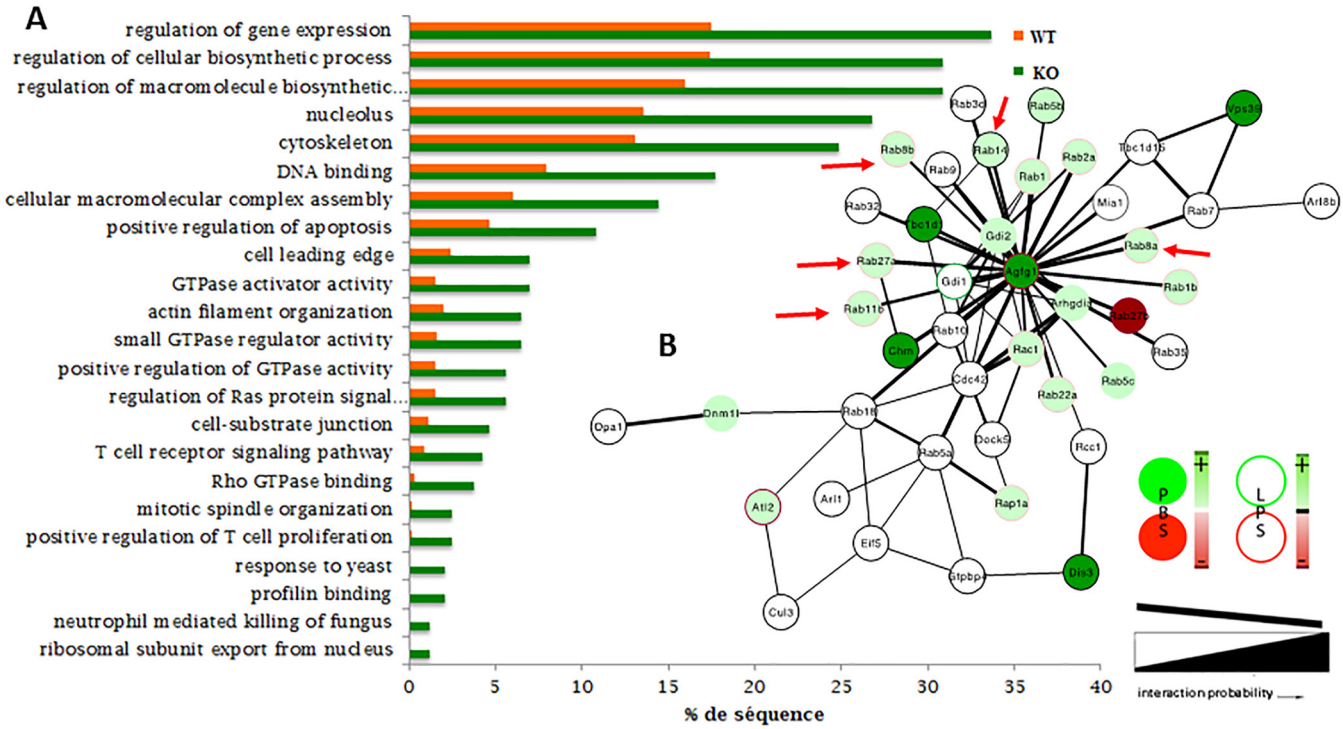

C

	KO-specific membrane-targeted molecules	
	N	Enrichment analysis
Unstimulated macrophages	428	"extracellular vesicular exosome" p = 1.75E-11
LPS-stimulated macrophages	493	"post-Golgi vesicle-mediated transport" P = 0.009

FIG. 5. **PC1/3 KO (KO) mice challenged by LPS exhibit disruption of molecular pathways secretion correlates with dysregulated cytokine secretion.** *A*, Ontogenic enrichment of proteins issued from proteomic analyses of peritoneal macrophages from wild type (WT) or PC1/3 KO (KO) mice challenged by LPS (8 h) *B*, Cytoscape followed by the Integrated Reactome FI analysis tools focus on vesicles trafficking has been realized. The network consists mainly of small G proteins and Rab proteins responsible for their regulation. Color code corresponds to : green over-expressed, red under-expressed of the selected proteins (KO *versus* WT) and including treatment (center of the circle untreated, outline treated with LPS). *C,* Macrophages from PC1 KO mice exhibit increased membrane targeted molecules involved in vesicle-associated functions. The number of membrane-targeted molecules, here defined as molecules with a membrane/cytoplasm ratio >2, was higher in macrophages derived from KO mice as compared with macrophages from WT mice. Genes coding for KO-specific membrane-targeted molecules were significantly enriched in genes annotated with GO terms describing vesicle-associated functions or cellular compartments. These included the GO term "extracellular vesicular exosome" (p = 1.75E-11) in unstimulated macrophages and the GO term "post-Golgi vesicle-mediated transport" (p = 0.009) in LPS-stimulated macrophages.

(Il1Rap), a known active factor in TLR4 signaling that functions by mediating IL-1-dependent activation of NF-κB in the MyD88-dependent pathway. Moreover, the cytoplasmic inhibitor of TLR4 signaling, NLRX1, was under-expressed in both resting and challenged PC1/3-K_D cells (49). Finally, we observed that molecules co-expressed with NF-κB1 in LPS-stimulated K_D cells comprised Stat1 and Stat2, two major pro-inflammatory transcription factors that were not co-expressed with NF-κB1 in LPS-stimulated NT cells (Fig. 7). To determine whether NF-κB showed greater activation in PC1/3-K_D cells, we conducted Western blot studies of the TLR4 signaling pathway by studying IκB-α phosphorylation and IRF3 nuclear translocation (Fig. 8).

The fold change represents the ratio of the band intensity between LPS-stimulated and nonstimulated samples at each time point. The kinetics of the phosphorylation of IκB-α after LPS challenge from 1 h to 6 h clearly showed that the fold change in phosphorylated IκB-α was higher at 3 h in K_D cells compared with NT cells (Fig. 8*A*a, a′ and 8*B*a). At 1 h, the phosphorylation of IκB-α was high in both NT and K_D cells. This phosphorylation remained high in K_D cells at 3 h, whereas it decreased in NT cells. In K_D cells, a decrease in IκB-α

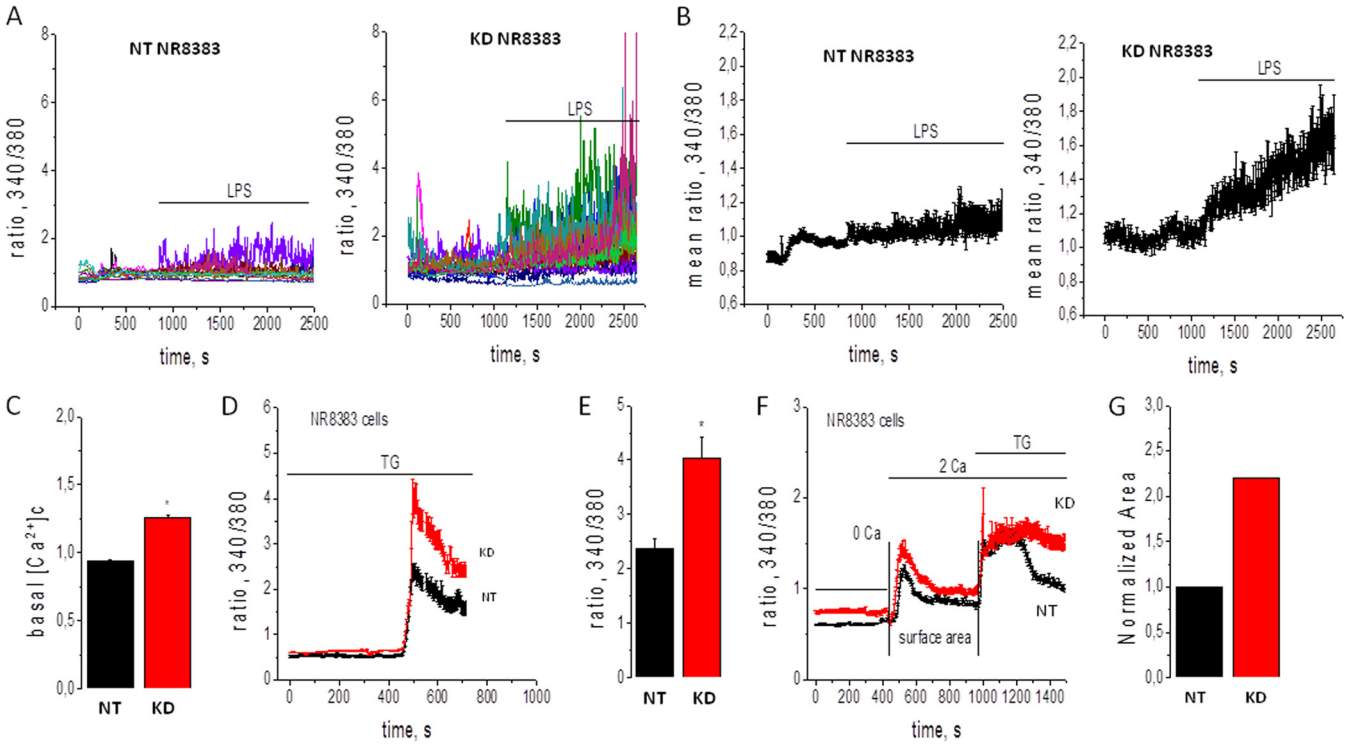

FIG. 6. **PC1/3-knockdown induces remodeling of Ca^{2+} homeostasis.** *A*, The cytosolic calcium concentration ((Ca^{2+})c) rose in NT and K_D NR8383 cells in response to LPS (horizontal bar). *B*, Quantification of the results presented in A. *C*, Quantification of the resting (Ca^{2+})c in NT and K_D NR8383 cells under basal conditions. *D*, Representative measurements of TG-activated SOCE, as indicated by the elevated (Ca^{2+})c in NR8383 cells. *E*, Quantification of SOCE in the results presented in *D*. *F*, The (Ca^{2+})c in the presence of 0 or 2 mM extracellular Ca^{2+} and after TG treatment in NT or K_D NR8383 cells. *G*, Quantification of the surface area presented in F following the application of 2 mM extracellular Ca^{2+}. $n = 3$.

TABLE V

List of selected identified proteins implicated in the immune system in NT and K_D PC1/3 resting (control) or LPS-stimulated macrophages

	Protein name	Gene name	NT		K_D	
			control	LPS	control	LPS
Chemokines and cytokines	Interleukin-1 receptor accessory protein	Il1rap	19.0246	19.2564	18.8126	20.2122
	C-X-C motif chemokine 2	Cxcl2	-	21.6242	-	22.83
	C-C motif chemokine 4	Ccl4	-	21.7711	21.7329	22.0981
	C-C motif chemokine 3	Ccl3	22.5974	27.755	24.8941	27.4812
	Macrophage migration inhibitory factor	Mif	28.5274	27.1267	26.8169	26.1873
Interferon-induced protein	Protein Ifit1	Ifit1	-	22.4039	-	24.6132
	Interferon-induced guanylate-binding protein 2	Gbp2	22.6232	24.1038	23.732	25.3116
TLR4 signaling	Nuclear factor NF-kappa-B p105 subunit	Nfkb1	19.4862	21.1055	21.2137	22.8011
	NF-kappa-B essential modulator	Ikbkg	20.5364	20.8487	20.5426	19.4019
	Interferon regulatory factor 3	Irf3	21.2062	20.5156	19.5384	19.2483
	Monocyte differentiation antigen CD14	Cd14	-	25.1175	-	18.7208
Other	Low affinity Fc-gamma receptor IIB isoform 1	Fcgr2b	26.4859	26.4101	20.9933	22.2522
	Interferon regulatory factor 5	Irf5	19.3744	19.9151	20.3435	20.7204

phosphorylation was observed at 6 h. These features demonstrate that in K_D cells, IκB-α phosphorylation was observed for a longer period, leading to NF-κB activation. The TLR4 MyD88-dependent pathway was involved at later stages compared with NT cells. We also focused on the TLR4 MyD88-independent pathway by examining the nuclear translocation of IRF3. After 3 h and 6 h of LPS stimulation, a duplication of the band corresponding to the various phosphorylated states of IRF3 was observed (Fig. 8*A*b′). However, no significant difference in IRF3 nuclear translocation was observed between NT and K_D cells over time (Fig. 8*B*b), suggesting that this pathway was not impacted by PC1/3 K_D (Fig. 8*A*b, b′ and 8*B*c). These data confirmed that NF-κB was mainly activated in PC1/3-K_D cells, as expected based on the proteomic analysis of the NR8383 cellular extracts. This phenomenon is also consistent with our results showing the remodeling of the endosomal compartment (10), (11) (Table IV) and perturbations in calcium homeostasis (Fig. 6).

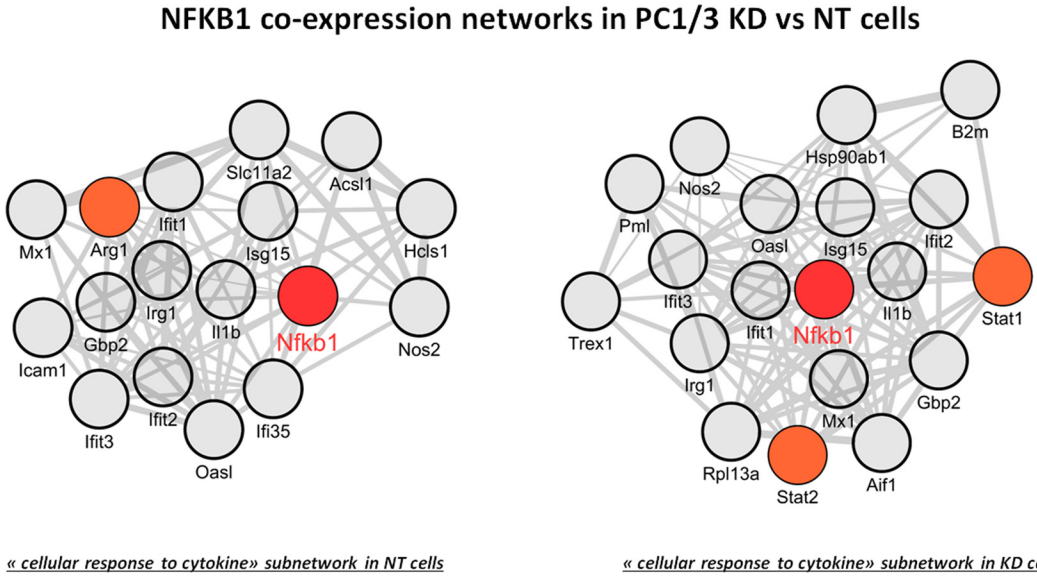

FIG. 7. **NFKB1 co-expression networks in PC1/3 K_D *versus* NT cells.** Lists of 100 genes which encoded molecules are the most tightly coregulated with NFKB1 in K_D or NT cells under LPS stimulation were established and assessed for gene set enrichment. Shown are subnetworks of genes annotated by the GO term "cellular response to cytokine stimuli" (adjusted p value for enrichment significance = 9.48e-6 in NT cells and 3.4e-7 in K_D cells). Note that Arg1, a prototypic M2 molecule, is specific to the NT subnetwork whereas Stat1 and Stat2, major pro-inflammatory transcription factors, are co-expressed with NFKB1 in K_D but not NT cells.

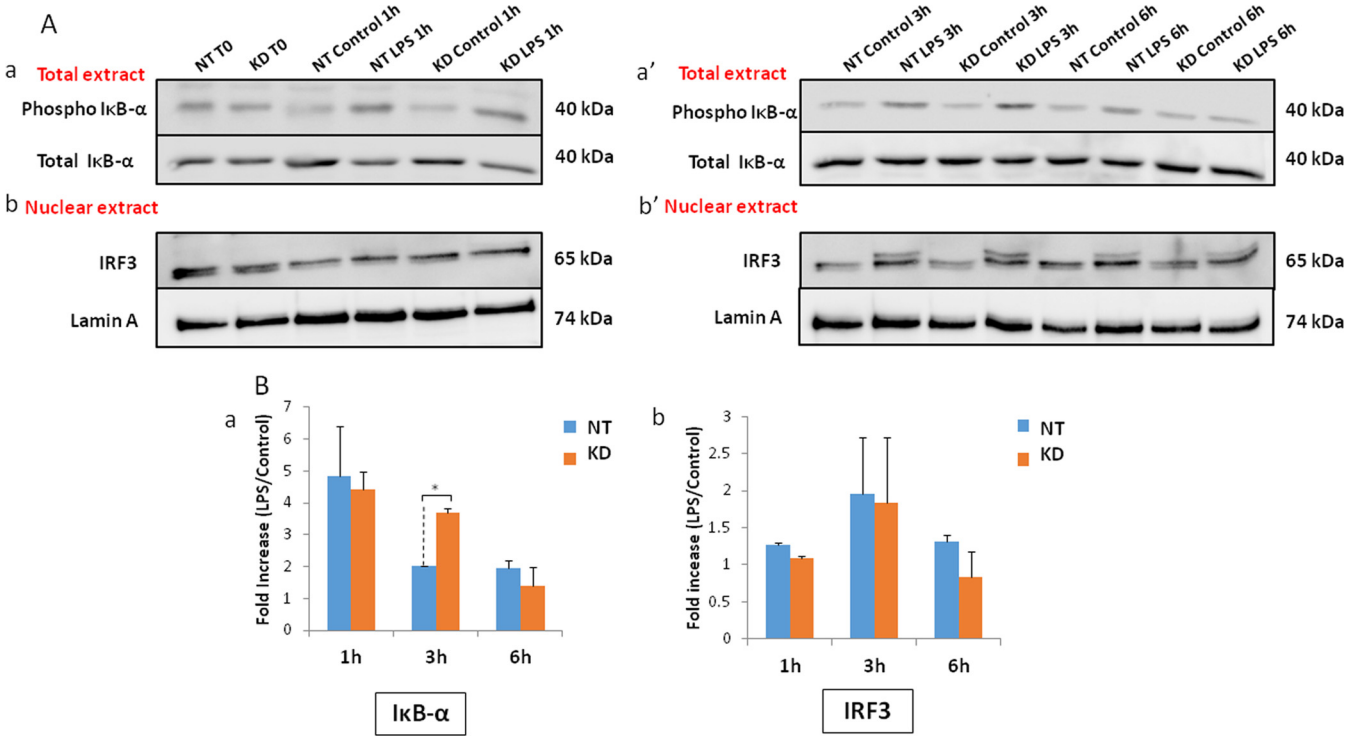

FIG. 8. **Western blot analysis of the TLR4 signaling pathway.** *A*, Western blot analysis of phospho IκB-α, total IκB-α (in total extracts, a and a'), IRF3 and Lamin A (in nuclear extracts, b and b') in NT or K_D PC1/3 NR8383 macrophages after LPS stimulation (200 ng/ml) or not at 1 h, 3 h and 6 h. *B*, Graphic representations of the quantification of phospho IκB-α (a) and IRF3 (b). The data are represented as the fold increase in samples stimulated with LPS relative to nonstimulated samples for phospho IκB-α and IRF3 and normalized to total IκB-α and Lamin A, respectively. * Significant differences between NT cells and K_D cells ($p \leq 0.05$) by t test. Experiments were performed in triplicate.

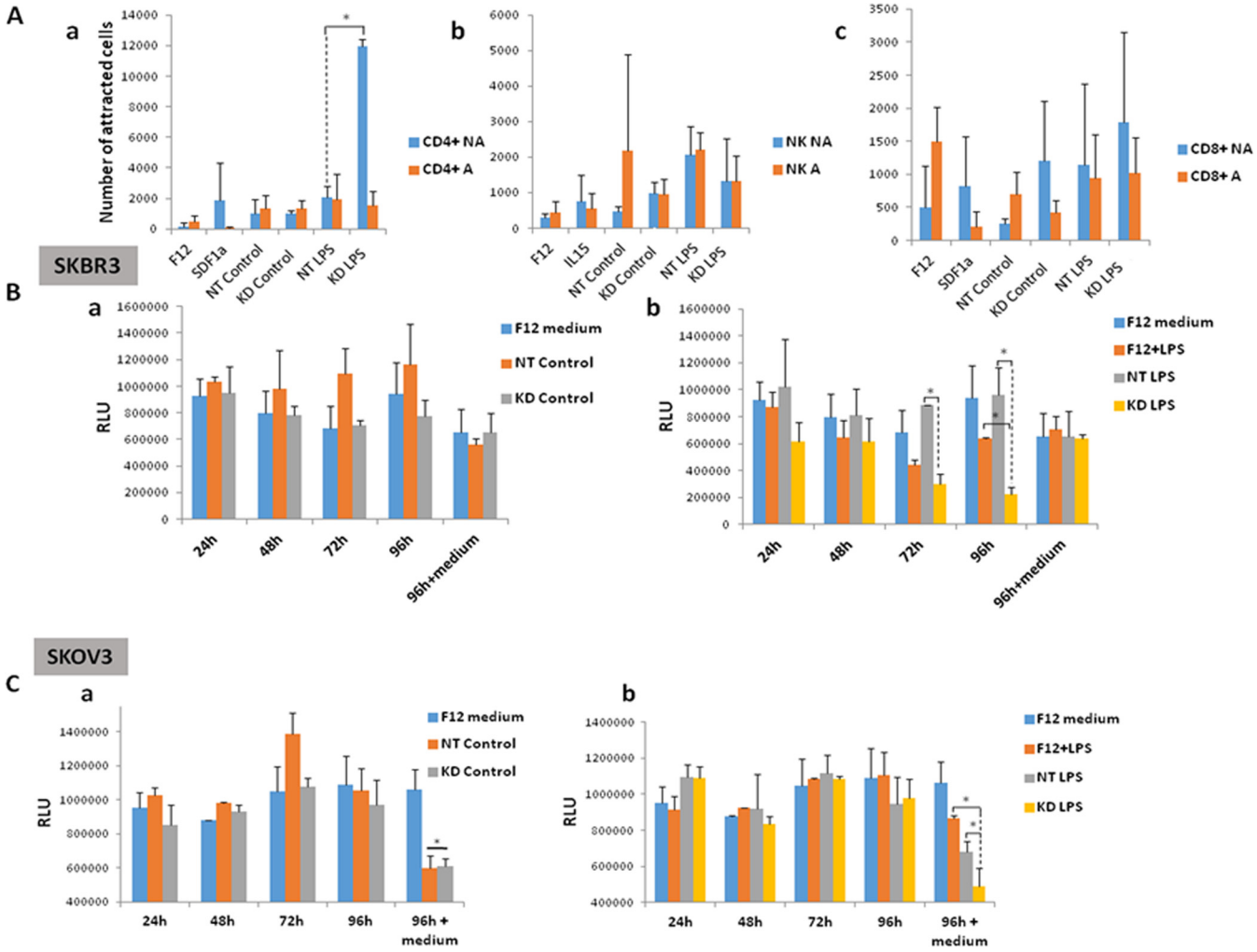

FIG. 9. **Chemoattraction and antitumor properties of NR8383 secretomes.** *A*, NR8383 PC1/3-K_D secretome enhanced CD4+ NA cell chemotaxis. Human primary leukocytes (CD4+ (a), natural killer (NK) cells (b) and CD8+ (c) cells that were activated (*A*) or nonactivated (NA)) were incubated in a Boyden chamber with NR8383 secretomes obtained at 24 h (control nonstimulated or stimulated with LPS) or F12 medium in the lower compartment. SDF1a and IL15 were used as controls for migration. Migration was conducted for 150 min. The results are presented as the number of cells that migrated. The experience was done in triplicates. *B*, *C*, The cell viability of SKBR3 cells (*B*) and SKOV3 cells (*C*) was determined using the CellTiter-Glo assay. The cells were incubated with NR8383 secretomes obtained at 24 h after no stimulation (a) or LPS stimulation (b). The assays were conducted for 24 h, 48 h, 72 h and 96 h. At 72 h, conditioned medium was replaced completely with fresh medium (96 h+ medium). The results were representative of three independent experiments. Significant differences were identified using Student's *t* test. $^*p < 0.05$.

Chemoattraction and Antitumor Activities of PC1/3-K_D Macrophage Secretomes—PC1/3 down-regulation in NR8383 macrophages strongly affected morphology and intracellular signaling pathways, leading to the secretion of large amounts of alarmins and pro-inflammatory chemokines and cytokines. These changes clearly suggest that PC1/3 K_D polarizes NR8383 toward an M1-like profile. M1 phenotype is characterized by high antigen presentation, high production of nitric oxide and high production of pro-inflammatory cytokines. They are known to have a killing function. In contract, M2 macrophages have repairing functions and produce high concentration of anti-inflammatory cytokines like IL-10.

The chemokines released by PC1/3-K_D macrophages are involved in leukocyte migration and activation (34) (Fig. 2*B*). CXCL10 (also known as IFN-γ-inducible protein of 10 kDa or IP-10) and CXCL9 (also known as monokine induced by IFN-γ or MIG) mainly function in T cell chemoattraction. These two chemokines share a common receptor: CXCR3. CXCR3 appears to be preferentially expressed on T lymphocytes (50). CCL20 is another chemokine that has been implicated in T cell chemoattraction, and the expression of its receptor, CCR6, has been detected in T and B lymphocytes (51). To investigate whether PC1/3-K_D NR8383 secretomes have chemotactic properties, assays were conducted in naïve (NA) or activated (A) T lymphocytes (CD4+, CD8+) and natural killer (NK) cells (Fig. 9*A*). Chemotaxis was performed in Boyden chambers using NR8383 secretomes as chemoattractant agents. The secretomes were obtained from

nonstimulated or LPS-stimulated NT or PC1/3-K_D macrophages after 24 h.

There was a significant attraction of CD4+ NA cells in the presence of the stimulated NR8383 PC1/3-K_D secretome (K_D LPS). We noticed a 6-fold increase in the attraction of CD4+ NA between NT LPS and K_D LPS secretomes (Fig. 9*A*a). No significant differences in chemoattraction were observed between NK and CD8+ cells (Figs. 9*A*b and c). The data indicated that immune factors produced by K_D cells following LPS challenge attracted naïve T helper lymphocytes (Th0; Fig. 9*A*a). Moreover, the nature of the chemokines and cytokines produced by the PC1/3-K_D cells could polarized these cells from a Th0 to a Th1 profile (TNF-α, IL-1α and IL-1β).

Next, we assessed the cytotoxic activities of NR8383 secretomes in the SKBR3 breast cancer cell line (Fig. 9*B*). The relative luminescence is proportional to cell viability and represents a measure of the level of ATP. Treatment with the supernatants of nonstimulated macrophages (control) did not affect the number of living cells (Fig. 9*B*a). Treatment with the supernatants of LPS-stimulated macrophages led to a decrease in the number of living cells at 72 h and 96 h (Fig. 9*B*b). A 3-fold decrease in the intensity of luminescence was observed between NT and K_D cell secretomes (LPS) at 72 h. At 96 h, a 5-fold decrease was observed. The decreased number of living SKBR3 cells demonstrated the anti-proliferative activity of PC1/3-K_D cell supernatants following LPS stimulation. Toxic tumor effects resulted from K_D macrophage activation and were mediated by soluble factors which is in line with the high level of chemokines secreted under LPS treatment. Moreover, LPS challenge triggers the release of specific factors impacting the viability of cancer cells. Such factors are absent in naive cells secretomes.

We then conducted these tests in an ovarian cancer cell line (SKOV3; Fig. 9*C*). The results confirmed that the secreted factors from PC1/3-K_D macrophages exerted antitumor activities, but in different ways, depending on the cell line considered. In SKOV3 cells, the effects were registered at 96 h after refreshing the conditioned medium with activated secreted factors from LPS-challenged PC1/3-K_D macrophages (Fig. 9*C*b). Under these conditions, NT and K_D cells in sterile conditions affected the viability of the SKOV3 tumor cells. A 1.7-fold decrease in luminescence intensity was observed when the cells were exposed to nonstimulated NT and K_D cell secretomes (Fig. 9*C*a). In LPS-challenged conditions, this decrease was 2.2 fold for the K_D secretome and 1.4-fold for the NT secretome.

These results suggested that these two cell lines did not have the same sensitivity toward factors secreted by PC1/3-K_D macrophages. SKBR3 cells were more sensitive to the direct actions of the secreted factors. SKOV3 cells were sensitized by these factors, and renewal of the conditioned medium with fresh medium containing the same secreted proteins affected their proliferation. This difference in response to treatment between SKBR3 and SKOV3 cells was noted recently (52). One major difference between these two cell lines is the production of inhibitory cytokines, such as IL-10: SKBR3 cells produce IL-10, whereas SKOV3 cells do not. Nevertheless, in both cases, the factors secreted by PC1/3-K_D NR8383 cells were active toward the tumor cells. In those conditions, we assessed whether PC1/3-K_D cells were susceptible to IL-10 in terms of their secretion of pro-inflammatory cytokines. As observed in Fig. 10, in response to Il-10 treatment, NT and K_D cells secreted decreased amounts of the pro-inflammatory chemokines CXCL1, CXCL2, TNF-α, and IL1–10. However, K_D cells were more resistant to this inhibition and could be more resistant to the tumor inhibitory medium. After IL-10 inhibition, cells were then challenged with LPS. In that case chemokine secretion was restored in both NT and K_D cells. Of note, a significant increase in chemokine release was again observed in K_D cells, especially for CXCL1, CXCL2, CXCL10, IL1-α, and IL-6. These results clearly demonstrate that PC1/3 K_D cells still conserve their M1-like phenotype under inhibitory conditions and that the immune profile is pro-inflammatory.

DISCUSSION

The data from our current work demonstrate that PC1/3 is a key enzyme involved in the regulation of cytokine secretion and, consequently, is important for the regulation of macrophage activation, as depicted in Fig. 11.

When PC1/3 was inhibited, immune factors such as pro-inflammatory chemokines as well as alarmins (GRP78, HSP84, HSP86, HSP73, calreticulin, capthepsin B, nucleolin, granulins) were secreted in the absence of challenge. These alarmins may act as autocrine and paracrine factors and activate an immune response through TLR4 (53). Immune factors, such as IL-6 and TNF-α, are known to be produced by immune cells through the canonical ER-Golgi secretion pathway. However, in NR8383-K_D macrophages, numerous unconventional vesicular or organellar pathways have been found. Indeed, proteomic analyses of cell extracts have revealed that the canonical secretion pathway is deregulated and the noncanonical secretion machinery, with an accumulation of endosomes and MVBs, is reinforced. A large number of studies have shown that many proteins known to regulate endocytosis also participate in nuclear signaling. Among them, an adaptor protein containing a pleckstrin homology domain, a phosphotyrosine binding domain and leucine zipper motif 1 (APPL1) has a role in the positive regulation of NF-κB signaling. The overexpression of APPL1 triggers p65 translocation to the nucleus in the absence of stimulation (54). Annexin A6 has been shown to increase NF-κB activity in response to activation signals (55). These two proteins are over-expressed in PC1/3-K_D macrophages and may have an impact on TLR4 signaling (Table IV). Co-expression networks analysis showed that two major pro-inflammatory transcription factors, Stat1 and Stat2, are co-expressed with NF-κB1 in PC1/3-K_D cells whereas Arg1, a prototypic M2 molecule, is

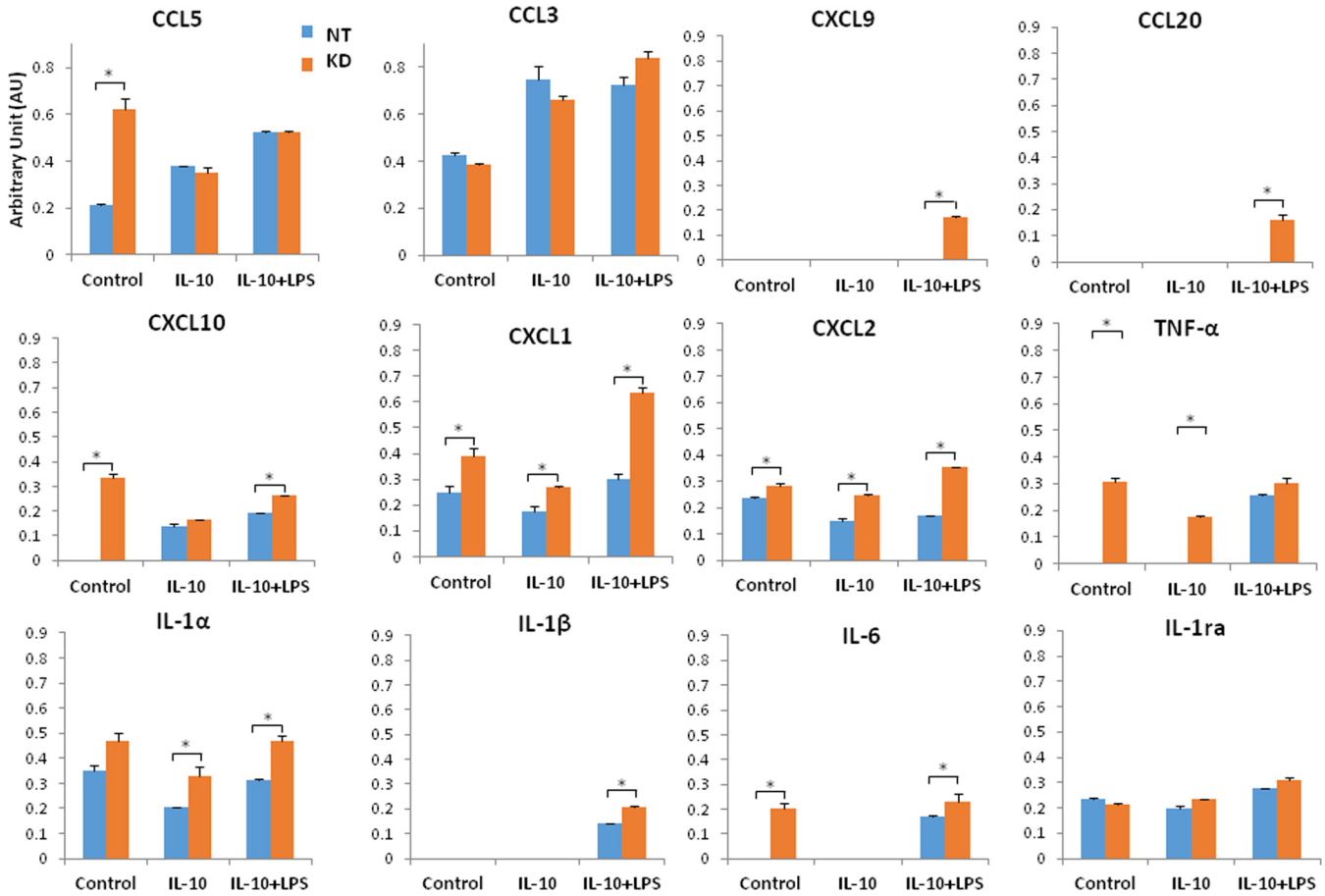

FIG. 10. **Effect of PC1/3 down-regulation on cytokine secretion under inhibitory conditions.** The rat cytokine array assay was performed in NR8383 secretomes (NT/K_D). The cells were untreated (control) or treated with IL-10 for 24 h without stimulation (IL-10) or with LPS for 24 h (IL-10+LPS). Blue shows NT cell secretomes, and orange indicates K_D cell secretomes. The bar diagrams represent the ratio of the spot mean pixel densities/reference point pixel densities. Significant differences were analyzed using Student's *t* test. *$p < 0.05$.

specific to the NT subnetwork (Fig. 7). Proteomics and Western blot analysis revealed that in PC1/3-K_D cells, the MyD88-dependent pathway was sustained. As a result, a greater activation of NF-κB was observed. This transcription factor is known to regulate the expression of the pore-forming Ca^{2+} channel unit, Orai1, and its activator, STIM1, to control Ca^{2+} entry and affect cellular functions (56). The induction of NF-κB by ER stress, *i.e.* Ca^{2+} efflux from the ER, has been also observed (57), and this induction is inhibited by Ca^{2+} chelators (58). Moreover, the treatment of cells with thapsigargin, which causes an efflux of Ca^{2+} from the ER, leads to NF-κB translocation (58). In the present study, we showed that, in PC1/3-K_D cells, both basal Ca^{2+} and constitutive Ca^{2+} influx increased. This result is consistent with our findings about NF-κB activation (Figs. 7 and 8). Calcium is also known to interact with cytoskeletal proteins. In PC1/3-K_D cells, cytoskeletal proteins were over-expressed, leading to the formation of a large number of filopodia (Figs. 3 and 4). The cell elasticity determines macrophage functions and is known to regulate phagocytosis or LPS responsiveness. In a positive feedback loop, the cytoskeleton can modulate the intracellular trafficking machinery through microtubules and calcium mobilization (59, 60). This event may amplify such a phenomenon and explain the spontaneous release of pro-inflammatory cytokines. In response to LPS challenge, amplified effects were registered in these PC1/3-K_D cells, provoking increased Ca^{2+} entry and thus impacting the morphology of the cells by producing a greater number of filopodia. As a result, these cells secreted more chemokines and cytokines to recruit naïve T helper lymphocytes (CD4+) and to orient the immune response from Th0 to Th1. Altogether, these findings show that PC1/3-K_D macrophages exhibit an M1-like phenotype.

It is known that, during the tumor development process, M1-polarized macrophages switch to an M2-like phenotype that is characterized by IL-12^{low} IL-10^{high} and lose their tumoricidal activities (61). According to our results, PC1/3 inhibition could be a relevant strategy to reverse the macrophage phenotype from an M2-like to an M1-like phenotype. As a first step, we tested whether the inhibitory cytokine IL-10 could

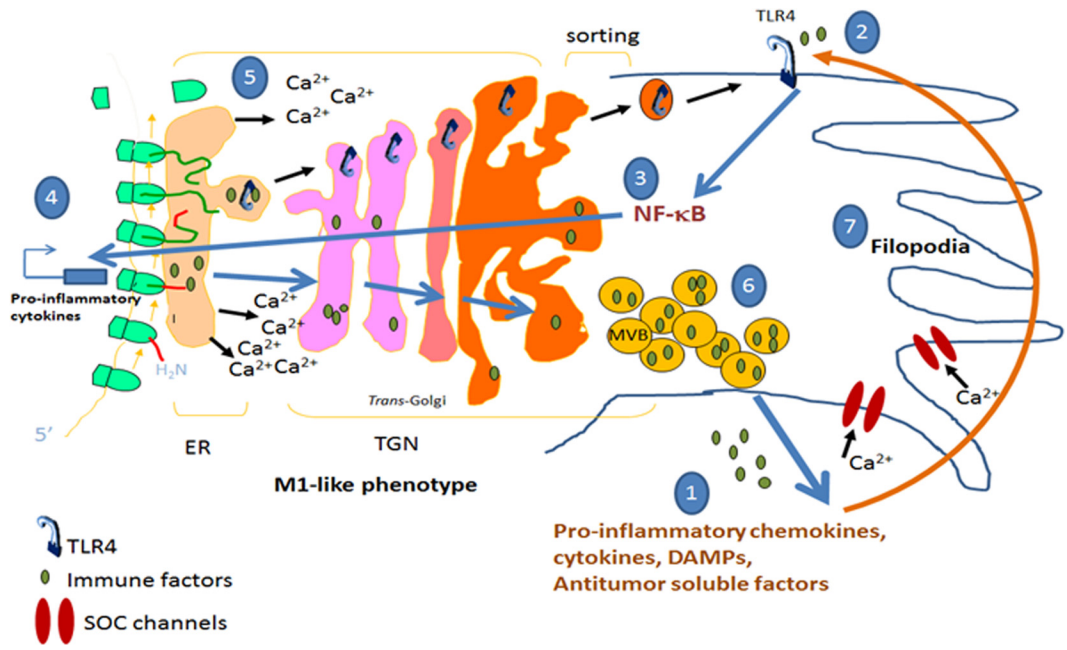

FIG. 11. **Schematic depicting how PC1/3 knockdown impacts macrophage activation based on the data presented in Figs. 1–8.** PC1/3 knockdown promotes the formation of endosomes and MVB release of inflammatory chemokines and cytokines via the noncanonical secretion pathway (1). Danger signal molecules (DAMs) can activate TLR4 (2) and induce the MyD88-dependent pathway with increased NF-κB (3) nuclear translocation (4) linked to Ca^{2+} mobilization in PC1/3 K_D macrophages (5). Both of these phenomena are also implicated in cytokines, chemokines, DAMs and tumor viability inhibitor release (6) as well as cytoskeletal rearrangements leading to the formation of filopodia (7). We then noticed that during LPS challenge, the amplification loop was amplified and driven toward the induction of increased Ca^{2+} release from the ER, greater numbers of filopodia and MVBs, the release of additional immune factors, an M1 phenotype refractive to IL-10 inhibition and a greater number of anti-tumor factors.

affect the secretion properties of PC1/3-K_D macrophages. Despite IL-10 treatment, these cells still spontaneously released pro-inflammatory cytokines and oriented the immune response toward a cytotoxic one. Thus, these cells clearly remained highly active. Moreover, in response to LPS challenge, their level of reactivity was restored to the same level of significance as that in cells challenged with LPS without IL-10. We also confirmed the antitumoral properties of their secretomes toward two different cell lines, *i.e.* one that is known to produce large amounts of IL-10 (SKBR3), whereas the other does not (SKOV3). Taken together, we demonstrated that PC1/3 K_D affected cell viability and resistance of cancer cells by the more abundant release of antitumoricidal factors such as TNF-α (62). PC1/3 is thus a promising target to reactivate dormant immune cells in tumors and in immunotherapeutic strategies.

Acknowledgments—We thank Elodie Richard of the CCMIC-Université de Lille 1 (BiCel) for her help and technical support in confocal microscopy experiments.

* This work was funded by grants from the Ministère de L'Education Nationale, de L'Enseignement Supérieur et de la Recherche, ANR (IF), Région Nord-Pas de Calais ARCIR (IF), the Université de Lille (MD) SIRIC ONCOLille (IF, MD), Grant INCa-DGOS-Inserm 6041aa, the CCMIC and INSERM.

S This article contains supplemental Data S1 to S6.

¶¶ To whom correspondence should be addressed: U-1192 Inserm, Laboratoire de Protéomique, Réponse Inflammatoire, Spectrométrie de Masse (PRISM), Université de Lille 1, Cité Scientifique, 59655 Villeneuve D'Ascq, France. Tel.: +33 (0)3 20 43 41 94; Fax: +33 (0)3 20 43 40 54; E-mail: michel.salzet@univ-lille1.fr.

Competing financial interests: The authors declare no competing financial interests.

REFERENCES

1. Ward, A. E., and Rosenthal, B. M. (2014) Evolutionary responses of innate immunity to adaptive immunity. *Infection, Genetics Evolution* **21,** 492–496
2. Buchmann, K. (2014) Evolution of Innate Immunity: Clues from Invertebrates via Fish to Mammals. *Front. Immunol.* **5,** 459
3. Wang, N., Liang, H., and Zen, K. (2014) Molecular mechanisms that influence the macrophage m1-m2 polarization balance. *Front. Immunol.* **5,** 614
4. Takeda, K., and Akira, S. (2004) TLR signaling pathways. *Sem. Immunol.* **16,** 3–9
5. Ostuni, R., Kratochvill, F., Murray, P. J., and Natoli, G. (2015) Macrophages and cancer: from mechanisms to therapeutic implications. *Trends Immunol* **36,** 229–239
6. Salzet, M., and Day, R. (2003) [Endocrine markers of cellular immunity: defining the endocrine phenotype). *J. Soc. Biol.* **197,** 97–101
7. Salzet, M. (2002) Immune cells express endocrine markers. *Neuro. Endocrinol. Lett.* **23,** 8–9
8. Salzet, M., Vieau, D., and Day, R. (2000) Crosstalk between nervous and immune systems through the animal kingdom: focus on opioids. *Trends Neurosci.* **23,** 550–555
9. Brogden, K. A., Guthmiller, J. M., Salzet, M., and Zasloff, M. (2005) The nervous system and innate immunity: the neuropeptide connection. *Nat. Immunol.* **6,** 558–564
10. Refaie, S., Gagnon, S., Gagnon, H., Desjardins, R., D'Anjou, F., D'Orléans-Juste, P., Zhu, X., Steiner, D. F., Seidah, N. G., and Lazure, C. (2012)

Disruption of Proprotein Convertase 1/3 (PC1/3) Expression in Mice Causes Innate Immune Defects and Uncontrolled Cytokine Secretion. *J. Biol. Chem.* **287,** 14703–14717
11. Gagnon, H., Refaie, S., Gagnon, S., Desjardins, R., Salzet, M., and Day, R. (2013) Proprotein convertase 1/3 (PC1/3) in the rat alveolar macrophage cell line NR8383: localization, trafficking and effects on cytokine secretion. *PLoS ONE* **8,** e61557
12. Lansac, G., Dong, W., Dubois, C. M., Benlarbi, N., Afonso, C., Fournier, I., Salzet, M., and Day, R. (2006) Lipopolysaccharide mediated regulation of neuroendocrine associated proprotein convertases and neuropeptide precursor processing in the rat spleen. *J. Neuroimmunol.* **171,** 57–71
13. Refaie, S., Gagnon, S., Gagnon, H., Desjardins, R., D'Anjou, F., D'Orleans-Juste, P., Zhu, X., Steiner, D. F., Seidah, N. G., Lazure, C., Salzet, M., and Day, R. (2012) Disruption of proprotein convertase 1/3 (PC1/3) expression in mice causes innate immune defects and uncontrolled cytokine secretion. *J. Biol. Chem.* **287,** 14703–14717
14. Wisniewski, J. R., Ostasiewicz, P., and Mann, M. (2011) High recovery FASP applied to the proteomic analysis of microdissected formalin fixed paraffin embedded cancer tissues retrieves known colon cancer markers. *J. Proteome Res.* **10,** 3040–3049
15. Meissner, F., Scheltema, R. A., Mollenkopf, H. J., and Mann, M. (2013) Direct proteomic quantification of the secretome of activated immune cells. *Science* **340,** 475–478
16. Polati, R., Castagna, A., Bossi, A., Campostrini, N., Zaninotto, F., Timperio, A. M., Zolla, L., Olivieri, O., Corrocher, R., and Girelli, D. (2009) High resolution preparation of monocyte-derived macrophages (MDM) protein fractions for clinical proteomics. *Proteome Sci.* **7,** 4
17. Searle, B. C. (2010) Scaffold: a bioinformatic tool for validating MS/MS-based proteomic studies. *Proteomics* **10,** 1265–1269
18. Shilov, I. V., Seymour, S. L., Patel, A. A., Loboda, A., Tang, W. H., Keating, S. P., Hunter, C. L., Nuwaysir, L. M., and Schaeffer, D. A. (2007) The Paragon Algorithm, a next generation search engine that uses sequence temperature values and feature probabilities to identify peptides from tandem mass spectra. *Mol. Cell. Proteomics* **6,** 1638–1655
19. Tang, W. H., Shilov, I. V., and Seymour, S. L. (2008) Nonlinear fitting method for determining local false discovery rates from decoy database searches. *J. Proteome Res.* **7,** 3661–3667
20. Colinge, J., Chiappe, D., Lagache, S., Moniatte, M., and Bougueleret, L. (2005) Differential proteomics via probabilistic peptide identification scores. *Anal. Chem.* **77,** 596–606
21. Gotz, S., Garcia-Gomez, J. M., Terol, J., Williams, T. D., Nagaraj, S. H., Nueda, M. J., Robles, M., Talon, M., Dopazo, J., and Conesa, A. (2008) High-throughput functional annotation and data mining with the Blast2GO suite. *Nucleic Acids Res.* **36,** 3420–3435
22. Szklarczyk, D., Franceschini, A., Kuhn, M., Simonovic, M., Roth, A., Minguez, P., Doerks, T., Stark, M., Muller, J., Bork, P., Jensen, L. J., and von Mering, C. (2011) The STRING database in 2011: functional interaction networks of proteins, globally integrated and scored. *Nucleic Acids Res.* **39,** D561–568
23. Smoot, M. E., Ono, K., Ruscheinski, J., Wang, P. L., and Ideker, T. (2011) Cytoscape 2.8: new features for data integration and network visualization. *Bioinformatics* **27,** 431–432
24. Saito, R., Smoot, M. E., Ono, K., Ruscheinski, J., Wang, P. L., Lotia, S., Pico, A. R., Bader, G. D., and Ideker, T. (2012) A travel guide to Cytoscape plugins. *Nat. Methods* **9,** 1069–1076
25. Cox, J., and Mann, M. (2008) MaxQuant enables high peptide identification rates, individualized p.p.b.-range mass accuracies and proteome-wide protein quantification. *Nat. Biotechnol.* **26,** 1367–1372
26. Cox, J., Neuhauser, N., Michalski, A., Scheltema, R. A., Olsen, J. V., and Mann, M. (2011) Andromeda: a peptide search engine integrated into the MaxQuant environment. *J. Proteome Res.* **10,** 1794–1805
27. Cox, J., Hein, M. Y., Luber, C. A., Paron, I., Nagaraj, N., and Mann, M. (2014) Accurate proteome-wide label-free quantification by delayed normalization and maximal peptide ratio extraction, termed MaxLFQ. *Mol. Cell. Proteomics* **13,** 2513–2526
28. Vizcaino, J. A., Deutsch, E. W., Wang, R., Csordas, A., Reisinger, F., Rios, D., Dianes, J. A., Sun, Z., Farrah, T., Bandeira, N., Binz, P. A., Xenarios, I., Eisenacher, M., Mayer, G., Gatto, L., Campos, A., Chalkley, R. J., Kraus, H. J., Albar, J. P., Martinez-Bartolome, S., Apweiler, R., Omenn, G. S., Martens, L., Jones, A. R., and Hermjakob, H. (2014) ProteomeXchange provides globally coordinated proteomics data submission and dissemination. *Nat. Biotechnol.* **32,** 223–226
29. Vizcaino, J. A., Cote, R. G., Csordas, A., Dianes, J. A., Fabregat, A., Foster, J. M., Griss, J., Alpi, E., Birim, M., Contell, J., O'Kelly, G., Schoenegger, A., Ovelleiro, D., Perez-Riverol, Y., Reisinger, F., Rios, D., Wang, R., and Hermjakob, H. (2013) The PRoteomics IDEntifications (PRIDE) database and associated tools: status in 2013. *Nucleic Acids Res.* **41,** D1063–1069
30. Montojo, J., Zuberi, K., Rodriguez, H., Kazi, F., Wright, G., Donaldson, S. L., Morris, Q., and Bader, G. D. (2010) GeneMANIA Cytoscape plugin: fast gene function predictions on the desktop. *Bioinformatics* **26,** 2927–2928
31. Chen, E. Y., Tan, C. M., Kou, Y., Duan, Q., Wang, Z., Meirelles, G. V., Clark, N. R., and Ma'ayan, A. (2013) Enrichr: interactive and collaborative HTML5 gene list enrichment analysis tool. *BMC Bioinformatics* **14,** 128
32. Azzaoui, I., Yahia, S. A., Chang, Y., Vorng, H., Morales, O., Fan, Y., Delhem, N., Ple, C., Tonnel, A. B., Wallaert, B., and Tsicopoulos, A. (2011) CCL18 differentiates dendritic cells in tolerogenic cells able to prime regulatory T cells in healthy subjects. *Blood* **118,** 3549–3558
33. Bianchi, M. E. (2007) DAMPs, PAMPs and alarmins: all we need to know about danger. *J. Leukoc. Biol.* **81,** 1–5
34. Franciszkiewicz, K., Boissonnas, A., Boutet, M., Combadiere, C., and Mami-Chouaib, F. (2012) Role of chemokines and chemokine receptors in shaping the effector phase of the antitumor immune response. *Cancer Res.* **72,** 6325–6332
35. Duitman, E. H., Orinska, Z., Bulanova, E., Paus, R., and Bulfone-Paus, S. (2008) How a cytokine is chaperoned through the secretory pathway by complexing with its own receptor: lessons from interleukin-15 (IL-15)/IL-15 receptor alpha. *Mol. Cell. Biol.* **28,** 4851–4861
36. Takenawa, T., and Suetsugu, S. (2007) The WASP-WAVE protein network: connecting the membrane to the cytoskeleton. *Nat. Rev. Mol. Cell Biol.* **8,** 37–48
37. Patel, N. R., Bole, M., Chen, C., Hardin, C. C., Kho, A. T., Mih, J., Deng, L., Butler, J., Tschumperlin, D., Fredberg, J. J., Krishnan, R., and Koziel, H. (2012) Cell elasticity determines macrophage function. *PLoS ONE* **7,** e41024
38. Bonnemaison, M. L., Eipper, B. A., and Mains, R. E. (2013) Role of adaptor proteins in secretory granule biogenesis and maturation. *Front. Endocrinol.* **4,** 101
39. Chaineau, M., Danglot, L., Proux-Gillardeaux, V., and Galli, T. (2008) Role of HRB in clathrin-dependent endocytosis. *J. Biol. Chem.* **283,** 34365–34373
40. Hutagalung, A. H., and Novick, P. J. (2011) Role of Rab GTPases in membrane traffic and cell physiology. *Physiol. Rev.* **91,** 119–149
41. Savina, A., Furlan, M., Vidal, M., and Colombo, M. I. (2003) Exosome release is regulated by a calcium-dependent mechanism in K562 cells. *J. Biol. Chem.* **278,** 20083–20090
42. Valitutti, S., Dessing, M., Aktories, K., Gallati, H., and Lanzavecchia, A. (1995) Sustained signaling leading to T cell activation results from prolonged T cell receptor occupancy. Role of T cell actin cytoskeleton. *J. Exp. Med.* **181,** 577–584
43. Nolz, J. C., Gomez, T. S., Zhu, P., Li, S., Medeiros, R. B., Shimizu, Y., Burkhardt, J. K., Freedman, B. D., and Billadeau, D. D. (2006) The WAVE2 complex regulates actin cytoskeletal reorganization and CRAC-mediated calcium entry during T cell activation. *Curr. Biol.* **16,** 24–34
44. Sun, H. Q., Yamamoto, M., Mejillano, M., and Yin, H. L. (1999) Gelsolin, a multifunctional actin regulatory protein. *J. Biol. Chem.* **274,** 33179–33182
45. Panther, E., Durk, T., Ferrari, D., Di Virgilio, F., Grimm, M., Sorichter, S., Cicko, S., Herouy, Y., Norgauer, J., Idzko, M., and Muller, T. (2012) AMP affects intracellular Ca2+ signaling, migration, cytokine secretion and T cell priming capacity of dendritic cells. *PLoS ONE* **7,** e37560
46. Heo, D. K., Lim, H. M., Nam, J. H., Lee, M. G., and Kim, J. Y. (2015) Regulation of phagocytosis and cytokine secretion by store-operated calcium entry in primary isolated murine microglia. *Cell Signal.* **27,** 177–186
47. Smyth, J. T., Hwang, S. Y., Tomita, T., DeHaven, W. I., Mercer, J. C., and Putney, J. W. (2010) Activation and regulation of store-operated calcium entry. *J. Cell. Mol. Med.* **14,** 2337–2349
48. Lytton, J., Westlin, M., and Hanley, M. R. (1991) Thapsigargin inhibits the sarcoplasmic or endoplasmic reticulum Ca-ATPase family of calcium pumps. *J. Biol. Chem.* **266,** 17067–17071
49. Xia, X., Cui, J., Wang, H. Y., Zhu, L., Matsueda, S., Wang, Q., Yang, X., Hong, J., Songyang, Z., Chen, Z. J., and Wang, R. F. (2011) NLRX1

negatively regulates TLR-induced NF-kappaB signaling by targeting TRAF6 and IKK. *Immunity* **34,** 843–853
50. Farber, J. M. (1997) Mig and IP-10: CXC chemokines that target lymphocytes. *J. Leukoc. Biol.* **61,** 246–257
51. Krzysiek, R., Lefevre, E. A., Bernard, J., Foussat, A., Galanaud, P., Louache, F., and Richard, Y. (2000) Regulation of CCR6 chemokine receptor expression and responsiveness to macrophage inflammatory protein-3alpha/CCL20 in human B cells. *Blood* **96,** 2338–2345
52. Bjorkelund, H., Gedda, L., and Andersson, K. (2011) Comparing the epidermal growth factor interaction with four different cell lines: intriguing effects imply strong dependency of cellular context. *PLoS ONE* **6,** e16536
53. Lee, K. H., Jeong, J., and Yoo, C. G. (2013) Positive feedback regulation of heat shock protein 70 (Hsp70) is mediated through Toll-like receptor 4-PI3K/Akt-glycogen synthase kinase-3beta pathway. *Exp. Cell Res.* **319,** 88–95
54. Hupalowska, A., Pyrzynska, B., and Miaczynska, M. (2012) APPL1 regulates basal NF-kappaB activity by stabilizing NIK. *J. Cell Sci.* **125,** 4090–4102
55. Campbell, K. A., Minashima, T., Zhang, Y., Hadley, S., Lee, Y. J., Giovinazzo, J., Quirno, M., and Kirsch, T. (2013) Annexin A6 interacts with p65 and stimulates NF-kappaB activity and catabolic events in articular chondrocytes. *Arthritis Rheum.* **65,** 3120–3129
56. Eylenstein, A., Schmidt, S., Gu, S., Yang, W., Schmid, E., Schmidt, E. M., Alesutan, I., Szteyn, K., Regel, I., Shumilina, E., and Lang, F. (2012) Transcription factor NF-kappaB regulates expression of pore-forming Ca2+ channel unit, Orai1, and its activator, STIM1, to control Ca2+ entry and affect cellular functions. *J. Biol. Chem.* **287,** 2719–2730
57. Prell, T., Lautenschlager, J., Weidemann, L., Ruhmer, J., Witte, O. W., and Grosskreutz, J. (2014) Endoplasmic reticulum stress is accompanied by activation of NF-kappaB in amyotrophic lateral sclerosis. *J. Neuroimmunol.* **270,** 29–36
58. Pahl, H. L., Sester, M., Burgert, H. G., and Baeuerle, P. A. (1996) Activation of transcription factor NF-kappaB by the adenovirus E3/19K protein requires its ER retention. *J. Cell Biol.* **132,** 511–522
59. Joseph, N., Reicher, B., and Barda-Saad, M. (2014) The calcium feedback loop and T cell activation: how cytoskeleton networks control intracellular calcium flux. *Biochim. Biophys. Acta* **1838,** 557–568
60. Murtazina, D. A., Chung, D., Ulloa, A., Bryan, E., Galan, H. L., and Sanborn, B. M. (2011) TRPC1, STIM1, and ORAI influence signal-regulated intracellular and endoplasmic reticulum calcium dynamics in human myometrial cells. *Biol. Reprod.* **85,** 315–326
61. Chanmee, T., Ontong, P., Konno, K., and Itano, N. (2014) Tumor-associated macrophages as major players in the tumor microenvironment. *Cancers* **6,** 1670–1690
62. Wallach, D., and Kovalenko, A. (2009) 12th international TNF conference: the good, the bad and the scientists. *Cytokine Growth Factor Rev.* **20,** 259–269

SCIENTIFIC REPORTS

OPEN

The proprotein convertase PC1/3 regulates TLR9 trafficking and the associated signaling pathways

Received: 04 September 2015
Accepted: 23 November 2015
Published: 18 January 2016

M. Duhamel[1,*], F. Rodet[1,*], A. N. Murgoci[1], R. Desjardins[2], H. Gagnon[2], M. Wisztorski[1], I. Fournier[1], R. Day[2] & M. Salzet[1]

Endosomal TLR9 is considered as a potent anti-tumoral therapeutic target. Therefore, it is crucial to decipher the mechanisms controlling its trafficking since it determines TLR9 activation and signalling. At present, the scarcity of molecular information regarding the control of this trafficking and signalling is noticeable. We have recently demonstrated that in macrophages, proprotein convertase 1/3 (PC1/3) is a key regulator of TLR4 Myd88-dependent signalling. In the present study, we established that PC1/3 also regulates the endosomal TLR9. Under CpG-ODN challenge, we found that PC1/3 traffics rapidly to co-localize with TLR9 in CpG-ODN-containing endosomes with acidic pH. In PC1/3 knockdown macrophages, compartmentalization of TLR9 was altered and TLR9 clustered in multivesicular bodies (MVB) as demonstrated by co-localization with Rab7. This demonstrates that PC1/3 controls TLR9 trafficking. This clustering of TLR9 in MVB dampened the anti-inflammatory STAT3 signalling pathway while it promoted the pro-inflammatory NF-kB pathway. As a result, macrophages from PC1/3 KO mice and rat PC1/3-KD NR8383 macrophages secreted more pro-inflammatory cytokines such as TNF-α, IL6, IL1α and CXCL2. This is indicative of a M1 pro-inflammatory phenotype. Therefore, PC1/3 KD macrophages represent a relevant mean for cell therapy as "Trojan" macrophages.

During tumorigenesis, key immune cells such as macrophages are recruited to the tumor site to become tumour associated macrophages (TAMs). However, the tumor creates an immune suppressive environment, which orients TAMs toward the anti-inflammatory M2 phenotype. In turn, these TAMs suppress immune cells function by secreting anti-inflammatory molecules and lack secretion of pro inflammatory immune components. Presence of TAMs has been closely correlated with vascularisation, metastasis and resistance to immunotherapy leading to a poor prognosis and outcome in most types of cancer[1]. Skewing TAMs towards pro-inflammatory phenotype is therefore extensively investigated as potential means for developing novel antitumor therapy. Such a strategy to reactivate TAMs consists in activating key innate immune receptors such as Toll-like receptors. In this context, the endosomal TLR9 is considered as a potent therapeutic target. It is involved in the recognition of double-stranded DNA rich in unmethylated CpG motifs of bacterial or viral origin[2,3]. At present, its synthetic ligand CpG ODN is currently tested as cancer vaccine adjuvant[4]. Indeed, intra-tumoral injection of CpG-ODN reduced the frequency of regulatory T cells (Tregs)[4] and decreased the number and suppressive activity of tumor infiltrating monocyte-derived suppressor cells (MDSC)[5]. These MDSC express TLR9 and respond to CpG-ODN stimulation by (i) losing their ability to suppress T cell function, (ii) producing Th1 cytokines and (iii) differentiating into tumoricidal macrophages. CpG-ODN delivery in the tumors also promoted cytotoxic responses by recruiting and inducing CD8 T cells[6,7]. Unexpectedly, intra-tumoral injection of CpG-ODN contributed to partial or complete remission of various tumors in humans[8] and rodents[7].

In our opinion, combining CpG-ODN intra-tumoral delivery and cell therapy with macrophages highly responsive to CpG-ODN is a promising strategy to treat tumors more efficiently. To obtain these highly reactive macrophages, it is crucial to decipher the mechanisms controlling TLR9 activation and signalling. TLR9 activation and signalling are intimately linked to TLR9 localization and trafficking. Indeed, recognition of CpG DNA by TLR9 is accompanied by changes in membrane dynamics and trafficking, resulting in their strict spatiotemporal

[1]Univ. Lille, INSERM, U1192 - Laboratoire Protéomique, Réponse Inflammatoire et Spectrométrie de Masse-PRISM, F-59000 Lille, France. [2]Institut de Pharmacologie, Département de Chirurgie/Service d'Urologie, Faculté de Médecine et des Sciences de la Santé, Université de Sherbrooke, 3001 12e Ave Nord, Sherbrooke, Qc, Canada, J1H 5N4. *These authors contributed equally to this work. Correspondence and requests for materials should be addressed to S.M. (email: michel.salzet@univ-lille1.fr)

compartmentalization[9]. During the resting state, TLR9 is synthesized in the endoplasmic reticulum (ER)[10]. After bacterial or viral infection, it translocates to the endolysosomal system to interact with its ligand and triggers associated signaling pathways. Nevertheless, apart from UNC93B1[11], PRAT4[12], HMGB1[13], GP96[14], protein kinase D1[15] and Ly49Q[16], the factors regulating TLR9 trafficking remain largely unknown.

We have recently demonstrated that proprotein convertase 1/3 (PC1/3) inhibition in macrophages led to marked perturbation of intracellular trafficking machinery through dysregulation of cytoskeletal protein expression. As a consequence, biogenesis of endosome carrier vesicle (ECV)/multivesicular body (MVB) transport intermediates from early endosomes was modified. Proteins involved in the late steps of the endosomal MVB pathway were also over-expressed. We have also pointed out that TLR4-Myd88 dependent signalling was exacerbated via the autocrine pathway. This promoted development of a pro-inflammatory M1-like phenotype in the presence or absence of endotoxin challenge[17]. In the present study, we wished to address if PC1/3 may also control the activity of the endosomal TLR9. We first demonstrated that macrophages from PC1/3-KO mice treated with CpG-ODN synthesized and secreted increased amounts of the pro-inflammatory cytokines TNF-α and IL-6. Since TLR9 signalling and the resulting cytokine secretion depend of TLR9 localization, we investigated the impact of PC1/3 inhibition on TLR9 dynamics and trafficking. For this purpose, we used the rat macrophage pulmonary cell line NR8383. Indeed, we have previously shown that it is a useful cell line to study the link between PC1/3 and regulation of cytokine secretion[18,19]. We found that PC1/3 travelled rapidly to co-localize with TLR9 in CpG-ODN-containing endosomes with acidic pH. Moreover, in PC1/3 knockdown (KD) cells, compartmentalization of TLR9 was altered and TLR9 formed clusters in multivesicular bodies. As a consequence, the NF-κB pro-inflammatory pathway was more rapidly and strongly activated whereas the STAT3 anti-inflammatory pathway was repressed. Because TLR9, NF-κB and STAT3 are key molecules involved in tumor propagation[20,21], control of their activation by PC1/3 represents a promising and potent antitumoral therapy. Therefore, PC1/3 KD macrophages represent a relevant mean for cell therapy as "Trojan" macrophages.

Results

Peritoneal macrophages isolated from PC1/3 KO mice exhibit excessive TNFα and IL-6 production and secretion. We have previously shown that PC1/3 regulated cytokine secretion in mice challenged with LPS[18]. Indeed, the plasma levels of proinflammatory cytokines (IL-6, IL-1β, and TNFα) were very significantly elevated in PC1/3 KO mice injected intraperitoneally with LPS. Peritoneal macrophages isolated from these mice and stimulated with this endotoxin also displayed uncontrolled cytokine secretion. To determine whether PC1/3 also controls signaling pathways and cytokine secretion associated with an endosomal TLR, such as TLR9, peritoneal macrophages were isolated from PC1/3 KO mice and challenged for 4 h with 1 μM CpG-ODN 2006 (Fig. 1). Following CpG-ODN stimulation, both WT and PC1/3 KO macrophages clearly produced (Fig. 1a) and secreted (Fig. 1b) an increased amount of TNFα. Comparison of the fold changes in cytokine levels between the stimulated and control cells revealed that the fold changes in TNFα synthesis (Fig. 1a) and release (Fig. 1b) were 2.12- and 14.41-fold higher, respectively, in the PC1/3 KO macrophages. Similar results were obtained for IL-6 production (Fig. 1c) and secretion (Fig. 1d) with a synthesis and release of IL-6, respectively 2.5- and 10-fold higher in PC1/3 KO macrophages. These findings demonstrate that PC1/3 has inhibitory effects on pro-inflammatory cytokine production and secretion induced by challenge with 1 μM CpG-ODN 2006. Thus, PC1/3 may regulate TLR9 signalling and the resulting cytokine secretion. The NR8383 rat pulmonary macrophage cell line is a cellular model used to study innate immunity. It also presents similar pro protein convertase expression as macrophages isolated from mice. Indeed, this cell line has been previously shown to be a good model for studying the role of PC1/3 in the macrophage innate immune response[18,19]. Therefore, we chose to use these cells to characterize the molecular and cellular mechanisms controlled by PC1/3. First, the effect of CpG-ODN treatment on PC1/3 activation was tested.

CpG-ODN induces PC1/3 cleavage and activation. PC1/3 activation requires specific proteolytic cleavage, which occurs during its trafficking from the endoplasmic reticulum (ER) to secretory granules (Fig. 2a)[22]. Five molecular forms of PC1/3 have been described to date. The 97 kDa form corresponds to the preproprotein. It is synthesized in the ER and rapidly cleaved to give rise to the 93 kDa proprotein, which traffics between the endoplasmic reticulum (ER) and the TGN. In the TGN, it is processed to generate full-length (87 kDa) PC1/3. A C-terminal truncated active 74 kDa form is then produced and transported to secretory granules, where it is processed into the full active 66 kDa form. TLR9 activation is also directly linked to its spatiotemporal compartmentalization and specific proteolytic cleavage (Fig. 2b). Following its trafficking to specific endolysosomes, it is cleaved to give rise either to its active or inactive form[23]. In endolysosomes with a low pH, the N-terminus of TLR9 is processed to generate a 64 kDa C-terminal fragment. TLR9 with this fragment is referred to as the active form because this fragment recruits MyD88 and induces signaling when it binds CpG-ODN. In contrast, in endolysosomes with a neutral pH, cleavage occurs in the C-terminus of the receptor to produce an 81.4 kDa N-terminal fragment. Despite its binding to CpG-ODN, this fragment cannot trigger any signaling since it lacks a TIR domain. It is thus considered as the inactive form of TLR9.

Therefore, we wished to determine whether there was a correlation between the active or inactive form of TLR9 and the active form of PC1/3. For this purpose, we performed subcellular fractionation using Optiprep™ density gradient centrifugation and western blotting with antibodies directed against PC1/3 and TLR9 (Fig. 2c). In untreated cells, we detected the various steady-state forms of PC1/3 and only unprocessed TLR9. After 15 min of CpG-ODN stimulation, a portion of TLR9 was detected in a PC1/3-positive compartment (Fig. 2b). At this time point, cleaved forms of TLR9 appeared, the majority of which were inactive. PC1/3 is also processed for activation, as reflected by detection of more of the active 74 kDa and 66 kDa forms (fractions 2 and 3). The 66 kDa form is typically weakly detected due to its natural instability[22]. Accordingly, after 1 h of stimulation, this form as well as the C-terminal truncated active 74 kDa form disappeared. In contrast, an increase in the 87 kDa form was

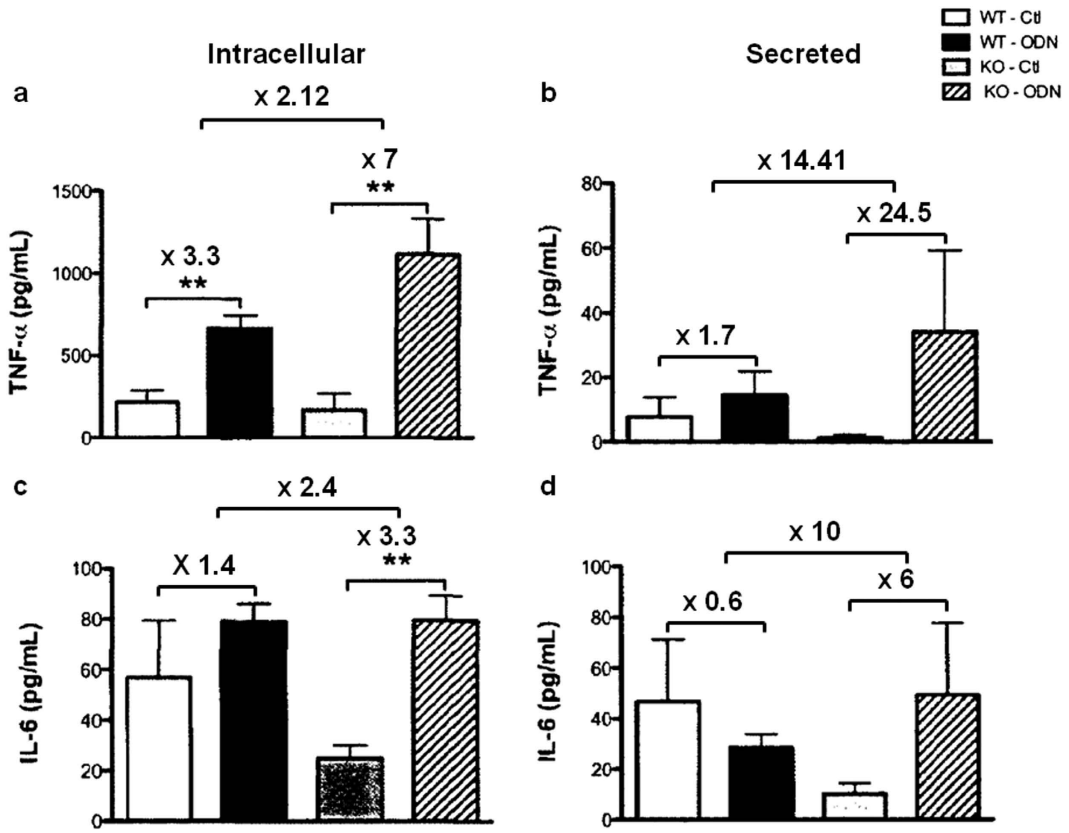

Figure 1. TNFα and IL-6 synthesis and secretion from peritoneal macrophages isolated from PC1/3 KO mice under CpG-ODN challenge. Under CpG-ODN challenge, peritoneal macrophages isolated from PC1/3 KO mice synthesize (**a**) and secrete (**b**) more TNFα than those harvested from WT mice. Similar results were obtained for IL-6 production (**c**) and secretion (**d**). Peritoneal macrophages were stimulated for 4 h with 1 μM CpG-ODN 2006 and TNFα or IL-6 concentration was measured using an ELISA kit. The data represent the mean ± SE. ($n = 4$; $^*p < 0.05$; $^{**}p < 0.01$ as determined by the t-test).

observed. These findings reflect the synthesis and trafficking of PC1/3 from the endoplasmic reticulum (ER) to the TGN to be processed and to produce a sufficient amount of active PC1/3. Interestingly, the majority of TLR9 was found to be active in all fractions except 11. This finding suggests that PC1/3 may control TLR9 activation. To test this hypothesis, we first examined the effect of CpG-ODN treatment on PC1/3 intracellular localization.

CpG-ODN induces PC1/3 translocation in endosomes. We have previously demonstrated that in resting NR8383 cells, PC1/3 is localized to the Golgi apparatus[19]. In the present study, we performed confocal microscopy (Fig. 3a) and showed that CpG-ODN treatment induced PC1/3 trafficking (Fig. 3b–d). After only 15 min of exposure to CpG-ODN, many vesicular structures containing PC1/3 began to appear (Fig. 3b). By 30 min of incubation, almost the whole cytoplasm was filled with these vesicular structures (Fig. 3c). After 1 h of stimulation, PC1/3-containing vesicular structures could be observed migrating toward the cell periphery and plasma membrane (Fig. 3d). Co-localization studies of PC1/3 and fluorescently labelled dextran identified these structures as endolysosomal compartments (Fig. 3e).

PC1/3 and TLR9 traffic and co-localize to the same acidic endosomes under CpG-ODN treatment. We performed time-lapse confocal microscopy to examine the spatial behaviours of PC1/3 and TLR9 after treatment with 100 nM CpG-ODN 2006 (Fig. 4a–f). In resting cells, we found that PC1/3 and TLR9 did not co-localize (Fig. 4a). However, after only 15 min of CpG-ODN stimulation, a portion of TLR9 was detected in a PC1/3-positive compartment (Fig. 4b). After 30 min and 1 h of incubation, the areas of co-localization extended progressively throughout the cytoplasm and toward the cell periphery (Fig. 4c,d). After longer incubation times (6 and 10 h), the co-localization signal became very strong and similar distributions of PC1/3 and TLR9 were observed (Fig. 4e–f′). To better characterize the exact organelle to which PC1/3 and TLR9 co-localized after stimulation, we conducted immunoelectron microscopic analysis. Double immunogold labelling clearly highlighted that PC1/3 and TLR9 coexisted in the same endosomes and lysosomes of treated NR8383 cells (Fig. 4g,h). Our results showed a correlation between TLR9 and PC1/3 activations (Fig. 2). TLR9 is cleaved to give rise to its active form in endosomes with a low pH and it is known that PC1/3 activity also requires an acidic pH. Therefore, the co-localization observed between the receptor and the proprotein convertase may occur in endosomes with low pH. To test this hypothesis, we examined the effect of bafilomycin A1 (bafA1) a compound which

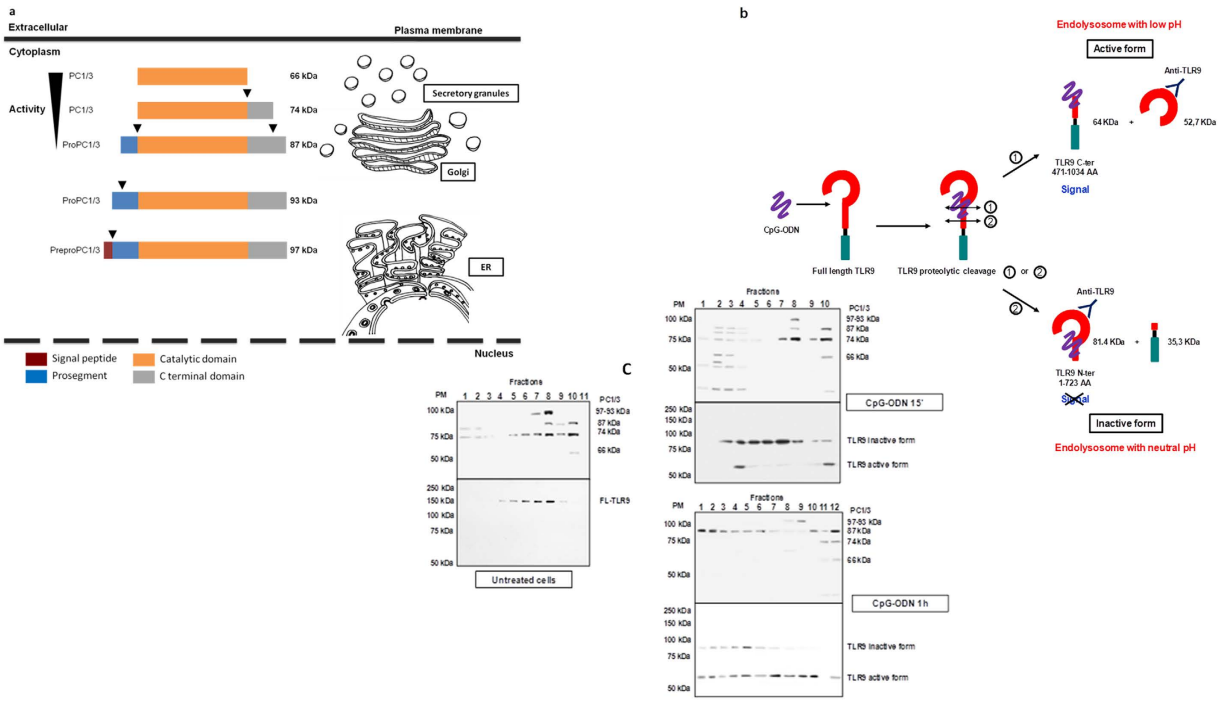

Figure 2. PC1/3 and TLR9 activation under CpG-ODN treatment. (**a**) Schematic representations of PC1/3 forms (realized by dr. F. Rodet). Cleavage sites are indicated by the black arrows. The apparent molecular weights of the various PC1/3 forms are indicated to the right of each bar. (**b**) Schematic representations of TLR9 cleavage forms. The antibody is directed against the extracellular domain of TLR9. The molecular weights of the various forms recognized by this antibody after proteolytic cleavage are indicated. (**c**) Subcellular fractionation of NR8383 cells. Cells were left untreated or stimulated with 1 μM CpG-ODN 2006 for 15 min or for 1 h and were then subjected to gradient fractionation. Next, aliquots of each collected gradient fraction were processed using SDS-PAGE (8%) and were immunoblotted with antibodies directed against PC1/3 and TLR9.

blocks endosomal acidification by inhibiting the intravesicular hydrogen pumps V-ATPase. After pre-incubation with bafA1 during 2 hours, NR8383 cells were exposed to CpG-ODN during 6 hours and examined by confocal microscopy. We found that PC1/3 did not co-localize anymore with TLR9 except in the ER (Fig. 5) demonstrating that PC1/3 and TLR 9 co-localized in endosomes with acidic pH. Thus, PC1/3 likely controls TLR9 cleavage and activation.

PC1/3 does not control TLR9 activation by proteolytic cleavage. To clarify if PC1/3 may control TLR9 activation, we took advantage of a PC1/3-knockdown (KD) NR8383 cell line obtained after lentiviral shRNA delivery[19]. Since TLR9 activation is directly linked to its spatiotemporal compartmentalization, Non-Target shRNA (NT) and PC1/3 KD NR8383 cells were challenged with CpG-ODN during 1 h, 3 h and 6 h. TLR9 proteolytic cleavage was then studied by western blot (Fig. 6a). Intensity of the 64 kDa band, corresponding to TLR9 active form (Fig. 2b), was quantified. However, after time course experiments, no differences were registered between NT and KD cells as revealed by three ways ANOVA followed by Holm-Sidak posthoc test (Fig. 6b). This demonstrates that PC1/3 doesn't control TLR9 cleavage and thus its activation.

PC1/3 regulates TLR9 trafficking. We next tested if PC1/3 may regulate TLR9 trafficking. Confocal imaging data of NT and PC1/3 KD cells in time course revealed that under CpG-ODN treatments TLR9 formed aggregates which were much more intense in KD cells (Fig. 7). Labelling with Rab7 indicated that TLR9 clusterization in KD cells occured in multivesicular bodies (Fig. 8). This demonstrates that PC1/3 is crucial for the proper trafficking of TLR9. In this context, we speculated that in PC1/3 KD cells, the targeting of TLR9 to MVBs may differentially trigger the associated signaling pathways. To address this hypothesis, we investigated both STAT3 and NF-κB activation.

Under CpG-ODN treatment, NF-κB activation occurs rapidly in PC1/3 KD cells. To examine NF-kB activation, we analyzed by western blot the degradation of IκB-α after CpG-ODN treatment for 1, 3, or 6 h (Fig. 9a). Data were then analyzed by three ways ANOVA followed by Holm-Sidak posthoc test. This revealed that IκB-α level was significantly lower at 1h ($p < 0.001$) in PC1/3 KD cells compared to NT cells (Fig. 9b). We next studied the fold increases between (Fig. 9c) CpG-ODN challenged cells vs. control cells to follow the dynamics of IκB-α degradation and synthesis. Despite a non-significant two ways ANOVA followed by Holm-Sidak posthoc test, the IκB-α level displayed a tendency to be lower in KD cells than in NT cells at 1 h after challenge. This reflected a more intense and quicker degradation of IκB-α and thus an increased activation of NF-κB in

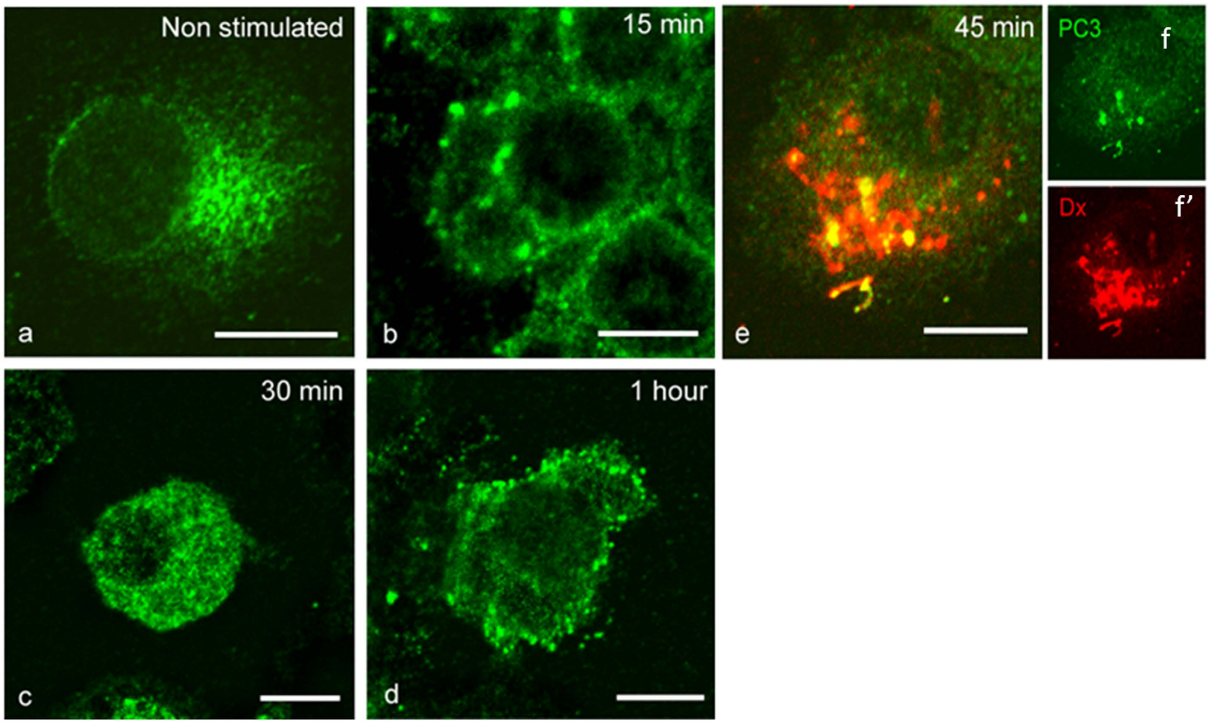

Figure 3. PC1/3 trafficking is affected by CpG-ODN internalization. PC1/3 was labelled by indirect immunofluorescence using anti-PC1/3 (green, Alexa488) and imaged by confocal microscopy. (**a**) Non-stimulated NR8383 cells. (**b–e**) NR8383 cells incubated with 100 nM CpG-ODN 2006 for the indicated durations. (**e**) Co-localization of PC1/3 (green, Alexa488) and Texas Red labelled dextran identified PC1/3-positive vesicular structures as lysosomes (big) and endosomes (small). Bars = 10 μm.

KD cells. At 3 h, we observed the opposite situation and at 6 h, both cell types had the same IκB-α protein level. Taken together, these results show that the NF-κB pathway is less repressed and more rapidly activated in KD cells. These effects may be the consequence of the clustering of TLR9 in MVBs, as observed in KD cells (Fig. 8).

STAT3 signaling is repressed in PC1/3 KD cells. As observed in Fig. 9, PC1/3 downregulation promoted the pro-inflammatory pathway via NF-κB activation. To address whether PC1/3 inhibition also favoured pro-inflammatory phenotype through repression of the anti-inflammatory pathway, we focused on STAT3 activation. Indeed, STAT3 has been described as a negative feedback inhibitor of TLR9 signalling[21]. To assess STAT3 activation, we analyzed by western blot the phosphorylation state of STAT3 after CpG-ODN treatment for 1, 3, or 6 h (Fig. 10a). Data were then analyzed by three ways ANOVA followed by Holm-Sidak posthoc test. This revealed that the level of phosphorylated STAT3 was significantly lower at 3 h and 6 h ($p < 0.001$) in PC1/3 KD cells than in NT cells (Fig. 10b). Differences in the dynamics of STAT3 phosphorylation under CpG-ODN challenge were also observed according to the fold changes in the CpG-ODN vs. control cells. Indeed, a two ways ANOVA followed by Holm-Sidak posthoc test pointed out a significant decrease of STAT3 phosphorylation in KD cells at 6 h post-treatment ($p < 0.001$, Fig. 10c). These data indicate that, in the presence or absence of CpG-ODN treatment, STAT3 pathway activation is reduced in KD cells.

After CpG-ODN treatment, PC1/3 KD cells secrete more pro-inflammatory cytokines than NT cells. To correlate TLR9 signaling and trafficking with cytokine secretion, cytokine arrays were performed after CpG-ODN treatment of NT and PC1/3 KD cells. At 4 h post-treatment, no significant differences in cytokine secretion were observed between NT and PC1/3 KD cells (data not shown). At 24 h post-treatment, the CXCL1, CXCL2, CXCL10, CCL3, CCL5 and IL1α levels were found to be altered (Fig. 11). The CXCL2 and IL1α levels were significantly increased in KD cells compared with those in NT cells after stimulation. The CXCL10 level was increased in KD cells compared with that in NT cells under basal condition and it dropped following the CpG-ODN treatment. In untreated and treated conditions, the CCL3 level in KD cells was lower than in NT cells. Finally, we observed that the CCL3 and CCL5 levels decreased in KD cells compared with those in NT cells after stimulation.

Discussion

In tumors, macrophages tend to acquire the anti-inflammatory M2 phenotype and to promote cancer growth by suppressing immune cell function[1]. Therefore, strategies need to be developed to reactivate macrophages. In this context, understanding how Toll-like receptors (TLRs) are activated, how they traffic and trigger their signaling pathways is crucial. Recently, studies have focused on TLR9 because it is considered as a potent therapeutic

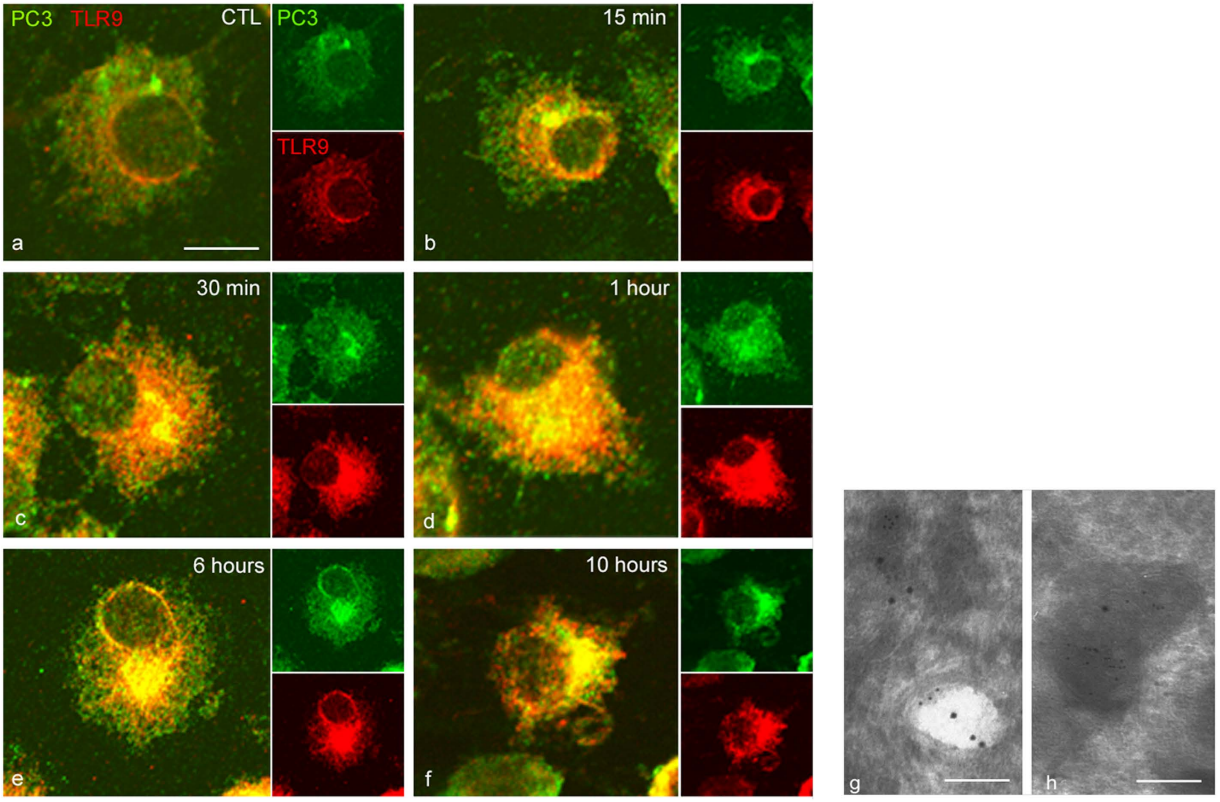

Figure 4. PC1/3 and TLR9 translocate to the same vesicular structures immediately upon exposure of cells to CpG-ODN. Confocal images of NR8383 cells double-labelled with anti-PC1/3 (green, Alexa488) and anti-TLR9 (red, Alexa546). (**a**) Untreated cells. (**b–f′**) Cells incubated with 100 nM CpG-ODN 2006 for the indicated durations. All of the confocal images are shown at the same scale, bar = 10 μm. (**g,h**) Immunogold electron micrographs, showing the coexistence of PC1/3 (small gold particles, 6 nM) and TLR9 (large gold particles, 12 nM) in the same endosome (**g**) and in the same lysosome (**h**) after incubation with 100 nM CpG-ODN 2006 for 6 h. Bar = 250 nM for both electron micrographs.

target for the effective treatment of some cancers[24]. TLR9 activation by CpG-DNA depends on its spatiotemporal compartmentalization in the endolysosomal compartment, where it undergoes specific proteolytic cleavage by cathepsins and asparagine endopeptidases[25–29]. Recently, we have demonstrated that the key endoprotease, proprotein convertase 1/3 (PC1/3) regulates intracellular trafficking machinery, the endosomal pathway and TLR4 activity[17]. We suspected that PC1/3 may also control TLR9 trafficking and activity. In neuroendocrine cells, PC1/3 activation requires specific proteolytic cleavages, which occurs during PC1/3 trafficking from the endoplasmic reticulum (ER) to secretory granules[18,19]. Here, we have demonstrated for the first time in macrophages that PC1/3 matures and co-traffics with TLR9 to the endolysosomal system after CpG-ODN treatment (Figs 2–4). In contrast, we have observed that when PC1/3 is inhibited, TLR9 targeting is modified and the receptor forms aggregates in multi vesicular bodies (MVBs) (Fig. 8). However, TLR9 cleavage is not impaired by PC1/3 inhibition (Fig. 6). These results are in contrast with those reported for the activity of another proprotein convertase family member, furin, in the TLR7 antiviral immune response[30]. In fact, furin is not required for TLR7 trafficking but is necessary for its proteolytic cleavage at a neutral pH, possibly in early endosomes or in a pre-endosomal compartment such as the ER, Golgi, or plasma membrane[30]. This finding is consistent with the reported activity of proprotein convertases as endoproteases. Taken together, our data suggest a new role for proprotein convertases as key molecules involved in TLR trafficking. Recently, a crucial role of neurite outgrowth inhibitory protein isoform B (NOGO-B) in proper TLR9 trafficking to the endolysosomal system has been demonstrated in macrophages[31]. Notably, we have previously observed that compared with NT cells, PC1/3 KD cells exclusively secrete Nogo[17]. Therefore, PC1/3 may control TLR9 targeting by mediating Nogo-B expression. We have also previously described overexpression of proteins involved in protein trafficking between the trans-Golgi network (TGN) and endosomes in PC1/3 KD cells[17]. Further, we have shown that the cytoskeleton is substantially reorganized following PC1/3 inhibition[17]. Therefore, another hypothesis is that PC1/3 may regulate TLR9 trafficking through regulation of trafficking machinery and cytoskeletal reorganization. This activity is similar to what occurs during UNC93B1-mediated recruitment of adaptor protein complex 2 (AP-2) for TLR9 delivery to endolysosomes[32]. It is also comparable to what happens during control of CpG-induced tubular endolysosomal extension and proper distribution of TLR9 by Ly49Q[16]. Thus, the precise mechanism exerted by PC1/3 to regulate TLR9 trafficking remains to be determined. However, we have showed here that the redistribution of TLR9 in MVBs in PC1/3 KD cells impacts the associated signalling pathways (Figs 9 and 10) and resulting cytokines secretion (Figs 1 and

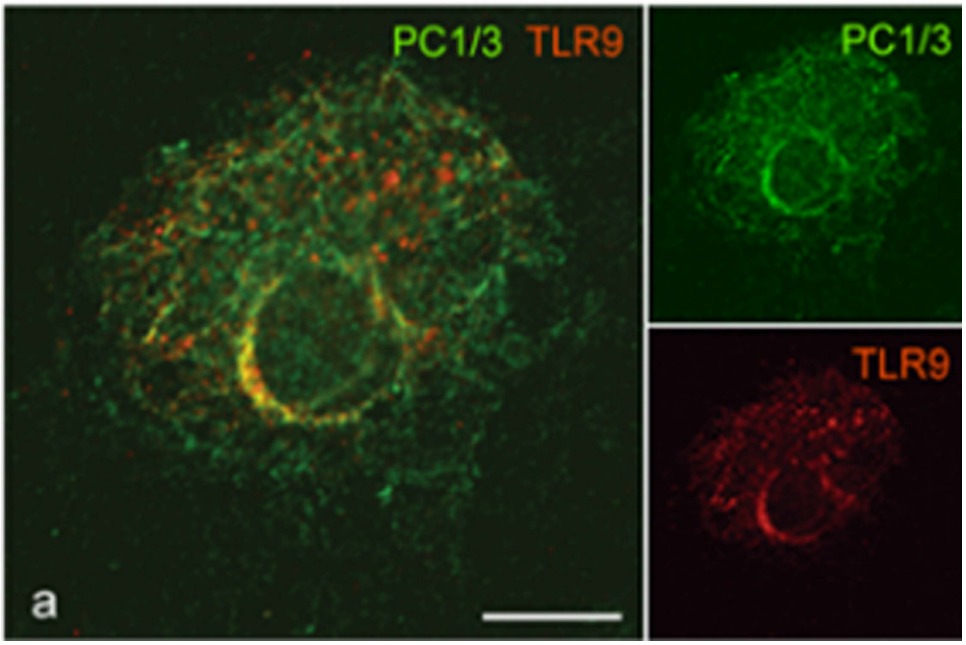

Figure 5. Bafilomycin A1 completely blocked PC1/3-TLR9 co-localization induced by CpG-ODN stimulation. NR8383 cells were stimulated for 6 h with 100 nM CpG-ODN 2006 in the presence of 100 nM bafilomycin A1, which was added to the cells 2 h prior to stimulation. The cells were then double labelled using anti-PC1/3 and anti-TLR9 and imaged by confocal microscopy. Bar = 10 μm.

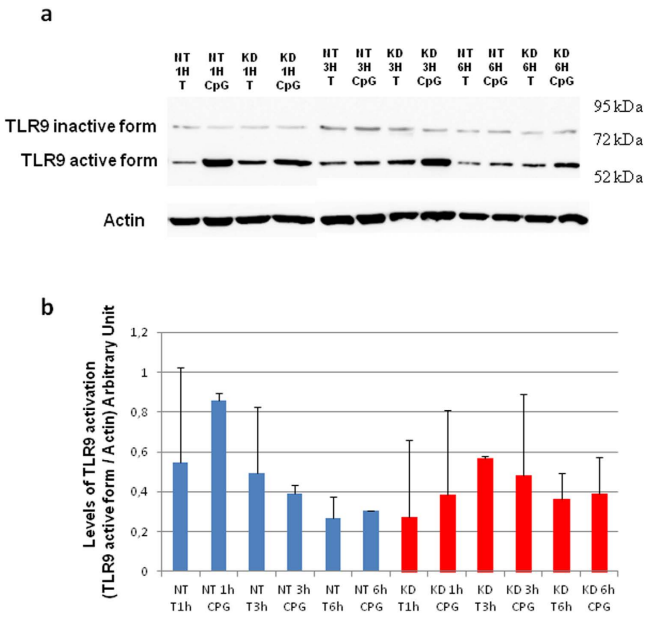

Figure 6. PC1/3 does not control TLR9 activation by proteolytic cleavage. Non-target (NT) and PC1/3 knockdown (KD) NR8383 cells were exposed to 1 μM CpG-ODN 2006 for 1, 3 or 6 h. (**a**) Proteins were then extracted, and western blotting was carried out with anti-TLR9. Intensities of 64 kDa bands corresponding to TLR9 active form were quantified and normalized to that of actin. (**b**) The results are depicted through graphic representations. Experiments were performed in triplicate and the data are presented as the mean ± SD. Data were then analyzed by three ways ANOVA followed by Holm-Sidak posthoc test.

11). Indeed, the NF-κB pro-inflammatory pathway was more rapidly and strongly activated (Fig. 9). This finding is supported by the fact that the anti-inflammatory cytokine IL1-Ra was not secreted by PC1/3 KD cells after challenge (data not shown). This is in contrast with what has been observed in wild type mouse macrophages after CpG-ODN stimulation[33]. We also depicted that PC1/3 inhibition in CpG-ODN-stimulated macrophages

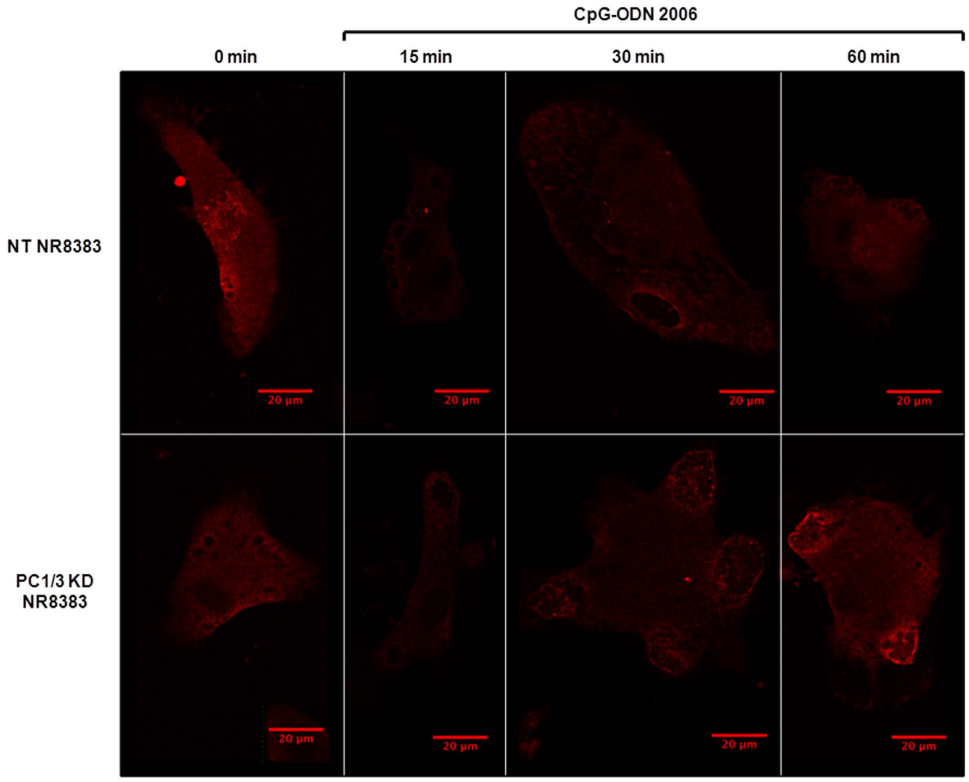

Figure 7. PC1/3 regulates TLR9 localization. Non-target (NT) and PC1/3 knockdown (KD) NR8383 cells were exposed to 100 nM CpG-ODN 2006 for 0, 15, 30 or 60 min, labelled with anti-TLR9 (red) and analyzed by confocal microscopy.

resulted in induction of secretion of pro-inflammatory cytokines, i.e., TNFα and IL-6 in PC1/3 KO mice (Fig. 1) and IL1α and CXCL2 in PC1/3 KD rat NR8383 (Fig. 11). Interestingly, we have previously demonstrated that the pro-inflammatory transcription factor STAT1 is co-expressed with NF-κB1 in LPS-stimulated KD cells, whereas this activity does not occur in LPS-stimulated NT cells[17]. KD cells also spontaneously secrete CXCL10[17], a cytokine whose gene expression is controlled by STAT1. Moreover, in myeloid cells, type I interferons activate STAT1 and STAT3[34]. STAT1 is sequestered by STAT3 to prevent STAT1 homodimer formation, thereby suppressing STAT1 activity. STAT3 has also been described to be a negative feedback inhibitor of TLR9 signaling in hematopoietic cells. Indeed, ablating *Stat3* in these cells results in rapid activation of innate immunity by CpG, with enhanced production of IFN-γ, TNFα and IL-12[21]. Our present study revealed that STAT3 activity was repressed in PC1/3 KD cells and that this repression was increased under CpG-ODN treatment (Fig. 10). We have also showed that after CpG-ODN challenge, the initially high level of CXCL10 also known as an interferon gamma-inducer, markedly dropped. It indicates that PC1/3 inhibition skews TLR9 signalling towards the NF-κB pathway instead of the IRF pathway as we have shown for TLR4. Taken together, these findings show that inhibition of PC1/3 orients macrophages toward a pro-inflammatory phenotype. TLR9[35], NF-κB and STAT3[20,21] are key molecules involved in tumor propagation. Therefore, control of their activation by PC1/3 is a promising strategy to reactivate tumor-associated macrophages and to develop a potent antitumor therapy.

Materials and Methods

Reagents. The rat alveolar macrophage NR8383 cell line (CRL-2192) was obtained from ATCC (USA). The rabbit anti-PC1/3 (Fus) antibody used has been previously described and characterized[18,19]. Mouse monoclonal anti-TLR9 (26C593.2) was purchased from NOVUS Biologicals. Rabbit anti-Rab7, mouse anti-IκB-α, rabbit anti-STAT3, rabbit anti-phospho-STAT3 and mouse anti-Actin were acquired from Cell Signaling Technology. Alexa Fluor® 488 donkey anti-rabbit, Alexa Fluor® 488 donkey anti-mouse, Alexa Fluor® 555 donkey anti-rabbit and Alexa Fluor® 555 donkey anti-mouse secondary antibodies were obtained from Molecular Probes. Phosphorothioate CpG-ODN 2006 was acquired from Invivogen. Ham's F12K medium, puromycin, phosphate-buffered saline (PBS), and fetal bovine serum (FBS) were purchased from Life Technologies (Milan, Italy). Nitrocellulose membranes and a Bio-Rad Protein Assay Kit were purchased from Bio-Rad (Marnes La Coquette, France). SuperSignal West Dura Chemiluminescent Substrate was acquired from Thermo Scientific. A peroxidase-conjugated secondary antibody was obtained from Jackson ImmunoResearch (West Grove, PA, USA). Rat Cytokine Array Panel A was purchased from R&D Systems (Minneapolis, MN, USA).

Mouse Experimental Models. The transgenic PC1/3 and wild-type (WT) mice used in this study were between 3 and 6 months of age. The mice were maintained in a pathogen-free environment and were provided

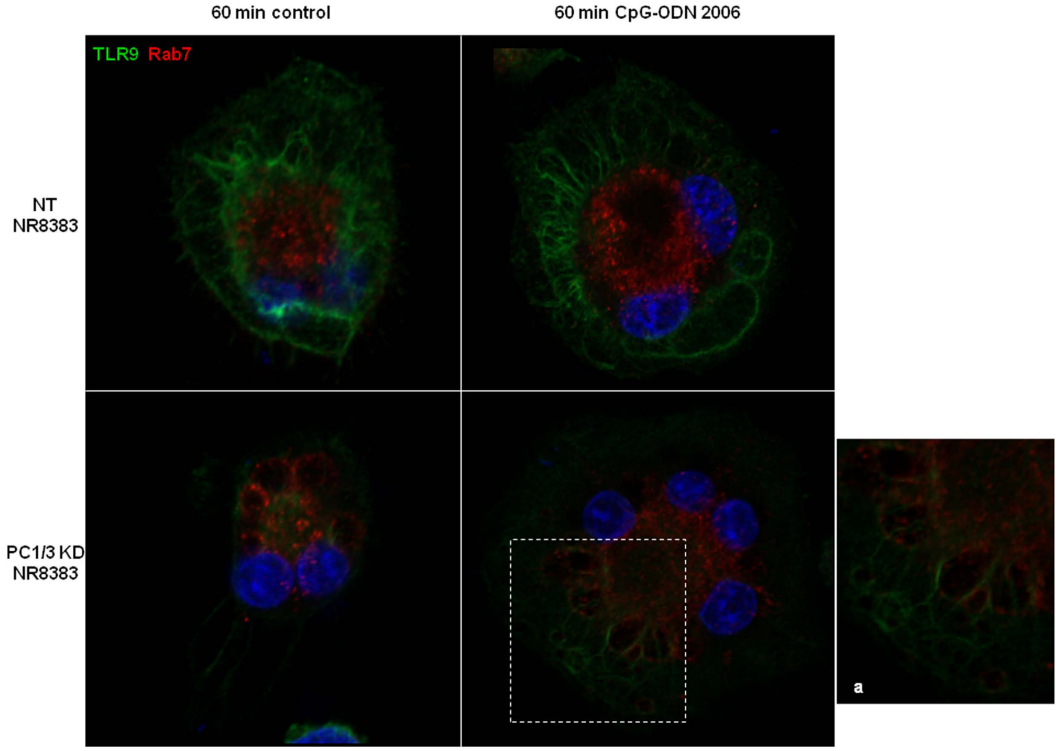

Figure 8. In the absence of PC1/3, TLR9 clusterizes in multivesicular bodies (MVB) after treatment with CpG-ODN. NT and PC1/3 KD NR8383 cells were exposed to CpG-ODN 2006 for 60 min and stained with anti-TLR9 (green) and anti-Rab7 (red). The nuclei were counterstained with Hoechst 33342 (blue). Confocal microscopy analysis was then performed. A higher magnification of the enclosed region is shown in (**a**). It points out the co-localization of TLR9 and Rab7 demonstrating the cluterization of TLR9 in MVB.

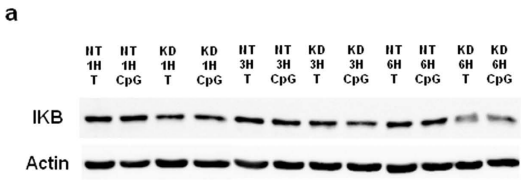

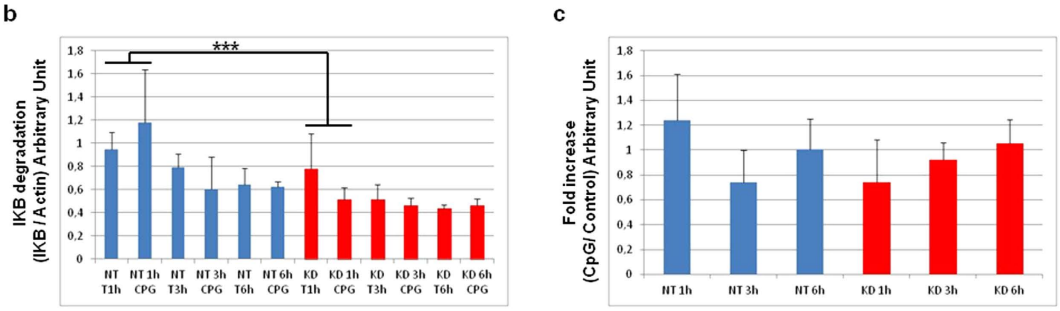

Figure 9. Time course of IκB-α degradation after CpG-ODN treatment. (**a**) Western blot analysis of total IκB-α in NT or KD PC1/3 NR8383 macrophages treated with 1 μM CpG-ODN 2006 for 1, 3 and 6 h. Intensities of total IκB-α bands were quantified and normalized to that of actin. (**b**) The results are depicted through graphic representations (**c**). The fold increases in the samples stimulated with CpG-ODN relative to the non-stimulated samples are shown. Experiments were performed in triplicate and data were then analyzed by two (**c**) or three (**b**) ways ANOVA followed by Holm-Sidak posthoc test. ***Significant differences between NT cells and KD cells ($p < 0.001$).

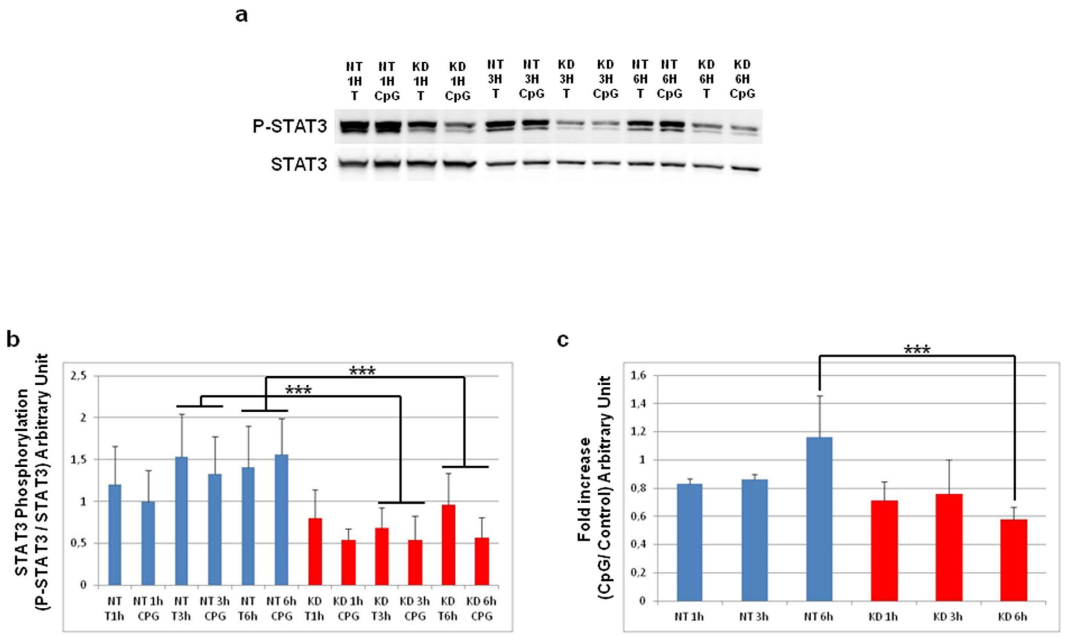

Figure 10. STAT3 signaling is repressed in PC1/3 KD cells. (**a**) Western blot analysis of phospho-STAT3 in NT or KD PC1/3 NR8383 macrophages treated with 1 μM CpG-ODN 2006 for 1, 3 and 6 h. Intensities of phospho-STAT3 bands were quantified and normalized to that of total STAT3. (**b**) The results are depicted through graphic representations. (**c**) The fold increases in the samples stimulated with CpG-ODN relative to the non-stimulated samples are shown. Experiments were performed in triplicate and data were then analyzed by two (**c**) or three (**b**) ways ANOVA followed by Holm-Sidak posthoc test. ***Significant differences between NT cells and KD cells ($p < 0.001$).

food and water *ad libitum*. PC1/3 KO mice have been previously described[18]. They were generated by deletion of exon 1 and several upstream transcriptional control elements of the PCSK1 gene by inserting a neomycin cassette in the C57BL/6 mouse background. All experimental protocol were approved by the Canadian Council on Animal Care and licensing committee from sherbrooke University. The methods were carried out in accordance with the approved guidelines.

Determination of Cytokine Secretion and Cellular Content of Primary Peritoneal Macrophages. Mice were injected intraperitoneally with 2 ml of sterile 3% thioglycolate (BD Biosciences) to increase the yield of peritoneal macrophages. Three days later, the mice were anesthetized with ketamine/xylazine (87/13 mg/kg intramuscularly) and were then sacrificed by cervical dislocation. Peritoneal cells were collected by peritoneal wash with a phosphate-buffered saline (PBS) solution. Red blood cells were lysed by incubation with hemolysis buffer. Cells were plated in a 6 or 24 well plate at 8×10^5 or 2.4×10^6 cells, respectively. They were cultured in RPMI 1640 medium containing penicillin/streptomycin for 24 h at 37 °C in a humidified atmosphere with 5% CO_2 in air. This allowed macrophage adherence, resulting in purification of the peritoneal exudates. The following day, the medium was replaced by serum free medium and the cells were stimulated for 4 h with PBS 1X or 1 μM CpG-ODN. Medium was collected and a cell lysate was obtained by adding 200 μl of 0.5 N HCl followed by three freeze-thaw cycles. Total protein was collected by centrifugation and cytokine levels were measured using ELISA kits specific for mouse TNFα and Mouse IL-6 according to the manufacturer's instructions (R&D Systems). Statistical analysis was performed using Student's t test with Prism 5 (GraphPad Software), which calculates the SE.

Culture of NR8383 cell lines. Rat alveolar wild-type (WT) NR8383 macrophages were cultured in Ham's F12K medium supplemented with 15% fetal bovine serum. NR8383 PC1/3 knockdown (PC1/3-KO) and NR8383 non-target (NT) shRNA cell lines were cultured in Ham's F12K medium supplemented with 15% fetal bovine serum and 12 μg/ml puromycin. NR8383 PC1/3 knockdown was carried out using lentiviral transduction, as described previously[19]. Culture was performed at 37 °C in a humidified atmosphere (5% CO2).

Confocal microscopy and co-localization studies. The NR8383 cells were grown on cover slip and treated or not as described. The cells were then fixed with 4% paraformaldehyde (PFA) for 10 min. After washes with PBS, cells were permeabilized with 0.2% Triton X-100 for 10 min at room temperature and blocked during 1 h with a blocking solution (PBS 1X, 1% Normal Donkey Serum, 1% BSA, 0.01% Triton). Cells were then incubated overnight at 4 °C with the primary antibodies diluted at 1:100 in blocking solution. After intensive washes with PBS 1X, secondary antibodies diluted at 10 μg/mL in blocking solution was applied for 1 h. After washes with PBS, the nuclei were stained with Hoechst 33342 (1/10000) and the cells were visualized by confocal microscopy. Fluorescence analysis was conducted using a Zeiss LSM 510 confocal microscope (488 nm excitation for Alexa 488 and 543 nm for Alexa 546) connected to a Zeiss Axiovert 200 M with a 63 × 1.4 numerical

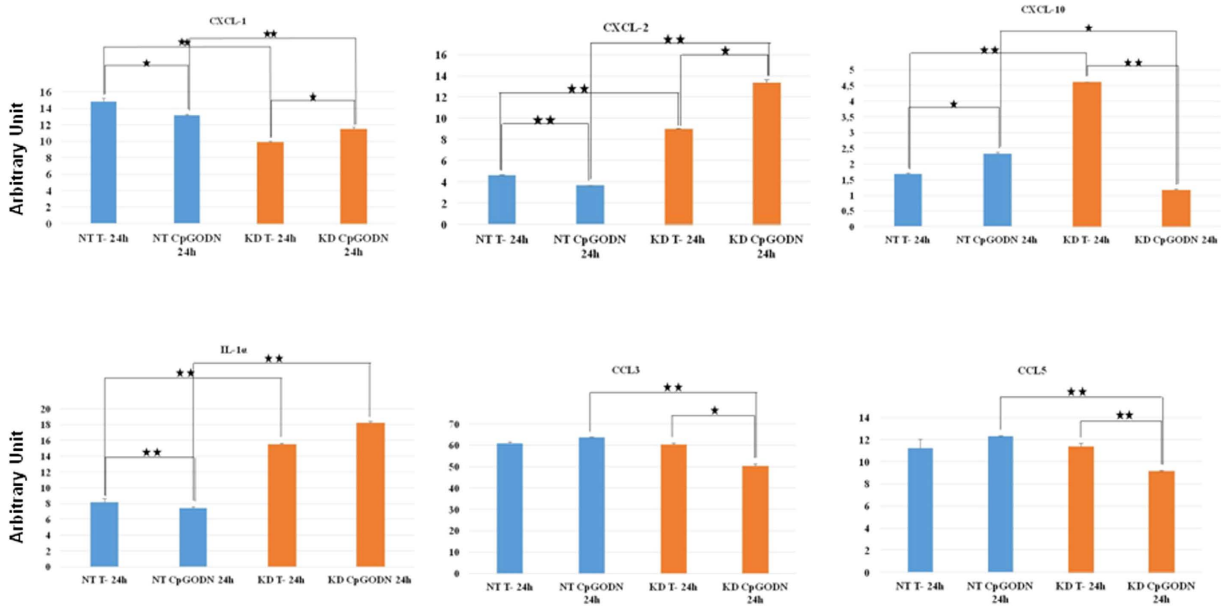

Figure 11. Cytokines secreted by NT and KD cells during challenge (or not) with CpG-ODN. Cells were untreated (control) or treated with 1 μM CpG-ODN for 24 h. A Rat Cytokine Array was used to probe cytokines in the secretomes. The NT cell secretomes are shown in blue and the KD cell secretomes are depicted in orange. The bar diagrams show the ratios of the spot mean pixel densities/reference point pixel densities. Significant differences were analyzed using Student's t-test. *P ≤ 0.05, **P ≤ 0.01.

aperture oil immersion objective. Both channels were excited, collected separately and then merged to examine the co-localization. The image acquisition characteristics (pinhole aperture, laser intensity, scan speed) were the same throughout the experiments to ensure comparability of the results.

Measurement of Texas red-dextran uptake. Endocytic activity was assessed by incubating cells for 2 h with 0.5 mg/ml Texas Red-dextran at 37 °C. Cells were washed extensively with PBS 1X and fixed with 4% paraformaldehyde (PFA) for 10 min. PC1/3 labelling with anti-PC1/3 was then performed as described above.

Bafilomycin A1 Treatment. NR8383 cells were stimulated for 6 hours with 100 nM CpG-ODN in the presence of 100 nM bafilomycin A1 added to the cells 2 hours prior to stimulation. The cells were then double labelled using anti-PC1/3 and anti-TLR9 and imaged by confocal microscopy.

Electron microscopy. After incubation or not with 100 nM CpG-ODN 2006, cells were harvested by scraping and the medium was removed by centrifugation. For the morphological experiments, cell pellets were fixed in 2.5% glutaraldehyde in 0.1 M cacodylate buffer, pH 7.4, for 15 min on ice. After washes, cell pellets were postfixed in 1% osmium tetroxide in the same buffer for another 15 min at room temperature. The pellets were subsequently processed for embedding in Epon resin after dehydration in graded acetonitrile. Double-contrasted sections (uranyl acetate and lead citrate[36]) were observed under a Hitachi H600 transmission electron microscope set at 75 kV. For ultrastructural immunodetection, cell pellets were fixed in 4% paraformaldehyde and 0.1% glutaraldehyde in PBS 1X for 15 min on ice. After several washes in PBS 1X, the pellets were infused overnight in 2.3 M sucrose and 20% polyvinyl pyrrolidone. The pellets were then frozen and kept in liquid nitrogen until use. Cryosections were harvested on Formvar-coated grids[37]. The grids were then incubated in PBS-glycerol (50 mM, pH 7.4) for 20 min at room temperature to inactivate the residual aldehydes. Next, they were transferred to a blocking solution (PBS, 5% activated BSA-C, 5% donkey serum albumin, and 0.1% fish gelatin) for 30 min at room temperature. After several washes, the samples were incubated with the respective primary antibodies for either 1 h at room temperature or overnight at 4 °C in a moist chamber. After thorough washes, the grids were incubated with their respective secondary antibodies labelled with colloidal gold (6 and 12 nM) for 1 h at 37 °C. The sections were finally contrasted with uranyl acetate and embedded in methyl cellulose[37].

Total protein extraction. NR8383 PC1/3-KD and NT cells were plated on sterile 6 well plates and cultured until they reached confluence. For CpG-ODN stimulation, cells were starved overnight in Ham's F12K medium supplemented with 2% FBS. They were then stimulated with 1 μM CpG-ODN 2006 in serum-free medium or were left untreated. At 24 h, cells were collected, washed once with ice-cold PBS and then lysed with RIPA buffer for total protein extraction (150 mM NaCl, 50 mM Tris, 5 mM EGTA, 2 mM EDTA, 100 mM NaF, 10 mM sodium pyrophosphate, 1% NP40, 1 mM PMSF, and 1X protease inhibitors). Cell debris was removed by centrifugation (20000 g, 10 min, 4 °C), supernatants were collected and protein concentrations were measured using a Bio-Rad Protein Assay Kit, according to the manufacturer's instructions.

Organelles sub-fractionation. 8 to 9×10^7 cells were harvested and processed for subcellular fractionation. The pellet was homogenized in 1 ml Tris 10 mM, sucrose 0.25 M, pH 7.5 and antiprotease cocktail, on ice in a Kontes glass homogenizer fitted with a 15 μm clearance pestle. The success of the homogenization process was checked by phase contrast microscopy (at least 90% broken cells). After two centrifugations at 800 g in order to remove the nuclei and the cellular debris, the post nuclear supernatant was laid on top of a preformed (two chamber gradient maker, CBS. Scientific) continuous (10–30%) gradient of Iodixanol (Optiprep™, Axis-Shield) and spun for 1H30 at 60,000 g in a swinging bucket rotor (SW41Ti, Beckman). The gradient was then collected from the bottom in 1 ml fractions which were 3 fold diluted in homogenization medium and centrifuged for 30 min in a fixed angle rotor (50Ti, Beckman) at 220,000 g. Each fraction was dissolved in Laemmli buffer and then processed through SDS-PAGE (8% acrylamide).

Western Blot Analysis. Total cell extracts (40 μg) were then analyzed by Western blotting. First, proteins were separated by SDS-PAGE electrophoresis and transferred onto nitrocellulose membranes. The membranes were blocked for 1 h at room temperature with TBS-Tween 0.1% + 5% nonfat dry milk and incubated overnight at 4 °C with primary antibodies against TLR9 (1:1000), IκBα (1:1000), phosphor-STAT3 (1:2000), STAT3 (1:1000) and actin (1:1000). The membranes were washed with TBS-Tween 0.1%, incubated for 1 h at room temperature with peroxidase-conjugated secondary antibodies (anti-mouse and anti-rabbit diluted at 1:30000 or 1:20000, respectively) and washed again with TBS-Tween 0.1%. Proteins were visualized with an enhanced chemiluminescence kit (West Dura from Pierce) according to the manufacturer's instructions. ImageJ software was used to quantify the bands.

Data were then analyzed by two or three ways ANOVA followed by Holm-Sidak posthoc test.

Identification of cytokines using rat cytokine antibody arrays. NR8383 PC1/3-KD and NT cells were plated on sterile 6 well plates and cultured until they reached confluence. The cells were starved overnight in Ham's F12K medium supplemented with 2% FBS and were stimulated for 4 h or 24 h with 1 μM CpG-ODN or were left untreated. Cell supernatants were collected, centrifuged at 500 g, passed through a 0.22 μm filter to remove cells and immediately frozen in liquid nitrogen. A Rat Cytokine Array Panel A (R&D Systems) was used to probe cytokines in the secretomes of stimulated and unstimulated NR8383 cells according to the manufacturer's recommendations. Briefly, array membranes were first incubated in blocking buffer for 1 h. In the meantime, secreted proteins were mixed with Detection Antibody Cocktail and incubated for 1 h at room temperature. The secreted protein volume used for this experiment was determined according to the cell count after stimulation. Next, after removal of the blocking buffer, sample/antibody mixtures were added to array membranes and incubated overnight at 4 °C. After incubation, the membranes were washed 3 times with Wash Buffer and then incubated with a streptavidin-HRP solution for 30 min at room temperature. The membranes were finally washed 3 times with Wash Buffer and bound antibodies were detected by chemiluminescence using Chemi Reagent Mix. The membranes were quantified by densitometry using ImageJ software. Statistical analysis was carried out by Student's t test.

References

1. Ostuni, R., Kratochvill, F., Murray, P. J. & Natoli, G. Macrophages and cancer: from mechanisms to therapeutic implications. *Trends Immunol* **36,** 229–239 (2015).
2. Pohar, J., Kuznik Krajnik, A., Jerala, R. & Bencina, M. Minimal sequence requirements for oligodeoxyribonucleotides activating human TLR9. *J Immunol* **194,** 3901–3908 (2015).
3. Rodriguez, J. M. *et al.* PyNTTTTGT and CpG immunostimulatory oligonucleotides: effect on granulocyte/monocyte colony-stimulating factor (GM-CSF) secretion by human CD56+ (NK and NKT) cells. *PLoS One* **10,** e0117484 (2015).
4. Kim, Y. H. *et al. In situ* vaccination against mycosis fungoides by intratumoral injection of a TLR9 agonist combined with radiation: a phase 1/2 study. *Blood* **119,** 355–363 (2012).
5. Shirota, Y., Shirota, H. & Klinman, D. M. Intratumoral injection of CpG oligonucleotides induces the differentiation and reduces the immunosuppressive activity of myeloid-derived suppressor cells. *J Immunol* **188,** 1592–1599 (2012).
6. Molenkamp, B. G. *et al.* Local administration of PF-3512676 CpG-B instigates tumor-specific CD8+ T-cell reactivity in melanoma patients. *Clin Cancer Res* **14,** 4532–4542 (2008).
7. Brody, J. D. *et al. In situ* vaccination with a TLR9 agonist induces systemic lymphoma regression: a phase I/II study. *J Clin Oncol* **28,** 4324–4332 (2010).
8. Hofmann, M. A. *et al.* Phase 1 evaluation of intralesionally injected TLR9-agonist PF-3512676 in patients with basal cell carcinoma or metastatic melanoma. *Journal of immunotherapy* **31,** 520–527 (2008).
9. Chockalingam, A., Brooks, J. C., Cameron, J. L., Blum, L. K. & Leifer, C. A. TLR9 traffics through the Golgi complex to localize to endolysosomes and respond to CpG DNA. *Immunology and cell biology* **87,** 209–217 (2009).
10. Latz, E. *et al.* TLR9 signals after translocating from the ER to CpG DNA in the lysosome. *Nat Immunol* **5,** 190–198 (2004).
11. Kim, Y. M., Brinkmann, M. M., Paquet, M. E. & Ploegh, H. L. UNC93B1 delivers nucleotide-sensing toll-like receptors to endolysosomes. *Nature* **452,** 234–238 (2008).
12. Takahashi, K. *et al.* A protein associated with Toll-like receptor (TLR) 4 (PRAT4A) is required for TLR-dependent immune responses. *J Exp Med* **204,** 2963–2976 (2007).
13. Demoulin, S. *et al.* HMGB1 secretion during cervical carcinogenesis promotes the acquisition of a tolerogenic functionality by plasmacytoid dendritic cells. *Int J Cancer* (2014).
14. Brooks, J. C., Sun, W., Chiosis, G. & Leifer, C. A. Heat shock protein gp96 regulates Toll-like receptor 9 proteolytic processing and conformational stability. *Biochem Biophys Res Commun* **421,** 780–784 (2012).
15. Park, J. E., Kim, Y. I. & Yi, A. K. Protein kinase D1: a new component in TLR9 signaling. *J Immunol* **181,** 2044–2055 (2008).
16. Yoshizaki, M. *et al.* Spatiotemporal regulation of intracellular trafficking of Toll-like receptor 9 by an inhibitory receptor, Ly49Q. *Blood* **114,** 1518–1527 (2009).
17. Duhamel, M. *et al.* Molecular consequences of proprotein convertase 1/3 inhibition in macrophages for application to cancer immunotherapy: a proteomic study. *Mol Cell Proteomics*, doi: 10.1074/mcp.M115.052480 (2015).
18. Refaie, S. *et al.* Disruption of proprotein convertase 1/3 (PC1/3) expression in mice causes innate immune defects and uncontrolled cytokine secretion. *J Biol Chem* **287,** 14703–14717 (2012).
19. Gagnon, H. *et al.* Proprotein convertase 1/3 (PC1/3) in the rat alveolar macrophage cell line NR8383: localization, trafficking and effects on cytokine secretion. *PLoS One* **8,** e61557 (2013).

20. Moreira, D. *et al.* TLR9 signaling through NF-kappaB/RELA and STAT3 promotes tumor-propagating potential of prostate cancer cells. *Oncotarget* **6,** 17302–17313 (2015).
21. Kortylewski, M. *et al.* Toll-like receptor 9 activation of signal transducer and activator of transcription 3 constrains its agonist-based immunotherapy. *Cancer Res* **69,** 2497–2505 (2009).
22. St Germain, C. *et al.* Expression and transient nuclear translocation of proprotein convertase 1 (PC1) during mouse preimplantation embryonic development. *Molecular reproduction and development* **72,** 483–493 (2005).
23. Manoury, B. TLR9 regulation by proteolysis: a friend or a foe. *Eur J Immunol* **41,** 2142–2144 (2011).
24. Carpentier, A. F. [Cancer immunotherapy with CpG-ODN]. *Med Sci (Paris)* **21,** 73–77 (2005).
25. Ewald, S. E. & Barton, G. M. Nucleic acid sensing Toll-like receptors in autoimmunity. *Current opinion in immunology* **23,** 3–9 (2011).
26. Ewald, S. E. *et al.* The ectodomain of Toll-like receptor 9 is cleaved to generate a functional receptor. *Nature* **456,** 658–662 (2008).
27. Ewald, S. E. *et al.* Nucleic acid recognition by Toll-like receptors is coupled to stepwise processing by cathepsins and asparagine endopeptidase. *J Exp Med* **208,** 643–651 (2011).
28. Sepulveda, F. E. *et al.* Critical role for asparagine endopeptidase in endocytic Toll-like receptor signaling in dendritic cells. *Immunity* **31,** 737–748 (2009).
29. Park, B. *et al.* Proteolytic cleavage in an endolysosomal compartment is required for activation of Toll-like receptor 9. *Nat Immunol* **9,** 1407–1414 (2008).
30. Hipp, M. M. *et al.* Processing of human toll-like receptor 7 by furin-like proprotein convertases is required for its accumulation and activity in endosomes. *Immunity* **39,** 711–721 (2013).
31. Kimura, T. *et al.* Endoplasmic Protein Nogo-B (RTN4-B) Interacts with GRAMD4 and Regulates TLR9-Mediated Innate Immune Responses. *J Immunol* **194,** 5426–5436 (2015).
32. Lee, B. L. *et al.* UNC93B1 mediates differential trafficking of endosomal TLRs. *eLife* **2,** e00291 (2013).
33. Chen, T. A. *et al.* Stimulation of Proliferation and Migration of Mouse Macrophages by Type B CpG-ODNs Is F-Spondin and IL-1Ra Dependent. *PLoS One* **10,** e0128926 (2015).
34. Ho, H. H. & Ivashkiv, L. B. Role of STAT3 in type I interferon responses. Negative regulation of STAT1-dependent inflammatory gene activation. *J Biol Chem* **281,** 14111–14118 (2006).
35. Kortylewski, M. & Pal, S. K. The dark side of Toll-like receptor signaling: TLR9 activation limits the efficacy cancer radiotherapy. *Oncoimmunology* **3,** e27894 (2014).
36. Reynolds, E. S. The use of lead citrate at high pH as an electron-opaque stain in electron microscopy. *J Cell Biol* **17,** 208–212 (1963).
37. Griffiths, G., Simons, K., Warren, G. & Tokuyasu, K. T. Immunoelectron microscopy using thin, frozen sections: application to studies of the intracellular transport of Semliki Forest virus spike glycoproteins. *Methods Enzymol* **96,** 466–485 (1983).

Acknowledgements

This research was supported by grants from the Ministère de L'Education Nationale, de L'Enseignement Supérieur et de la Recherche, ANR (IF), Région Nord-Pas de Calais ARCIR (IF), the Université de Lille (MD) SIRIC ONCOLille (IF, MD), Grant INCa-DGOS-Inserm 6041aa, the CCMIC and INSERM. The authors are indebted to Elodie Richard of the CCMIC–Université de Lille 1 (BiCel) for her help and technical support in confocal microscopy experiments.

Author Contributions

M.S., F.R. and R.D. have written the paper. M.D., F.R., A.N.M., M.W., D.R. and G.H. have done the experiments. M.S., I.F. and R.D. have got financial support for the project and corrected the manuscript. All authors have reviewed the manuscript.

Additional Information

Competing financial interests: The authors declare no competing financial interests.

How to cite this article: Duhamel, M. *et al.* The proprotein convertase PC1/3 regulates TLR9 trafficking and the associated signaling pathways. *Sci. Rep.* **6**, 19360; doi: 10.1038/srep19360 (2016).

EuPA Open Proteomics 11 (2016) 20–22

Contents lists available at ScienceDirect

EuPA Open Proteomics

journal homepage: www.elsevier.com/locate/euprot

Proprotein convertase 1/3 inhibited macrophages: A novel therapeutic based on drone macrophages

Marie Duhamel[a], Franck Rodet[a], Adriana Murgoci[a], Maxence Wisztorski[a], Robert Day[b], Isabelle Fournier[a], Michel Salzet[a,*]

[a] Univ. Lille, INSERM, U1192—Laboratoire Protéomique, Réponse Inflammatoire et Spectrométrie de Masse-PRISM, F-59000 Lille, France
[b] Institut de Pharmacologie, Département de Chirurgie/Service d'Urologie, Faculté de Médecine et des Sciences de la Santé, Université de Sherbrooke, Sherbrooke, J1H 5N4 Québec, Canada

ARTICLE INFO

Article history:
Received 24 October 2015
Received in revised form 1 March 2016
Accepted 2 March 2016
Available online 5 March 2016

ABSTRACT

We demonstrated here thanks to proteomic, that proprotein convertase 1/3 knockdown macrophages present all the characteristic of activated pro-inflammatory macrophages. TLR4 and TLR9 signaling pathways can be enhanced leading to the secretion of pro-inflammatory factors and antitumor factors. We can control their activation by controlling one enzyme, PC1/3. In a tumor context, PC1/3 inhibition in macrophages may reactivate them and lead to a cytokine storm after stimulation "at distance" with a TLR ligand. Therefore, we name these proprotein convertase inhibited macrophages the "drone macrophages". They constitute an innovative cell therapy to treat efficiently tumors.

Macrophages are involved in almost every disease. They are recruited during inflammation to exert their inflammatory and phagocytosis functions. Tissue-resident macrophages are not a homogenous population. In fact, they present different phenotypes which can be influenced by their environment. Macrophages activation is often represented in two ways: M1 pro-inflammatory and M2 anti-inflammatory polarization. This description is over-simplified because macrophages activation depends on many parameters such as their origin, environment etc. During tumorigenesis, macrophages are recruited to the tumor site to become tumour associated macrophages (TAMs). However, the tumor creates an immune suppressive environment, which orients TAMs toward the anti-inflammatory M2 phenotype. One challenge is to counteract this local immune suppression observed in numerous cancers. More and more therapies are being developed in order to find a way to control macrophages' phenotype switching in order to boost the immune response in cancer patients. Pro-inflammatory macrophages can be activated by several stimuli triggering signaling cascades. As stimuli, we can find Toll-like receptors (TLR) ligands (LPS, CpG-ODN, Taxol . . .). TLR-based therapies could be thus very interesting.

Our research goes in that direction. In fact, we work on an enzyme called proprotein convertase 1/3 (PC1/3). PC1/3 was first associated with the neuroendocrine system. More recent studies have demonstrated that this enzyme is also expressed in immune cells like macrophages and lymphocytes. In PC1/3 knockout mice, a massive cytokine response was registered following the stimulation of TLR4 [1]. Another study confirmed the role of PC1/3 in cytokines release in rat alveolar NR8383 macrophages [2]. In the present study, we want to know the impact of PC1/3 knockdown (KD) on NR8383 macrophages activation after TLR4 (LPS) and TLR9 (CpG-ODN) stimulations. We used a complete proteomic approach to answer this question. In the first part, a shotgun experiment was performed on the macrophages supernatants stimulated with LPS from 1 h to 72 h. More than 1400 proteins were identified and 18 proteins were specific to PC1/3 inhibition. Some of them are involved in Th1-cell activation and inflammatory response. We also identified immune factors such as danger signals, cytokines and chemokines which are secreted by PC1/3 KD macrophages earlier compared to non-target shRNA (NT) macrophages [3]. We then focused on the secretion of chemokines and cytokines by cytokines arrays and confirmed the fact that PC1/3 KD macrophages secrete more pro-inflammatory factors such as IL6, TNF-α, CXCL10, IL-1α and β. After LPS treatment, the secretion of some of these factors was enhanced. Interestingly, the stimulation with CpG-ODN triggered a slightly different secretion than the one observed under LPS. In fact, PC1/3 KD macrophages secrete more

Abbreviations: PC, proprotein convertase; TAM, tumor associated macrophages; TLR, toll like receptor; KD, knockdown; NT, non-target; LPS, lipopolysaccharides; MVB, multivesicular bodies; CCL, chemokine (C–C motif) ligand; CXCL, chemokine (C–X–C motif) ligand.

* Corresponding author at: U−1192 Inserm, Laboratoire de Protéomique, Réponse Inflammatoire, Spectrométrie de Masse (PRISM), Université de Lille 1, Cité Scientifique, 59655 Villeneuve D'Ascq, France.
E-mail address: michel.salzet@univ-lille1.fr (M. Salzet).

http://dx.doi.org/10.1016/j.euprot.2016.03.003

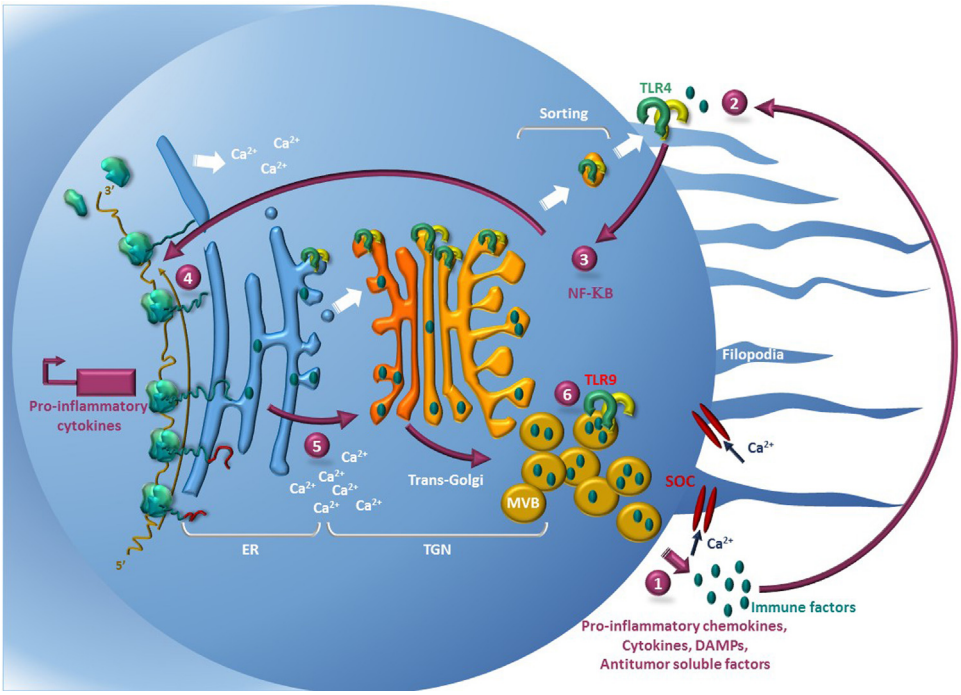

Fig. 1. Schematic depicting how PC1/3 knockdown impacts macrophage activation. PC1/3 knockdown promotes the formation of endosomes and MVB release of inflammatory chemokines and cytokines via the non-canonical secretion pathway (1). Danger signal molecules (DAMs) can activate TLR4 and TLR9 (2) and induce the MyD88-dependent pathway with increased NF-κB (3) nuclear translocation (4) linked to Ca^{2+} mobilization in PC1/3 KD macrophages (5). Both of these phenomena are also implicated in cytokines, chemokines, DAMs and tumor viability inhibitor release as well as cytoskeletal rearrangements leading to the formation of filopodia (6). We then noticed that during LPS challenge, the loop was amplified and driven toward the induction of increased Ca^{2+} release from the ER, greater numbers of filopodia and MVBs, the release of additional immune factors and a greater number of anti-tumor factors. Under ODN-CpG challenge, we observed that PC1/3 moved rapidly to CpG-ODN-containing endosomes and lysosomes and subsequently co-localized with TLR9. In PC1/3 knockdown macrophages, compartmentalization of TLR9 was altered, and formed clusters at the cell periphery. Under CpG-ODN treatment, PC1/3-KD macrophages secreted more pro-inflammatory cytokines (TNF-α, CXCL2, and IL1α) and less CCL5 and CXCL10. We have thus established that PC1/3 inhibition clearly affects TLR9 trafficking and signaling and not its activation. All experimental procedures have been published in [3].

CXCL2 and IL1-α. One important observation was that PC1/3 KD macrophages secretomes, obtained after LPS stimulation, have an antitumor activity on breast (SKBR3) and ovarian (SKOV3) cancer cells, meaning that these macrophages secrete killing factors [3]. To understand why such secretion is observed in PC1/3 KD macrophages, we studied the intracellular proteins by mass spectrometry. The first finding from these proteomic data was the big impact of PC1/3 knockdown on the cytoskeleton. Co-expression network analysis showed that actin-related proteins and exosomal proteins were overexpressed in PC1/3 KD macrophages. A complete reorganization of the cytoskeleton was highlighted with the development of a lot of filopodia in PC1/3 KD cells leading us to affirm that macrophages are more active when PC1/3 is inhibited. This cytoskeleton reorganization has a huge impact on the formation of multivesicular bodies (MVB) and the trafficking of some proteins such as the TLR9 receptor [4]. In fact, immunofluorescence studies showed that TLR9 trafficking is modulated in PC1/3 KD macrophages and is aggregated within MVB. The higher number of MVB and exosomes can be one explanation for the cytokines release observed in PC1/3 KD macrophages. Moreover, calcium homeostasis is also modulated as a consequence of cytoskeleton rearrangement. Basal calcium concentration is higher in PC1/3 KD macrophages compared to NT macrophages and increases following LPS stimulation. Calcium and cytokines release are often linked. Furthermore, calcium can also influenced the TLR signaling pathway. We investigated TLR9 and TLR4 signaling pathways by studying the level of degradation of IκB-α after LPS or CpG-ODN stimulation. We noticed that the NF-κB transcription factor is enhanced in both cases in PC1/3 KD macrophages. By proteomic, we also demonstrated that the two pro-inflammatory transcription factors STAT1 and STAT2 are over-expressed whereas the level of phosphorylation of STAT3, which is known to inhibit NF-κB signaling, is lower in PC1/3 KD macrophages. This last point could be interesting because STAT3 is a known target in immunotherapy of cancer.

In this study, we demonstrated, thanks to proteomic, that PC1/3 KD macrophages present all the characteristic of activated pro-inflammatory macrophages. We are able to enhance TLR4 and TLR9 signaling pathways leading to the secretion of pro-inflammatory factors and antitumor factors (Fig. 1). We can control their activation by controlling one enzyme, PC1/3. In this perspective, it should be interesting to verify our concept on other TLR. In a tumor context, PC1/3 inhibition in macrophages may reactivate them and lead to a cytokine storm after stimulation “at distance” with a TLR ligand. Therefore, we name these PC1/3 inhibited macrophages the “drone macrophages”. They constitute an innovative cell therapy to treat efficiently tumors.

Conflict of interest

None.

Acknowledgements

This research was supported by grants from the Ministère de L’Education Nationale, de L’Enseignement Supérieur et de la Recherche,ANR (IF), Région Nord-Pas de Calais ARCIR (IF), the Université de Lille (MD) SIRIC ONCOLille (IF, MD), Grant INCa-DGOS-Inserm 6041aa, theCCMIC and INSERM.

Appendix A. Supplementary data

Supplementary data associated with this article can be found, in the online version, at http://dx.doi.org/10.1016/j.euprot.2016.03.003.

References

[1] S. Refaie, S. Gagnon, H. Gagnon, R. Desjardins, F. D'Anjou, P. D'Orleans-Juste, et al., Disruption of proprotein convertase 1/3 (PC1/3) expression in mice causes innate immune defects and uncontrolled cytokine secretion, J. Biol. Chem. 287 (2012) 14703–14717.

[2] H. Gagnon, S. Refaie, S. Gagnon, R. Desjardins, M. Salzet, R. Day, Proprotein convertase 1/3 (PC1/3) in the rat alveolar macrophage cell line NR8383: localization, trafficking and effects on cytokine secretion, PLoS One 8 (2013) e61557.

[3] M. Duhamel, F. Rodet, N. Delhem, F. Vanden Abeele, F. Kobeissy, S. Nataf, et al., Molecular consequences of proprotein convertase 1/3 (PC1/3) inhibition in macrophages for application to cancer immunotherapy: a proteomic study, Mol. Cell Proteom. 14 (2015) 2857–2877.

[4] M. Duhamel, F. Rodet, A.N. Murgoci, R. Desjardins, H. Gagnon, M. Wisztorski, et al., The proprotein convertase PC1/3 regulates TLR9 trafficking and the associated signaling pathways, Sci. Rep. 6 (2016) 19360.

Conclusion

Notre étude démontre que l'inhibition de PC1/3 dans les macrophages permet d'induire un phénotype pro-inflammatoire. La combinaison de l'inhibition de PC1/3 et de la stimulation des récepteurs TLR4 et TLR9 renforce encore plus ce phénotype. Il serait également intéressant de savoir si la stimulation d'autres récepteurs TLR déclencherait le même phénomène.

Afin de vérifier si la stimulation au CpG-ODN des macrophages permet la libération de facteurs anti-tumoraux, nous avons réalisé des tests de viabilité sur une lignée cellulaire de gliome de rat (C6). En effet, des essais cliniques précoces ont démontré que le CpG-ODN pouvait stimuler les activités anti-tumorales des cellules immunitaires (Carpentier 2005). Le CpG-ODN peut induire la production de cytokines telles que l'IFN-α par les cellules dendritiques pour activer les cellules « natural killer » cytotoxiques (Ballas et al. 1996). Des essais cliniques du CpG-ODN sur des patients atteints de glioblastome montrent des effets significatifs (Carpentier 2005). Les tests de viabilité sur les cellules C6 ont été faits avec le sécrétome des macrophages PC1/3 KD et NT stimulés au CpG-ODN pendant 24h. La viabilité a été mesurée à 24h, 48h, 72h et 96h. Le point à « 96h+medium » signifie que le milieu a été renouvelé au bout de 72h et la viabilité mesurée 24h après (**Figure 14**). Les résultats nous montrent que les macrophages sécrètent également des facteurs anti-tumoraux sous stimulation au CpG-ODN. La viabilité des cellules C6 diminue en présence du sécrétome des macrophages par rapport au contrôle contenant uniquement du milieu et du CpG-ODN. Par contre, on remarque qu'au cours du temps, les cellules ne meurent pas, ni ne prolifèrent. Elles restent dans un état quiescent. De plus, les différences de viabilité entre le sécrétome des cellules NT et KD ne sont pas significatives. Cela est différent des résultats observés sous LPS, notamment pour les cellules cancéreuses du sein SKBR3, où l'on pouvait voir une mort des cellules au cours du temps et plus particulièrement avec le sécrétome des macrophages PC1/3 KD et pour les SKOV3, où le renouvellement du milieu a entraîné une chute de viabilité importante avec le sécrétome des macrophages et notamment avec celui des cellules PC1/3 KD (article MCP, Figure 9).

De plus, la combinaison du CpG-ODN avec différents agents chimiothérapeutiques n'a pas montré d'effet supplémentaire par rapport à la chimiothérapie seule (étude clinique réalisée par Pfizer en 2005).

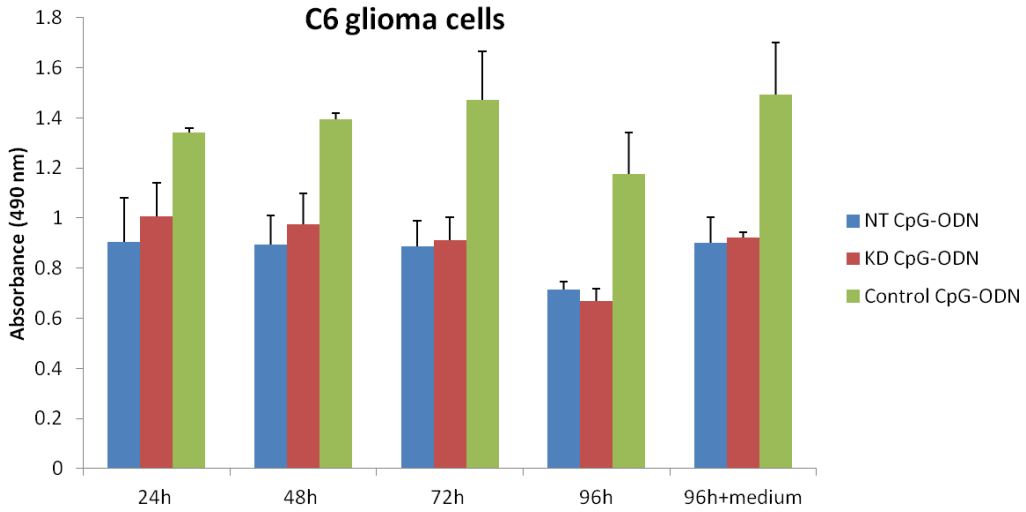

Figure 14 : Viabilité des cellules cancéreuses C6 de gliome de rat en présence des sécrétomes des macrophages NT et PC1/3 KD stimulés au CpG-ODN. La viabilité des cellules C6 de gliome de rat a été mesurée avec le test MTS. Les cellules ont été mises en présence du sécrétome des macrophages durant 24h, 48h, 72h et 96h. Le point de mesure « 96h+medium » signifie que le milieu a été renouvelé à 72h et la viabilité a été mesurée 24h après.

Nous nous sommes donc basés sur nos observations pour la suite de nos expériences, c'est-à-dire cibler l'activation du récepteur TLR4 pour une stratégie thérapeutique. La combinaison à la fois d'un ligand du récepteur TLR4 et de l'inhibition de PC1/3 dans les macrophages pourrait permettre de les réactiver et ainsi ils pourraient réattaquer les cellules cancéreuses. L'application des ligands naturels des récepteurs TLR est bien sûr exclue. Etant donné leur nature infectieuse, ils déclencheraient une très forte inflammation. Une « inflammation stérile » peut être obtenue en utilisant des agonistes du récepteur TLR4. Un agoniste connu est le taxol. Le taxol est un agent anti-cancéreux mimant l'action du LPS. Ces travaux font l'objet de mon troisième chapitre de thèse où nous avons cherché à activer les macrophages PC1/3 KD avec le taxol dans un contexte immuno-oncologique. Ce chapitre a pour but de répondre aux questions suivantes :

1. Le taxol induit-il le même état d'activation que le LPS dans nos macrophages?
2. L'utilisation du taxol couplée à l'inhibition de PC1/3 est-elle une bonne stratégie thérapeutique pour la réactivation des macrophages au sein de la tumeur?

CHAPITRE 3

Inhibition de la proprotéine convertase 1/3 (PC1/3) dans les macrophages pré-activés au Taxol pour le traitement des glioblastomes

Introduction

Le taxol est une drogue utilisée pour le traitement contre différents cancers tels que les cancers de la prostate, de l'ovaire, du sein et du poumon. Son mécanisme d'action est lié à sa capacité de stabiliser les microtubules et de perturber leur dynamique. Le taxol a été isolé il y a plus de 28 ans et extrait à partir de certaines espèces d'ifs (*Taxus baccata*). Il inhibe la prolifération cellulaire en stabilisant les microtubules durant la phase G2-M du cycle cellulaire. Dans le contexte des glioblastomes, on lui préfère le témozolomide**,** l'alkylant le plus efficace. Cependant, depuis le développement de nanoparticules contenant du Taxol, ce dernier est désormais utilisé en thérapie contre les gliomes (Wang et al. 2015). Les cellules microgliales et macrophages peuvent représenter jusqu'à 30% de la masse tumorale totale des glioblastomes. Les macrophages associés aux tumeurs (TAM) ne permettent pas seulement de promouvoir la croissance tumorale et sa progression mais ils modulent aussi l'efficacité de certaines thérapies anti-cancéreuses (De Palma & Lewis 2013). La chimiosensibilité des thérapies est améliorée quand les agents cytotoxiques augmentent la cytotoxicité des TAM ou permettent de diminuer leur nombre au niveau de la tumeur. Les TAM peuvent aussi subir une reprogrammation de leur phénotype par certains agents. Au contraire, la chimiorésistance est plus importante quand les agents cytotoxiques augmentent le nombre de TAM infiltrant la tumeur. Par exemple, le taxol déclenche une infiltration importante des macrophages car les cellules cancéreuses surexpriment le facteur CSF-1. La forte augmentation du nombre de TAM dans les tumeurs traitées avec le taxol, limite l'infiltration des cellules T CD8+ cytotoxiques et réduit leur activité tumoricide. Les TAM peuvent limiter l'activité thérapeutique du taxol dans le cancer du sein en supprimant les réponses immunitaires anti-tumorales (DeNardo et al. 2011).

Le taxol a une autre activité potentiellement intéressante. En effet, il peut mimer l'action du LPS. Son action passe par la liaison au récepteur TLR4. Une fois lié au récepteur, le taxol induit, à la fois, les voies de signalisation MyD88-dépendante et indépendante menant à l'activation de MAPK et à la translocation dans le noyau du facteur de transcription NF-κB (Byrd-Leifer et al. 2001). La stimulation des cellules microgliales et des TAM, par les

récepteurs TLR4 et TLR3, déclenche une réponse tumorale cytotoxique et entraîne l'élimination des cellules de gliome résistantes (Kees et al. 2012; Mora et al. 2009). De plus dans notre étude précédente, nous avons démontré que l'activation via le récepteur TLR4 des macrophages, dans lesquels PC1/3 est inhibée, déclenchait la sécrétion de facteurs anti-tumoraux. Une inhibition de PC1/3, avec l'ajout d'une stimulation de différents TLR, pourrait donc représenter un nouveau type d'immunothérapie pour réactiver les macrophages et cellules microgliales intra-tumoraux.

Nous avons donc voulu savoir si nos macrophages PC1/3 knock-down répondaient de la même façon au taxol qu'au LPS, en nous intéressant à leur sécrétion cytokinique, aux voies de signalisation et à leurs activités anti-tumorales.

Résultats

Dans cette étude, nous avons cherché à savoir si le taxol pouvait induire une activation des macrophages PC1/3 knock-down, via le récepteur TLR4, et ainsi induire une réponse anti-tumorale. Dans notre étude précédente, nous avions stimulé les macrophages PC1/3 knock-down avec du LPS et observé une forte sécrétion cytokinique comparée aux cellules contrôles. Les facteurs sécrétés permettaient de recruter des lymphocytes T CD4+ et induisaient une diminution de viabilité de différentes lignées de cellules cancéreuses (cancers du sein et de l'ovaire).

Nous avons démontré que le taxol induisait, de la même façon que le LPS, l'activation de la voie NF-κB et la sécrétion de cytokines et chémokines pro-inflammatoires. De plus, la phosphorylation de STAT3 diminue dans les cellules PC1/3 KD et cette diminution est accentuée sous taxol dans les cellules KD et les cellules NT. Lorsque l'on active la voie STAT3 avec de l'IL10, la phosphorylation de STAT3 n'est pas induite dans les cellules PC1/3 KD. Il est connu que les TAM présentent un fort taux d'activation de la voie de signalisation STAT3. Ils permettent à la tumeur de progresser quand STAT3 est activé. L'activation de STAT3 dans le microenvironnement tumoral déclenche l'expression de médiateurs pro-tumoraux et de facteurs de croissance (Kortylewski et al. 2005; Kortylewski et al. 2009). L'inhibition de STAT3 dans les macrophages PC1/3 KD présente donc un fort intérêt pour la réactivation des TAM. STAT3 inhibe aussi l'expression de gènes induits par le facteur de transcription NF-κB. Or, nous avons observé ici que le facteur NF-κB était plus activé dans les macrophages PC1/3

KD. La signalisation déclenchée sous taxol entraîne la libération de chémokines et cytokines dont le pattern est différent de celui observé sous LPS. En effet, le taxol induit la sécrétion de chémokines dites GRO telles que les CXCL1, CXCL2 et CXCL3 et d'interleukines 1 (α et β). Cette sécrétion est plus abondante dans les cellules PC1/3 KD même lorsque l'on stimule les macrophages avec de l'IL10, qui est une cytokine inhibitrice de la sécrétion. Nous avons ensuite voulu évaluer l'effet des facteurs sécrétés sur la viabilité de trois lignées cellulaires de gliomes (U87, J3T et C6). Les sécrétomes des macrophages PC1/3 KD entraînent une diminution de viabilité des cellules de rat C6 par rapport au milieu contrôle. Des co-cultures de macrophages et sphéroïdes C6 dans une matrice de collagène ont montré que l'invasion des cellules cancéreuses est altérée quand les macrophages sont pré-activés avec le taxol, sans différence entre les macrophages NT ou KD. Par contre, l'analyse des sécrétomes obtenus à 6 jours de co-culture montre des différences. Les inhibiteurs de tumeurs Nqo1, ANP32A et le facteur de coagulation IX ont été détectés dans les sécrétomes des sphéroïdes en co-culture avec les macrophages PC1/3 KD pré-activés au taxol alors que les protéines qui supportent la croissance tumorale telles que les protéines Mortalin et SH3BGRL sont moins exprimées.

Nous avons également étudié l'impact intracellulaire du taxol sur les macrophages par des analyses protéomiques. Les protéines qui sont surexprimées dans les macrophages PC1/3 KD sont majoritairement impliquées dans la modulation du cytosquelette et l'homéostasie calcique. Ces résultats sont similaires à ceux observés lorsque les macrophages sont stimulés avec du LPS. De plus, des résultats d'imagerie calcique ont montré que le calcium intracellulaire augmentait fortement suite à la stimulation au taxol dans les cellules PC1/3 KD. En s'intéressant un peu plus aux protéines qui sont surexprimées suite à la stimulation avec le taxol, que ce soit dans les macrophages NT ou PC1/3 KD, on remarque qu'elles sont fortement impliquées dans le cytosquelette et l'organisation du réseau des filaments d'actine. Cela concorde avec l'effet du taxol sur la stabilisation des microtubules. Ensuite, nous avons déterminé quelles protéines étaient co-régulées avec les tubulines, qui sont les cibles primaires du taxol. De nombreuses protéines associées aux mitochondries sont co-régulées avec les tubulines dans les cellules NT et KD. Les protéines anti-inflammatoires IL1rn et Arg1 sont co-surexprimées avec les tubulines dans les cellules NT tandis que les protéines pro-inflammatoires Aif1, B2m, CD44, Sod1 et Calr sont co-surexprimées avec les tubulines dans les cellules PC1/3 KD. D'autres protéines surexprimées dans les macrophages PC1/3 KD et impliquées dans la réponse immunitaire sont les galectines 1 et 3 et la molécule CD36. Il a été démontré que des ligands de CD36 déclenchaient une réponse immunitaire stérile suite à

l'activation de l'hétérodimère TLR4-TLR6 (Stewart et al. 2010). Sous taxol, l'expression de la protéine CD36 est modulée différemment dans les cellules NT et PC1/3 KD, suggérant un rôle de CD36 dans l'activation du récepteur TLR4 sous taxol.

Notre étude a permis de démontrer que le taxol induisait, de la même façon que le LPS, l'activation de la voie NF-κB de façon plus importante dans les macrophages PC1/3 KD. Le taxol module le cytosquelette de ces cellules et leur état d'activation. Des chémokines et cytokines sont sécrétées de façon abondante par les cellules PC1/3 KD. Les sécrétomes des macrophages PC1/3 KD obtenus sous taxol diminuent la viabilité des cellules de gliome de rat C6 par rapport au milieu contrôle ne contenant que du taxol. Les études de co-culture en 3 dimensions montrent un effet significatif des macrophages pré-activés au taxol, sans différence entre les macrophages NT et KD. Les différences sont observées au niveau des facteurs sécrétés qui sont majoritairement anti-tumoraux dans la co-culture des sphéroïdes C6 avec les macrophages PC1/3 KD.

A novel treatment for glioblastoma based on Taxol activation of PC1/3-depleted macrophages: evidence from a proteomic and functional study.

Duhamel M[1], Murgoci A[1], Rodet F[1], Zografidou L[2], Régnier-Vigouroux A[2], Vanden Abeele F[3], Kobeissy F[4], Nataf S[5], Laurent Pays[5], Wisztorski M[1], Day R[6], Fournier I[1], Salzet M[1]**

[1] Inserm U-1192, Laboratoire de Protéomique, Réponse Inflammatoire, Spectrométrie de Masse (PRISM), Université Lille 1, Cité Scientifique, 59655 Villeneuve D'Ascq, France

[2] Zoology / Molecular Cell Biology, Johannes Gutenberg-Universität Mainz, Johann-Joachim-Becher-Weg 15, D-55128 Mainz

[3] Inserm U-1003, Equipe labellisée par la Ligue Nationale contre le cancer, Laboratory of Excellence, Ion Channels Science and Therapeutics, Université Lille 1, Cité Scientifique, 59655 Villeneuve d'Ascq, France

[4] Department of Biochemistry and Molecular Genetics, Faculty of Medicine, American University of Beirut.

[5] Inserm U-1060, CarMeN Laboratory, Banque de Tissus et de Cellules des Hospices Civils de Lyon, Université Lyon-1.

[6] Institut de Pharmacologie, Département de Chirurgie/Service d'Urologie, Faculté de Médecine et des Sciences de la Santé, Université de Sherbrooke, Sherbrooke, Canada.

** Corresponding author

ABSTRACT (120 words)

Tumor-associated macrophages contribute to tumor pathogenesis and represent an attractive therapeutic target. We report that the proprotein convertase PC1/3 inhibits the TLR4 Myd88-pathway induced in macrophages by the anti-cancer agent Taxol. Thus, PC1/3 knock-down in these cells exacerbates the TLR4 MyD88-dependent pathway triggered by Taxol. In PC1/3 knock-down macrophages, Taxol drives the secretion of pro-inflammatory cytokines, inhibits STAT3 signaling and counteracts tumor-supportive activities, thus inhibiting viability, growth and invasion of glioblastoma cells. Proteomic analyses indicate that their secretomes are characterized by a unique protein profile supporting a specific paracrine anti-tumoral effect. These findings unravel the potential value of a new therapeutic strategy combining PC1/3 inhibition and activation of the TLR4 MyD88-dependent pathway to switch intra-tumoral macrophages toward an anti-tumoral immunophenotype.

Significance (120 words)

Taxol stimulation of PC1/3 knock-down macrophages leads to the production of a unique set of soluble factors that exert pro-inflammatory activities and inhibit glioma viability, invasion and growth. The signaling pathway involved in such effect relies on the TLR4 MyD88-mediated translocation of NF-κB and STAT3 signaling inhibition. Viability tests performed with different glioma cell lines confirmed the sensitivity of these lines to Taxol. Invasion assay conducted in 3D spheroid culture confirmed the protective effect of macrophages, which was overridden by their pre-activation with Taxol. Taxol up-regulated proteins involved in microtubule cytoskeleton assembly and impacting the endosomal and phagosome movements. These results establish the possibility to combine Taxol with inhibition of PC1/3 in macrophages as a novel treatment for glioblastoma.

Highlights

- Taxol pre-activated macrophages inhibit glioma growth and viability
- Taxol activates the TLR4 MyD88-dependent pathway leading to inflammatory cytokines
- Taxol inhibits STAT3 signaling in PC1/3 knock-down macrophages
- Taxol impacts endosomal and phagosome movements of macrophages

Key words: Proprotein convertase PC1/3, Taxol, STAT3, TLR4 signaling, calcium, intracellular trafficking, macrophage, shotgun proteomic, tumors

INTRODUCTION

Cancer cells share eight common traits ("hallmarks") that govern their transformation from normal cells and their maintenance in the host environment: (1) they stimulate their own growth (self-sufficiency in growth signals), (2) they resist inhibitory signals that might otherwise stop their growth (insensitivity to anti-growth signals), (3) they resist their programmed cell death (evading apoptosis), (4) they can multiply indefinitely (limitless replicative potential), (5) they stimulate the growth of blood vessels to supply nutrients to tumors (sustained angiogenesis), (6) they invade local tissues and spread to distant sites (tissue invasion and metastasis), (7) they have abnormal metabolic pathways, and (8) they evade the immune system (1). This last-mentioned feature has radically changed our view on cancer pathophysiology by pointing the crucial instructing effects exerted by cancer cells on both local and systemic immune responses. Working towards new immunotherapeutic approaches for cancer is now considered as a priority task.

Among the many mechanisms that drive tumoral immune escape, tumor-associated macrophages (TAM) greatly contribute to promote resistance to immune responses. Indeed the local and systemic environments shaped by tumors suppress the anti-tumoral functions of macrophages (2, 3). Moreover TAMs do promote tumor growth and the correlation of a high number of TAMs with a low number of T cells in the tumor establishes a poor prognosis for cancer patients (4, 5). Expression of the chemokine CCL2 is correlated with TAM migration to the tumor, resulting in a higher number of TAMs (6). CSF-1 secreted by tumor cells is also a major tumor-derived factor that shapes TAM functional behavior. Indeed CSF-1 not only attracts TAMs (7) but induces a switch from a pro-inflammatory M1 into an anti-inflammatory M2 immunophenotype (8). Accordingly, elevated systemic or local levels of CSF-1 are associated with poor outcomes (7, 9, 10), and persisting elevated levels after treatment are indicators of recurrence of progression. Also, constitutive production of TNF from the tumor microenvironment is a characteristic of many malignant tumors, and the increased expression of TNF, a potent macrophage activator, is often associated with poor prognosis (11). Thus, TAMs play an important role in tumor growth and metastasis, which implies that the interaction between tumor cells and TAM provides an opportunity for cancer treatment.

Considering the above, we recently demonstrated in proprotein convertase PC1/3 knock-out mice (12), as well as in the pulmonary resident NR8383 rat macrophage PC1/3 knock-down (PC1/3-KD) cell line (13), that PC1/3-deficient macrophages produce high levels of cytokines and chemokines through autocrine and paracrine pathways. Challenging these cells with endotoxic/LPS results in a cytokine storm that impacts the cell survival of cancer cells (14). Indeed, PC1/3 protein regulates cytokines and chemokines secretion in macrophages and under LPS stimulation, the TLR4 MyD88-dependent signaling pathway is exacerbated in PC1/3-deficient macrophages which promotes a stable pro-inflammatory activated phenotype. Secreted factors from these PC1/3-KD macrophages not only attract naïve T helper cells but inhibit ovarian and breast cancer cell lines viability via innate immune mechanisms (14). However, achieving an activation of TAM via the LPS/TLR4/Myd88 pathway appears yet unfeasible in cancer patients. In this paper, we explored the possibility of using Taxol as a pro-inflammatory trigger that could induce TAM to engage an effective activation program under conditions of systemic PC1/3 inhibition.

Taxol has been widely used for the treatment of breast, ovarian, lung, and colon cancers (15). Taxol is an anti-neoplastic agent that stabilizes microtubules against depolymerization and blocks cells at the G2/M junction of the cell cycle. Although treatment with Taxol has led to improvement in the duration and quality of life for some cancer patients, the majority of Taxol-treated patients eventually develop drug resistance leading to disease progression (16). Besides its cytostatic and cytotoxic effects Taxol is endowed with immunomodulatory properties that may partly hamper its antitumoral effects (Javeed et al, 2009), Taxol stimulates tumor cells to secrete some chemo-attractant factors such as macrophage colony-stimulating factor 1 (CSF1) that promote immune evasion. Taxol is known to activate the TLR4 MyD88-dependent signaling pathway mimicking LPS action (17, 18) Nevertheless, Taxol is known to stabilize microtubules and to promote tumor resistance. We thus try to understand in our PC1/3-KD macrophage cell models in which microtubules network is disorganized, the impact of Taxol in term of intracellular signaling, trafficking and anti-tumor activities.

RESULTS

Proteomic study of PC1/3-KD cells under Taxol treatment

To better understand the intracellular impact of Taxol treatment on NT and KD macrophages, we performed proteomic analyses of cell lysates. From these results, we used the ANOVA test to perform a non a priori clustering of samples. Two clear clusters were highlighted. Cluster number 1 represents overexpressed proteins in PC1/3-KD cells, while cluster number 2 groups overexpressed proteins in NT cells (**Figure 1Aa, Suppl. data 1**). The proteins in each cluster were then analyzed using PANTHER software to determine the biological functions based on the protein classes. Using this analysis, we demonstrated that overexpressed proteins in PC1/3-KD cells, after Taxol treatment, included calcium binding proteins, extracellular matrix proteins, receptors, transporter proteins or cytoskeleton proteins, whereas in NT cells, overexpressed proteins were involved in enzymatic functions such as transferase, hydrolase, isomerase or oxidoreduction (**Figure 1Ab**). A String analysis of global pathways analyses (**Figure 1B**) established that overexpressed proteins under Taxol treatment in both NT or PC1/3-KD cells were involved in microtubule cytoskeleton assembly, actin organization, cell-cell adhesion and cell matrix adhesion modifications (**Figure 1Ba**). Proteins involved in cell differentiation were highly impacted (**Figure 1Bb**) as well as the ones involved in the immune response (**Figure 1Bc**). A deeper analysis taking into account proteins that are over- and underexpressed in NT and PC1/3-KD cells after Taxol treatment was performed (**Figure 1C, Suppl. data 2**). Data showed the underexpression of COP9 signalosome and AP-1 complex, which are known to play a role in protein sorting in the trans-Golgi network (TGN) and endosomes. Moreover, among the identified proteins, we found cytoplasmic dynein 1, which acts as a motor for the intracellular retrograde motility of vesicles and organelles along microtubules. Another interesting protein is fodrin, which seems to be involved in secretion. This protein interacts with calmodulin in a calcium-dependent manner and is thus a candidate for the calcium-dependent movement of the cytoskeleton at the membrane. The tandem HSP 90-beta and beclin 1 is involved in TLR mediated autophagy, and the Gamma-interferon-inducible lysosomal thiol reductase is involved in MHC class II-restricted antigen processing (19).

To complement these systematic biological approaches based on unsupervised clustering, we performed co-expression network analyses to identify molecules that, in Taxol-treated NT or KD cells, were co-upregulated with tubulins, the primary molecular targets of Taxol (20, 21) (**Figures 1Da and 1Db**). We chose

Tuba1c and Tuba4a proteins as query molecules because these 2 tubulins have shown the highest fold change among the 6 identified tubulins that were overexpressed in Taxol-treated cells (i.e., Tubb4b, Tubb2b, Tubb6, Tuba4a, Tuba1c, and Tuba1b; Table 2). We found that in both NT and KD cells, the Taxol-induced up-regulation of Tuba1ac and Tuba4a was accompanied by the co-upregulation of a highly significant number of mitochondria-related molecules (**Figure 1Db**). This result was in line with previous studies that demonstrated that Taxol targets mitochondria (22), possibly as a direct consequence of microtubule network alterations (23). Interestingly, we also observed that Tuba1ac/Tuba4a co-expression networks comprised immune-related molecules that, for some, were distinct when comparing Taxol-treated NT cells vs. Taxol-treated KD cells. In particular, these included the anti-inflammatory molecules IL1rn and Arg1 in Taxol-treated NT cells, while the pro-inflammatory molecules Aif1, B2m, CD44, Sod1 and Calr were co-upregulated with Tuba1ac/Tuba4a in Taxol-treated KD, but not Taxol-treated NT, cells (**Figure1Db**).

Further supervised proteomic data analyses were then performed in which samples were a priori grouped on the basis of PC1/3 deficiency (NT vs PC1/3-KD cells) and Taxol treatment (treated vs untreated cells) (**Figure 1Ea, Suppl. Data 3**). Eight specific clusters were identified. Cluster 1 was specific for overexpressed proteins under Taxol treatment in PC1/3-KD cells and cluster 3 for overexpressed proteins under Taxol in both cell lines. Cluster 2 was specific for PC1/3-KD cells whether they were treated or not. Cluster 6 represents proteins overexpressed in resting PC1/3-KD cells. We thus investigated, using systems biology analysis, network identification of the overexpressed proteins in PC1/3-KD cells after Taxol treatment or not using GeoSoftware corresponding to clusters 1 and 2 (**Figure 1Eb**). Differential pathways were generated using the “direct interaction” algorithm to map the relationships of the identified proteins. We found that among the 50 altered proteins, 35 proteins had direct regulatory relationships, including integrins (i.e., integrin beta 2 precursor, Protein Itgax, integrin alpha-5), cytoskeleton proteins (i.e., twinfilin, filamin-A, calponin 2, emerin, moesin, Alpha-actinin-4, gelsolin, lymphocyte specific 1, coronin 1c), and proteasomes (i.e., Proteasome subunit beta type-10; Proteasome activator complex subunit 2, WD repeat-containing protein and ionic channels (the voltage-gated potassium channel subunit beta-2 or the anoctamin-6) (**Figure 1Eb**). Anoctamin-6 (Ano6) produces large ion currents by stimulation of $P2X_7$ receptors and contributes to phagocytosis (24) and macrophage migration. Cell

migration requires constant depolymerization and repolymerization of the actin cytoskeleton, which permanently changes cell-matrix adhesions. In that context, Ano6 modulates Cl^- currents, which are under the control of the actin cytoskeleton associated with the signaling/scaffolding proteins ezrin, radixin, moesin and RhoA proteins (25). These proteins are known to connect plasma membrane proteins to the cytoskeleton. Moreover, it has recently been suggested that there is interaction of Ano6 with a number of proteins related to cell attachment and migration, such as zyxin, fibulin 1, S100A11, twinfilin and catenin, of which some have been identified in our proteomic study. Moreover, some specific proteins involved in the immune response were also overexpressed in PC1/3-KD macrophages, i.e., galectins (1 and 3), and CD36. Galectins have been identified as modulators of many monocyte/macrophage functions (26).

Taxol Signaling in NT and PC1/3-KD Macrophages

Taxol triggers CD36

Proteomic studies revealed that CD36 is overexpressed in PC1/3-KD cells upon Taxol challenge. Recently it has been shown that Taxol is a CD36 ligand and is promoting sterile inflammation through assembly of a Toll-like receptor 4 and 6 heterodimer (27, 28). We confirm by western blot study the modulation of CD36 by Taxol. According to the fold increases (**Figure 2A**) in Taxol-challenged vs. control cells, results obtained between PC1/3-KD and NT cells presents an opposite evolution. At 1h, in PC1/3-KD cells, the level of CD36 is the same between NT cells and KD cells. At 3h, it decreases in PC1/3-KD cells whereas it increases in NT cells. At 6h, CD36 increases in PC1/3-KD and decreases in NT cells but both get back at the same level that the one registered at 1h. To further confirm the involvement of CD36 in Taxol activation, we investigated whether its expression correlates with activation of the NF-κB signaling pathway.

Taxol leads to NF-κB activation in PC1/3-KD cells

To examine NF-κB activation in macrophages, we analyzed the degradation of IκB-α after Taxol treatment for 1, 3, or 6 h. According to the fold change (**Figure 2B**) in Taxol-challenged vs. control cells, the dynamics of IκB-α degradation and synthesis differed between the two types of cells under Taxol treatment. At 1h the

fold change was higher in PC1/3-KD cells compared to NT cells but without statistical difference. At 3h, this fold change dropped in PC1/3-KD cells whereas it increased in NT cells. At 6h, the level was identical in PC1/3-KD cells and NT cells. This demonstrates that in NT cells the level of NF-κB activation diminished from 1h to 3h whereas in PC1/3-KD cells, it increased from 1h to 3h. These kinetics of NF-κB activation correlate with the decrease of CD36 level in PC1/3-KD cells. In fact, the level of CD36 diminished from 1h to 3h and was back to the starting level at 6h, which could be explained by recruitment of CD36 between 1h and 3h and then its recycling from 3h to 6h that brings it back to the initial level.

Taxol acts as a signalosome by stimulating $[Ca^{2+}]c$

Considering the fact that NF-κB activation is linked to cytosolic calcium increases, we performed calcium imaging experiments using a fura-2AM calcium probe to evaluate the cytosolic calcium concentration ($[Ca^{2+}]c$) after Taxol treatment on NT and PC1/3-KD macrophages (**Figure 2C**). We demonstrated that Taxol (30 µM) rapidly induced a pronounced elevation of $[Ca^{2+}]c$ in KD cells compared to NT cells (**Figure 2Ca**). Quantification of these experiments is given in **Figure 2Cb**. We also observed that other features of calcium homeostasis were affected in KD NR8383 cells. Indeed, **Figures 2Cb and 2Cc** show that the resting $[Ca^{2+}]c$ levels were significantly increased in PC1/3-KD cells compared to NT cells. Thus, Taxol induced a higher increase of $[Ca^{2+}]c$ in PC1/3-KD cells compared to NT cells, which can act as signaling molecules. The Ca^{2+} signals can activate transcription factors such as nuclear factors of activated T cells (NFAT) or nuclear factor-κB (NF-κB).

Taxol decreases STAT3 phosphorylation

Several studies have demonstrated that inhibition of STAT3 leads to the activation of pro-inflammatory pathways such as the NF-κB signaling (29). A time course of the signal transducer and activator of transcription 3 (STAT3) phosphorylation was studied (**Figure 2D**). The level of the ratio of phosphorylated/total STAT3 was lower in PC1/3-KD compared to NT cells at any time point and in any condition. Following Taxol treatment, it dropped after 1h in PC1/3-KD cells and went back after 6h to the control level observed after 1h. IL-10 treatment, which is known to induce STAT3 phosphorylation, induced a similar

kinetics but a weaker effect than the one induced by Taxol. Taken together, these results clearly indicate that in PC1/3-KD cells, Taxol leads to the decrease of STAT3 phosphorylation resulting in the degradation of IκB-α and NF-κB activation (**Figure 2E**).

Taxol induces secretion of pro-inflammatory cytokines by PC1/3-KD cells

To place the macrophages under conditions similar to those in tumor environment, they were placed in an inhibitory medium, with the addition of the anti-inflammatory cytokine IL10, and then stimulated or not with Taxol (**Figure 3A**). In the absence of IL10, PC1/3-KD cells produced, as is already known, TNF-α, IL6, and CXCL10 (30). In the presence of IL10, TNF-α and CXCL10 are still produced by the PC1/3-KD cells, but in lower levels. However, in response to Taxol treatment, these molecules disappeared, whereas CXCL3 was secreted in PC1/3-KD cells. IL1β appeared after Taxol in non-targeted (NT) cells, but was present in a higher amount in PC1/3-KD cells, whereas in IL10 treatment, the amount was identical in NT and PC1/3-KD cells. For the other cytokines, the results were quite different. CXCL1 (CINC-1), CXCL2 (CINC-3), CCL3 and CCL5 were produced in both NT and PC1/3-KD cells in the control and under IL10 conditions as well as under Taxol stimulation. In PC1/3-KD cells, the amount of each of these chemokines was always higher compared to NT cells, regardless of the conditions. For CXCL1 and CXCL2, the amount in the controls was higher compared to the other conditions in PC1/3-KD cells. For CCL5, the amount is the same between control and Taxol treatment in PC1/3-KD cells. CCL3 cytokine showed the opposite behavior, i.e., its amount was higher under Taxol regardless of the presence of IL10 in PC1/3-KD cells. For the interleukin 1 family (i.e., IL1α, IL1β and IL1ra) some differences were registered. The amount of IL1α and IL1β was higher under Taxol stimulation in PC1/3-KD cells. The secretion of IL1ra was also higher under Taxol challenge but in NT cells, it was similar to that of soluble ICAM-1 factor (**Figure 3A**). Thus, it appears that the pro-inflammatory factors (i.e., IL6, TNFα and CXCL10), which are over-produced in KD-PC1/3 cells under LPS challenge, were inhibited by Taxol addition. In contrast, under Taxol challenge, the profile switched to secretion of GRO (α, β, γ) and interleukin 1 (α, β), which are attractive factors for Polymorphonuclear leukocyte (PMN) cells and which are over-produced in PC1/3-KD cells. In contrast, the inhibitory factors (i.e.,

Il1ra and sICAM 1) were only over-produced in NT cells under Taxol stimulation. In the presence of IL10, the secretion of the PC1/3- KD cells was nearly not affected. The same pattern was observed as the one registered with Taxol. This suggests that these PC1/3-KD cells were more resistant to the inhibitory effects of IL10.

Taxol activated macrophages produce tumor viability inhibitor factors

Tumor viability tests on different glioma cell lines (rat C6, canine J3T, human U87 cells) were performed with the secretome of cells treated with Taxol for 24h (**Figures 3B, 3C & 3D**). Controls are medium alone or medium with Taxol. Viability tests were performed during 24h, 48h, 72h and 96h. The time point 96h+medium means that the medium was renewed at 72h and the viability of cancer cells was registered 24h latter.

For C6 glioma cell line (**Figure 3Ba**), differences were registered at 48h and 72h between PC1/3-KD cells secreted factors and control medium with Taxol. The viability of the C6 glioma is decreased by 19% at 48h and 24% at 72h between PC1/3-KD treated cells and the medium with Taxol and 35% at 48h and 43% at 72h with control medium without Taxol. Anova test reveals significant differences between KD Taxol secretomes and medium with Taxol alone and KD control secretomes and medium alone (**Figure 3Bb**) which is not observed for NT cells secretomes. A decrease of viability of C6 glioma cells is observed over time with a more striking difference between 24h and 96h for KD cells secretomes (**Figure 3Bb**). Nevertheless, no significant differences are observed between NT and PC1/3-KD cells.

For J3T glioma cell line (**Figure 3Ca**), Taxol cytotoxicity is registered whatever the time considered for both conditions *i.e.* cells incubated with Taxol in medium (direct effect) or cells incubated with the secretomes of Taxol-activated NT or PC1/3-KD cells. At 24h, we can observe a decrease of viability of 36% between cells treated with Taxol or secretomes and control cells. At 48h, 72h, 96h and 96h+medium, the decrease is 67%, 59%, 54% and 65% respectively. It is thus difficult to distinguish the intrinsic effect of the secreted factors from Taxol activated macrophages and the one from Taxol itself. Anova test showed a significant difference between 24h and 96h for KD cells secretomes only (**Figure 3Cb**).

For U87 glioma cell line (**Figure 3Da**), as observed with the J3T cells, Taxol is directly active towards the glioma cells. Taxol alone is more active than secretomes

obtained from NT and KD macrophages stimulated with Taxol. At 96h, we can observe a decrease of viability of 51% of cells treated with Taxol or secretomes compare to control untreated cells. At 48h and 72h, factors secreted from NT cells are 26% more active towards the U87 glioma cells than the one secreted from PC1/3-KD cells. With Anova test we can observe a significant difference, for KD cells secretomes, between 96h + medium and all the other time points (**Figure 3Db**).

For each of these three cancer cell lines, Taxol treatment has an effect. For C6 rat glioma cells, factors secreted by KD cells have a higher impact on their viability, compared to NT cells secreted-factors and to Taxol alone. For J3T dog glioma cells, it is difficult to distinguish the effects from Taxol alone and factors secreted by macrophages. For U87 human glioma cells, the most important effect of KD factors, is observed when we renew the medium (condition 96h+medium) meaning that cancer cells may have been sensitized during the previous time points. Such differences observed between these three glioma cell lines may be explained by the fact that they belong to three different organisms. Thus, the factors secreted by our rat macrophages may be less efficient on other organisms.

To validate our results, we performed co-culture of macrophages and C6 rat glioma cells spheroids.

Taxol triggers the secretion of anti-glioblastoma factors by PC1/3-KD cells

The impact of Taxol treatment in a direct co-culture of macrophages and glioblastoma cells was investigated using a 3D culture system. Spheroids generated with C6 rat glioma cells were co-cultured for 6 days in a collagen matrix containing untreated or Taxol-treated macrophages (NT or PC1/3-KD cells). The growth of the spheroids and the invasion of the matrix by cells migrating out the initial core were monitored over 6 days. As shown in **Figure 4Aa**, neither the NT nor the KD cells present in the collagen impaired the growth and invasion of the spheroids, an observation in line with their reported tumour-supportive effects. Addition to the co-cultures of Taxol at 30 µM (i.e. the concentration used to induce the pro-inflammatory secretome) led to a complete growth and invasion arrest of the spheroids, irrespective of the presence or absence of the macrophages (data not shown). This indicated a strong inhibitory effect of Taxol on both C6 spheroids and macrophages. By contrast, when the macrophages (NT or PC1/3-KD cells) were pre-activated by 30

µM Taxol before their embedding in collagen, tumour growth and invasion was inhibited (**Figure 4Ab).** Quantification of the growth and invasion rate confirmed that pre-activated NT and KD cells exerted a similar inhibitory effect (**Figure 4Ac**).

Interestingly, time course analyses of the secretomes of these co-cultures indicated clear differences in their composition according to the presence of Taxol pre-activated NT or PC1/3-KD cells in the collagen matrix (**Figure 4B**). At day 6, i.e. after 6 days of co-culture of macrophages and C6 spheroids, secretomes were collected and analysed by LC-MS/MS. Only 5 unique proteins are detected in spheroids secretomes with PC1/3-KD cells and 10 proteins in spheroids secretomes with NT cells (**Figures 4Ba, Table2**). These proteins are mostly related to tumor suppression (**Table 2**). For example, the NAD(P)H dehydrogenase [quinone] 1 (Nqo1) is known to stabilize the *tumor* suppressor gene p53 and inhibits its degradation. It is also involved in metabolism of Vitamin K known to be a highly potent inhibitor of glioma cell growth (31). We recently shown that PC1/3-KD macrophage contain and can produce through exosomes Nqo1 (14). Similarly the acidic leucine-rich nuclear phosphoprotein 32 family member A (ANP32A, pp32) is also produced in macrophages exosomes during inflammation (32). ANP32A has been shown to inhibit pancreatic cancer cells survival by disrupting human antigen R (HuR) binding to target mRNAs encoding key proteins for cancer cell survival and drug efficacy (33). Coagulation factor IX (F9) is known to regulate carcinoma migration (34). Beside these factors involved in tumor suppression, the secretome contained Rac1, which is described as a major player in glioma invasion and progression (35) and myosin light polypeptide 6 (Myl6), which is found in glioblastoma exosomes (36). For secretomes obtained from spheroids in co-culture with NT macrophages, 10 unique proteins are detected (**Figure 4Ba, Table 2**). Among them, we can find Ezrin which is an actin-binding protein involved in several cellular functions such as cell adhesion and migration. Ezrin has been associated with tumor invasion and increase malignancy of astrocytic tumors (37, 38). Sorcin protein is a calcium binding protein involved in the resistance to chemotherapeutics in cancer cells and is overexpressed in various cancer cells ((39). LRP1 protein is also over-represented. Activation of LRP1 allows the initiation and maintenance of AKT signaling, contributing to the aggressiveness of glioblastoma (40). C1QBP protein is up-regulated by Myc in malignant brain tumors. Inhibition of C1QBP in glioma cell lines impaired cell proliferation *in vitro* (41). NPM1 protein is also up-regulated in high

grade glioma and its depletion leads to a higher apoptosis when cancer cell are exposed to actinomycin D (42)**.** We also found 2 proteins which are overexpressed in secretomes obtained from NT cells co-culture compared to secretomes obtained from KD cells secretomes co-culture (**Figure 4Bb**). These proteins are Mortalin (HSPA9) and SH3 domain-binding glutamic acid-rich-like protein 3 (Sh3bgrl). Both are underexpressed in PC1/3-KD secretomes co-culture. These proteins are known to be involved in cancer progression. Mortalin interacts with tumor suppressor protein-p53 (both wild and mutant types), inactivates its transcriptional activation and shares apoptotic functions in cancer cells (43). SH3BGRL functions as a c-Src activator and metastasis promoter in mice and tumor suppressive in human (44).

Taken together, we have established that PC1/3-KD cells and NT cells challenged with Taxol produce a distinct set of factors that, together with factors secreted by glioma cells, similarly impact the growth of C6 glioma cells spheroids and their invasion. In the case of the co-culture of spheroids with PC1/3-KD cells, the profile of secreted factors suggests a possible scenario whereby these factors stabilize P53, inhibit its degradation through Nqo1 and inhibit cancer cell survival, facilitate drug efficacy due to ANP32A production and blocks tumor migration through Coagulation factor IX combined to immune factors. In contrast, unique proteins found in secretomes from the co-culture of NT cells and glioma spheroid, are mainly involved in cancer cells proliferation and aggressiveness.

DISCUSSION

Since the last decade, many studies have demonstrated that the density of TAMs is associated with a poor prognosis, suggesting macrophages as a target for clinical therapy (45-51). Macrophages can be activated through the cytokines and other small molecules and a secondary signal is supplied by either antibody or LPS/endotoxin/TLR stimulants. Both of the signals can activate macrophage mediated tumor cytotoxicity (MTC) and can withstand the immunosuppressive activities of tumor cells (52-55) . Thus, new therapeutic strategies have been elaborated to counteract tumour outgrowth by inhibiting macrophages infiltration, or promoting M2 to M1 conversion in TAM (45). In this context, several studies reporting the use of “anti-macrophage” approaches have primarily focused on counteracting monocyte chemokines and receptors as anticancer targets (56-65) . As M1

macrophages induce an effective pro-inflammatory anti-tumoral response, converting the M2 pro-tumoral phenotype of TAMs into a M1 anti-tumoral one represents an attractive alternative to the “anti-macrophage” approaches. This can be realized by reprogramming in vitro macrophage phenotype switching, e.g. through activation of TLRs. In a mouse model, CpG, a TLR9 ligand, combined with anti-interleukin-10 receptor antibody, promptly switched infiltrating macrophages from M2 to M1 and triggered innate response towards large tumors (66). Strategies targeting TLR4 signalling pathway have also shown some success in anti-tumoral activity (67, 68). In addition, accumulating studies report using macrophages as natural vectors to deliver therapeutic molecules to the neoplastic sites such as Taxol treatment (47). Taxol stimulates macrophages to express high levels of NO, TNF-α, and IL-1β. Through the increased levels of these substances, Taxol can enhance tumor cell cytotoxicity and restore IL-12 production by macrophages in tumor-bearing mice (47). Taxol has been widely used for the treatment of breast, ovarian, lung, and colon cancers (15). More recently different strategies based on liposomes or nanoparticles with Taxol have been investigated in brain glioma (69-72). However, Taxol induces drug resistance (16). Based on such knowledge, in this work, we investigated the possibility to trigger the macrophage mediated tumor cytotoxicity based on a TLR4 activation using Taxol drug as ligand. Our previous data obtained on PC1/3-KO mice and PC1/3-KD NR8383 macrophage cell lines showed their ability to produce pro-inflammatory cytokines in autocrine and paracrine ways (12, 13). Under endotoxin/LPS challenge, these cells produce a high amount of pro-inflammatory cytokines such like TNF-α, IL6, and CXCL10. The secreted factors attract naïve T helper cells and orientate the immune response to the cytotoxic Th1 immune response (14). Moreover, these cells also produce danger signal molecules impacting viability of cancer cell lines *in vitro* such as the SKOV3 ovarian and SKBR3 breast cancer cell lines (14). In that context, we show in the present report that Taxol activates NF-κB pathway like LPS does. A more intense and quicker degradation of IκB-α is observed at 3h in PC1/3-KD cells, indicating an increased NF-κB activation. Same observations can be made for the decrease in STAT3 phosphorylation. This activation leads to the production of pro-inflammatory cytokines but with a different profile than that observed for LPS. In PC1/3-KD cell, Taxol stimulates the secretion of growth related oncogene (GRO) (α, β, γ) and interleukin 1 (α, β), which are known to elicit recruitment of PMN cells. GRO

(α, β, γ), also known as chemokines (CXCL1, CXCL2, CXCL3) mediates varied functions, such as attracting neutrophils to sites of inflammation, regulating angiogenesis, and modulating neurotransmitter release but in cancer, they are involved in tumor initiation, progression, and metastasis (73, 74). For example, GRO-β forms an autocrine loop that activates the Ras-Erk1/2 signaling pathway (75) which is linked to phosphorylation of STAT3 (76) signal transducer activator of transcription which is important for cell proliferation. STAT3 is an important molecule that mediates tumor-induced immuno-suppression (77). Interestingly, we observed that PC1/3-KD cells present a decreased level of phosphorylated STAT3 compared to NT cells, indicating a higher level of inhibition of STAT3 signaling. Taxol treatment further enhanced this decrease in both macrophages lines. Such a decrease would be expected to result in an increased resistance of PC1/3-KD cells towards the inhibitory effect of IL10. Taxol is known to inhibit STAT3 signaling (30, 78, 79), which is also the case in PC1/3-KD cells but here the effect is amplified. Concomitant to the effect of Taxol on NF-kB activation, STAT3 decreased phosphorylation and release of pro-inflammatory cytokines, we observed a decrease in the viability of 3 glioma cell lines exposed to the secretomes of Taxol-treated macrophages. This anti-tumor activity was further evidenced in co-cultures of spheroids of C6 glioma cells and macrophages. Growth of spheroids and cell invasion in the matrix were severely halted when the macrophages were pre-activated with Taxol. We could identify unique proteins in the secretome of the co-cultures that may contribute to these inhibitory activities. For instance, tumor inhibitors like Nqo1, ANP32A, Coagulation factor IX were detected in the secretome of C6 glioma spheroids co-cultured with Taxol pretreated PC1/3 cells which showed as well as lower expression of tumor supportive proteins such as Mortalin or SH3BGRL. The mechanism by which Taxol induces such activities was investigated. We establish that in contrary to classically activated macrophages, in PC1/3-KD macrophages, Taxol up-regulates proteins involved in microtubule cytoskeleton assembly, actin organization, cell-cell adhesion and cell matrix adhesion modifications. The overexpression of cytoskeleton proteins is expected to impact the endosomal and phagosome movements (80, 81), which would also lead to a higher secretion of immune factors. This is in line with the presence of 6 overexpressed proteins *i.e.* the natural resistance-associated macrophage protein 1 [Nramp1], intercellular adhesion molecule 1 [ICAM 1], Talin 1 [Tln1], Solute carrier family 2 [Slc2], Sequestosome-1 [Sqstm1], Integrin beta-1

[Itg1b]) which are implicated in TLR signaling. In fact, Sqstm1 is associated with Traf6, which is linked to TLR4, TLR2, TLR9 and IL1R (82, 83). Nramp1 modulates p38 MAPK and PKCζ activity in TLR7 activation (84). TLR2 or TLR5 ligation rapidly activated integrin-dependent leukocyte adhesion (integrin beta-1 or beta 2) to immobilized ICAM-1, fibronectin and Talin1 (85-87). A supervised clustering analysis using Nramp1, ICAM1, Tln1, Slc2, Sqstm1 and Itgb1 as query molecules, indicated that these proteins belonged to a shared subnetwork that was significantly enriched in molecules coded by genes annotated with the GO term «extravesicular exosome ».

Taken together, these data clearly show that Taxol treatment in macrophages favors lysosomal and multivesicular body trafficking, diminishes TLR4 autophagy, and increases constitutive secretion and endosomal sorting through AP-1 complex inhibition. Taxol activates the TLR4 Myd88-dependant pathway through modulation of CD36 and leads to IKB-α degradation, increase of the cytosolic calcium concentration ([Ca^{2+}]c. Taxol also diminishes STAT3 phosphorylation and reveals a potential of the co-action of PC1/3 inhibition and Taxol treatment in macrophage for glioma therapy. As expected from previous observations with murine microglia and human tumor-associated microglia/macrophages (88, 89), untreated rat macrophages supported the growth and invasion of tumor cells from the spheroids. These supportive activities were suppressed by a pre-treatment with Taxol, which triggered an efficient anti-tumor response borne by macrophage-secreted factors. We did not observe a difference in the inhibitory effects of NT and KD cells in the spheroids co-culture and viability tests on 2D culture, although these cells induced a distinct pattern of proteins secreted during the co-culture with C6 spheroids. Further experiments are needed to explain these observations, which might be linked to problems of macrophage motility in collagen and/or cell death triggered by the TLR activation. Nevertheless, the invasion assays in complement to proteomic analyses of the secretomes of C6 spheroids cultured with Taxol pre-activated NT or PC1/3-KD cells, demonstrate that PC1/3 cells secrete factors active towards C6 glioma.

To conclude, these experimental observations lay the basis for a cell therapy targeting macrophages, based on their activation by Taxol and inhibition of the PC1/3 expression. The next step will be the development of a specific PC1/3 inhibitor that can be used in conjunction withTLR4 activation. This is part of the strategy we would

like to develop and that we call the Trojan macrophage therapy based on PC1/3 inhibited macrophages (90).

Author information

Contributions

MS, MD have written the paper

MD, FR, MW, FVA, ND, FK, DC, LZ have done the experiments

MS, IF, have got financial support to the project and corrected the manuscript

All authors have reviewed the manuscript

Competing financial interests

The authors declare no Competing Financial Interests

Corresponding author

Pr Michel Salzet, U-1192 Inserm, Laboratoire de Protéomique, Réponse Inflammatoire, Spectrométrie de Masse (PRISM), Université de Lille 1, Cité Scientifique, 59655 Villeneuve D'Ascq, France. Email: **michel.salzet@univ-lille1.fr,**

Acknowledgements

This research was supported by grants from the Ministère de L'Education Nationale, de L'Enseignement Supérieur et de la Recherche, ANR (IF), Région Nord-Pas de Calais ARCIR (IF), the Université de Lille (MD) SIRIC ONCOLille (IF, MD), Grant INCa-DGOS-Inserm 6041aa, the CCMIC and INSERM.

MATERIALS AND METHODS

Reagents. The rat alveolar macrophage NR8383 cell line (CRL-2192) and the U87 cell line (HTB-14) were obtained from ATCC (USA). The rat C6 glioma cell line was kindly provided by Prof. Dr. Bernd Kaina (Institute of Toxicology, University Medical Center, Mainz, Germany). The canine J3T glioma was kindly provided by Professor Berens (Translational Genomics Research Institute (TGen), Phoenix, USA). Paclitaxel (Taxol) was obtained from Sigma. Polyclonal rabbit anti-CD36 (NB400-144) was obtained from NOVUS Biologicals (Cambridge, UK). We obtained

secondary antibodies Alexa Fluor® 488 donkey anti-rabbit and Alexa Fluor® 546 goat anti-mouse from Molecular Probes (Interchim, France). Ham's F12K, puromycin, phosphate buffer saline (PBS), fetal bovine serum (FBS) were obtained from Invitrogen Life Technologies (Milan, Italy). LysC/Trypsin was obtained from Promega (USA). Antibodies against IκBα and phospho-STAT3 were obtained from CellSignaling Technology. Nitrocellulose membrane and Bio-Rad Protein Assay were obtained from Bio-Rad (Marnes La Coquette, France). SuperSignal West Dura Chemiluminescent substrate was obtained from Thermo Scientific. Peroxydase-conjugated secondary antibodies were obtained from Jackson ImmunoResearch (West Grove, PA, USA). Rat Cytokine Array Panel A was obtained from R&D Systems (Minneapolis, MN, USA). The CellTiter-Glo assay was purchased from Promega (Southampton, UK).

Culture of the NR8383 cell line. The rat alveolar NR8383 wild type (WT) macrophages were cultured with Ham's F12K medium supplemented with 15% fetal bovine serum. NR8383 PC1/3 knockdown (KD) and NR8383 non-target (NT) shRNA cell lines were cultured in Ham's F12K medium supplemented with 15% fetal bovine serum and 12 µg/ml puromycin at 37°C in a humidified atmosphere (5% CO_2). NR8383 PC1/3 knockdown was performed using lentivirus transduction, as described previously (13).

Culture of C6, J3T and U87, cell lines. C6 cells were cultured in high-glucose Dulbecco's Modified Eagle's Medium (DMEM) and supplemented with 10% heat-inactivated fetal calf serum (FCS), 1% L-glutamine (2 mM) and 1% gentamicin (50 units per ml), all from Sigma-Aldrich. This medium is referred to as complete DMEM (cDMEM). The FCS concentration was reduced to 5% in medium used for the co-culture experiments (c-DMEM-5). J3T and U87 were cultured in Dulbecco's Modified Eagle's Medium (DMEM) and supplemented with 10% heat inactivated fetal bovine serum (FBS), 1% L-glutamine (2mM) and 1% penicillin-streptomycin all from Life Technologies. Cells were maintained in standard culture conditions (37 °C in humidified air with 5% CO2).

Spheroid generation and embedding in a collagen matrix. C6 rat glioma cells were resupended in cDMEM at the final concentration of 12500 cells in 200 µl. Cells (200 µl per well) were distributed in flat 96-well low attachment surface plates (Corning®). Plates were incubated at standard culture conditions for 96 h. The newly formed C6 cell spheroids were then implanted in the center of each well of a 24-well plate coated with a 2.2 mg/ml collagen mixture (one spheroid per well in 400 µl of collagen mixture per well). The collagen mixture was prepared by mixing 2 ml of PureCol® bovine collagen type I solution (3 mg/ml; Advanced BioMatrix) with 250 µl of 10X minimal essential medium (MEM) (Sigma-Aldrich) and 500 µl of sodium hydroxide 0.1 M. After cell spheroid embedding, the plate was incubated for 30 min at standard culture conditions to solidify the gels. Thereafter 400 µl of cDMEM was overlaid on the collagen matrix in each well. The complete system was incubated for a total of 6 days (91).

Co-culture of Taxol pre-treated macrophages and C6 spheroids. For co-culture experiments, PC1/3-KD and NT cell lines were grown in cDMEM containing 15% FCS and complemented with 12 µg/ml puromycin. Taxol was dissolved in DMSO at a concentration of 30mM. Following trypsinisation, 800.000 cells were seeded in a T25 flask and treated for 24 h with 30 µM Taxol in cDMEM-5 with 12 µg/ml puromycin or with the corresponding volume of DMSO (control, untreated macrophages). The cells were trypsinised, resuspended in MEM 10X and mixed with components of the collagen mixture as described above. The collagen mixture containing macrophages was distributed in 24-well plates (400 µl / 100.000 macrophages per well) for embedding of C6 spheroids as described above. Supernatants of all conditions were collected at the end of the co-culture, immediately frozen and stored at – 80°C for further proteome analysis (secretome day 6).

Quantification of spheroid size and invaded area. After the spheroids were embedded, cell invasion out of the spheroid was monitored by digital photography using a Leica® DM IL LED Fluo inverted light microscope (Leica® DFC450C camera) at room temperature, with the Leica Application Suite (LAS V4.4). Images were acquired every day (day 0 = time of embedding in collagen; picture taken immediately after embedding) using a 4x/0.10 objective. Image processing and quantification of spheroids and of invasion areas was performed using an in-house

software. This in-house software takes into account cell density and not the (observer-dependent) limits of cell migration in the collagen matrix. The implemented algorithm uses local fluctuations of the image intensity for an automated estimation of the invasion magnitude. It is robust enough to handle micrographs of different generation methods and various qualities without the concept of an invasive front of the spheroids (Cisneros et al., 2016). Invasion and spheroid areas are normalized for each day to the invasion and spheroid areas measured at day 0 and expressed in protocol defined units (PDU). These normalized data are reported as relative size to day zero. Relative size of day 0 thus equals 1.

Cell viability measured by the CellTiter-Glo assay. J3T, U87 and C6 cells were seeded into 96-well white plates at 70% confluence with NR8383 secretomes obtained after 24 h of Taxol (30 µM) stimulation or no stimulation. The assay was conducted for 24, 48, 72 or 96 h. For the 96h + medium, conditioned secretomes were removed at 72 h and replaced with fresh ones. CellTiter 96® AQ_{ueous} One Solution Cell Proliferation reagent (Promega) was added to the wells and incubated at 37°C for 1 hour protected from light. The absorbance was recorded at 490 nm using a 96-well plate reader. The results are expressed either as absorbance or as the fold change of each conditions compared to control. For U87, CellTiter Glo reagent (Promega) was added to the wells and incubated at room temperature for 10 min protected from light. The luminescence was recorded using a Berthold luminometer Centro LB960. The results are either expressed as relative light units (RLU) or as fold change of each condition compared to control.

Identification of cytokines and chemokines using rat cytokine antibody arrays. NR8383 KD and NT cells were plated on sterile 6-well plates to reach confluence. The cells were starved overnight with Ham's F12K medium supplemented with 2% FBS and stimulated for 24 h with 20 ng/ml IL-10 in serum-free medium or were left untreated. Then, the medium was replaced, and the cells were stimulated for 24 h with 30µM Taxol or were left untreated. Cell supernatants were collected, centrifuged at 500 g, passed through a 0.22 µm filter to remove cells and immediately frozen in liquid nitrogen. The Rat Cytokine Array Panel A from the R&D system was used to probe cytokines in the secretome of stimulated and unstimulated NR8383 cells by following the procedures recommended by the manufacturer. Briefly, the array

membranes were first incubated in the blocking buffer for 1 hour. In the meantime, secretomes were mixed with the Detection Antibody Cocktail and incubated for 1 hour at room temperature. The volume of secretome used for this experiment was determined according to the number of cells counted after stimulation. Then, after removing the blocking buffer, the sample/antibody mixture was added to array membranes and incubated overnight at 4°C. After incubation, the membranes were washed 3 times with the wash buffer and then incubated with the Streptavidin-HRP solution for 30 min at room temperature. The membranes were finally washed with wash buffer 3 times, and the bound antibodies were detected by chemoluminescence using the Chemi Reagent Mix. The membranes were quantified by densitometry using ImageJ software. Statistical analysis was carried out using a paired *t* test.

Total protein extractions. NR8383 KD and NT cells were plated on sterile 6-well plates to reach confluence. For Taxol stimulation, the cells were starved overnight with Ham's F12K medium supplemented with 2% FBS. The cells were stimulated with 30 µM Taxol in serum-free medium or left untreated. At 24 hours, cells were collected, washed once with ice-cold PBS and then lysed with RIPA buffer for total protein extraction (150 mM NaCl, 50 mM Tris, 5 mM EGTA, 2 mM EDTA, 100 mM NaF, 10 mM sodium pyrophosphate, 1% NP40, 1 mM PMSF, and 1X proteases inhibitors). Cells debris were removed by centrifugation (20,000 g, 10 min, 4°C), and supernatants were collected and protein concentrations were measured using a Bio-Rad Protein Assay according to the manufacturer's instructions.

Western Blot Analysis*.* Total cell extracts (40 µg) were then analyzed by Western blot assays. First, proteins were separated by SDS-PAGE electrophoresis and then transferred on to a nitrocellulose membrane. Membranes were blocked for 1 hour at room temperature in TBS-Tween 0.1% + milk 5% and incubated overnight at 4°C with primary antibodies directed against mouse anti-IκB-α (1:1000, from Cell Signaling Technology, Leiden, The Netherlands), rabbit anti-CD36 antibody (1:1000, from Novus Biologicals), rabbit anti-phospho STAT3 (1:2000, from Cell Signalling), rabbit anti-STAT3 (1:1000, from Cell Signaling) and rabbit anti-actin (1:400, from Thermo-Fisher). Horseradish peroxidase-coupled goat anti-mouse and goat anti-rabbit secondaries (Jackson ImmunoResearch) were used at 1:30000 and 1:20000 respectively. The proteins were visualized with the enhanced chemiluminescence kit

(West Dura from Pierce) according to the manufacturer's instructions. ImageJ software was used to quantify the bands.

Filter-aided Sample Preparation (FASP). Total protein extract (0.1 mg) was used for FASP analysis as described previously We performed FASP using Microcon devices YM-30 (Millipore) before adding trypsin (Promega) for protein digestion (40 µg/ml in 0.05 MNH4HCO3). The samples were incubated overnight at 37°C. The digests were collected by centrifugation, and the filter device was rinsed with 50 µl of NaCl 0.5 M. Next, 5%TFA was added to the digests, and the peptides were desalted with a Millipore ZipTip device before LC-MS/MS analysis (14).

Proteomics analysis of secretomes. Secretomes obtained from spheroids were centrifuged at 500 g and passed through a 0.22-µm filter to remove cells and debris. The experiments were performed in biological triplicates. Four hundred microliters of the secretome was collected for each condition. The volume was reduced to 100 µl in a SpeedVac. Secretome digestion was performed as previously described (92). In brief, the cell supernatants were denatured with 2 M urea in 10 mM HEPES, pH 8.0 by sonication on ice. The proteins were reduced with 10 mM DTT for 40 min followed by alkylation with 55 mM iodoacetamide for 40 min in the dark. The iodoacetamide was quenched with 100 mM thiourea. The proteins were digested with 1 µg LysC/Trypsin mixture (Promega) overnight at 37°C. The digestion was stopped with 0.5% TFA. The peptides were desalted with a Millipore ZipTip device in a final volume of 20 µl of 80% ACN elution solution. The solution was then dried using the SpeedVac. Dried samples were solubilized in water/0.1% formic acid before LC MS/MS analysis.

LC MS/MS analysis. Samples were separated by online reversed-phase chromatography using a Thermo Scientific Proxeon Easy-nLC system equipped with a Proxeon trap column (100 µm ID x 2 cm, Thermo Scientific) and a C18 packed-tip column (75 µm ID x 50 cm, Thermo Scientific). Peptides were separated using an increasing amount of acetonitrile (5–35% for 100 min) at a flow rate of 300 nL/min. The LC eluent was electrosprayed directly from the analytical column, and a voltage of 1.7 kV was applied via the liquid junction of the nanospray source. The chromatography system was coupled with a Thermo Scientific Q Exactive mass

spectrometer programmed to acquire a data dependent Top 10 method. Survey scans were acquired at a resolution of 70 000 at m/z 400.

Data analyses. All the MS data were processed with MaxQuant (93) using the Andromeda (94) search engine. Proteins were identified by searching MS and MS/MS data against Decoy version of the complete proteome for *Rattus norvegicus* of the UniProt database (95) (Release June 2014, 33,675 entries) combined with 262 commonly detected contaminants. Trypsin specificity was used for the digestion mode with N-terminal acetylation and methionine oxidation selected as the variable. Carbarmidomethylation of cysteines was set as a fixed modification, and we allowed up to two missed cleavages. For MS spectra, an initial mass accuracy of 6 ppm was selected, and the MS/MS tolerance was set to 20 ppm for HCD data. For identification, the FDR at the peptide spectrum matches (PSMs) and protein level was set to 0.01. Relative, label-free quantification of proteins was performed using the MaxLFQ algorithm (96) integrated into MaxQuant with the default parameters. The data sets and the Perseus result files used for analysis were deposited at the ProteomeXchange Consortium *(97)* (http://proteomecentral.proteomexchange.org) via the PRIDE partner repository *(98)* with the dataset identifier PXD001984 for cellular extracts. Analysis of the proteins identified was performed using Perseus software (http://www.perseus-framework.org/) (version 1.5.0.31). The file containing the information from identification was used with hits to the reverse database, and proteins only identified with modified peptides and potential contaminants were removed. Then, the LFQ intensity was logarithmized (log2[x]). Categorical annotation of rows was used to define different groups depending on the following: 1) the cell line (NT or KD), 2) the treatment (Control/Taxol). Multiple-samples tests were performed using an ANOVA test with a FDR of 5% and preserved grouping in randomization. To determine enrichment of categorical annotations (Gene Ontology terms and KEGG pathway), a Fisher's exact test was used, taking in account the results of the ANOVA test for each group. Normalization was achieved using a Z-score with matrix access by rows. Only proteins presenting as significant by the ANOVA tests were used for statistical analysis. A hierarchical clustering was first performed using the Euclidean parameter for distance calculation and an average option for linkage in row and column trees using a maximum of 300 clusters. To quantify fold changes of proteins across samples, we used MaxLFQ. To visualize

these fold changes in the context of individual protein abundances in the proteome, we projected them onto the summed peptide intensities normalized by the number of theoretically observable peptides. Functional annotation and characterization of identified proteins were obtained using PANTHER software (version 9.0, http://www.pantherdb.org) and STRING (version 9.1, http://string-db.org). The GeneMANIA Cytoscape plugin (99) was used to generate 2 distinct co-expression networks from cell extract proteomics data: i) a « Taxol-treated NT cells » network composed of 99,556 recognized interactions, generated from the analysis of a data subset gathering control NT cells and Taxol-treated NT cells and iii) a « Taxol-treated KD cells » network composed of 86,780 recognized interactions, generated from the analysis of a data subset gathering control KD cells and Taxol-treated KD cells. A supervised clustering was then performed to identify the top 100 molecules that co-regulated with the following query molecules: Itgb1/Slc2a1/Icam1/SQSTM1 or Tuba1c/Tuba4a. The list of 100 genes that encoded molecules was identified and was then assessed for gene set enrichment using EnrichR (100) and the GO classification. Finally, subnetworks of genes presenting significant enrichments for specific GO terms were selected and visualized on Cytoscape. For presentation purposes, nodes were assigned equal weights and subnetworks were slightly distorted to avoid node superimposition.

Calcium Imaging. NT and PC1/3-KD cells were plated onto glass coverslips and were loaded with 4 µM Fura-2 AM at room temperature for 45 min in the growth medium. Recordings were performed in HBSS containing 140 mM NaCl, 5 mM KCl, 2 mM $MgCl_2$, 0.3 mM Na_2HPO_3, 0.4 mM KH_2PO_4, 4 mM $NaHCO_3$, 5 mM glucose and 10 mM HEPES adjusted to pH 7.4 with NaOH. The cells were then washed three times in HBSS. Taxol (30 µM) was added at the time of analysis. The fluorescent intensity of Fura-2 in each cell was monitored and recorded at 340 nm and 380 nm. To represent the variation in the intracellular free calcium concentration, the fluorescence intensity ratio represented by F340/F380 was used as an indicator of changes in cytosolic Ca^{2+} concentrations.

REFERENCES

1. Hanahan D, Weinberg RA. Hallmarks of cancer: the next generation. Cell. 2011;144:646-74.

2. De Palma M, Lewis CE. Cancer: Macrophages limit chemotherapy. Nature. 2011;472:303-4.
3. Fukuda K, Kobayashi A, Watabe K. The role of tumor-associated macrophage in tumor progression. Frontiers in bioscience. 2012;4:787-98.
4. Taskinen M, Karjalainen-Lindsberg ML, Nyman H, Eerola LM, Leppa S. A high tumor-associated macrophage content predicts favorable outcome in follicular lymphoma patients treated with rituximab and cyclophosphamide-doxorubicin-vincristine-prednisone. Clin Cancer Res. 2007;13:5784-9.
5. Shree T, Olson OC, Elie BT, Kester JC, Garfall AL, Simpson K, et al. Macrophages and cathepsin proteases blunt chemotherapeutic response in breast cancer. Genes Dev. 2011;25:2465-79.
6. Svensson S, Abrahamsson A, Vazquez Rodriguez G, Olsson AK, Jensen L, Cao Y, et al. CCL2 and CCL5 are novel therapeutic targets for estrogen-dependent breast cancer. Clin Cancer Res. 2015.
7. Laoui D, Van Overmeire E, De Baetselier P, Van Ginderachter JA, Raes G. Functional Relationship between Tumor-Associated Macrophages and Macrophage Colony-Stimulating Factor as Contributors to Cancer Progression. Frontiers in immunology. 2014;5:489.
8. Mantovani A, Locati M. Tumor-associated macrophages as a paradigm of macrophage plasticity, diversity, and polarization: lessons and open questions. Arterioscler Thromb Vasc Biol. 2013;33:1478-83.
9. Zhu Y, Knolhoff BL, Meyer MA, Nywening TM, West BL, Luo J, et al. CSF1/CSF1R blockade reprograms tumor-infiltrating macrophages and improves response to T-cell checkpoint immunotherapy in pancreatic cancer models. Cancer Res. 2014;74:5057-69.
10. Hung JY, Horn D, Woodruff K, Prihoda T, LeSaux C, Peters J, et al. Colony-stimulating factor 1 potentiates lung cancer bone metastasis. Lab Invest. 2014;94:371-81.
11. Hagemann T, Wilson J, Kulbe H, Li NF, Leinster DA, Charles K, et al. Macrophages induce invasiveness of epithelial cancer cells via NF-kappa B and JNK. J Immunol. 2005;175:1197-205.
12. Refaie S, Gagnon S, Gagnon H, Desjardins R, D'Anjou F, D'Orleans-Juste P, et al. Disruption of proprotein convertase 1/3 (PC1/3) expression in mice causes innate immune defects and uncontrolled cytokine secretion. J Biol Chem. 2012;287:14703-17.
13. Gagnon H, Refaie S, Gagnon S, Desjardins R, Salzet M, Day R. Proprotein convertase 1/3 (PC1/3) in the rat alveolar macrophage cell line NR8383: localization, trafficking and effects on cytokine secretion. PLoS One. 2013;8:e61557.
14. Duhamel M, Rodet F, Delhem N, Vanden Abeele F, Kobeissy F, Nataf S, et al. Molecular Consequences of Proprotein Convertase 1/3 (PC1/3) Inhibition in Macrophages for Application to Cancer Immunotherapy: A Proteomic Study. Mol Cell Proteomics. 2015;14:2857-77.
15. Edwards SJ, Barton S, Thurgar E, Trevor N. Topotecan, pegylated liposomal doxorubicin hydrochloride, paclitaxel, trabectedin and gemcitabine for advanced recurrent or refractory ovarian cancer: a systematic review and economic evaluation. Health technology assessment. 2015;19:1-480.
16. Orr GA, Verdier-Pinard P, McDaid H, Horwitz SB. Mechanisms of Taxol resistance related to microtubules. Oncogene. 2003;22:7280-95.
17. Kawasaki K, Nogawa H, Nishijima M. Identification of mouse MD-2 residues important for forming the cell surface TLR4-MD-2 complex recognized by anti-TLR4-MD-2 antibodies, and for conferring LPS and taxol responsiveness on mouse TLR4 by alanine-scanning mutagenesis. J Immunol. 2003;170:413-20.

18. Kawasaki K, Akashi S, Shimazu R, Yoshida T, Miyake K, Nishijima M. Involvement of TLR4/MD-2 complex in species-specific lipopolysaccharide-mimetic signal transduction by Taxol. Journal of endotoxin research. 2001;7:232-6.
19. Hastings KT. GILT: Shaping the MHC Class II-Restricted Peptidome and CD4(+) T Cell-Mediated Immunity. Frontiers in immunology. 2013;4:429.
20. Schiff PB, Horwitz SB. Taxol stabilizes microtubules in mouse fibroblast cells. Proc Natl Acad Sci U S A. 1980;77:1561-5.
21. Schiff PB, Fant J, Horwitz SB. Promotion of microtubule assembly in vitro by taxol. Nature. 1979;277:665-7.
22. Patel N, Chatterjee SK, Vrbanac V, Chung I, Mu CJ, Olsen RR, et al. Rescue of paclitaxel sensitivity by repression of Prohibitin1 in drug-resistant cancer cells. Proc Natl Acad Sci U S A. 2010;107:2503-8.
23. Shprung T, Gozes I. A novel method for analyzing mitochondrial movement: inhibition by paclitaxel in a pheochromocytoma cell model. J Mol Neurosci. 2009;37:254-62.
24. Ousingsawat J, Wanitchakool P, Kmit A, Romao AM, Jantarajit W, Schreiber R, et al. Anoctamin 6 mediates effects essential for innate immunity downstream of P2X7 receptors in macrophages. Nat Commun. 2015;6:6245.
25. Takesono A, Heasman SJ, Wojciak-Stothard B, Garg R, Ridley AJ. Microtubules regulate migratory polarity through Rho/ROCK signaling in T cells. PLoS One. 2010;5:e8774.
26. Dhirapong A, Lleo A, Leung P, Gershwin ME, Liu FT. The immunological potential of galectin-1 and -3. Autoimmunity reviews. 2009;8:360-3.
27. Tsai TH, Chen SF, Huang TY, Tzeng CF, Chiang AS, Kou YR, et al. Impaired Cd14 and Cd36 expression, bacterial clearance, and Toll-like receptor 4-Myd88 signaling in caveolin-1-deleted macrophages and mice. Shock. 2011;35:92-9.
28. Chavez-Sanchez L, Garza-Reyes MG, Espinosa-Luna JE, Chavez-Rueda K, Legorreta-Haquet MV, Blanco-Favela F. The role of TLR2, TLR4 and CD36 in macrophage activation and foam cell formation in response to oxLDL in humans. Hum Immunol. 2014;75:322-9.
29. McFarland BC, Gray GK, Nozell SE, Hong SW, Benveniste EN. Activation of the NF-kappaB pathway by the STAT3 inhibitor JSI-124 in human glioblastoma cells. Mol Cancer Res. 2013;11:494-505.
30. Walker SR, Chaudhury M, Nelson EA, Frank DA. Microtubule-targeted chemotherapeutic agents inhibit signal transducer and activator of transcription 3 (STAT3) signaling. Mol Pharmacol. 2010;78:903-8.
31. Oztopcu P, Kabadere S, Mercangoz A, Uyar R. Comparison of vitamins K1, K2 and K3 effects on growth of rat glioma and human glioblastoma multiforme cells in vitro. Acta neurologica Belgica. 2004;104:106-10.
32. Eldh M, Ekström K, Valadi H, Sjöstrand M, Olsson B, Jernås M, et al. Exosomes communicate protective messages during oxidative stress; possible role of exosomal shuttle RNA. PloS one. 2010;5:e15353.
33. Williams TK, Costantino CL, Bildzukewicz NA, Richards NG, Rittenhouse DW, Einstein L, et al. pp32 (ANP32A) expression inhibits pancreatic cancer cell growth and induces gemcitabine resistance by disrupting HuR binding to mRNAs. PLoS One. 2010;5:e15455.
34. Kitano H, Mamiya A, Tomomi I, Shinichiro K, Chiaki H. Coagulation factor IX regulates cell migration and adhesion in vitro. Cell biology international. 2015;39:1162-72.

35. Chan AY, Coniglio SJ, Chuang Y-y, Michaelson D, Knaus UG, Philips MR, et al. Roles of the Rac1 and Rac3 GTPases in human tumor cell invasion. Oncogene. 2005;24:7821-9.
36. Skog J, Würdinger T, van Rijn S, Meijer DH, Gainche L, Curry WT, et al. Glioblastoma microvesicles transport RNA and proteins that promote tumour growth and provide diagnostic biomarkers. Nature cell biology. 2008;10:1470-6.
37. Tynninen O, Carpen O, Jaaskelainen J, Paavonen T, Paetau A. Ezrin expression in tissue microarray of primary and recurrent gliomas. Neuropathol Appl Neurobiol. 2004;30:472-7.
38. Geiger KD, Stoldt P, Schlote W, Derouiche A. Ezrin immunoreactivity is associated with increasing malignancy of astrocytic tumors but is absent in oligodendrogliomas. Am J Pathol. 2000;157:1785-93.
39. Zheng BB, Zhang P, Jia WW, Yu LG, Guo XL. Sorcin, a potential therapeutic target for reversing multidrug resistance in cancer. Journal of physiology and biochemistry. 2012;68:281-7.
40. Gopal U, Bohonowych JE, Lema-Tome C, Liu A, Garrett-Mayer E, Wang B, et al. A novel extracellular Hsp90 mediated co-receptor function for LRP1 regulates EphA2 dependent glioblastoma cell invasion. PLoS One. 2011;6:e17649.
41. Fogal V, Babic I, Chao Y, Pastorino S, Mukthavaram R, Jiang P, et al. Mitochondrial p32 is upregulated in Myc expressing brain cancers and mediates glutamine addiction. Oncotarget. 2015;6:1157-70.
42. Holmberg Olausson K, Elsir T, Moazemi Goudarzi K, Nister M, Lindstrom MS. NPM1 histone chaperone is upregulated in glioblastoma to promote cell survival and maintain nucleolar shape. Scientific reports. 2015;5:16495.
43. Lu W, Lee N, Kaul S, Lan F, Poon R, Wadhwa R, et al. Mortalin–p53 interaction in cancer cells is stress dependent and constitutes a selective target for cancer therapy. Cell Death & Differentiation. 2011;18:1046-56.
44. Wang H, Liu B, Al-Aidaroos A, Shi H, Li L, Guo K, et al. Dual-faced SH3BGRL: oncogenic in mice, tumor suppressive in humans. Oncogene. 2015.
45. Tang X, Mo C, Wang Y, Wei D, Xiao H. Anti-tumour strategies aiming to target tumour-associated macrophages. Immunology. 2013;138:93-104.
46. Tang X. Tumor-associated macrophages as potential diagnostic and prognostic biomarkers in breast cancer. Cancer Lett. 2013;332:3-10.
47. Siveen KS, Kuttan G. Role of macrophages in tumour progression. Immunol Lett. 2009;123:97-102.
48. Laoui D, Movahedi K, Van Overmeire E, Van den Bossche J, Schouppe E, Mommer C, et al. Tumor-associated macrophages in breast cancer: distinct subsets, distinct functions. Int J Dev Biol. 2011;55:861-7.
49. Jung KY, Cho SW, Kim YA, Kim D, Oh BC, Park do J, et al. Cancers with Higher Density of Tumor-Associated Macrophages Were Associated with Poor Survival Rates. Journal of pathology and translational medicine. 2015;49:318-24.
50. Chen P, Huang Y, Bong R, Ding Y, Song N, Wang X, et al. Tumor-associated macrophages promote angiogenesis and melanoma growth via adrenomedullin in a paracrine and autocrine manner. Clin Cancer Res. 2011;17:7230-9.
51. Allavena P, Mantovani A. Immunology in the clinic review series; focus on cancer: tumour-associated macrophages: undisputed stars of the inflammatory tumour microenvironment. Clinical and experimental immunology. 2012;167:195-205.
52. Sudheerkumar P, Shiras A, Das G, Jagtap JC, Prasad V, Shastry P. Independent activation of Akt and NF-kappaB pathways and their role in resistance to TNF-alpha mediated cytotoxicity in gliomas. Mol Carcinog. 2008;47:126-36.

53. Mamidi S, Hone S, Teufel C, Sellner L, Zenz T, Kirschfink M. Neutralization of membrane complement regulators improves complement-dependent effector functions of therapeutic anticancer antibodies targeting leukemic cells. Oncoimmunology. 2015;4:e979688.
54. Ishimoto T, Sugihara H, Watanabe M, Sawayama H, Iwatsuki M, Baba Y, et al. Macrophage-derived reactive oxygen species suppress miR-328 targeting CD44 in cancer cells and promote redox adaptation. Carcinogenesis. 2014;35:1003-11.
55. Friedberg JW, Kelly JL, Neuberg D, Peterson DR, Kutok JL, Salloum R, et al. Phase II study of a TLR-9 agonist (1018 ISS) with rituximab in patients with relapsed or refractory follicular lymphoma. Br J Haematol. 2009;146:282-91.
56. Viola A, Sarukhan A, Bronte V, Molon B. The pros and cons of chemokines in tumor immunology. Trends Immunol. 2012;33:496-504.
57. Matsuo Y, Takeyama H, Guha S. Cytokine network: new targeted therapy for pancreatic cancer. Curr Pharm Des. 2012;18:2416-9.
58. Knutson KL, Karyampudi L, Lamichhane P, Preston C. Targeted immune therapy of ovarian cancer. Cancer Metastasis Rev. 2015;34:53-74.
59. Kawakami Y, Yaguchi T, Sumimoto H, Kudo-Saito C, Iwata-Kajihara T, Nakamura S, et al. Improvement of cancer immunotherapy by combining molecular targeted therapy. Frontiers in oncology. 2013;3:136.
60. Katholnig K, Linke M, Pham H, Hengstschlager M, Weichhart T. Immune responses of macrophages and dendritic cells regulated by mTOR signalling. Biochemical Society transactions. 2013;41:927-33.
61. Hamdan R, Zhou Z, Kleinerman ES. Blocking SDF-1alpha/CXCR4 downregulates PDGF-B and inhibits bone marrow-derived pericyte differentiation and tumor vascular expansion in Ewing tumors. Mol Cancer Ther. 2014;13:483-91.
62. Gorbachev AV, Fairchild RL. Regulation of chemokine expression in the tumor microenvironment. Crit Rev Immunol. 2014;34:103-20.
63. Fridman WH, Pages F, Sautes-Fridman C, Galon J. The immune contexture in human tumours: impact on clinical outcome. Nat Rev Cancer. 2012;12:298-306.
64. Becht E, Goc J, Germain C, Giraldo NA, Dieu-Nosjean MC, Sautes-Fridman C, et al. Shaping of an effective immune microenvironment to and by cancer cells. Cancer Immunol Immunother. 2014;63:991-7.
65. Abastado JP. The next challenge in cancer immunotherapy: controlling T-cell traffic to the tumor. Cancer Res. 2012;72:2159-61.
66. Guiducci C, Vicari AP, Sangaletti S, Trinchieri G, Colombo MP. Redirecting in vivo elicited tumor infiltrating macrophages and dendritic cells towards tumor rejection. Cancer Res. 2005;65:3437-46.
67. Palsson-McDermott EM, Curtis AM, Goel G, Lauterbach MA, Sheedy FJ, Gleeson LE, et al. Pyruvate kinase M2 regulates Hif-1alpha activity and IL-1beta induction and is a critical determinant of the warburg effect in LPS-activated macrophages. Cell Metab. 2015;21:65-80.
68. Tarassishin L, Suh HS, Lee SC. Interferon regulatory factor 3 plays an anti-inflammatory role in microglia by activating the PI3K/Akt pathway. J Neuroinflammation. 2011;8:187.
69. Nance E, Zhang C, Shih TY, Xu Q, Schuster BS, Hanes J. Brain-penetrating nanoparticles improve paclitaxel efficacy in malignant glioma following local administration. ACS Nano. 2014;8:10655-64.
70. Liu Y, Ran R, Chen J, Kuang Q, Tang J, Mei L, et al. Paclitaxel loaded liposomes decorated with a multifunctional tandem peptide for glioma targeting. Biomaterials. 2014;35:4835-47.

71. Hu Q, Gao X, Gu G, Kang T, Tu Y, Liu Z, et al. Glioma therapy using tumor homing and penetrating peptide-functionalized PEG-PLA nanoparticles loaded with paclitaxel. Biomaterials. 2013;34:5640-50.
72. Chirio D, Gallarate M, Peira E, Battaglia L, Muntoni E, Riganti C, et al. Positive-charged solid lipid nanoparticles as paclitaxel drug delivery system in glioblastoma treatment. Eur J Pharm Biopharm. 2014;88:746-58.
73. Zhu Q, Han X, Peng J, Qin H, Wang Y. The role of CXC chemokines and their receptors in the progression and treatment of tumors. J Mol Histol. 2012;43:699-713.
74. Keeley EC, Mehrad B, Strieter RM. CXC chemokines in cancer angiogenesis and metastases. Advances in cancer research. 2010;106:91-111.
75. Wang B, Khachigian LM, Esau L, Birrer MJ, Zhao X, Parker MI, et al. A key role for early growth response-1 and nuclear factor-kappaB in mediating and maintaining GRO/CXCR2 proliferative signaling in esophageal cancer. Mol Cancer Res. 2009;7:755-64.
76. Plaza-Menacho I, van der Sluis T, Hollema H, Gimm O, Buys CH, Magee AI, et al. Ras/ERK1/2-mediated STAT3 Ser727 phosphorylation by familial medullary thyroid carcinoma-associated RET mutants induces full activation of STAT3 and is required for c-fos promoter activation, cell mitogenicity, and transformation. J Biol Chem. 2007;282:6415-24.
77. Dobi E, Monnien F, Kim S, Ivanaj A, N'Guyen T, Demarchi M, et al. Impact of STAT3 phosphorylation on the clinical effectiveness of anti-EGFR-based therapy in patients with metastatic colorectal cancer. Clinical colorectal cancer. 2013;12:28-36.
78. Walker SR, Chaudhury M, Frank DA. STAT3 Inhibition by Microtubule-Targeted Drugs: Dual Molecular Effects of Chemotherapeutic Agents. Molecular and cellular pharmacology. 2011;3:13-9.
79. Abubaker K, Luwor RB, Escalona R, McNally O, Quinn MA, Thompson EW, et al. Targeted Disruption of the JAK2/STAT3 Pathway in Combination with Systemic Administration of Paclitaxel Inhibits the Priming of Ovarian Cancer Stem Cells Leading to a Reduced Tumor Burden. Frontiers in oncology. 2014;4:75.
80. Jahraus A, Egeberg M, Hinner B, Habermann A, Sackman E, Pralle A, et al. ATP-dependent membrane assembly of F-actin facilitates membrane fusion. Mol Biol Cell. 2001;12:155-70.
81. Guerin I, de Chastellier C. Disruption of the actin filament network affects delivery of endocytic contents marker to phagosomes with early endosome characteristics: the case of phagosomes with pathogenic mycobacteria. European journal of cell biology. 2000;79:735-49.
82. Zotti T, Scudiero I, Settembre P, Ferravante A, Mazzone P, D'Andrea L, et al. TRAF6-mediated ubiquitination of NEMO requires p62/sequestosome-1. Mol Immunol. 2014;58:27-31.
83. Into T, Inomata M, Niida S, Murakami Y, Shibata K. Regulation of MyD88 aggregation and the MyD88-dependent signaling pathway by sequestosome 1 and histone deacetylase 6. J Biol Chem. 2010;285:35759-69.
84. Moisan J, Thuraisingam T, Henault J, De Sanctis J, Radzioch D. Role of SLC11A1 (formerly NRAMP1) in regulation of signal transduction induced by Toll-like receptor 7 ligands. FEMS immunology and medical microbiology. 2006;47:138-47.
85. Verma S, Hoffmann FW, Kumar M, Huang Z, Roe K, Nguyen-Wu E, et al. Selenoprotein K knockout mice exhibit deficient calcium flux in immune cells and impaired immune responses. J Immunol. 2011;186:2127-37.

86. Meiler S, Baumer Y, Huang Z, Hoffmann FW, Fredericks GJ, Rose AH, et al. Selenoprotein K is required for palmitoylation of CD36 in macrophages: implications in foam cell formation and atherogenesis. J Leukoc Biol. 2013;93:771-80.
87. Huang Z, Hoffmann FW, Norton RL, Hashimoto AC, Hoffmann PR. Selenoprotein K is a novel target of m-calpain, and cleavage is regulated by Toll-like receptor-induced calpastatin in macrophages. J Biol Chem. 2011;286:34830-8.
88. Kees T, Lohr J, Noack J, Mora R, Gdynia G, Todt G, et al. Microglia isolated from patients with glioma gain antitumor activities on poly (I:C) stimulation. Neuro Oncol. 2012;14:64-78.
89. Mora R, Abschuetz A, Kees T, Dokic I, Joschko N, Kleber S, et al. TNF-alpha- and TRAIL-resistant glioma cells undergo autophagy-dependent cell death induced by activated microglia. Glia. 2009;57:561-81.
90. Duhamel M, Rodet F, Murgoci A, Wisztorski M, Day R, Fournier I, et al. Proprotein convertase 1/3 inhibited macrophages: A novel therapeutic based on drone macrophages. EuPA open proteomics. 2016;11:20-2.
91. Cisneros L O, AD, Stüllein C, Régnier-Vigouroux. Evaluation of Consistency in Spheroid Invasion Assays. Scientific reports. 2016;In press.
92. Meissner F, Scheltema RA, Mollenkopf HJ, Mann M. Direct proteomic quantification of the secretome of activated immune cells. Science. 2013;340:475-8.
93. Cox J, Mann M. MaxQuant enables high peptide identification rates, individualized p.p.b.-range mass accuracies and proteome-wide protein quantification. Nat Biotechnol. 2008;26:1367-72.
94. Cox J, Neuhauser N, Michalski A, Scheltema RA, Olsen JV, Mann M. Andromeda: a peptide search engine integrated into the MaxQuant environment. J Proteome Res. 2011;10:1794-805.
95. UniProt C. Reorganizing the protein space at the Universal Protein Resource (UniProt). Nucleic Acids Res. 2012;40:D71-5.
96. Cox J, Hein MY, Luber CA, Paron I, Nagaraj N, Mann M. Accurate proteome-wide label-free quantification by delayed normalization and maximal peptide ratio extraction, termed MaxLFQ. Mol Cell Proteomics. 2014;13:2513-26.
97. Vizcaino JA, Deutsch EW, Wang R, Csordas A, Reisinger F, Rios D, et al. ProteomeXchange provides globally coordinated proteomics data submission and dissemination. Nat Biotechnol. 2014;32:223-6.
98. Vizcaino JA, Cote RG, Csordas A, Dianes JA, Fabregat A, Foster JM, et al. The PRoteomics IDEntifications (PRIDE) database and associated tools: status in 2013. Nucleic Acids Res. 2013;41:D1063-9.
99. Montojo J, Zuberi K, Rodriguez H, Bader GD, Morris Q. GeneMANIA: Fast gene network construction and function prediction for Cytoscape. F1000Res. 2014;3:153.
100. Chen EY, Tan CM, Kou Y, Duan Q, Wang Z, Meirelles GV, et al. Enrichr: interactive and collaborative HTML5 gene list enrichment analysis tool. BMC Bioinformatics. 2013;14:128.

Figure Legends

Figure 1: A) Shot-gun proteomic strategy. a) NR8383 cells were stimulated with Taxol (30 µM) or not (control) and lysed before FASP and LC-MS/MS analysis. MaxQuant and Perseus software were used for the statistical analysis, and a heat map was generated to show proteins that were significantly different between NT and PC1/3-KD NR8383 macrophages in

the cell extracts. Two clusters are highlighted. b) The proteins in each cluster were analyzed using Panther software. The biological functions associated with these proteins are shown. The functions framed in orange correspond to those of the proteins that were overexpressed in PC1/3-KD cells, whereas the functions framed in blue correspond to the proteins that were overexpressed in NT cells. **B) Specific molecular pathway analyses after Taxol treatment** a) cytoskeleton, b) cell differentiation and c) inflammation of the over- and under- expressed proteins identified in NT and PC1/3-KD cells after Taxol treatment using string analysis followed by Ingenuity software. The different colors reflect the degree of expression. Under Taxol treatment, proteins in blue are underexpressed whereas those in orange show overexpression. **C) Global pathway analysis**, **D) Co-expression network analyses** a) Co-expression of Tuba1c/Tuba4a with mitochondria-related molecules in Taxol-treated NT vs Taxol-treated KD cells. The 100 genes which encoded molecules were the most tightly co-expressed with Tuba4a/Tuba1c were identified in Taxol-treated NT vs Taxol-treated KD cells. Shown are subnetworks of genes annotated by the GO term “mitochondrion” (adjusted p value for enrichment significance = 0.11e-3 in Taxol-treated NT cells and 0.10e-5 in Taxol-treated KD cells). b) Co-expression of tubulins with immune-related molecules in Taxol-treated NT vs Taxol-treated KD cells. The 100 genes which encoded molecules were the most tightly co-expressed with Tuba4a/Tuba1c were identified in Taxol-treated NT vs Taxol-treated KD cells. Shown are subnetworks of immune-related genes. Note that Arg1 and IL1rn, two anti-inflammatory molecules, are specific to the Tuba4a/Tuba1c network in Taxol-treated NT cells. In contrast, the Tuba4a/Tuba1c network in Taxol-treated KD cells is characterized by the following pro-inflammatory signature: B2m, Calr, Aif1, CD44 and Sod1. **E) Whole-cell extract proteomic analysis strategy.** a) A heat map was generated to show proteins that were significantly different between NT and PC1/3-KD NR8383 macrophages in all conditions. Eight clusters are highlighted. b) Global pathway analysis of the overexpressed proteins specifically identified in PC1/3-KD cells. The relationship between the overexpressed proteins with PCSk1/3 (pink) is also showed.

Figure 2: A) Taxol modulates CD36 expression. Western blot analysis of CD36 (in total extracts) in NT or KD PC1/3 NR8383 macrophages after Taxol stimulation (30 µM) or not at 1 h, 3 h and 6 h. The data is represented as the fold change in samples stimulated with Taxol relative to non-stimulated samples for CD36 and normalized to actin. * Significant differences between NT cells and PC1/3-KD cells (P≤0.05) by t-test. Experiments were performed in duplicates. **B) Time course of IκB-α degradation after Taxol treatment a)** Western blot analysis of total IκB-α in NT or KD PC1/3 NR8383 macrophages treated with 30 µM of Taxol

for 1, 3 and 6 h. Intensities of total IκB-α bands were quantified and normalized with actin. **b**) The results are depicted through graphic representations The fold change in the samples stimulated with Taxol relative to the non-stimulated samples are shown. * Significant differences between NT cells and KD cells (P≤0.05) by t-test. Experiments were performed in duplicates. **C) Taxol stimulates $[Ca^{2+}]$c production a)** $[Ca^{2+}]$c rise in NT and KD NR8383 cells in response to Taxol (horizontal bar). **b)** Quantification of Taxol mediated $[Ca^{2+}]$c increase for NT and KD NR8383 cells. **c)** Quantification of resting $[Ca^{2+}]$c for NT and KD NR8383 cells in basal condition. **D) Taxol inhibits STAT3 signalization. a)** Western blot analysis of phospho STAT3 and total STAT3 in NT or KD PC1/3 NR8383 macrophages after Taxol stimulation (30 µM), IL10 stimulation (20 ng/ml) or not at 1 h, 3 h and 6 h. **b)** Graphic representations of the quantification of phospho STAT3. The data are represented as the ratio of phosphorylated STAT3 on total STAT3 in samples for each conditions. * Significant differences between NT cells and PC1/3-KD cells (P≤0.05) by t-test. Experiments were performed in triplicates. **E)** Schematic representation of Taxol signaling in PC1/3-KD cells. Taxol can modulate CD36 and activate TLR4 MyD88-dependent pathway leading to NF-κB activation, calcium mobilization and pro-inflammatory cytokine secretion. Similarly, STAT3 phosphorylated pathway is blocked leading to an ineffective action of IL-10.

Figure 3: **A) Effect of PC1/3 down-regulation on cytokine secretion under inhibitory conditions**. The rat cytokine array assay was performed with NR8383 secretomes (NT/KD). The cells were untreated (control) or treated with IL-10 for 24 h without stimulation (IL-10) or with Taxol for 24 h (IL-10+Taxol). Blue shows NT cell secretomes, and orange indicates KD cell secretomes. The bar diagrams represent the ratio of the spot mean pixel densities/reference point pixel densities. Significant differences were analyzed using Student's t-test. *P<0.05. **B)** to **D)** The cell viability of C6 rat glioma (B)~~,~~ and J3T canine glioma (C) was determined by the CellTiter Aqueous One Solution Cell Proliferation reagent and the viability of U87 human glioma cells (D) was determined using the CellTiter-Glo assay. The cells were incubated with NR8383 secretomes obtained at 24 h with or without Taxol Treatment. The assays were conducted for 24 h, 48 h, 72 h and 96 h. At 72 h, conditioned medium was replaced with fresh medium (96 h+ medium). Graphs are presented in (a) and significant differences are presented in (b). Significant differences were identified using Anova test with +++P<0.001, ++P<0.01 and NS non-significant. "+" means that NT or KD secretomes are significant compared to control and "–" means that controls are significant compared to NT or KD secretomes.

Figure 4: A) Antitumor properties of NR8383 secretomes on glioma cells in a 3D co-culture. a) Invasion of rat glioma cells (C6) spheroids in the absence (No Mϕ) and in the presence of NR8383 non target (NT) or PC1/3 knockdown (KD) macrophages. Representative images of the invasion of C6 spheroids in the collagen matrix at day 0, day 3 and day 6. All images were acquired with an inverted light microscope at 4x magnification. Scale bar: 500 µm. **b**) Effect of Taxol pre-activated macrophages on C6 spheroids invasion. NT and KD macrophages were treated with 3 µl Taxol for 24 h prior to embedding (Taxol, 30 µM final). Control macrophages were left untreated (medium) or were treated with 3 µl DMSO (DMSO). Representative images of the invasion of C6 spheroids are shown at day 0 and day 6. All images were acquired with an inverted light microscope at 4x magnification. Scale bar: 500 µm. **c**) Images were quantified with the in-house software as described in Material and Methods. **B)** Proteomic analyses of secretome from co-cultures of C6 spheroids with PC1/3-KD cells and NT cells. At day 6, the secretomes were harvested and analysed (Time 6 days). Veen diagram of the co-cultures at day 6. **a)** Venn Diagram of the all co-culture conditions used (Taxol, control DMSO) for PC1/3-KD and NT cells **b)** MaxQuant and Perseus software were used for the statistical analysis and a heat map was generated to show proteins that significantly differed between the secretomes of NT and PC1/3-KD NR8383 macrophages after 6 days of co-culture.

Table 1: Identified unique proteins from secretomes issued from 3D Spheroids experiments.

Supplementary data 1: List of overexpressed proteins in NT and PC1/3-KD macrophages.
Supplementary data 2: List of overexpressed and underexpressed proteins after Taxol stimulation.
Supplementary data 3: List of proteins overexpressed in the different clusters of the global heatmap (Figure 1Ea).

Table 1: Identified unique proteins from secretomes issued from 3D Spheroids experiments

Unique identified proteins			
NT cells Taxol Time 6 days (Co-culture)	NT cells Control Time 6 days (Co-culture)	KD cells Taxol Time 6 days (Co-culture)	KD cells Control Time 6 days (Co-culture)
Rbmxrtl	Hist1h3e	Myl6	Thbs4
Grpel1	Atp6v1g1	Rac1	Tgfbi
Ezr	Flna	Anp32a	Sumo2
Sri	Nucb2	Nqo1	Fmod
Lrp1	Hist1h1e	F9	Ywhah
C1qbp	Akr1b7		Pgd
Npm1	Fkbp1a		Thbs4
Fh	Hnrnpa3		Tgfbi
H1f0	Lasp1		Hba1
Eif2s2			Plod1
			Inhba
			Dpysl2
			Cand1
			Wdr1
			Eef1g
			Dstn
			Hba1
			Plod1
			Inhba

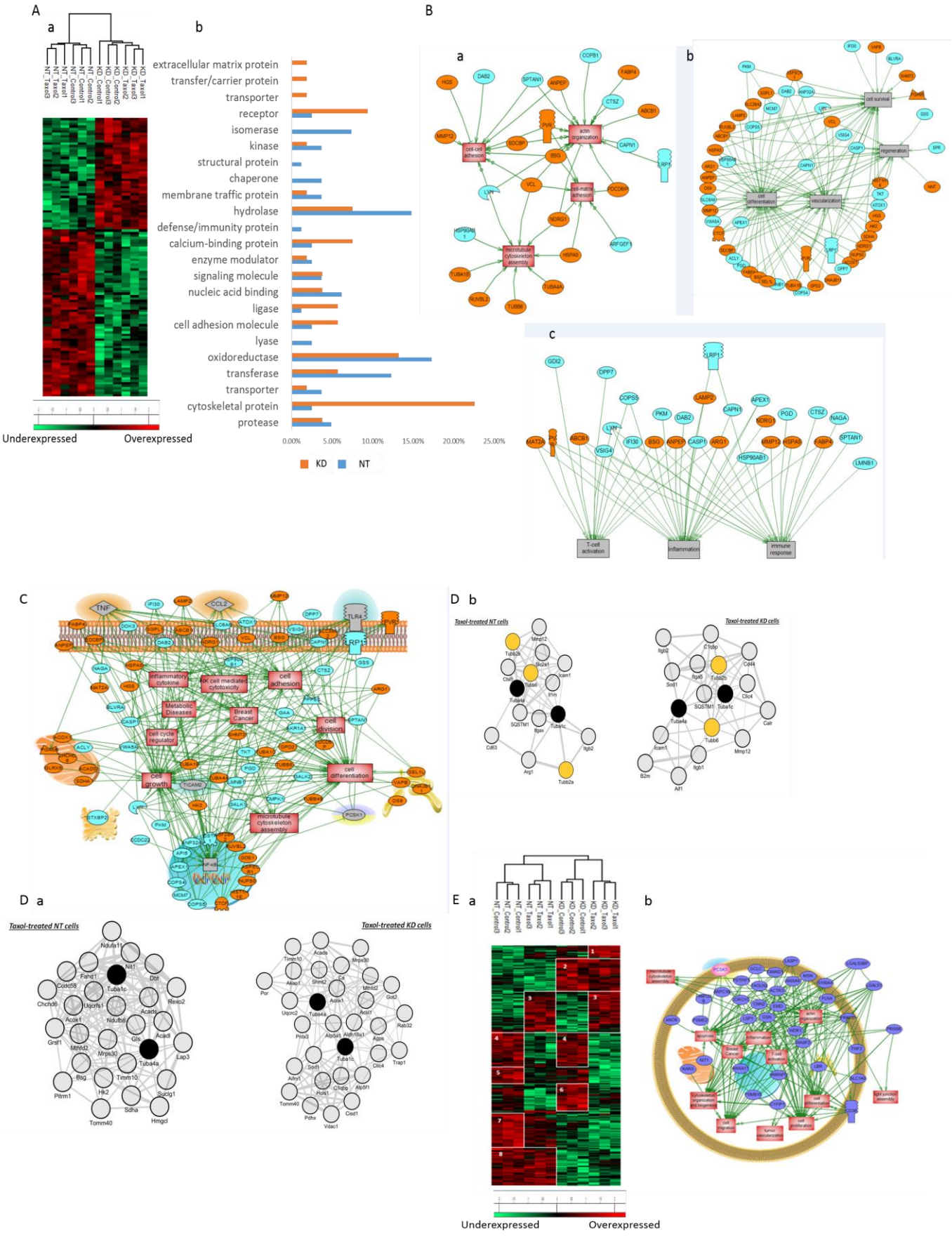

Figure 1

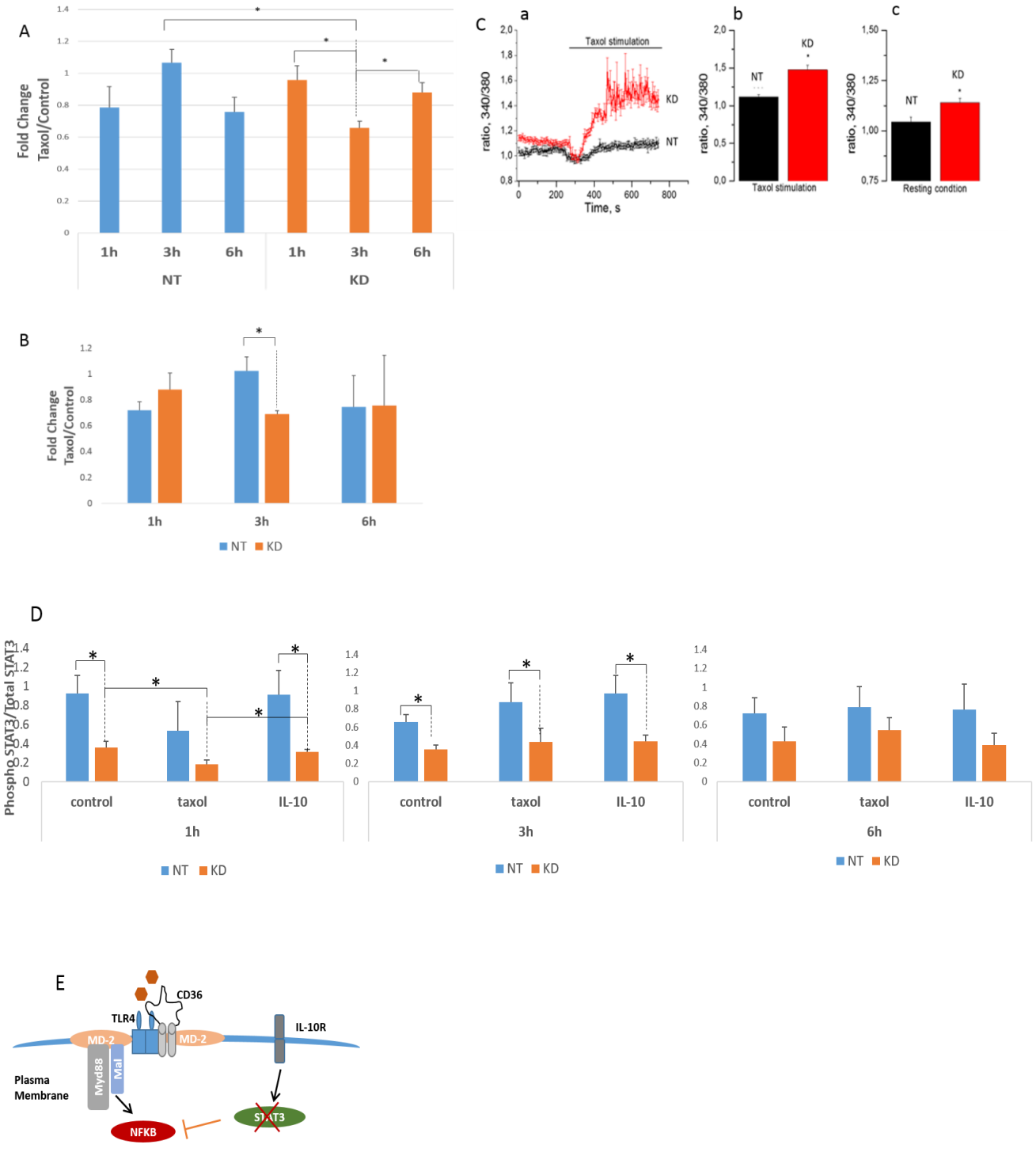

Figure 2

B

a

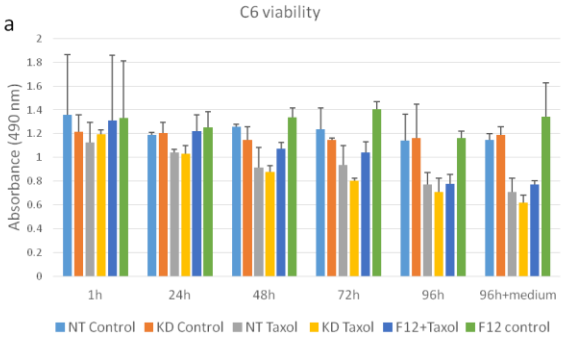

b

No treatment vs Taxol treatment (24h, 48h, 72h)	F12	NT	KD
	+++	+++	+++

F12 Taxol	NS	++
	NT Taxol	NS
		KD Taxol

F12 Control	NS	++
	NT Control	NS
		KD Control

Taxol treatment

24H	NS	++	+++	+++
	48H	NS	+++	++
		72H	+++	++
			96H	NS
				96H + medium

KD

24H	NS	NS	++	NS
	48H	NS	NS	NS
		72H	NS	NS
			96H	NS
				96H + medium

NT

24H	NS	NS	NS	NS
	48H	NS	NS	NS
		72H	NS	NS
			96H	NS
				96H + medium

C

a

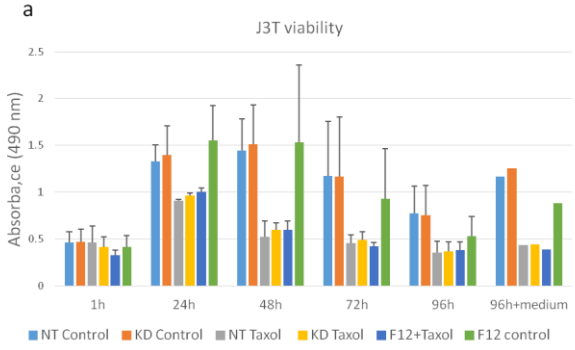

b

No treatment vs Taxol treatment	F12	NT	KD
	+++	+++	+++

F12 Taxol	NS	NS
	NT Taxol	NS
		KD Taxol

F12 Control	NS	NS
	NT Control	NS
		KD Control

Taxol treatment

24H	NS	++	+++	++
	48H	NS	NS	NS
		72H	NS	NS
			96H	NS
				96H + medium

KD

24H	NS	NS	++	NS
	48H	NS	NS	NS
		72H	NS	NS
			96H	NS
				96H + medium

NT

24H	NS	NS	NS	NS
	48H	NS	NS	NS
		72H	NS	NS
			96H	NS
				96H + medium

D

a

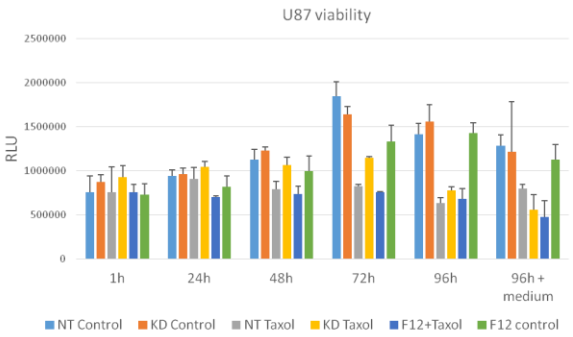

b

No treatment vs Taxol treatment	F12	NT	KD
	+++	+++	+++

F12 Taxol	--	---
	NT Taxol	NS
		KD Taxol

F12 Control	---	--
	NT Control	NS
		KD Control

Taxol treatment

24H	NS	++	++	+++
	48H	NS	NS	+++
		72H	NS	+++
			96H	NS
				96H + medium

KD

24H	NS	++	NS	++
	48H	NS	NS	+++
		72H	NS	+++
			96H	+++
				96H + medium

NT

24H	NS	++	NS	NS
	48H	NS	NS	NS
		72H	NS	NS
			96H	NS
				96H + medium

Figure 3

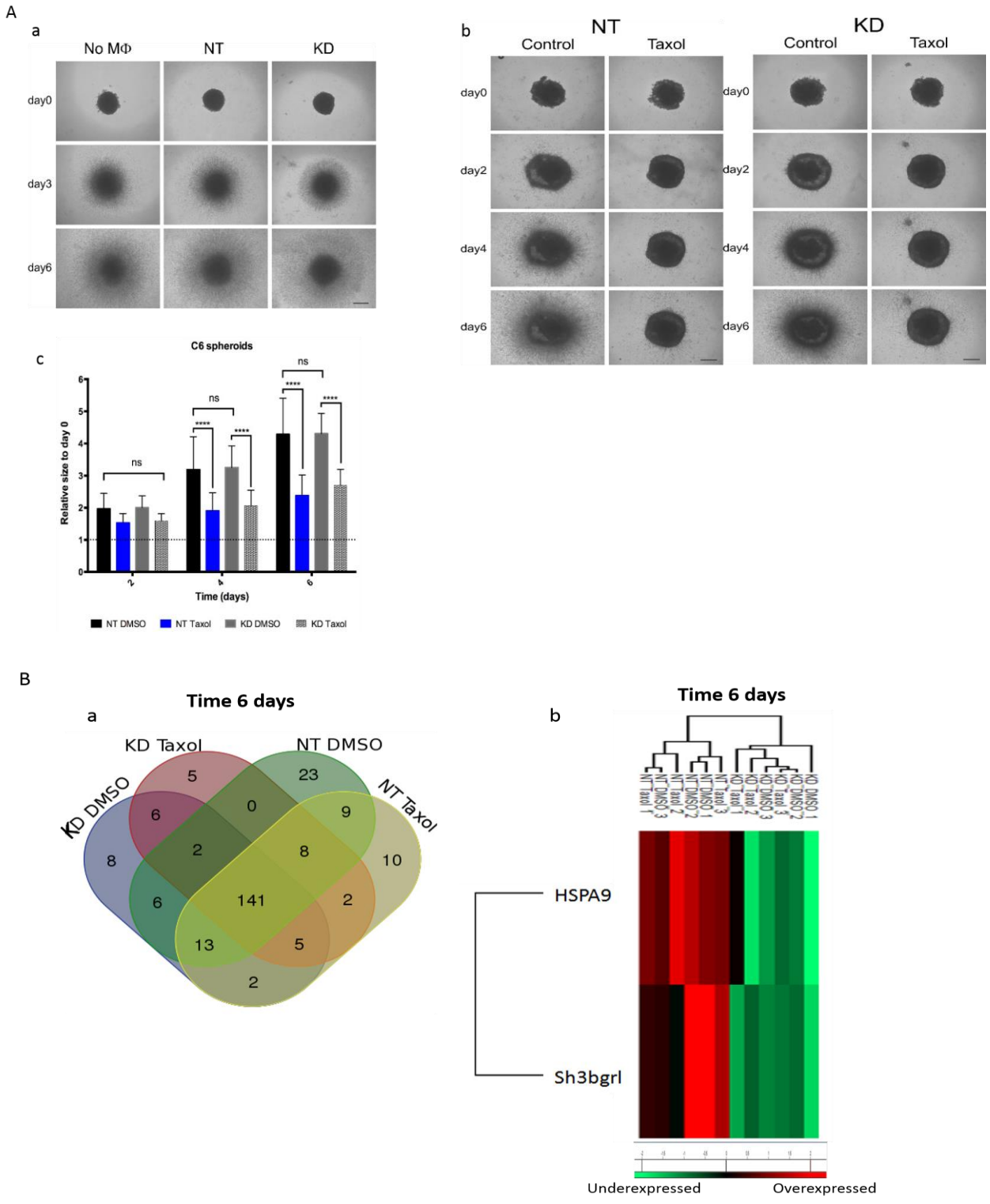

Figure 4

Conclusion

Cette étude apporte donc des informations sur l'effet du taxol sur les macrophages. L'inhibition de PC1/3 et la stimulation au taxol induisent, encore une fois, une activation plus importante des macrophages. L'effet des macrophages PC1/3 KD sur l'invasion des cellules cancéreuses n'est pas différent par rapport aux macrophages NT. Par contre, les cellules PC1/3 KD sécrètent des facteurs actifs contre les cellules de gliome C6. Des expériences complémentaires sont, cependant, nécessaires afin de savoir si des effets sur l'invasion peuvent être observés à des temps plus longs.

La résistance au taxol est couramment observée lors du traitement des patients. Les mécanismes de résistance sont nombreux tels que la surexpression d'un gène de résistance aux drogues MDR-1, des mutations de la β-tubuline qui est la molécule cible du taxol ou encore des changements de la composition lipidique (Yusuf et al. 2003). D'autres études ont démontré que le taxol induisait la sécrétion de facteurs qui attirent les macrophages tels que le facteur CSF-1. L'infiltration macrophagique permet aux cellules tumorales de devenir résistantes aux chimiothérapies, en partie dû à la sécrétion de cathepsine B par les macrophages (Shree et al. 2011; Bruchard et al. 2013; DeNardo et al. 2011). Nous avons réalisé une expérience de titration du taxol en présence ou absence de macrophages en co-culture avec les sphéroïdes de cellules C6 (**Figure 15**). Les résultats indiquent que l'invasion des cellules cancéreuses est taxol-dépendante : plus la concentration en taxol est importante (80 nM), plus l'invasion est réduite. La diminution d'invasion est plus prononcée en l'absence de macrophages, surtout à de plus faible concentrations de taxol (20 nM et 40 nM). Ceci indique donc que la résistance au taxol passe par les macrophages. Les macrophages protègent la tumeur contre les effets tumoricides du taxol.

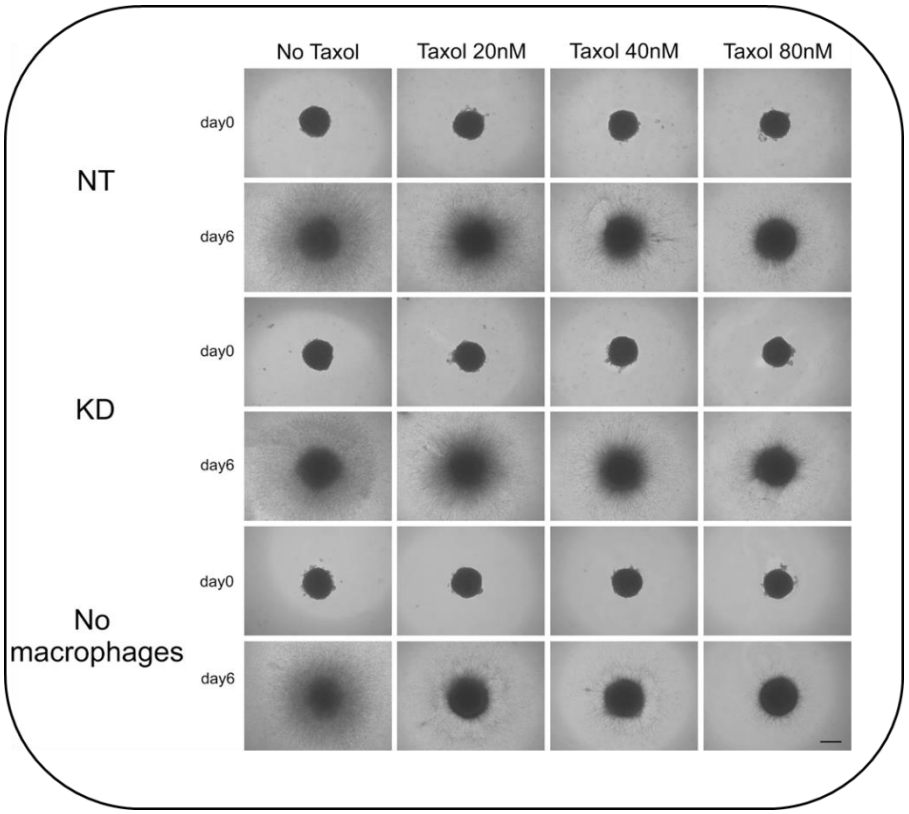

Figure 15 : Effet de l'augmentation de la concentration de taxol sur l'invasion des cellules tumorales C6 en l'absence ou présence de macrophages NT ou PC1/3 KD. Le contrôle a été fait en l'absence de taxol (No Taxol). Les images ont été prises à 0 et 6 jours. Toutes les images ont été acquises avec un microscope inversé à l'objectif 4x. Echelle : 500 µm.

Dans l'article, nous avons démontré que la pré-activation des macrophages avec le taxol pendant 24h permettait de contrer cet effet de résistance. La résistance est donc présente lorsque le taxol est appliqué directement sur les macrophages présents au niveau de la tumeur. La pré-activation avec le taxol permet d'induire un état d'activation des macrophages, même après 6 jours de co-culture, qui diminue l'invasion des cellules cancéreuses.

La prochaine étape de notre travail sera le développement d'un inhibiteur de PC1/3 qui pourrait être utilisé en combinaison avec différents ligands des récepteurs TLR. Actuellement, aucun inhibiteur strict de PC1/3 n'existe. Par contre, un inhibiteur ciblant plusieurs proprotéines convertases différentes a été développé (Becker et al. 2012). Nous avons commencé des analyses préliminaires avec cet inhibiteur. Il cible la furine, PC1/3, PC4, PACE4 et PC5/6. Ces proprotéines convertases ont des implications dans différents cancers. Par exemple, PACE4 est surexprimée dans le cancer de la prostate (D'Anjou et al. 2011) et dans le cancer des ovaires (Longuespée et al. 2014). La furine est associée à la transformation maligne des cellules

cancéreuses dans différents cancers (tête et cou, ovaires, sein) (Bassi et al. 2001; Cheng et al. 1997; Page et al. 2007). PC1/3 a un rôle dans les cancers neuroendocriniens et les tumeurs du poumon (Jin et al. 1999). De plus, elles peuvent avoir des rôles dans la progression tumorale car elles clivent différents substrats comme les métalloprotéases, les molécules d'adhésion, les facteurs de croissance et leur récepteur (Khatib et al. 2002). Un autre rôle important de ces proprotéines convertases est leur rôle dans l'immunité comme nous l'avons démontré tout au long des chapitres 2 et 3 de ma thèse pour PC1/3. Par exemple, la furine est exprimée dans les lymphocytes T. Elle clive plusieurs protéines impliquées dans l'activation des cellules T dont Notch1 et TGF-β. L'inhibition de la furine dans les lymphocytes T induit la sécrétion de cytokines pro-inflammatoires (Thomas 2002). L'ensemble de ces éléments tend à démontrer que l'inhibition de ces différentes proprotéines convertases permettrait d'agir à la fois sur les cellules cancéreuses mais aussi sur les cellules immunitaires infiltrantes pour leur réactivation.

Nous avons quelques résultats préliminaires sur l'effet de l'inhibiteur sur les macrophages. Tout d'abord, des études protéomiques ont été menées sur les protéines sécrétées par les macrophages sous inhibiteur. Les macrophages NT ont été mis en présence de l'inhibiteur pendant 24h puis stimulés au LPS pendant 24h. Les sécrétomes ont ensuite été analysés par nanoLC-MS/MS. Nous les avons comparés aux sécrétomes des cellules KD et NT sans inhibiteur. Parmi toutes les protéines identifiées, nous avons ciblé l'analyse sur les protéines impliquées dans l'inflammation telles que les cytokines et chémokines (**Figure 16**). On remarque que les chémokines CCL3, CCL4 et CXCL2 sont sécrétées de façon abondantes par les cellules KD et NT sous inhibiteur. La chémokine CCL6 est sécrétée de façon abondante par les cellules NT sous inhibiteur. Les CCL3 et CCL4 sont des chémokines qui permettent le recrutement des cellules NK cytotoxiques (Cassetta & Pollard 2016). L'ensemble de ces chémokines sont pro-inflammatoires. Les cytokines IL1RA et IL1RAP sont également plus sécrétées par les macrophages sous inhibiteur. L'IL1RA se lie au récepteur de l'IL1 sans l'activer. Cette protéine diminue la croissance tumorale, l'angiogenèse et les métastases dans des modèles de souris xénogreffées (Lewis et al. 2006). D'autres protéines sécrétées abondamment par les cellules NT sous inhibiteur ont été identifiées comme la galectine 1, le facteur AIF1 (ou IBA1), le cluster de différenciation CD14 et la protéine CSF3. IBA1 est un marqueur de cellules microgliales et macrophages activés (Garzetti et al. 2014; Ito et al. 1998). Suite à l'activation des macrophages, CD14 est libéré sous sa forme soluble (Shive et al. 2015). Le pattern de sécrétion des chémokines des cellules NT sous inhibiteur ressemble à celui des macrophages KD. D'autres molécules sont sécrétées de façon plus importante par les

macrophages sous inhibiteur. Cela peut être dû à l'inhibition des autres proprotéines convertases. L'inhibiteur déclenche donc la sécrétion de facteurs qui sont caractéristiques des macrophages activés. Ces expériences sont à poursuivre afin de valider ces résultats.

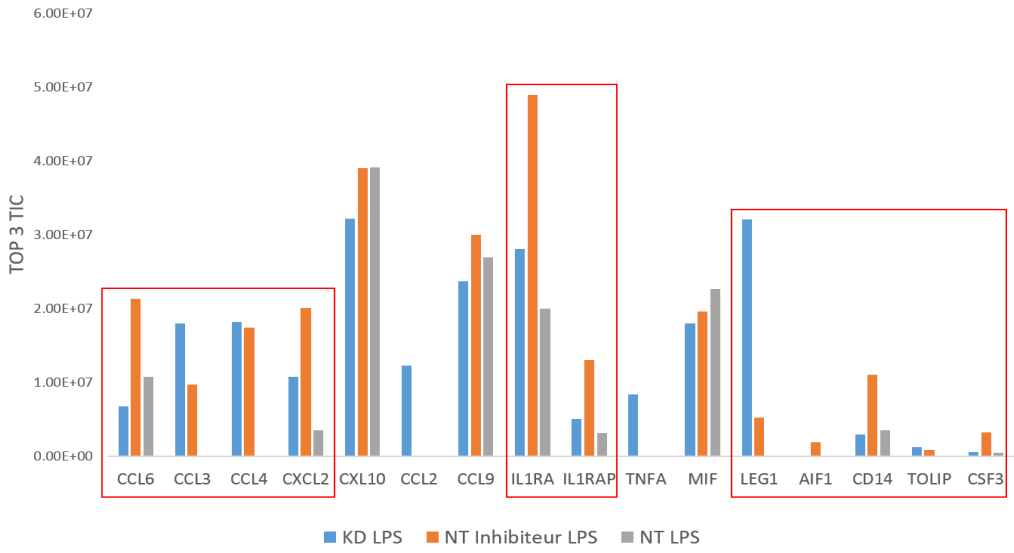

Figure 16 : TOP 3 TIC des protéines inflammatoires différentiellement sécrétées par les macrophages KD, NT en présence de l'inhibiteur et NT sans l'inhibiteur. L'inhibiteur (50 µM) a été ajouté aux cellules NT pendant 24h puis les cellules ont été stimulées avec le LPS (200 ng/ml) pendant 24h. Les sécrétomes ont été récoltées puis une approche shotgun a été réalisée avant l'analyse nanoLC-MS/MS.

Afin de connaître le potentiel de l'inhibiteur en onco-immunothérapie, il a ensuite été testé sur des co-cultures de sphéroïdes de cellules de gliomes et de macrophages. Pour ces expériences, nous avons utilisé des cellules de gliome de chien, appelées cellules J3T. Comme nous l'avons montré par protéomique, dans le chapitre 1, les gliomes canins sont proches d'un point de vue moléculaire des gliomes humains. Ils sont un bon modèle de translation à l'homme car ils partagent les mêmes stress environnementaux et développent des gliomes de façon spontanée. Ils permettraient de valider l'efficacité de nouvelles stratégies thérapeutiques (Bentley et al. 2016). Nous avons donc fait les tests de l'inhibiteur dans un modèle en trois dimensions. Le sphéroïde, composé de cellules de gliome canin, est mis en co-culture dans une matrice de collagène contenant, ou non, les macrophages de rat. L'invasion des cellules cancéreuses dans le collagène a ensuite été mesurée. Plusieurs concentrations d'inhibiteur ont été testées sur ce système (**Figure 17**). On remarque que l'inhibiteur entraîne une forte diminution de l'invasion des cellules cancéreuses dans le collagène quelle que soit sa concentration. Pour la suite, nous avons donc choisi la concentration de 50 µM.

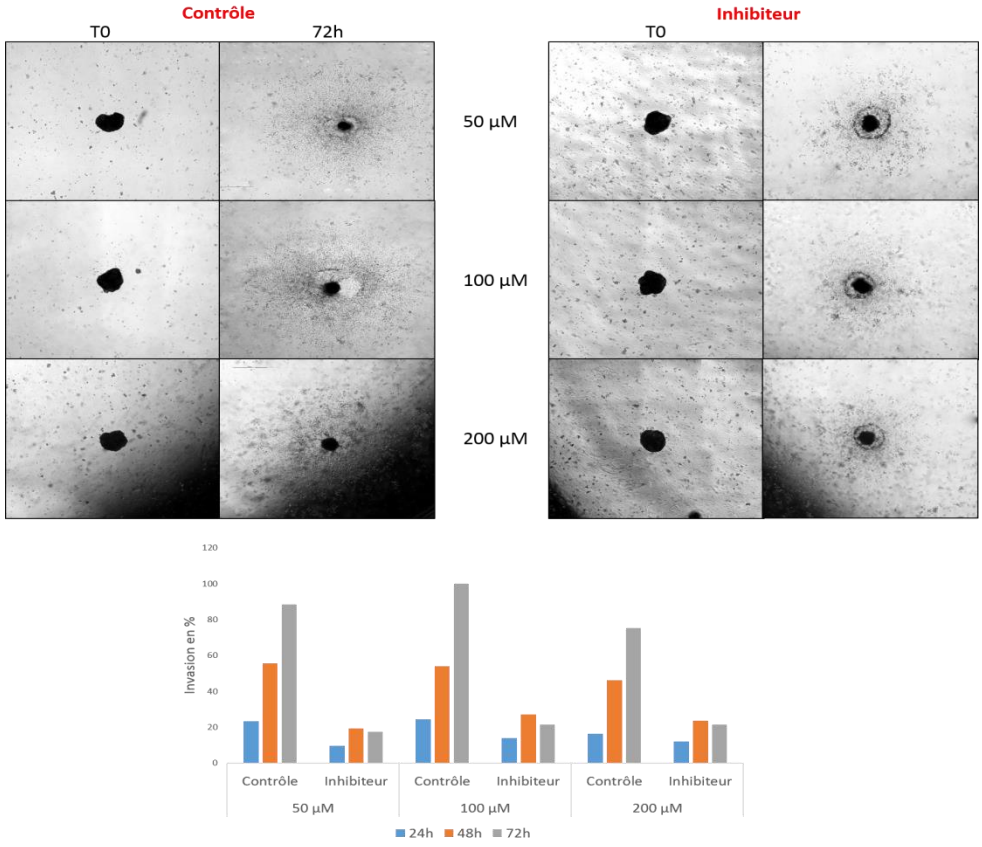

Figure 17 : Test de différentes concentrations d'inhibiteur des proprotéines convertases sur les sphéroïdes de cellules J3T en co-culture avec les macrophages NR8383 dans le collagène. Les sphéroïdes J3T sont composés de 10 000 cellules et mis en co-culture avec 50 000 macrophages. L'inhibiteur est dilué dans le collagène à 50, 100 ou 200 µM. Le contrôle contient l'équivalent en DMSO. L'aire d'invasion est mesurée avec le logiciel Photoshop de 24h à 72h et rapportée à l'aire du sphéroïde à T0.

L'inhibiteur a également été testé sur le sphéroïde de cellules J3T sans les macrophages (**Figure 18**). On remarque que l'invasion des cellules cancéreuses en présence de l'inhibiteur est moins prononcée que dans la condition contrôle. L'inhibiteur agit donc directement sur l'invasion des cellules cancéreuses. Afin de savoir sur quelles proprotéines convertases agit l'inhibiteur, il serait intéressant de savoir lesquelles sont exprimées par ces cellules canines.

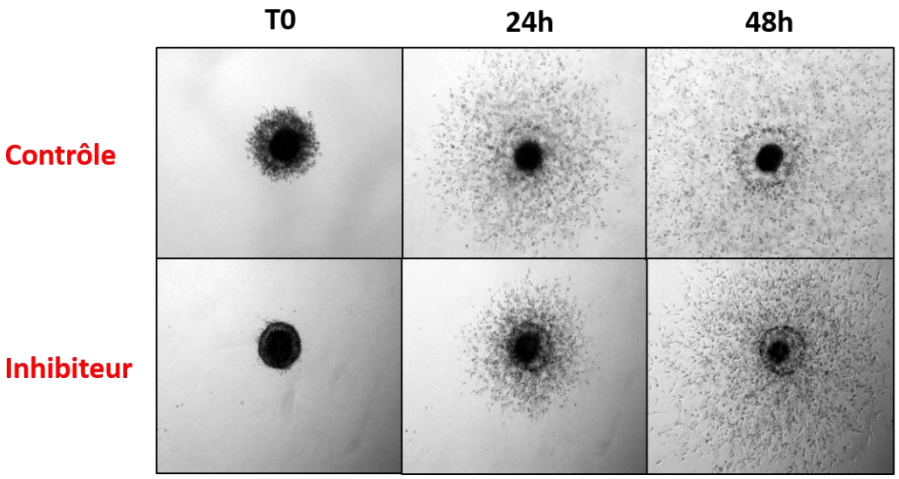

Figure 18 : Test de l'inhibiteur (50 µM) sur les sphéroïdes de cellules J3T sans macrophages. L'inhibiteur est dilué à 50 µM dans le collagène. Le contrôle contient l'équivalent en DMSO.

L'inhibiteur a ensuite été utilisé avec différents ligands des TLR. Nous pensons que la combinaison de l'inhibiteur et des ligands des TLR permettrait d'activer les macrophages et ainsi de limiter l'invasion. Le premier ligand est le LPS qui cible le TLR4. Comme nous l'avons vu dans le chapitre 2, l'inhibition de PC1/3 et l'activation du récepteur TLR4 par le LPS déclenchent la sécrétion de facteurs anti-tumoraux par les macrophages. On remarque sur la **Figure 19** que l'inhibiteur permet de diminuer l'invasion des cellules cancéreuses mais l'ajout de LPS ne permet pas d'améliorer l'effet observé.

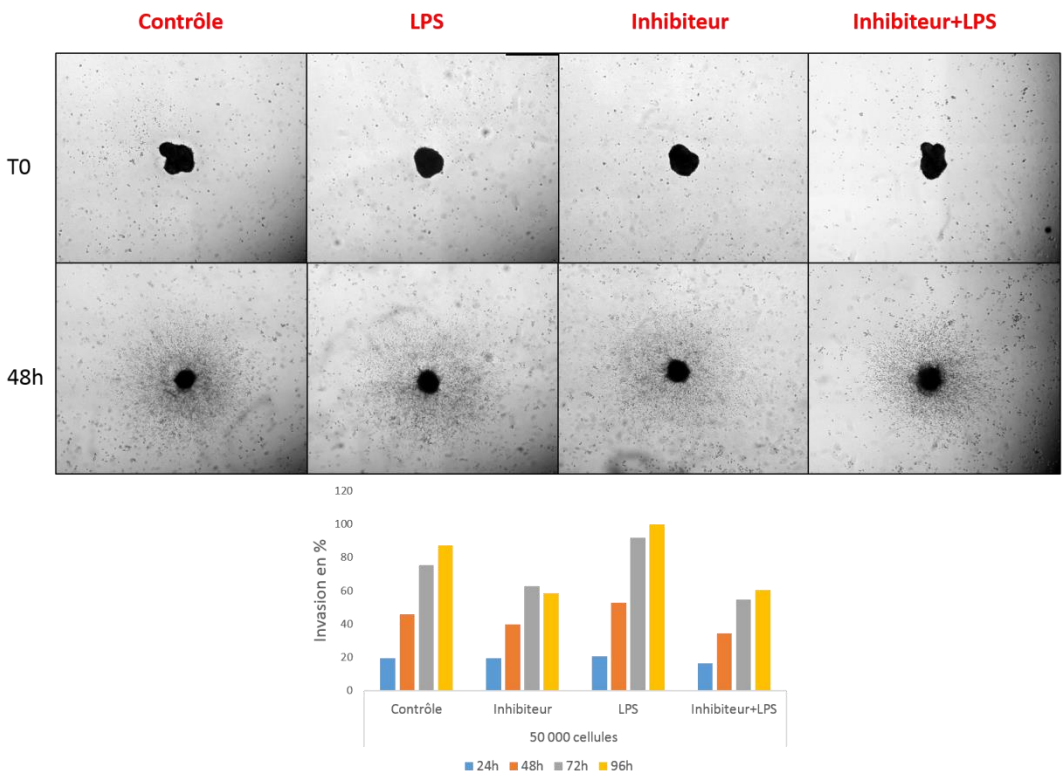

Figure 19 : Test de l'inhibiteur (50 µM) +/- LPS (200 ng/ml) sur les sphéroïdes de cellules J3T en co-culture avec les macrophages. L'inhibiteur est dilué dans le collagène à 50 µM. Le contrôle contient l'équivalent en DMSO. Le LPS est ajouté 24h après l'incorporation dans le collagène. L'aire d'invasion est mesurée avec le logiciel Photoshop de 24h à 96h et rapportée à l'aire du sphéroïde à T0.

L'inhibiteur en combinaison avec le CpG-ODN, ligand du TLR9, a aussi été utilisé (**Figure 20**). Nous pouvons observer le même effet que sous LPS, c'est-à-dire que l'invasion des cellules cancéreuses est plus faible sous inhibiteur, par contre l'ajout de CpG-ODN ne module pas l'invasion.

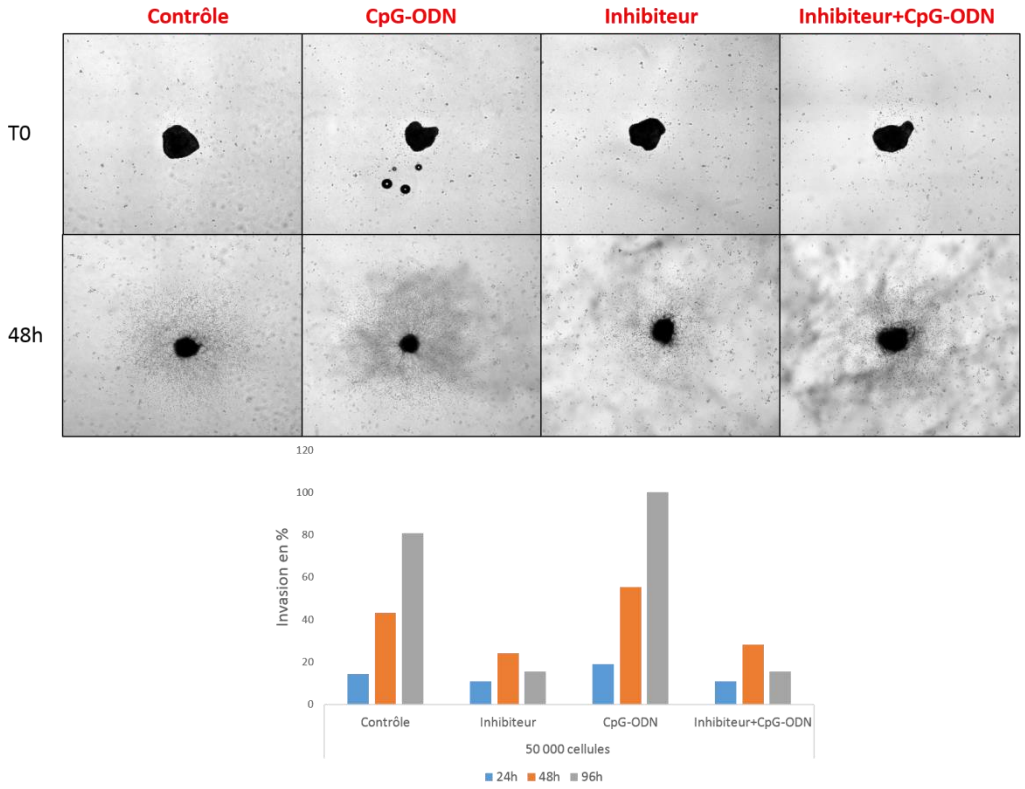

Figure 20 : Test de l'inhibiteur (50 µM) +/- CpG-ODN (1 µM) sur les sphéroïdes de cellules J3T en co-culture avec les macrophages. L'inhibiteur est dilué dans le collagène à 50 µM. Le contrôle contient l'équivalent en DMSO. Le CpG-ODN est ajouté 24h après l'incorporation dans le collagène. L'aire d'invasion est mesurée avec le logiciel Photoshop de 24h à 96h et rapportée à l'aire du sphéroïde à T0.

Avec ces expériences, nous avons démontré que l'inhibiteur permet de diminuer l'invasion en agissant directement sur les cellules cancéreuses. L'ajout de macrophages dans le collagène ne change pas l'effet de l'inhibiteur. Il faut maintenant savoir s'il a une action sur l'activation des macrophages. Cela semble être le cas d'après les chémokines sécrétées par les macrophages sous inhibiteur. L'ajout de ligands des TLR4 et TLR9 n'améliore pas l'effet sur l'invasion. D'autres ligands seront testés pour activer les macrophages. Il faut améliorer le système car actuellement nous sommes dans un système hétérologue de cellules de gliome canin et de macrophages de rat. Il se peut que les facteurs sécrétés par les macrophages de rat ne soient pas aussi actifs sur des cellules de chien. Une de nos priorités est donc d'isoler des monocytes sanguins de chien. Nous serons ainsi dans un système homologue plus représentatif de la réalité.

Dans le cas des gliomes outre les macrophages infiltrant, les cellules microgliales jouent un rôle important comme nous l'avons mis en évidence dans le premier chapitre. Nous nous

sommes donc demandé si des sphéroïdes mixtes cellules microgliales humaines avec la lignée de glioblastome NCH82 pourraient être sensibles à l'inhibiteur (**Figure 21**). Les résultats montrent qu'une activation du TLR3 par le Poly(I:C) est faiblement efficace comparé au couple inhibiteur et Poly(I:C). Ces résultats ont été faits en collaboration avec le Dr Anne Régnier Vigouroux. Sur la base de ces résultats, une étude complète avec le Poly(I:C) et l'inhibiteur est en cours.

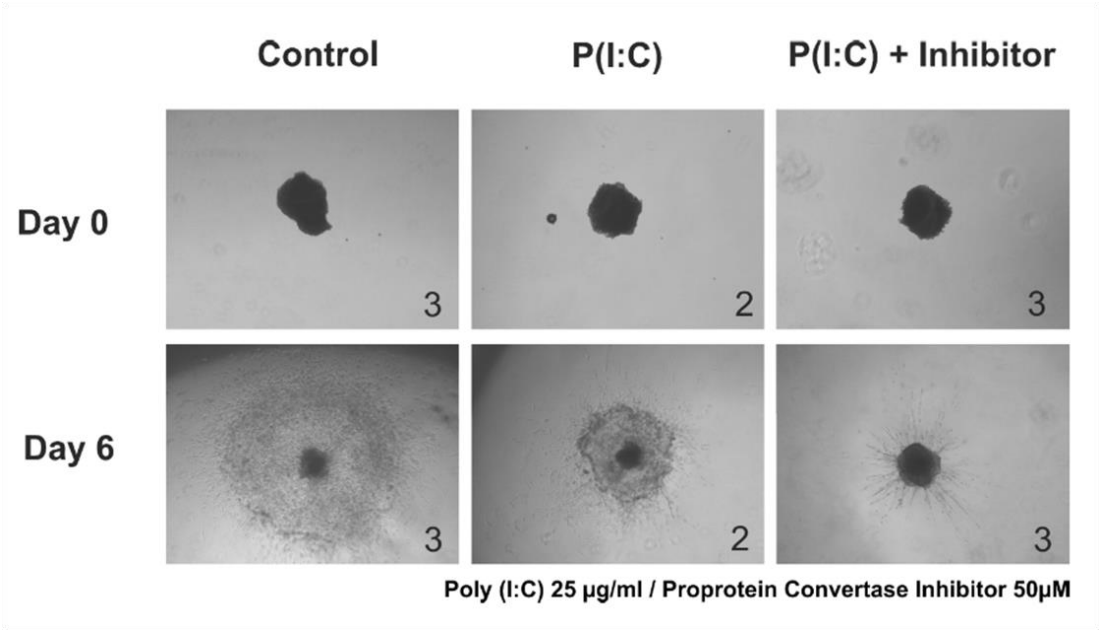

Figure 21 : Test de l'inhibiteur (50 µM) en combinaison avec le Poly(I:C) (25 µg/ml) sur les sphéroïdes mixtes de cellules de glioblastome humain NCH82 et de cellules microgliales humaines. L'inhibiteur et le Poly(I:C) sont dilués dans le collagène à 50 µM et 25 µg/ml respectivement.

DISCUSSION GENERALE

Les tumeurs se développent dans un microenvironnement complexe qui influence leur croissance, leur transformation et la formation de métastases. Dans le microenvironnement de nombreuses tumeurs, différents types cellulaires non néoplasiques coexistent, incluant les fibroblastes, les cellules du système immunitaire et les cellules endothéliales. Chacun de ces types cellulaires produit des facteurs de croissance et de survie, des chémokines, des composants de la matrice extracellulaire et des molécules favorisant l'angiogenèse. Ces molécules permettent de créer un environnement dans lequel les cellules néoplasiques peuvent se multiplier. Dans le cas des gliomes, les cellules microgliales et macrophages représentent 30 à 50% de la masse tumorale (Rossi et al. 1987; Morantz et al. 1979). Cela en fait des cibles de choix pour le développement de nouvelles thérapies contre les gliomes qui sont, la plupart du temps, difficile à traiter. Les gliomes représentent une pathologie complexe à la fois due à leur traitement qui n'est souvent pas adapté et leur classification qui est basée sur des critères histologiques peu reproductibles inter- et intra-observateur. De nouveaux critères moléculaires sont donc nécessaires afin d'améliorer cette classification et de déterminer des sous-populations de gliomes. Cela permettrait d'adapter le traitement en fonction du profil moléculaire de chaque patient. Mes travaux de thèse se sont placés dans cette problématique avec deux questions principales : la première concerne le développement d'une nouvelle classification des gliomes de haut grade basée sur des techniques de protéomique ; la deuxième porte sur le développement d'une immunothérapie contre le cancer reposant sur la réactivation des macrophages présents dans le microenvironnement tumoral.

Une classification par la protéomique des gliomes de haut grade

Le système actuel de classification histologique est un moyen pratique et rapide de classer les gliomes mais est enclin à la subjectivité des observateurs. De nombreux cas n'entrent pas dans les catégories établies dus à leur grande hétérogénéité. Des tumeurs de même grade peuvent avoir des issues cliniques différentes. Une solution est de compléter cette classification avec les informations moléculaires des patients. Dans la mise à jour de la classification de l'OMS de 2016, de nouveaux critères sont intégrés tels que la mutation des gènes IDH, la co-délétion 1p/19q et la mutation du gène ATRX (Louis et al. 2016b). Une classification

multiparamétrique des tumeurs représente le système le plus complet et le plus informatif de la pathologie. En plus des données génomiques, les données protéomiques peuvent fournir de nouvelles informations pour chaque sous-type de gliomes déjà établi et l'identification de protéines ou de profils protéiques permettrait de compléter la classification actuelle. A la différence des études déjà menées par protéomique, notre approche prend en compte l'hétérogénéité des échantillons. En effet, dans la plupart des études, les biopsies sont lysées avant une analyse en gel-LC-MS/MS. Notre approche consiste à utiliser l'imagerie par spectrométrie de masse pour caractériser l'hétérogénéité des tissus et ensuite la microprotéomique pour identifier les protéines de chaque sous-région.

L'étude que nous avons menée souligne l'hétérogénéité tumorale des gliomes de grade III. Au sein de ces tumeurs de même grade, trois sous-groupes ont pu être mis en évidence. Une discordance entre la classification réalisée par l'anatomopathologiste et la classification obtenue grâce à l'imagerie par spectrométrie de masse a été observée. Les protéines identifiées au sein de ces trois groupes appartiennent à des réseaux moléculaires différents. L'hétérogénéité est donc observée à la fois d'un point de vue histologique et moléculaire. Un des sous-groupes présente une forte expression de protéines reliées au métabolisme des ARN. Une étude de (Polisetty et al. 2013) a également démontré que de nombreuses protéines impliquées dans la régulation des ARN étaient surexprimées dans les gliomes de grade III. Le deuxième sous-groupe présente des protéines impliquées dans la réponse inflammatoire caractéristique d'une infiltration en cellules immunitaires. Le troisième sous-groupe est lié à la différenciation cellulaire et neuronale. Le principal objectif de cette première partie était de démontrer que l'imagerie par spectrométrie de masse couplée à la microprotéomique était un bon outil pour établir de nouvelles classifications des tumeurs. Cependant, cette première étude ne repose que sur dix tumeurs de grade III et n'est donc pas suffisante pour valider notre classification. Une étude sur une cohorte de 50 patients atteints de glioblastomes est en cours en utilisant la même technologie. La cohorte étant suffisamment importante, une corrélation avec les données cliniques des patients pourra être établie. Une valeur pronostique sera également ajoutée à notre classification en prenant en compte la survie des patients. Au cours de cette étude, nous avons également mis en évidence la présence de protéines issues d'ORF alternatif (Vanderperre et al. 2013; Mouilleron et al. 2016). La présence de ces protéines ouvre une porte supplémentaire en vue d'une meilleure classification moléculaire et également en vue du théranostic. En effet, les protéines alternatives issues de ces ORF alternatifs ont pour certaines pu être classées dans un des deux groupes définis à l'issue de l'étude protéomique. Ces protéines dont on ne connait pas

la fonction pour l'instant peuvent refléter chez les patients des mutations particulières. Nous prendrons désormais en compte de façon systématique la présence de ces protéines alternatives et les associerons aux données cliniques. Les travaux au sein de l'unité montrent que ces protéines alternatives sont des protéines régulatrices et certaines, du fait de leur petite taille, pourraient agir sur des récepteurs. Il n'est pas non plus à exclure qu'une partie de ces protéines alternatives (10362 identifiées chez l'homme) pourrait être les ligands des récepteurs orphelins. Il nous faut donc désormais intégrer ces nouvelles données.

L'hétérogénéité des tumeurs peut expliquer les difficultés rencontrées lors du traitement des patients. En effet, le traitement actuel est le même pour tous les patients et consiste en la résection chirurgicale de la tumeur suivie de radiothérapie et chimiothérapie. La chimiothérapie conventionnelle est le témozolomide. L'avantage de détailler le profil moléculaire de chaque patient est de pouvoir ensuite adapter la thérapie. Le problème à l'heure actuelle est de trouver le bon modèle animal avant la translation à l'homme. Les essais thérapeutiques précliniques se font actuellement sur des modèles de souris xénogreffées immunodéficientes. Cependant, la plupart du temps, ils échouent en phase clinique précoce chez l'homme. Une bonne alternative est de travailler sur les modèles canins. Les chiens partagent le même environnement que les hommes et développent spontanément des gliomes. De plus, nos résultats préliminaires semblent démontrer que les réseaux protéiques dérégulés chez l'homme sont également retrouvés chez le chien. Ils partagent leur hétérogénéité moléculaire et donc les mêmes mécanismes moléculaires et cellulaires dans le processus de tumorisation.

La réactivation des macrophages basée sur une enzyme : la proprotéine convertase 1/3

Comme nous l'avons observé précédemment, de nombreuses protéines identifiées dans les gliomes de grade III sont impliquées dans la réponse immunitaire. Les cellules microgliales et macrophages participent à la croissance tumorale en sécrétant différents facteurs pro-tumoraux. Ils vont également inhiber les réponses anti-tumorales des lymphocytes T. Dans ce cas, les macrophages présentent un phénotype anti-inflammatoire. De plus en plus de thérapies anti-cancéreuses consistent soit à dépléter la tumeur en macrophages soit à réactiver le phénotype de ces macrophages. Cependant, la déplétion des macrophages de la tumeur provoque très souvent des rechutes dès l'interruption du traitement (Bonapace et al. 2014). Notre approche consiste donc à réactiver les macrophages via l'enzyme PC1/3. PC1/3 est largement associée aux cellules neuroendocriniennes. Cependant, cette enzyme est également

exprimée dans les macrophages (Lansac, Dong, Claire M. Dubois, et al. 2006). PC1/3 joue un rôle important comme modulateur de l'immunité au sein des macrophages comme cela a été démontré chez des souris PC1/3 KO et dans un modèle de macrophages de rat PC1/3 KD (Refaie et al. 2012; Gagnon et al. 2013). Nous avons donc voulu utiliser cette capacité de PC1/3 à moduler la réponse immunitaire pour le développement d'une immunothérapie. Nous avons tout d'abord cherché à expliquer ce phénotype. L'inhibition de PC1/3 déclenche une sécrétion cytokinique importante par les macrophages due à une modulation du cytosquelette qui dérégule complètement la signalisation et le trafic intracellulaire suivant l'activation des récepteurs TLR4 et TLR9. PC1/3 est une protéase qui clive différents substrats et notamment des hormones. Les substrats de PC1/3 dans les macrophages n'ont, pour le moment, jamais été décrits. Il est essentiel de connaître ces substrats afin de comprendre exactement le mode d'action de PC1/3 et son rôle dans l'immunité.

Un point important que nous avons observé est que la stimulation des récepteurs TLR4 (LPS ou Taxol) et TLR9 (CpG-ODN) ne déclenche pas la sécrétion des mêmes facteurs lorsque PC1/3 est inhibé. Cela est intéressant car une thérapie ciblée en fonction de la sensibilité des tumeurs à ces facteurs pourrait être établie. Nous avons démontré que les cellules cancéreuses du sein, des ovaires ou des gliomes ne répondent pas de la même façon aux facteurs sécrétés par les macrophages PC1/3 KD. De plus, les macrophages PC1/3 KD sécrètent les mêmes facteurs sous IL10. L'IL10 est une cytokine majeure sécrétée par les cellules cancéreuses dans le microenvironnement pour orienter les macrophages vers un phénotype anti-inflammatoire. Il serait intéressant d'étudier leur phénotype suite à leur présence directe avec les cellules cancéreuses. La voie STAT3 qui est impliquée dans la prolifération, la survie, l'invasion des cellules cancéreuses et l'immunosuppression, est également modulée par PC1/3. Les sécrétomes des macrophages PC1/3 KD ont bien une action tumoricide mais ne reflètent pas la complexité tumorale. Il faudrait pour cela inhiber PC1/3 dans les macrophages de l'environnement tumoral afin d'observer leur réponse. Un inhibiteur des proprotéines convertases a été utilisé pour cet objectif. Il inhibe plusieurs proprotéines convertases dont la furine, PC1/3 et PACE4. Il a été démontré que la furine est également associée au système immunitaire en régulant la voie Th1 (Lin et al. 2012; Pesu et al. 2006). L'inhibiteur pourrait donc augmenter l'effet observé par rapport au knock-down de PC1/3. Des études de cet inhibiteur sur notre modèle macrophagique sont actuellement en cours afin de déterminer son effet sur la réponse immunitaire. Nous avons démontré que l'inhibiteur agissait également directement sur l'invasion des cellules cancéreuses de gliome canin. Cela peut s'expliquer par

le rôle de ces différentes proprotéines convertases dans le clivage de substrats essentiels à la croissance tumorale. De plus, l'expression de la furine est augmentée dans les cancers tête et cou et le cancer de l'ovaire (Bassi et al. 2001; Page et al. 2007) et l'expression de PC1/3 est augmentée dans les cancers neuroendocriniens (Jin et al. 1999; Konoshita et al. 1994). Nous avons également mis en évidence le rôle de PACE4 dans le cadre du cancer de l'ovaire et de la prostate en collaboration avec le Pr. R. Day (Université de Sherbrooke) (Longuespée et al. 2014; D'Anjou et al. 2011). L'inhibiteur pourrait donc agir à la fois sur les cellules cancéreuses et sur les macrophages et cellules microgliales pour réactiver la réponse immunitaire. Le développement d'aptamères spécifiques de chaque enzyme serait également intéressant afin de comparer l'effet de l'inhibition multiple ou isolée de chaque proprotéine convertase. Cependant nous nous sommes rendu compte que l'activation des macrophages par les ligands des TLR est dépendante de la tumeur concernée. Par exemple, pour les sphéroïdes de gliome canin, le LPS ou le CpG-ODN ne permettent pas aux macrophages d'agir sur l'invasion des cellules cancéreuses. D'autres ligands sont en cours d'essai tels que le Poly(I:C) qui a montré des effets significatifs sur l'invasion de sphéroïdes mixtes composés de cellules de gliome humain et de microglie humaine. Le Poly(I:C) seul permet de réduire l'invasion des cellules cancéreuses. La combinaison de l'inhibiteur et du Poly(I:C) est encore plus efficace. Ces résultats sont très encourageants quant à la faisabilité de notre approche.

Notre prochaine étape sera donc de trouver les meilleures conditions d'application de cette stratégie thérapeutique en prenant en compte la possibilité de faire des applications multiples de l'inhibiteur au cours du temps, de changer de ligands au cours du traitement et de l'évolution de la tumeur en suivant la nature des facteurs qu'elle secrète dans le milieu des sphéroïdes. Il faudra également réaliser des tests d'apoptose, d'autophagie, de résistance et de réactivation de TILs (Tumor Infiltrated Lymphocytes) avant de réaliser la première étude préclinique chez le chien. Ce travail ouvre donc une nouvelle possibilité de thérapie que nous appelons : le drone macrophage i .e la réactivation à distance des macrophages associés à la tumeur via l'action conjuguée d'un inhibiteur des proprotéines convertases et la stimulation des TLR.

LISTE DES REFERENCES

Adamson, C. et al., 2009. Glioblastoma multiforme: a review of where we have been and where we are going. *Expert Opinion on Investigational Drugs*.

Addona, T.A. et al., 2009. Multi-site assessment of the precision and reproducibility of multiple reaction monitoring-based measurements of proteins in plasma. *Nature biotechnology*, 27(7), pp.633–41.

Affara, N.I. et al., 2014. B cells regulate macrophage phenotype and response to chemotherapy in squamous carcinomas. *Cancer cell*, 25(6), pp.809–21.

Aldape, K. et al., 2015. Glioblastoma: pathology, molecular mechanisms and markers. *Acta neuropathologica*, 129(6), pp.829–48.

Almand, B. et al., 2001. Increased production of immature myeloid cells in cancer patients: a mechanism of immunosuppression in cancer. *Journal of immunology (Baltimore, Md. : 1950)*, 166(1), pp.678–89.

Anderson, H.J. & Galileo, D.S., 2016. Small-molecule inhibitors of FGFR, integrins and FAK selectively decrease L1CAM-stimulated glioblastoma cell motility and proliferation. *Cellular oncology (Dordrecht)*, 39(3), pp.229–42.

Angel, P.M. & Caprioli, R.M., 2013. Matrix-assisted laser desorption ionization imaging mass spectrometry: in situ molecular mapping. *Biochemistry*, 52(22), pp.3818–28.

Artenstein, A.W. & Opal, S.M., 2011. Proprotein convertases in health and disease. *The New England journal of medicine*, 365(26), pp.2507–18.

Baeza, N. et al., 2003. PTEN methylation and expression in glioblastomas. *Acta Neuropathologica*, pp.479–485.

Balkwill, F. & Mantovani, A., 2001. Inflammation and cancer: back to Virchow? *Lancet*, 357(9255), pp.539–45.

Ballas, Z.K., Rasmussen, W.L. & Krieg, A.M., 1996. Induction of NK activity in murine and human cells by CpG motifs in oligodeoxynucleotides and bacterial DNA. *Journal of immunology (Baltimore, Md. : 1950)*, 157(5), pp.1840–5.

Balluff, B. et al., 2011. MALDI imaging identifies prognostic seven-protein signature of novel tissue markers in intestinal-type gastric cancer. *The American journal of pathology*, 179(6), pp.2720–9.

Bassi, D.E. et al., 2001. Elevated furin expression in aggressive human head and neck tumors and tumor cell lines. *Molecular carcinogenesis*, 31(4), pp.224–32.

Bassi, D.E. et al., 2005. PACE4 expression in mouse basal keratinocytes results in basement membrane disruption and acceleration of tumor progression. *Cancer research*, 65(16), pp.7310–9.

Bates, G.J. et al., 2006. Quantification of regulatory T cells enables the identification of high-risk breast cancer patients and those at risk of late relapse. *Journal of clinical oncology : official journal of the American Society of Clinical Oncology*, 24(34), pp.5373–80.

Becker, G.L. et al., 2012. Highly potent inhibitors of proprotein convertase furin as potential drugs for treatment of infectious diseases. *The Journal of biological chemistry*, 287(26), pp.21992–2003.

van den Bent, M.J. et al., 2013. Adjuvant procarbazine, lomustine, and vincristine chemotherapy in newly diagnosed anaplastic oligodendroglioma: long-term follow-up of

EORTC brain tumor group study 26951. *Journal of clinical oncology : official journal of the American Society of Clinical Oncology*, 31(3), pp.344–50.

Bentley, R.T. et al., 2016. Dogs are man's best friend: in sickness and in health. *Neuro-oncology*.

Bergamaschi, A. et al., 2008. Extracellular matrix signature identifies breast cancer subgroups with different clinical outcome. *The Journal of pathology*, 214(3), pp.357–67.

Bhatia, S. et al., 2015. Pilot Study Of Intratumoral G100, Toll-like Receptor-4 (TLR4) Agonist, Therapy In Patients With Merkel Cell Carcinoma (MCC). *2015 ASCO Annual M*.

von Boehmer, H. & Daniel, C., 2013. Therapeutic opportunities for manipulating T(Reg) cells in autoimmunity and cancer. *Nature reviews. Drug discovery*, 12(1), pp.51–63.

Bonapace, L. et al., 2014. Cessation of CCL2 inhibition accelerates breast cancer metastasis by promoting angiogenesis. *Nature*, 515(7525), pp.130–3.

Brinkmann, M.M. et al., 2007. The interaction between the ER membrane protein UNC93B and TLR3, 7, and 9 is crucial for TLR signaling. *The Journal of cell biology*, 177(2), pp.265–75.

Bruchard, M. et al., 2013. Chemotherapy-triggered cathepsin B release in myeloid-derived suppressor cells activates the Nlrp3 inflammasome and promotes tumor growth. *Nature medicine*, 19(1), pp.57–64.

Byrd-Leifer, C.A. et al., 2001. The role of MyD88 and TLR4 in the LPS-mimetic activity of Taxol. *European journal of immunology*, 31(8), pp.2448–57.

Cairncross, G. et al., 2013. Phase III trial of chemoradiotherapy for anaplastic oligodendroglioma: long-term results of RTOG 9402. *Journal of clinical oncology : official journal of the American Society of Clinical Oncology*, 31(3), pp.337–43.

Carpentier, A.F., 2005. Cancer immunotherapy with CpG-ODN. *Medecine sciences : M/S*, 21(1), pp.73–77.

Carvalho Da Fonseca, A.C. & Badie, B., 2013. Microglia and macrophages in malignant gliomas: Recent discoveries and implications for promising therapies. *Clinical and Developmental Immunology*, 2013.

Cassetta, L. & Pollard, J.W., 2016. Cancer immunosurveillance: role of patrolling monocytes. *Cell Research*, 26(1), pp.3–4.

Chan, E. et al., 2015. Open-label phase 1b study of FOLFIRI plus cetuximab plus IMO-2055 in patients with colorectal cancer who have progressed following chemotherapy for advanced or metastatic disease. *Cancer Chemotherapy and Pharmacology*, 75(4), pp.701–709.

Chen, J. et al., 2011. CCL18 from tumor-associated macrophages promotes breast cancer metastasis via PITPNM3. *Cancer cell*, 19(4), pp.541–55.

Cheng, M. et al., 1997. Pro-protein convertase gene expression in human breast cancer. *International journal of cancer*, 71(6), pp.966–71.

Chicoine, M.R. et al., 2007. The in vivo antitumoral effects of lipopolysaccharide against glioblastoma multiforme are mediated in part by Toll-like receptor 4. *Neurosurgery*, 60(2), pp.372–80; discussion 381.

Choi, B.D. et al., 2009. EGFRvIII-Targeted Vaccination Therapy of Malignant Glioma. *Brain Pathology*, 19(4), pp.713–723.

Chow, K.K.H. et al., 2015. Combining immunotherapy with radiation for the treatment of glioblastoma. *Journal of Neuro-Oncology*, 123(3), pp.459–464.

Colegio, O.R. et al., 2014. Functional polarization of tumour-associated macrophages by tumour-derived lactic acid. *Nature*, 513(7519), pp.559–563.

Cortez-Retamozo, V. et al., 2012. Origins of tumor-associated macrophages and neutrophils. *Proceedings of the National Academy of Sciences of the United States of America*, 109(7), pp.2491–6.

D'Anjou, F. et al., 2011. Molecular Validation of PACE4 as a Target in Prostate Cancer. *Translational oncology*, 4(3), pp.157–72.

Day, R. et al., 1992. Distribution and regulation of the prohormone convertases PC1 and PC2 in the rat pituitary. *Molecular endocrinology (Baltimore, Md.)*, 6(3), pp.485–497.

Day, R. & Salzet, M., The neuroendocrine phenotype, cellular plasticity, and the search for genetic switches: redefining the diffuse neuroendocrine system. *Neuro endocrinology letters*, 23(5-6), pp.447–51.

De Palma, M. & Lewis, C.E., 2013. Macrophage Regulation of Tumor Responses to Anticancer Therapies. *Cancer Cell*, 23(3), pp.277–286.

Deltour, I. et al., 2009. Time trends in brain tumor incidence rates in Denmark, Finland, Norway, and Sweden, 1974-2003. *Journal of the National Cancer Institute*, 101(24), pp.1721–4.

DeNardo, D.G. et al., 2011. Leukocyte Complexity Predicts Breast Cancer Survival and Functionally Regulates Response to Chemotherapy. *Cancer Discovery*, 1(1), pp.54–67.

Dong, W. et al., 1995. Distinct mRNA expression of the highly homologous convertases PC5 and PACE4 in the rat brain and pituitary. *The Journal of neuroscience : the official journal of the Society for Neuroscience*, 15(3 Pt 1), pp.1778–96.

Erez, N. et al., 2010. Cancer-Associated Fibroblasts Are Activated in Incipient Neoplasia to Orchestrate Tumor-Promoting Inflammation in an NF-kappaB-Dependent Manner. *Cancer cell*, 17(2), pp.135–47.

Ferjančič, Š. et al., 2013. VCAM-1 and VAP-1 recruit myeloid cells that promote pulmonary metastasis in mice. *Blood*, 121(16), pp.3289–97.

Fife, B.T. & Bluestone, J.A., 2008. Control of peripheral T-cell tolerance and autoimmunity via the CTLA-4 and PD-1 pathways. *Immunological reviews*, 224, pp.166–82.

Fisher, J.L. et al., 2007. Epidemiology of Brain Tumors. *Neurologic Clinics*, 25(4), pp.867–890.

Franck, J. et al., 2009. MALDI imaging mass spectrometry: state of the art technology in clinical proteomics. *Molecular & cellular proteomics : MCP*, 8(9), pp.2023–33.

Frey, D.M. et al., 2010. High frequency of tumor-infiltrating FOXP3(+) regulatory T cells predicts improved survival in mismatch repair-proficient colorectal cancer patients. *International journal of cancer*, 126(11), pp.2635–43.

Fu, J. et al., 2007. Increased regulatory T cells correlate with CD8 T-cell impairment and poor survival in hepatocellular carcinoma patients. *Gastroenterology*, 132(7), pp.2328–39.

Fukumura, D. et al., 1998. Tumor induction of VEGF promoter activity in stromal cells. *Cell*, 94(6), pp.715–25.

Gagnon, H. et al., 2013. Proprotein Convertase 1/3 (PC1/3) in the Rat Alveolar Macrophage Cell Line NR8383: Localization, Trafficking and Effects on Cytokine Secretion. *PLoS*

ONE, 8(4).

Galdiero, M.R. et al., 2013. Tumor associated macrophages and neutrophils in cancer. *Immunobiology*, 218(11), pp.1402–1410.

Gallagher, B. et al., 2001. Cancer incidence in New York State acquired immunodeficiency syndrome patients. *American journal of epidemiology*, 154(6), pp.544–56.

Garzetti, L. et al., 2014. Activated macrophages release microvesicles containing polarized M1 or M2 mRNAs. *J. Leukoc. Biol*, 95, pp.0–0.

Gautam, P. et al., 2012. Proteins with altered levels in plasma from glioblastoma patients as revealed by iTRAQ-based quantitative proteomic analysis. *PloS one*, 7(9), p.e46153.

Germano, G. et al., 2013. Role of macrophage targeting in the antitumor activity of trabectedin. *Cancer cell*, 23(2), pp.249–62.

Germano, I., Swiss, V. & Casaccia, P., 2010. Primary brain tumors, neural stem cell, and brain tumor cancer cells: where is the link? *Neuropharmacology*, 58(6), pp.903–10.

Gocheva, V. et al., 2010. IL-4 induces cathepsin protease activity in tumor-associated macrophages to promote cancer growth and invasion. *Genes & development*, 24(3), pp.241–55.

Gollapalli, K. et al., 2012. Investigation of serum proteome alterations in human glioblastoma multiforme. *Proteomics*, 12(14), pp.2378–90.

Grivennikov, S.I., Greten, F.R. & Karin, M., 2010. Immunity, inflammation, and cancer. *Cell*, 140(6), pp.883–99.

Gyamera-Acheampong, C. & Mbikay, M., 2009. Proprotein convertase subtilisin/kexin type 4 in mammalian fertility: a review. *Human reproduction update*, 15(2), pp.237–47.

Hambardzumyan, D., Gutmann, D.H. & Kettenmann, H., 2015. The role of microglia and macrophages in glioma maintenance and progression. *Nature neuroscience*, 19(1), pp.20–7.

Hardell, L. et al., 2007. Long-term use of cellular phones and brain tumours: increased risk associated with use for > or =10 years. *Occupational and environmental medicine*, 64(9), pp.626–32.

Hegi, M. et al., 2004. Clinical trial substantiates the predictive value of O-6-methylguanine-DNA methyltransferase promoter methylation in glioblastoma patients treated with temozolomide. *Clin Cancer Res*, pp.1871–1874.

Hegi, M.E. et al., 2005. MGMT gene silencing and benefit from temozolomide in glioblastoma. *The New England journal of medicine*, 352, pp.997–1003.

Vander Heiden, M.G., Cantley, L.C. & Thompson, C.B., 2009. Understanding the Warburg effect: the metabolic requirements of cell proliferation. *Science (New York, N.Y.)*, 324(5930), pp.1029–33.

Heo, D.K. et al., 2015. Regulation of phagocytosis and cytokine secretion by store-operated calcium entry in primary isolated murine microglia. *Cellular Signalling*, 27(1), pp.177–186.

Hipp, M.M. et al., 2013. Processing of human toll-like receptor 7 by furin-like proprotein convertases is required for its accumulation and activity in endosomes. *Immunity*, 39(4), pp.711–21.

Hochberg, F.H. & Pruitt, A., 1980. Assumptions in the radiotherapy of glioblastoma. *Neurology*, 30(9), pp.907–11.

Hofseth, L.J. et al., 2003. Nitric oxide-induced cellular stress and p53 activation in chronic inflammation. *Proceedings of the National Academy of Sciences of the United States of America*, 100(1), pp.143–8.

Iribarren, K. et al., 2016. Trial Watch: Immunostimulation with Toll-like receptor agonists in cancer therapy. *Oncoimmunology*, 5(3), p.e1088631.

Ito, D. et al., 1998. Microglia-specific localisation of a novel calcium binding protein, Iba1. *Molecular Brain Research*, 57(1), pp.1–9.

Iwadate, Y., 2004. Molecular Classification and Survival Prediction in Human Gliomas Based on Proteome Analysis. *Cancer Research*, 64(7), pp.2496–2501.

Jiang, R. et al., 2006. Pathway alterations during glioma progression revealed by reverse phase protein lysate arrays. *Proteomics*, 6(10), pp.2964–71.

Jin, L. et al., 1999. Distribution and regulation of proconvertases PC1 and PC2 in human pituitary adenomas. *Pituitary*, 1(3-4), pp.187–95.

Johannesen, T.B. et al., Trends in incidence of brain and central nervous system tumors in Norway, 1970-1999. *Neuroepidemiology*, 23(3), pp.101–9.

Jones, E.A. et al., 2012. Imaging mass spectrometry statistical analysis. *Journal of proteomics*, 75(16), pp.4962–89.

Jung, C.S. et al., 2007. Serum GFAP is a diagnostic marker for glioblastoma multiforme. *Brain : a journal of neurology*, 130(Pt 12), pp.3336–41.

Kakinoki, K. et al., 2010. Prevention of intrahepatic metastasis of liver cancer by suicide gene therapy and chemokine ligand 2/monocyte chemoattractant protein-1 delivery in mice. *The journal of gene medicine*, 12(12), pp.1002–13.

Kalluri, R. & Zeisberg, M., 2006. Fibroblasts in cancer. *Nature reviews. Cancer*, 6(5), pp.392–401.

Karas, M. & Krüger, R., 2003. Ion Formation in MALDI: The Cluster Ionization Mechanism. *Chemical Reviews*, 103(2), pp.427–440.

Karavitis, J. et al., 2012. Regulation of COX2 expression in mouse mammary tumor cells controls bone metastasis and PGE2-induction of regulatory T cell migration. *PloS one*, 7(9), p.e46342.

El Kasmi, K.C. et al., 2008. Toll-like receptor-induced arginase 1 in macrophages thwarts effective immunity against intracellular pathogens. *Nature immunology*, 9(12), pp.1399–406.

Kees, T. et al., 2012. Microglia isolated from patients with glioma gain antitumor activities on poly (I:C) stimulation. *Neuro-Oncology*, 14(1), pp.64–78.

Khatib, A.-M. et al., 2002. Proprotein convertases in tumor progression and malignancy: novel targets in cancer therapy. *The American journal of pathology*, 160(6), pp.1921–35.

Kitamura, T., Qian, B.-Z. & Pollard, J.W., 2015. Immune cell promotion of metastasis. *Nature Reviews Immunology*, 15(2), pp.73–86.

Klatzmann, D. et al., 1998. A phase I/II study of herpes simplex virus type 1 thymidine kinase "suicide" gene therapy for recurrent glioblastoma. Study Group on Gene Therapy for Glioblastoma. *Human gene therapy*, 9(17), pp.2595–604.

Klug, F. et al., 2013. Low-dose irradiation programs macrophage differentiation to an iNOS^{+}/M1 phenotype that orchestrates effective T cell immunotherapy. *Cancer cell*, 24(5), pp.589–602.

Kodumudi, K.N. et al., 2010. A novel chemoimmunomodulating property of docetaxel: suppression of myeloid-derived suppressor cells in tumor bearers. *Clinical cancer research : an official journal of the American Association for Cancer Research*, 16(18), pp.4583–94.

Konoshita, T. et al., 1994. Expression of PC2 and PC1/PC3 in human pheochromocytomas. *Molecular and cellular endocrinology*, 99(2), pp.307–14.

Kortylewski, M. et al., 2005. Inhibiting Stat3 signaling in the hematopoietic system elicits multicomponent antitumor immunity. *Nature Medicine*, 11(12), pp.1314–1321.

Kortylewski, M. et al., 2009. Toll-like receptor 9 activation of signal transducer and activator of transcription 3 constrains its agonist-based immunotherapy. *Cancer Res*, 69(6), pp.2497–2505.

Lansac, G., Dong, W., Dubois, C.M., et al., 2006. Lipopolysaccharide mediated regulation of neuroendocrine associated proprotein convertases and neuropeptide precursor processing in the rat spleen. *Journal of Neuroimmunology*, 171(1-2), pp.57–71.

Lansac, G., Dong, W., Dubois, C.M., et al., 2006. Lipopolysaccharide mediated regulation of neuroendocrine associated proprotein convertases and neuropeptide precursor processing in the rat spleen. *Journal of neuroimmunology*, 171(1-2), pp.57–71.

Lee, B.L. et al., 2013. UNC93B1 mediates differential trafficking of endosomal TLRs. *eLife*, 2, p.e00291.

Lemaire, R. et al., 2007. Specific MALDI imaging and profiling for biomarker hunting and validation: fragment of the 11S proteasome activator complex, Reg alpha fragment, is a new potential ovary cancer biomarker. *Journal of proteome research*, 6(11), pp.4127–34.

Lewis, A.M. et al., 2006. Interleukin-1 and cancer progression: the emerging role of interleukin-1 receptor antagonist as a novel therapeutic agent in cancer treatment. *Journal of translational medicine*, 4, p.48.

Lin, H. et al., 2012. Protective role of systemic furin in immune response-induced arthritis. *Arthritis and rheumatism*, 64(9), pp.2878–86.

Longuespée, R. et al., 2014. Implications of Proprotein Convertases in Ovarian Cancer Cell Proliferation and Tumor Progression: Insights for PACE4 as a Therapeutic Target. *Translational oncology*, 7(3), p.410.

Louis, D.N. et al., 2007. The 2007 WHO classification of tumours of the central nervous system. *Acta Neuropathologica*, 114(2), pp.97–109.

Louis, D.N. et al., 2016a. The 2016 World Health Organization Classification of Tumors of the Central Nervous System: a summary. *Acta neuropathologica*, 131(6), pp.803–20.

Louis, D.N. et al., 2016b. The 2016 World Health Organization Classification of Tumors of the Central Nervous System: a summary. *Acta neuropathologica*.

Lusson, J. et al., 1993. cDNA structure of the mouse and rat subtilisin/kexin-like PC5: a candidate proprotein convertase expressed in endocrine and nonendocrine cells. *Proceedings of the National Academy of Sciences of the United States of America*, 90(14), pp.6691–5.

Magnavita, N. et al., 2003. Occupational head injury and subsequent glioma. *Neurological sciences : official journal of the Italian Neurological Society and of the Italian Society of Clinical Neurophysiology*, 24(1), pp.31–3.

Marsh, T., Pietras, K. & McAllister, S.S., 2013. Fibroblasts as architects of cancer

pathogenesis. *Biochimica et biophysica acta*, 1832(7), pp.1070–8.

Maxwell, K.N., Fisher, E.A. & Breslow, J.L., 2005. Overexpression of PCSK9 accelerates the degradation of the LDLR in a post-endoplasmic reticulum compartment. *Proceedings of the National Academy of Sciences of the United States of America*, 102(6), pp.2069–74.

McKinley, B.P. et al., 2000. The impact of age and sex on the incidence of glial tumors in New York state from 1976 to 1995. *Journal of neurosurgery*, 93(6), pp.932–9.

Melchior, K. et al., 2009. Proteomic study of human glioblastoma multiforme tissue employing complementary two-dimensional liquid chromatography- and mass spectrometry-based approaches. *Journal of proteome research*, 8(10), pp.4604–14.

Miletic, H. et al., 2009. Anti-VEGF therapies for malignant glioma: treatment effects and escape mechanisms. *Expert Opinion on Investigational Drugs*, 13(4), pp.455–468.

Mora, R. et al., 2009. TNF-α- and TRAIL-resistant glioma cells undergo autophagy-dependent cell death induced by activated microglia. *Glia*, 57(5), pp.561–581.

Morantz, R.A. et al., 1979. Macrophages in experimental and human brain tumors. Part 2: studies of the macrophage content of human brain tumors. *Journal of neurosurgery*, 50(3), pp.305–11.

Motomura, K. et al., 2011. Benefits of interferon-β and temozolomide combination therapy for newly diagnosed primary glioblastoma with the unmethylated MGMT promoter: A multicenter study. *Cancer*, 117(8), pp.1721–30.

Mouilleron, H., Delcourt, V. & Roucou, X., 2016. Death of a dogma: eukaryotic mRNAs can code for more than one protein. *Nucleic acids research*, 44(1), pp.14–23.

Müller, E.J., Caldelari, R. & Posthaus, H., 2004. Role of subtilisin-like convertases in cadherin processing or the conundrum to stall cadherin function by convertase inhibitors in cancer therapy. *Journal of molecular histology*, 35(3), pp.263–75.

Murdoch, C., Muthana, M. & Lewis, C.E., 2005. Hypoxia Regulates Macrophage Functions in Inflammation. *The Journal of Immunology*, 175(10), pp.6257–6263.

Nathan, C., 2002. Points of control in inflammation. *Nature*, 420(6917), pp.846–52.

Németh, Z.H. et al., 2004. Disruption of the actin cytoskeleton results in nuclear factor-kappaB activation and inflammatory mediator production in cultured human intestinal epithelial cells. *Journal of cellular physiology*, 200(1), pp.71–81.

Niclou, S.P., Fack, F. & Rajcevic, U., 2010. Glioma proteomics: status and perspectives. *Journal of proteomics*, 73(10), pp.1823–38.

Nijaguna, M.B. et al., 2015. Definition of a serum marker panel for glioblastoma discrimination and identification of Interleukin 1β in the microglial secretome as a novel mediator of endothelial cell survival induced by C-reactive protein. *Journal of Proteomics*, 128, pp.251–261.

Noy, R. & Pollard, J.W., 2014. Tumor-Associated Macrophages: From Mechanisms to Therapy. *Immunity*, 41(1), pp.49–61.

Ohgaki, H. & Kleihues, P., 2013. The definition of primary and secondary glioblastoma. *Clinical cancer research : an official journal of the American Association for Cancer Research*, 19(4), pp.764–72.

Ohnishi, M. et al., 2009. Proteomics of tumor-specific proteins in cerebrospinal fluid of patients with astrocytoma: usefulness of gelsolin protein. *Pathology international*, 59(11), pp.797–803.

Oppenheimer, S.R. et al., 2010. Molecular analysis of tumor margins by MALDI mass spectrometry in renal carcinoma. *Journal of proteome research*, 9(5), pp.2182–90.

Ostrom, Q.T. et al., 2015. CBTRUS Statistical Report: Primary Brain and Central Nervous System Tumors Diagnosed in the United States in 2008-2012. *Neuro-oncology*, 17 Suppl 4(suppl_4), pp.iv1–iv62.

Ostuni, R. et al., 2015. Macrophages and cancer: from mechanisms to therapeutic implications. *Trends in Immunology*, 36(4), pp.229–39.

Padfield, E., Ellis, H.P. & Kurian, K.M., 2015. Current Therapeutic Advances Targeting EGFR and EGFRvIII in Glioblastoma. *Frontiers in oncology*, 5, p.5.

Page, R.E. et al., 2007. Increased expression of the pro-protein convertase furin predicts decreased survival in ovarian cancer. *Cellular oncology : the official journal of the International Society for Cellular Oncology*, 29(4), pp.289–99.

Pallotta, M.T. et al., 2011. Indoleamine 2,3-dioxygenase is a signaling protein in long-term tolerance by dendritic cells. *Nature immunology*, 12(9), pp.870–8.

Park, S.W., Moon, Y.-A. & Horton, J.D., 2004. Post-transcriptional regulation of low density lipoprotein receptor protein by proprotein convertase subtilisin/kexin type 9a in mouse liver. *The Journal of biological chemistry*, 279(48), pp.50630–8.

Parsons, D.W. et al., 2008. An integrated genomic analysis of human glioblastoma multiforme. *Science (New York, N.Y.)*, 321(5897), pp.1807–12.

Patel, N.R. et al., 2012. Cell Elasticity Determines Macrophage Function. *PLoS ONE*, 7.

Persson, O. et al., 2009. Proteomic expression analysis and comparison of protein and mRNA expression profiles in human malignant gliomas. *PROTEOMICS - CLINICAL APPLICATIONS*, 3(1), pp.83–94.

Pesu, M. et al., 2006. Proprotein convertase furin is preferentially expressed in T helper 1 cells and regulates interferon gamma. *Blood*, 108(3), pp.983–5.

Pesu, M. et al., 2008. T-cell-expressed proprotein convertase furin is essential for maintenance of peripheral immune tolerance. *Nature*, 455(7210), pp.246–50.

Polisetty, R.V. et al., 2013. Heterogeneous nuclear ribonucleoproteins and their interactors are a major class of deregulated proteins in anaplastic astrocytoma: a grade III malignant glioma. *Journal of proteome research*, 12(7), pp.3128–38.

Pollard, J.W., 2004. Tumour-educated macrophages promote tumour progression and metastasis. *Nature reviews. Cancer*, 4(1), pp.71–8.

Porter, A., 2012. A Dead End: A Review of Glioblastoma Multiforme. *Eukaryon*, pp.64–68.

Puente, X.S. et al., 2003. Human and mouse proteases: a comparative genomic approach. *Nature reviews. Genetics*, 4(7), pp.544–58.

Pullikotil, P. et al., 2007. The proprotein convertase SKI-1/S1P: alternate translation and subcellular localization. *The Journal of biological chemistry*, 282(37), pp.27402–13.

Pyonteck, S.M. et al., 2013. CSF-1R inhibition alters macrophage polarization and blocks glioma progression. *Nature medicine*, 19(10), pp.1264–72.

Qian, B.-Z. et al., 2011. CCL2 recruits inflammatory monocytes to facilitate breast-tumour metastasis. *Nature*, 475(7355), pp.222–5.

Quail, D.F. & Joyce, J.A., 2013. Microenvironmental regulation of tumor progression and metastasis. *Nature medicine*, 19(11), pp.1423–37.

Quanico, J. et al., 2013. Development of liquid microjunction extraction strategy for improving protein identification from tissue sections. *Journal of proteomics*, 79, pp.200–18.

Rahat, M.A. & Hemmerlein, B., 2013. Macrophage-tumor cell interactions regulate the function of nitric oxide. *Frontiers in physiology*, 4, p.144.

Refaie, S. et al., 2012. Disruption of proprotein convertase 1/3 (PC1/3) expression in mice causes innate immune defects and uncontrolled cytokine secretion. *Journal of Biological Chemistry*, 287(18), pp.14703–14717.

Ries, C.H. et al., 2014. Targeting tumor-associated macrophages with anti-CSF-1R antibody reveals a strategy for cancer therapy. *Cancer cell*, 25(6), pp.846–59.

Rossi, M.L. et al., 1987. Immunohistological study of mononuclear cell infiltrate in malignant gliomas. *Acta neuropathologica*, 74(3), pp.269–77.

Rousselet, E. et al., 2011. The proprotein convertase PC7: unique zymogen activation and trafficking pathways. *The Journal of biological chemistry*, 286(4), pp.2728–38.

Ruffell, B. et al., 2014. Macrophage IL-10 blocks CD8+ T cell-dependent responses to chemotherapy by suppressing IL-12 expression in intratumoral dendritic cells. *Cancer cell*, 26(5), pp.623–37.

Salzet, M., 2002. Immune cells express endocrine markers [1]. *Neuroendocrinology Letters*, 23(1), pp.8–9.

Salzet, M., Vieau, D. & Day, R., 2000. Crosstalk between nervous and immune systems through the animal kingdom: focus on opioids. *Trends in Neurosciences*, 23(11), pp.550–555.

Sangaletti, S. et al., 2008. Macrophage-derived SPARC bridges tumor cell-extracellular matrix interactions toward metastasis. *Cancer research*, 68(21), pp.9050–9.

Sangiovanni, A. et al., 2004. Increased survival of cirrhotic patients with a hepatocellular carcinoma detected during surveillance. *Gastroenterology*, 126(4), pp.1005–14.

Schäfer, N. et al., 2016. Phase I trial of dovitinib (TKI258) in recurrent glioblastoma. *Journal of cancer research and clinical oncology*, 142(7), pp.1581–9.

Schmid, M.C. & Varner, J.A., 2010. Myeloid cells in the tumor microenvironment: modulation of tumor angiogenesis and tumor inflammation. *Journal of oncology*, 2010, p.201026.

Schuhmann MU, Zucht HD, Nassimi R, Heine G, Schneekloth CG, Stuerenburg HJ, S.H., 2010. Peptide screening of cerebrospinal fluid in patients with glioblastoma multiforme. *European Journal of Surgical Oncology*, 36(2), pp.201–207.

Seidah, N.G. et al., 1999. Mammalian subtilisin/kexin isozyme SKI-1: A widely expressed proprotein convertase with a unique cleavage specificity and cellular localization. *Proceedings of the National Academy of Sciences of the United States of America*, 96(4), pp.1321–6.

Seidah, N.G. & Prat, A., 2012. The biology and therapeutic targeting of the proprotein convertases. *Nature Reviews Drug Discovery*, 11(5), pp.367–383.

Semenza, G.L., 2013. HIF-1 mediates metabolic responses to intratumoral hypoxia and oncogenic mutations. *The Journal of clinical investigation*, 123(9), pp.3664–71.

Shen, F. et al., 2014. Proteomic analysis of cerebrospinal fluid: toward the identification of biomarkers for gliomas. *Neurosurgical review*, 37(3), pp.367–80; discussion 380.

Shive, C.L. et al., 2015. Soluble CD14 is a nonspecific marker of monocyte activation. *AIDS (London, England)*, 29(10), pp.1263–5.

Shree, T. et al., 2011. Macrophages and cathepsin proteases blunt chemotherapeutic response in breast cancer. *Genes & Development*, 25(23), pp.2465–2479.

Siezen, R.J. & Leunissen, J.A., 1997. Subtilases: the superfamily of subtilisin-like serine proteases. *Protein science : a publication of the Protein Society*, 6(3), pp.501–23.

Siveen, K.S. et al., 2014. Targeting the STAT3 signaling pathway in cancer: Role of synthetic and natural inhibitors. *Biochimica et Biophysica Acta (BBA) - Reviews on Cancer*, 1845(2), pp.136–154.

Smith, D.A. et al., 2014. Antitumor activity and safety of combination therapy with the Toll-like receptor 9 agonist IMO-2055, erlotinib, and bevacizumab in advanced or metastatic non-small cell lung cancer patients who have progressed following chemotherapy. *Cancer Immunology, Immunotherapy*, 63(8), pp.787–796.

Smith, J.S. & Jenkins, R.B., 2000. Genetic alterations in adult diffuse glioma: occurrence, significance, and prognostic implications. *Frontiers in bioscience : a journal and virtual library*, 5, pp.D213–D231.

Stewart, C.R. et al., 2010. CD36 ligands promote sterile inflammation through assembly of a Toll-like receptor 4 and 6 heterodimer. *Nature immunology*, 11(2), pp.155–161.

Stewart, T. et al., 1995. Incidence of de-novo breast cancer in women chronically immunosuppressed after organ transplantation. *Lancet (London, England)*, 346(8978), pp.796–8.

Stupp, R. et al., 2005. Radiotherapy plus concomitant and adjuvant temozolomide for glioblastoma. *The New England journal of medicine*, 352(10), pp.987–96.

Tabatabai, G. et al., 2010. Molecular diagnostics of gliomas: The clinical perspective. *Acta Neuropathologica*, 120(5), pp.585–592.

Talmadge, J.E. & Gabrilovich, D.I., 2013. History of myeloid-derived suppressor cells. *Nature reviews. Cancer*, 13(10), pp.739–52.

Thomas, G., 2002. Furin at the cutting edge: from protein traffic to embryogenesis and disease. *Nature reviews. Molecular cell biology*, 3(10), pp.753–66.

Tsuchiyama, T. et al., 2008. Optimal amount of monocyte chemoattractant protein-1 enhances antitumor effects of suicide gene therapy against hepatocellular carcinoma by M1 macrophage activation. *Cancer science*, 99(10), pp.2075–82.

Vanderperre, B. et al., 2013. Direct detection of alternative open reading frames translation products in human significantly expands the proteome. *PloS one*, 8(8), p.e70698.

Varlet, P. et al., 2005. Criteria of diagnosis and grading of oligodendrogliomas or oligo-astrocytomas according to the WHO and Sainte-Anne classifications. *Neuro-Chirurgie*, 51(3-4 Pt 2), pp.239–246.

Verhaak, R.G.W. et al., 2010. Integrated genomic analysis identifies clinically relevant subtypes of glioblastoma characterized by abnormalities in PDGFRA, IDH1, EGFR, and NF1. *Cancer cell*, 17(1), pp.98–110.

Vicari, A.P. et al., 2002. Reversal of tumor-induced dendritic cell paralysis by CpG immunostimulatory oligonucleotide and anti-interleukin 10 receptor antibody. *The Journal of experimental medicine*, 196(4), pp.541–9.

Viegas, C. et al., 2011. Occipital WHO grade II gliomas: Oncological, surgical and functional

considerations. *Acta Neurochirurgica*, 153(10), pp.1907–1917.

Vogel, T.W. et al., 2005. Proteins and protein pattern differences between glioma cell lines and glioblastoma multiforme. *Clinical cancer research : an official journal of the American Association for Cancer Research*, 11(10), pp.3624–32.

Walley, K.R. et al., 2014. PCSK9 is a critical regulator of the innate immune response and septic shock outcome. *Science translational medicine*, 6(258), p.258ra143.

Walter, A. et al., 2013. Aldara activates TLR7-independent immune defence. *Nature Communications*, 4, p.1560.

Wang, B. et al., 2015. Improved anti-glioblastoma efficacy by IL-13Rα2 mediated copolymer nanoparticles loaded with paclitaxel. *Scientific Reports*, 5, p.16589.

West, R.B. et al., 2006. A landscape effect in tenosynovial giant-cell tumor from activation of CSF1 expression by a translocation in a minority of tumor cells. *Proceedings of the National Academy of Sciences of the United States of America*, 103(3), pp.690–5.

Wisztorski, M. et al., 2013. Microproteomics by liquid extraction surface analysis: application to FFPE tissue to study the fimbria region of tubo-ovarian cancer. *Proteomics. Clinical applications*, 7(3-4), pp.234–40.

Wisztorski, M. et al., 2016. Spatially-resolved protein surface microsampling from tissue sections using liquid extraction surface analysis. *Proteomics*, 16(11-12), pp.1622–32.

Wong, A. et al., 1987. Increased expression of the epidermal growth factor receptor gene in malignant gliomas is invariably associated with gene amplification. *Proceedings of the National Academy of Sciences of the United States of America*, pp.6899–6903.

Wyckoff, J. et al., 2004. A paracrine loop between tumor cells and macrophages is required for tumor cell migration in mammary tumors. *Cancer research*, 64(19), pp.7022–9.

Xue, J. et al., 2014. Transcriptome-based network analysis reveals a spectrum model of human macrophage activation. *Immunity*, 40(2), pp.274–88.

Yang, B. et al., 2010. Molecular mechanisms of "off-on switch" of activities of human IDH1 by tumor-associated mutation R132H. *Cell research*, 20(11), pp.1188–1200.

Yusuf, R.Z. et al., 2003. Paclitaxel resistance: molecular mechanisms and pharmacologic manipulation. *Current cancer drug targets*, 3(1), pp.1–19.

Zacher, A. et al., 2016. Molecular diagnostics of gliomas using next generation sequencing of a glioma-tailored gene panel. *Brain Pathology*, 7(9), p.e41024.

Zaid, A. et al., 2008. Proprotein convertase subtilisin/kexin type 9 (PCSK9): hepatocyte-specific low-density lipoprotein receptor degradation and critical role in mouse liver regeneration. *Hepatology (Baltimore, Md.)*, 48(2), pp.646–54.

Zeng, J. et al., 2013. Anti-PD-1 blockade and stereotactic radiation produce long-term survival in mice with intracranial gliomas. *Int J Radiat Oncol Biol Phys*, pp.343–349.

Zhang, Q. et al., 2012. Prognostic significance of tumor-associated macrophages in solid tumor: a meta-analysis of the literature. *PloS one*, 7(12), p.e50946.

Zhu, X., Zhou, A., et al., 2002. Disruption of PC1/3 expression in mice causes dwarfism and multiple neuroendocrine peptide processing defects. *Proceedings of the National Academy of Sciences of the United States of America*, 99(16), pp.10293–8.

Zhu, X., Orci, L., et al., 2002. Severe block in processing of proinsulin to insulin accompanied by elevation of des-64,65 proinsulin intermediates in islets of mice lacking prohormone convertase 1/3. *Proceedings of the National Academy of Sciences of the*

United States of America, 99(16), pp.10299–304.

Zouaoui, S. et al., 2012. [French brain tumor database: general results on 40,000 cases, main current applications and future prospects]. *Neuro-Chirurgie*, 58(1), pp.4–13.

RÉSUMÉ

Les tumeurs sont des régions très hétérogènes à la fois au niveau moléculaire et au niveau de la diversité cellulaire composant le microenvironnement tumoral. La classification des gliomes repose actuellement sur des critères histologiques qui sont enclins à de fortes subjectivités inter- et intra-observateurs. Au sein du même grade, des sous-groupes de tumeurs se différencient. Le but de ce projet est de réaliser une classification moléculaire des gliomes de haut grade en se basant sur des données protéiques permettant de localiser des biomarqueurs potentiels directement sur le tissu. Des sous-régions ayant des profils moléculaires différents ont été mises en évidence et les molécules les composants ont ensuite été identifiées de façon localisée. Les résultats démontrent que les annotations histologiques ne concordent pas forcément avec la classification moléculaire. Cette hétérogénéité est également retrouvée dans le microenvironnement des tumeurs où l'on retrouve des cellules immunitaires telles que les macrophages. Les macrophages sont détournés de leur fonction première par la tumeur pour lui permettre de se développer. Une stratégie thérapeutique pour contrer sa croissance est de réorienter le phénotype des macrophages vers un phénotype antitumoral. L'inhibition de la proprotéine convertase 1/3 s'est révélée être une stratégie prometteuse pour la réactivation des macrophages via les récepteurs TLR. Les facteurs sécrétés par ces macrophages ont un effet sur la viabilité et l'invasion de différentes cellules cancéreuses (gliomes, cancer de l'ovaire et cancer du sein) en fonction des ligands des récepteurs TLR utilisés. La première partie nous a permis d'identifier des sous-groupes de gliomes qui en fonction de leur profil moléculaire pourront, dans une perspective à long terme, recevoir des traitements plus personnalisés basés, par exemple, sur l'inhibition de proprotéines convertases en combinaison avec des ligands des récepteurs TLR.

Mots clés : Gliome, Imagerie par Spectrométrie de Masse, Microprotéomique, Classification, Proprotéine convertase 1/3, Macrophages, Récepteurs TLR, Oncoimmunologie

SUMMARY

Tumors are highly heterogeneous both histologically and molecularly. In fact, several non-neoplasic cell types are present in the microenvironment. Glioma classification is based on histological criteria that are prone to inter- and intra-observers subjectivities. Within tumors of same grade, subgroups can be differentiated. The aim of this project is to realize a molecular classification of high grade glioma based on proteomics data allowing the localization of potential biomarkers directly on the tissue. Subregions having different molecular profiles have been highlighted and the molecules comprising them have been identified in a localized way. Results prove that histological annotations do not necessarily correspond to molecular classification. This heterogeneity is also found in the tumor microenvironment where we can find immune cells such as macrophages. Macrophages are changed from their primary function by the tumor to allow it to grow. A therapeutic strategy to counter the tumor growth has been developed in order to switch macrophages phenotype toward an antitumor one. The inhibition of proprotein convertase 1/3 has proven to be a promising therapy to reactivate macrophages via TLR receptors. Secreted factors by these PC1/3 inhibited macrophages have an effect on cancer cells viability and invasion according to TLR ligand used. The first part will allow us to identify subgroups of glioma which, depending on their molecular profiles, could, in a long-term view, receive personalized treatments based on the inhibition of proproteins convertases combined to TLR ligands.

Keywords: Glioma, Mass Spectrometry Imaging, Microproteomics, Classification, Proprotein Convertase 1/3, Macrophages, TLR Receptors, Oncoimmunology.